

BIBLIOGRAPHIC INFORMATION

PB94-219185

Report Nos:

Title: Seismic Energy Based Fatigue Damage Analysis of Bridge Columns. Part 1. Evaluation of Seismic Capacity.

Date: 14 Mar 94

Authors: G. A. Chang and J. B. Mander.

Performing Organization: State Univ. of New York at Buffalo. Dept. of Civil Engineering.

Performing Organization Report Nos: NCEER-94-0006

Sponsoring Organization: *National Center for Earthquake Engineering Research, Buffalo, NY. *Federal Highway Administration, Washington, DC. *National Science Foundation, Arlington, VA. *New York State Science and Technology Foundation, Albany.

Contract Nos: DTFH-61-92-C-00106, NSF-BCS-90-25010, NYSSTF-NEC-91029

Type of Report and Period Covered: Technical rept.

NTIS Field/Group Codes: 50A (Highway Engineering), 89D (Structural Analyses)

Price: PC A15/MF A03

Availability: Available from the National Technical Information Service, Springfield, VA. 22161

Number of Pages: 238p

Keywords: *Bridge piers. *Damage assessment. *Earthquake engineering. Seismic design. Computerized simulation. Mathematical models. Energy absorption. Cyclic loads. Pile structures. Bridge foundations.

Abstract: The study is concerned with the computational modeling of energy absorption (fatigue) capacity of reinforced concrete bridge columns by using a cyclic dynamic Fiber Element computational model. The results may be used with a hysteretic rule to generate seismic energy demand. By comparing the ratio of energy demand to capacity, inferences of column damageability or fatigue resistance can be made. A complete analysis methodology for bridge columns is developed.



PB94-219185

**NATIONAL CENTER FOR EARTHQUAKE
ENGINEERING RESEARCH**

State University of New York at Buffalo

**Seismic Energy Based Fatigue Damage Analysis
of Bridge Columns:
Part I — Evaluation of Seismic Capacity**

by

G.A. Chang and J.B. Mander
State University of New York at Buffalo
Department of Civil Engineering
Buffalo, New York 14260

Technical Report NCEER-94-0006

March 14, 1994

REPRODUCED BY:
U.S. Department of Commerce
National Technical Information Service
Springfield, Virginia 22161

This research was conducted at the State University of New York at Buffalo and was partially supported by the Federal Highway Administration under contract number DTFH161-92-C-00106, the National Science Foundation under Grant No. BCS 90-25010 and the New York State Science and Technology Foundation under Grant No. NEC-91029.

NOTICE

This report was prepared by the State University of New York at Buffalo as a result of research sponsored by the National Center for Earthquake Engineering Research (NCEER) through a contract from the Federal Highway Administration and grants from the National Science Foundation, the New York State Science and Technology Foundation, and other sponsors. Neither NCEER, associates of NCEER, its sponsors, the State University of New York at Buffalo, nor any person acting on their behalf:

- a. makes any warranty, express or implied, with respect to the use of any information, apparatus, method, or process disclosed in this report or that such use may not infringe upon privately owned rights; or
- b. assumes any liabilities of whatsoever kind with respect to the use of, or the damage resulting from the use of, any information, apparatus, method or process disclosed in this report.

Any opinions, findings, and conclusions or recommendations expressed in this publication are those of the author(s) and do not necessarily reflect the views of NCEER, the Federal Highway Administration, the National Science Foundation, the New York State Science and Technology Foundation, or other sponsors.



PB94-219185

1. REPORT DOCUMENTATION PAGE		2. REPORT NO. NCEER-94-0006			
4. Title and Subtitle Seismic Energy Based Fatigue Damage Analysis of Bridge Columns: Part I - Evaluation of Seismic Capacity				5. Report Date March 14, 1994	
7. Author(s) G.A. Chang and J.B. Mander				8. Performing Organization Rept. No.	
9. Performing Organization Name and Address State University of New York at Buffalo Department of Civil Engineering Buffalo, New York 14260				10. Project/Task/Work Unit No.	
				11. Contract(s) or Grant(s) No. (a) BCS 90-25010 (b) NEC-91029 (c) DTFH61-92-C-00106	
12. Sponsoring Organization Name and Address National Center for Earthquake Engineering Research State University of New York at Buffalo Red Jacket Quadrangle Buffalo, New York 14261				13. Type of Report & Period Covered Technical report	
				14.	
15. Supplementary Notes This research was conducted at the State University of New York at Buffalo and was partially supported by the Federal Highway Administration under contract #DTFH61-92-C-00106, the National Science Foundation under Grant No. BCS 90-25010 and the New York State Science and Technology Foundation under Grant No. NEC-91029.					
16. Abstract (Limit: 200 words) This study is concerned with the computational modeling of energy absorption (fatigue) capacity of reinforced concrete bridge columns by using a cyclic dynamic Fiber Element computational model. The results may be used with a hysteretic rule to generate seismic energy demand. By comparing the ratio of energy demand to capacity, inferences of column damageability or fatigue resistance can be made. A complete analysis methodology for bridge columns is developed. The hysteretic behavior of ordinary mild steel as well as high threadbar prestressing reinforcement--stability, degradation and consistency of cyclic behavior--is explained. An energy based universally applicable low cycle fatigue model for such reinforcing steels is proposed. A hysteretic model for confined and unconfined concrete subjected to both tension or compression cyclic loading is developed. The model is also capable of simulating gradual crack closure under cyclic loading. A Cyclic Inelastic Strut-Tie (CIST) model is developed, in which the compressive concrete model stress-strain proved to be suitable. A fiber element based column analysis program UB-COLA is also developed, which is capable of accurately predicting the behavior of reinforced concrete columns subjected to inelastic cyclic deformations. The program is useful in predicting the failure model of high axial load columns. For shear critical columns, the cyclic inelastic behavior is accurately simulated through the CIST modeling technique.					
17. Document Analysis a. Descriptors					
b. Identifiers/Open-Ended Terms Reinforced concrete bridge columns. Fatigue capacity. Energy absorption. Hysteresis. Damage analysis. Fiber element models. Mild steel reinforcement. Computer programs. Prestressing reinforcement. Stress strain relationships. Earthquake engineering. UB-COLA. Cyclic Inelastic Strut Tie (CIST) model.					
c. COSATI Field/Group					
18. Availability Statement Release unlimited			19. Security Class (This Report) Unclassified		21. No. of Pages 240
			20. Security Class (This Page) Unclassified		22. Price



**Seismic Energy Based Fatigue Damage Analysis of Bridge Columns:
Part I - Evaluation of Seismic Capacity**

by

G.A. Chang¹ and J.B. Mander²

March 14, 1994

Technical Report NCEER-94-0006

NCEER Task Numbers 91-3412 and 10693-E-5.2

FHWA Contract Number DTFH61-92-C-00106

NSF Master Contract Number BCS 90-25010

and

NYSSTF Grant Number NEC-91029

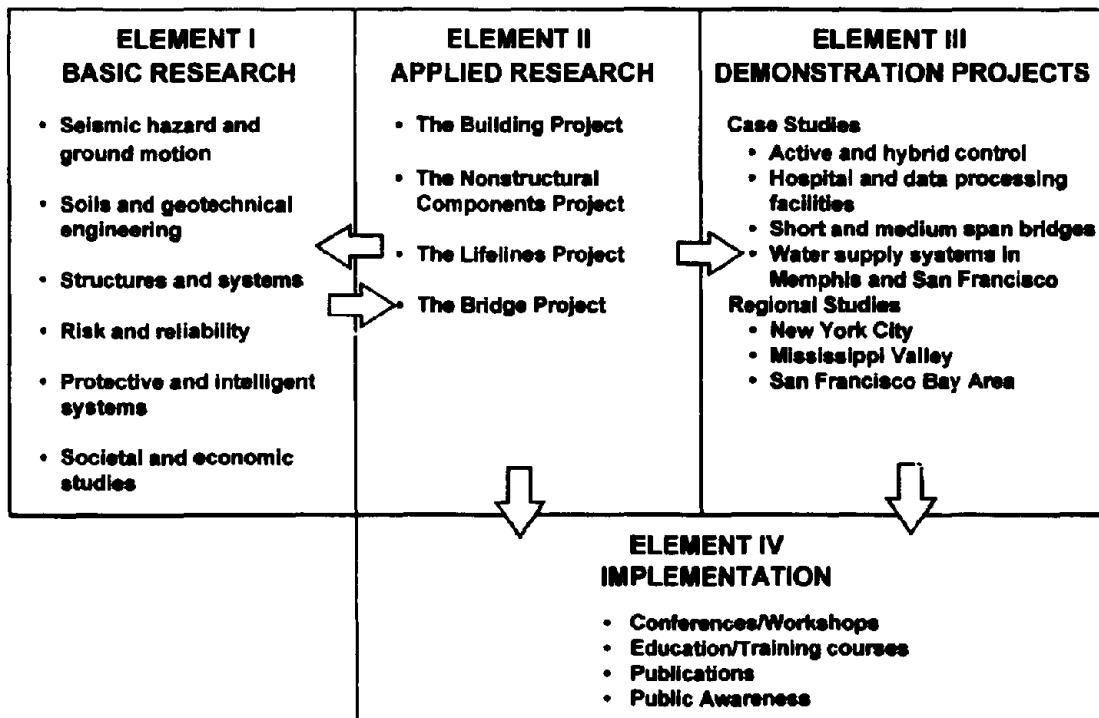
- 1 Teaching Staff Professor, Department of Civil Engineering, Universidad Tecnológica de Panamá. Former Fullbright-LASPAU Scholar, Department of Civil Engineering, State University of New York at Buffalo
- 2 Assistant Professor, Department of Civil Engineering, State University of New York at Buffalo

NATIONAL CENTER FOR EARTHQUAKE ENGINEERING RESEARCH
State University of New York at Buffalo
Red Jacket Quadrangle, Buffalo, NY 14261

PREFACE

The National Center for Earthquake Engineering Research (NCEER) was established to expand and disseminate knowledge about earthquakes, improve earthquake-resistant design, and implement seismic hazard mitigation procedures to minimize loss of lives and property. The emphasis is on structures in the eastern and central United States and lifelines throughout the country that are found in zones of low, moderate, and high seismicity.

NCEER's research and implementation plan in years six through ten (1991-1996) comprises four interlocked elements, as shown in the figure below. Element I, Basic Research, is carried out to support projects in the Applied Research area. Element II, Applied Research, is the major focus of work for years six through ten. Element III, Demonstration Projects, have been planned to support Applied Research projects, and will be either case studies or regional studies. Element IV, Implementation, will result from activity in the four Applied Research projects, and from Demonstration Projects.



Research tasks in the **Bridge Project** expand current work in the retrofit of existing bridges and develop basic seismic design criteria for eastern bridges in low-to-moderate risk zones. This research parallels an extensive multi-year research program on the evaluation of gravity-load design concrete buildings. Specifically, tasks are being performed to:

1. Determine the seismic vulnerability of bridge structures in regions of low-to-medium seismicity, and in particular of those bridges in the eastern and central United States.
2. Develop concepts for retrofitting vulnerable bridge systems, particularly for typical bridges found in the eastern and central United States.
3. Develop improved design and evaluation methodologies for bridges, with particular emphasis on soil-structure mechanics and its influence on bridge response.
4. Review seismic design criteria for new bridges in the eastern and central United States.

The end product of the **Bridge Project** will be a collection of design manuals, pre-standards and design aids which will focus on typical eastern and central United States highway bridges. Work begun in the **Bridge Project** has now been incorporated into the **Highway Project**.

One of the key goals of the Bridge Project is the development of reliable analytical tools so that the response of a wide variety of structures can be predicted. Currently, nonlinear analysis programs rely mostly on macromodels and empirical data for the force-deformation relationships of members. This report summarizes various micromodels and presents important advancements which can be used to predict nonlinear member behavior. The model can predict low-cycle failure of steel, confined or unconfined response of concrete, and steel buckling. It provides a significant tool that will enhance our analytical capabilities related to reinforced and prestressed concrete.

Abstract

This study is concerned with the computational modeling of energy absorption (fatigue) capacity of reinforced concrete bridge columns by using a cyclic dynamic Fiber Element computational model. The results may be used with a hysteretic rule to generate seismic energy demand. By comparing the ratio of energy demand to capacity, inferences of column damageability or fatigue resistance can be made.

The complete analysis methodology for bridge columns is developed starting from basic principles. The hysteretic behavior of ordinary mild steel as well as high threadbar prestressing reinforcement is dealt with in detail: stability, degradation and consistency of cyclic behavior is explained. An energy based universally applicable low cycle fatigue model for such reinforcing steels is proposed.

A hysteretic model for confined and unconfined concrete subjected to both tension or compression cyclic loading is developed. This concrete stress-strain model is a model version of the well-known Mander, Priestley and Park (1984, 1988) model and has been enhanced to predict the behavior of high strength concrete. The model is also capable of simulating gradual crack closure under cyclic loading. A Cyclic Inelastic Strut-Tie (CIST) model is developed, in which the comprehensive concrete model stress-strain proved to be suitable. The CIST model is capable of assessing inelastic shear deformations under cyclic loading with high accuracy.

A fiber element based column analysis program UB-COLA is developed, which is capable of accurately predicting the behavior of reinforced concrete columns subjected to inelastic cyclic deformations. A parabolic fiber element with parabolic stress function element for uniaxial flexure is developed, as well as a rectangular fiber element with a quadratic interpolation function suitable for biaxial flexure. The axial, flexural and shear cyclic behavior are modeled, as well as the low cycle fatigue properties of reinforcing and high strength prestressing steel bars. Fracture of transverse confining steel is modeled through an energy balance theory. The program proved to be useful in predicting the failure mode of either low axial load (low cycle fatigue of longitudinal reinforcement) or high axial load columns (fracture of confining reinforcement and crushing of concrete). For shear critical columns, the cyclic inelastic behavior is accurately simulated through the CIST modeling technique.

Acknowledgments

This research was conducted at the Department of Civil Engineering of the State University of New York at Buffalo.

The authors wish to thank former graduate student F.D. Panthaki and Ph.D. student L.E. Aycardi for providing experimental data.

Special thanks to Professors Andrei M., Reinhorn, Ian G. Buckle and Peter Gergely.

The financial support of the first author from LASPAU and the Universidad Tecnológica de Panamá is deeply appreciated. The second author also wishes to thank the National Center for Earthquake Engineering Research for partial support of this project.

Table of Contents

Title	Page
1. Introduction	
1.1 Background	1-1
1.2 Integration of Previous Research Work	1-2
1.3 Seismic Evaluation Methodologies	1-5
1.4 Scope of Present Investigation	1-5
2. Hysteretic and Damage Modeling of Reinforced Steel Bars	
2.1 Introduction	2-1
2.2 Monotonic Stress-Strain Curve	2-1
2.2.1 The Elastic Branch	2-1
2.2.2 The Yield Plateau	2-2
2.2.3 Strain Hardened Branch	2-2
2.3 The Menegotto-Pinto Equation	2-2
2.3.1 Computation of Parameters Q , f_{ch} and R	2-3
2.3.2 Menegotto-Pinto Equation Limiting Case	2-7
2.4 Cyclic Properties of Reinforcing Steel	2-10
2.4.1 Envelope Branches (Rules 1 and 2)	2-10
2.4.2 Reversal Branches (Rules 3 and 4)	2-12
2.4.3 Returning Branches (Rules 5 and 6)	2-15
2.4.4 First Transition Branches (Rules 7 and 8)	2-23
2.4.5 Second Transition Branches (Rules 9 and 10)	2-24
2.4.6 Strength Degradation	2-26
2.5 Stress-Strain Model Verification	2-26
2.6 Damage Modeling	2-36
2.7 Damage Model Implementation and Verification	2-41
2.8 Strain Rate Effects	2-57
2.9 Conclusions	2-58
3. Modeling Stress-Strain Cyclic Behavior of Concrete	
3.1 Introduction	3-1
3.2 Review of Previous Work in Stress-Strain Relations for Concrete	3-2

Table of Contents (con'd)

Title	Page
3.2.1 Monotonic Compression Stress-Strain Equation	3-2
3.2.2 Initial Modulus of Elasticity	3-12
3.2.3 Strain at Peak Stress for Unconfined Concrete	3-14
3.2.4 Characteristic of the Descending Branch of the Monotonic Stress-Strain Curve for Unconfined Concrete	3-16
3.3 Recommended Complete Stress-Strain Curve for Unconfined Concrete	3-17
3.4 Confinement of Concrete	3-22
3.4.1 Confinement Models	3-23
3.4.2 Confinement Mechanism	3-29
3.4.2.1 Confinement of Circular Sections	3-29
3.4.2.2 Confinement of Rectangular Sections	3-30
3.4.3 Confinement Effect on Strength	3-32
3.4.4 Confinement Effect on Ductility	3-34
3.4.5 Confinement Effect on the Descending Branch	3-35
3.5 Concrete in Tension	3-35
3.6 Compression Softening Effect	3-37
3.7 Dynamic Effects on Concrete Behavior	3-40
3.8 Modeling Hysteretic Behavior	3-42
3.8.1 Basic Components of a Hysteretic Model	3-42
3.8.2 A General Approach to Assessing Degradation Within Partial Looping in a Rule-Based Hysteretic Model	3-43
3.8.2.1 First Partial Reversal	3-44
3.8.2.2 Partial Reloading	3-45
3.8.2.3 Partial Unloading from a Partial Reloading	3-48
3.8.3 A Smooth Transition Curve for Mathematical Modeling	3-49
3.9 Cyclic Properties of Confined and Unconfined Concrete	3-52
3.9.1 Compression Envelope Curve (Rules 1 and 5)	3-52
3.9.2 Tension Envelope Curve (Rules 2 and 6)	3-54
3.9.3 Pre-Cracking Unloading and Reloading Curves	3-55
3.9.4 Post-Cracking Unloading and Reloading Curves	3-61

Table of Contents (con'd)

Title	Page
3.9.5 Pre-Cracking Transition Curves	3-62
3.9.6 Post-Cracking Transition Curve	3-64
3.10 Model Verification	3-67
3.11 Damage Analysis	3-67
3.12 Conclusions	3-69
4. Damage Modeling of Reinforced Concrete Columns using Fiber-Element Analysis	
4.1 Introduction	4-1
4.2 Moment-Curvature Analysis for Uniaxial Bending	4-1
4.3 Moment-Curvature Analysis for Biaxial Bending	4-9
4.4 Force-Displacement Analysis	4-16
4.4.1 Elastic Flexural Deformation	4-16
4.4.2 Plastic Flexural Deformation	4-17
4.4.3 Elastic Shear Deformation	4-18
4.4.4 Inelastic Shear Deformation	4-20
4.4.4.1 Proposed Cyclic Inelastic Strut-Tie (CIST) Model for Shear Deformations	4-21
4.4.4.2 Crack Inclination Angle	4-30
4.5 Validation of Fiber-Element Model	4-32
4.6 Conclusions	4-35
5. Summary, Conclusions and Recommendations	
5.1 Summary	5-1
5.2 Some Specific Conclusions	5-2
5.3 Recommendations for Future Research	5-3
6. References	

List of Figures

	Title	Page
Section 1		
Fig. 1-1	Summary of Research Significance of this Study in the Context of a Seismic Evaluation Methodology	1-4
Section 2		
Fig. 2-1	The Menegotto-Pinto Equation	2-3
Fig. 2-2	Different Curves Having the Same Starting and Ending Properties	2-4
Fig. 2-3	Tension and Compression Envelope Curves	2-11
Fig. 2-4	Effect of the Strain Amplitude of the Reversal on the Equation Parameters	2-15
Fig. 2-5	Reversal From Yield Plateau	2-16
Fig. 2-6	Definition of the Reversal Unloading Branch	2-16
Fig. 2-7	Effect of the Strain Amplitude of Loop on the Initial Modulus and R parameter for Reinforcing Bars ($f_y = 53$ ksi) (Loading)	2-17
Fig. 2-8	Effect of the Strain Amplitude of Loop on the Initial Modulus and R parameter for Reinforcing Bars ($f_y = 53$ ksi) (Unloading)	2-18
Fig. 2-9	Effect of the Strain Amplitude of Loop on the Initial Modulus and R parameter for High Strength Bars ($f_y = 123$ ksi) (Loading)	2-19
Fig. 2-10	Effect of the Strain Amplitude of Loop on the Initial Modulus and R parameter for High Strength Bars ($f_y = 123$ ksi) (Unloading)	2-20
Fig. 2-11	Fitting of M-P Equation to a Loading Loop of Reinforcing Steel Bars ($f_y = 53$ ksi)	2-21
Fig. 2-12	Fitting of M-P Equation to an Unloading Loop of Reinforcing Steel Bars ($f_y = 53$ ksi)	2-21
Fig. 2-13	Fitting of M-P Equation to a Loading Loop of High Strength Steel Bars ($f_y = 123$ ksi)	2-22
Fig. 2-14	Fitting of M-P Equation to an Unloading Loop of High Strength Steel Bars ($f_y = 123$ ksi)	2-22
Fig. 2-15	Sequence of Partial Reversals	2-23
Fig. 2-16	Flow of Rules at Every Reversal and Target Strain	2-25
Fig. 2-17	Degradation of Reinforcing and High Strength Steel Bars	2-27
Fig. 2-18	Comparison of Degrading Model with Experimental Results	2-27
Fig. 2-19	Stress Degradation Simulation and Fracture Prediction on Steel Bars	2-28
Fig. 2-20	Stress-Strain Experiment by Kent and Park (1973), Specimen 6	2-29
Fig. 2-21	Stress-Strain Experiment by Kent and Park (1973), Specimen 8	2-29
Fig. 2-22	Stress-Strain Experiment by Kent and Park (1973), Specimen 9	2-30
Fig. 2-23	Stress-Strain Experiment by Kent and Park (1973), Specimen 15	2-30
Fig. 2-24	Stress-Strain Experiment by Kent and Park (1973), Specimen 11	2-31
Fig. 2-25	Stress-Strain Experiment by Kent and Park (1973), Specimen 17	2-31

List of Figures (cont'd)

Title	Page
Fig. 2-26 Stress-Strain Experiment by Ma, Bertero and Popov (1976), Specimen 1	2-32
Fig. 2-27 Stress-Strain Experiment by Ma, Bertero and Popov (1976), Specimen 4	2-32
Fig. 2-28 Stress-Strain Experiment by Panthaki (1991), Specimen P2	2-33
Fig. 2-29 Stress-Strain Experiment by Panthaki (1991), Specimen P3	2-33
Fig. 2-30 Stress-Strain Experiment by Panthaki (1991), Specimen P16	2-34
Fig. 2-31 Stress-Strain Experiment by Panthaki (1991), Specimen P19	2-34
Fig. 2-32 Stress-Strain Experiment by Panthaki (1991), Specimen R1	2-35
Fig. 2-33 Stress-Strain Experiment by Panthaki (1991), Specimen R4	2-35
Fig. 2-34 Stress-Strain Experiment by Panthaki (1991), Specimen R5	2-36
Fig. 2-35 Determination of Equivalent Strain Amplitude	2-40
Fig. 2-36 High Strength Bar, Specimen P18 (Panthaki, 1991)	2-42
Fig. 2-37 High Strength Bar, Specimen P10	2-43
Fig. 2-38 High Strength Bar, Specimen P13	2-44
Fig. 2-39 High Strength Bar, Specimen P12	2-45
Fig. 2-40 High Strength Bar, Specimen P4	2-46
Fig. 2-41 High Strength Bar, Specimen P7	2-47
Fig. 2-42 High Strength Bar, Specimen P14	2-48
Fig. 2-43 High Strength Bar, Specimen P9	2-49
Fig. 2-44 High Strength Bar, Specimens P11, P2 and P3	2-50
Fig. 2-45 Reinforcing Bar, Specimen R1	2-51
Fig. 2-46 Reinforcing Bar, Specimen R9	2-52
Fig. 2-47 Reinforcing Bar, Specimen R5	2-53
Fig. 2-48 Reinforcing Bar, Specimens R11, R7 and R10	2-54
Fig. 2-49 High Strength Bar, Specimen P20, Low-High Step Test	2-55
Fig. 2-50 High Strength Bar, Specimen P21, High-Low Step Test	2-56
Fig. 2-51 Incipient Failure Prediction	2-57
 Section 3	
Fig. 3-1 Characteristics of the Stress-Strain Relation for Concrete	3-2
Fig. 3-2 Comparison of Different Stress-Strain Equations for Concrete	3-6
Fig. 3-3 Equation Suggested by Young (1960)	3-6
Fig. 3-4 Equation Suggested by Saenz (1964)	3-7
Fig. 3-5 Equation Proposed by Popovics (1973)	3-7
Fig. 3-6 Equation Suggested by Saenz (1964)	3-10
Fig. 3-7 Equation Suggested by Sargin (1968)	3-10

List of Figures (cont'd)

Title	Page
Fig. 3-8 Equation Proposed by Tsai (1988)	3-11
Fig. 3-9 Comparison of Different Equations for the Secant Modulus of Concrete	3-20
Fig. 3-10 Comparison of Different Equations for the Strain at Peak Stress	3-20
Fig. 3-11 Proposed Theoretical Stress-Strain Curves for Unconfined Concrete	3-21
Fig. 3-12 Theoretical Stress-Strain Curves Suggested by Collins and Mitchell	3-21
Fig. 3-13 Tsai's Equation Parameters for Unconfined Concrete	3-22
Fig. 3-14 Some Proposed Stress-Strain Curves for Confined Concrete	3-28
Fig. 3-15 Confinement Mechanism for Circular and Rectangular Cross Sections	3-31
Fig. 3-16 Confined Concrete Strength Ratio	3-33
Fig. 3-17 Comparison of Different Models for Triaxial Confinement	3-33
Fig. 3-18 Characteristic of the Falling Branch for Confined Concrete	3-39
Fig. 3-19 Definition of Falling Branch for Confined Concrete	3-41
Fig. 3-20 Relationship Between Curves in a Rule-Based Model	3-43
Fig. 3-21 Target Point and Reloading Point in a Complete Reversal	3-46
Fig. 3-22 Reloading from a Partial Unloading	3-46
Fig. 3-23 Unloading from a Partial Reloading	3-47
Fig. 3-24 A Smooth Transition Curve	3-51
Fig. 3-25 Tension and Compression Envelope Curves	3-53
Fig. 3-26 Cyclic Compression Characteristics of Concrete	3-57
Fig. 3-27 Complete Unloading Branch	3-58
Fig. 3-28 Complete Loading Branch	3-59
Fig. 3-29 Loading and Unloading Curves after Cracking	3-61
Fig. 3-30 Partial Unloading Curves for Tension and Compression	3-63
Fig. 3-31 Transition Curves (Before Cracking)	3-65
Fig. 3-32 Transition Curves (After Cracking)	3-65
Fig. 3-33 Relationship Among the Model Rules	3-66
Fig. 3-34 Unconfined Cyclic Compression Test by Sinha, Gerstle and Tullin (1964)	3-71
Fig. 3-35 Unconfined Cyclic Compression Test by Karsan and Jirsa (1969)	3-71
Fig. 3-36 Unconfined Cyclic Compression Test by Okamoto (1976)	3-72
Fig. 3-37 Unconfined Cyclic Compression Test by Okamoto (1976)	3-72
Fig. 3-38 Unconfined Cyclic Compression Test by Tanigawa (1979)	3-73
Fig. 3-39 Cyclic Tension Test by Yankelovsky and Reinhardt (1987)	3-73
Fig. 3-40 Confined Concrete Cyclic Test by Mander et al. (1984)	3-74

List of Figures (cont'd)

	Title	Page
	Fig. 3-41 Confined Concrete Cyclic Test by Mander et al. (1984)	3-74
	Fig. 3-42 Comparison of the Proposed Tension Branch Equation with other Analytical Equations	3-75
Section 4		
	Fig. 4-1 Definition of Global and Local Coordinates	4-5
	Fig. 4-2 Definition of Variables on a Fiber Element	4-7
	Fig. 4-3 Definition of Variables for Biaxial Bending	4-10
	Fig. 4-4 Element Node Numbering	4-13
	Fig. 4-5 Flexural Deformation on a Column	4-16
	Fig. 4-6 Shear Deformation on a Column	4-22
	Fig. 4-7 Equivalent Strut-Tie Model for Shear Deformations	4-22
	Fig. 4-8 Equilibrium and Strain Deformation in the Cyclic Inelastic Strut-Tie Shear Model	4-23
	Fig. 4-9 Definition of Average Longitudinal Strain on Shear Concrete Strut	4-24
	Fig. 4-10 Comparison of the Analytical Stress-Strain Relationship with the Experimental Behavior of Plain Concrete from Aycardi et al. (1992) for Specimens 2 and 4	4-33
	Fig. 4-11 Comparison of Proposed Fiber Element Model with Experimental Results from Aycardi et al. (1992) Specimen 4, $P = 0.10 f_c A_g$	4-37
	Fig. 4-12 Comparison of Proposed Fiber Element Model with Experimental Results from Aycardi et al. (1992) Specimen 2, $P = 0.30 f_c A_g$	4-38
	Fig. 4-13 Comparison of Proposed Fiber Element Analysis with Experimental and Analytical Results from Mander et al. (1984) Column A	4-39
	Fig. 4-14 Prediction of Low Cycle Fatigue Fracture of Longitudinal Bars for Column A	4-40
	Fig. 4-15 Comparison of Proposed Fiber Element Analysis with Experimental and Analytical Results from Mander et al. (1984) Column C	4-41
	Fig. 4-16 Comparison of Proposed Fiber Element Analysis with Experimental and Analytical Results from Mander et al. (1984) Column D	4-42
	Fig. 4-17 Analytical Simulation of a Full Size Shear Critical Bridge Pier Tested by Mander et al. (1993)	4-43

Section 1

Introduction

1.1 Background

In order to design or analyze the behavior of bridge substructures (piles and columns of piers) that may be either reinforced, or fully or partially prestressed concrete, it is essential that analytical models be developed that accurately reflect the true non-linear dynamic cyclic loading behavior of those members. Current analytical modeling techniques of structural elements use either a macro modeling approach (e.g. DRAIN, Kanaan and Powell, 1973; Allahabadi and Powell, 1988) or micro finite element approach (e.g. ANSYS, Kohnke, 1983). It is considered that a coarse macro approach in which lumped plasticity within elements is used to predict response behavior, in many instances, is too crude when looking at detailed behavior of joints and plastic hinges. On the other hand, sophisticated finite element models may require a mesh representation that is too fine, thus prohibiting the analysis of large or even moderate size bridges. It is considered that the most appropriate compromise is to use a combination of the two. Fiber elements can be used for this purpose. Fiber elements can be incorporated into a non-linear time-history structural analysis computer program using two different approaches: direct fiber modeling, or indirect fiber modeling. The first has recently been incorporated into the latest version of DRAIN-2DX, but is in a relatively crude form and still may require some further refinement, but the approach shows great promise. The second approach is the subject of this study for the purpose of use with programs such as IDARC (Park et al., 1987) (or DRAIN-2DX). A fiber model representation can capture details of features such as the critical concrete and steel strains as part of the analysis process through the direct integration of stress-strain response. Most existing time-history computer programs focus on determining the *inelastic demands* caused by a given seismic excitation. As part of a fiber element analysis of components the *inelastic capacity* of members can also be determined as part of a preprocessing / post-processing analysis. Further, as part of a post-processing analysis, the damage sustained

by components and subassemblages can be determined as the ratio of demand versus capacity. This investigation focuses on this damageability concept as part of the modeling for bridge substructures.

1.2 Integration of Previous Research Work

Considerable work has been undertaken by Mander, Priestley and Park (1984) in developing moment-curvature and force-deformation models based on a fiber approach, directly integrating stress-strain relations for reinforced concrete members (Mander et al., 1988a, 1988b). Dynamic reversed cyclic loading of members is accounted for and inelastic buckling of longitudinal reinforcement, transverse hoop fracture, and concrete crushing modes of failure are determined from energy considerations. Good agreement has been demonstrated when tested against a variety of physical model experimental results. This fundamental work was followed by Zahn et al. (1990) who developed energy-based design charts for bridge piers with ductile detailing.

The need for sophisticated tools to analyze structures subjected to earthquake loadings has produced a great deal of research. Much of this research is the coordinated effort of many researchers that share a common purpose, to gain insight into this very complex problem. The complexity of the problem underlies in both the randomness of earthquake motions and the nonlinear hysteretic behavior of structural components. The end goal is to develop rational methods of design, that will consider both the *demand* that the ground motion will impose on the structure and the *capacity* of the structure to meet those requirements.

The *demand* on a structure can be of two types: displacement ductility demand and energy demand. The former dictates bearing seat width requirements and secondary P- Δ load effects, while the latter leads to failure of the constituent materials, steel and concrete, through low cycle fatigue. It will subsequently be shown that the two are also interrelated. Much of the research effort had been concentrated on the ductility demand, although energy demand research is gaining popularity among researchers. The *capacity* of structural elements is, of course, a fundamental problem.

This first report of a two-part series is concerned with the evaluation of seismic capacity of bridge columns. The purpose is to build on past work and specifically address issues that were avoided previously, namely:

i) Investigate the behavior and develop appropriate stress-strain models for high performance reinforcing steels. This study focuses on high strength, high alloy threadbars with ultimate tensile strengths of 160 ksi (1100 MPa).

ii) To model the low cycle fatigue behavior of reinforcing steels (of both mild steel and high strength grades) and use such models in predicting the failure modes/life of structural concrete bridge columns.

iii) To investigate the behavior and develop appropriate stress-strain models for high performance/high strength concrete.

iv) To model the effect of the gradual crack closure of concrete to enable a more reliable prediction of the moment curvature behavior of bridge columns particularly with low levels of axial load. This requires a better understanding of the tensile/crack opening/closing behavior at the constitutive level.

v) To incorporate the above features into a computationally efficient moment-curvature and force-flexural deformation model for bridge columns.

vi) To provide a better understanding and modeling of the nonlinear shear force-shear displacement behavior of reinforced concrete columns, particularly in the nonlinear cyclic loading regime.

A computer program to simulate the cyclic behavior of reinforced concrete is presented in this study. Every major aspect of its development is presented. Advanced models for concrete and steel are proposed, with improvements over previous models. Mathematical models for the description of damage in steel elements are incorporated. A uniaxial moment-curvature and force-deformation micro model is presented as well as a biaxial moment-curvature fiber element model. A general purpose macro model with system identification for uniaxial moment-curvature or force deformation was implemented.

These programs can be integrated as part of an analysis methodology outlined in Fig. 1-1.

SEISMIC EVALUATION METHODOLOGY

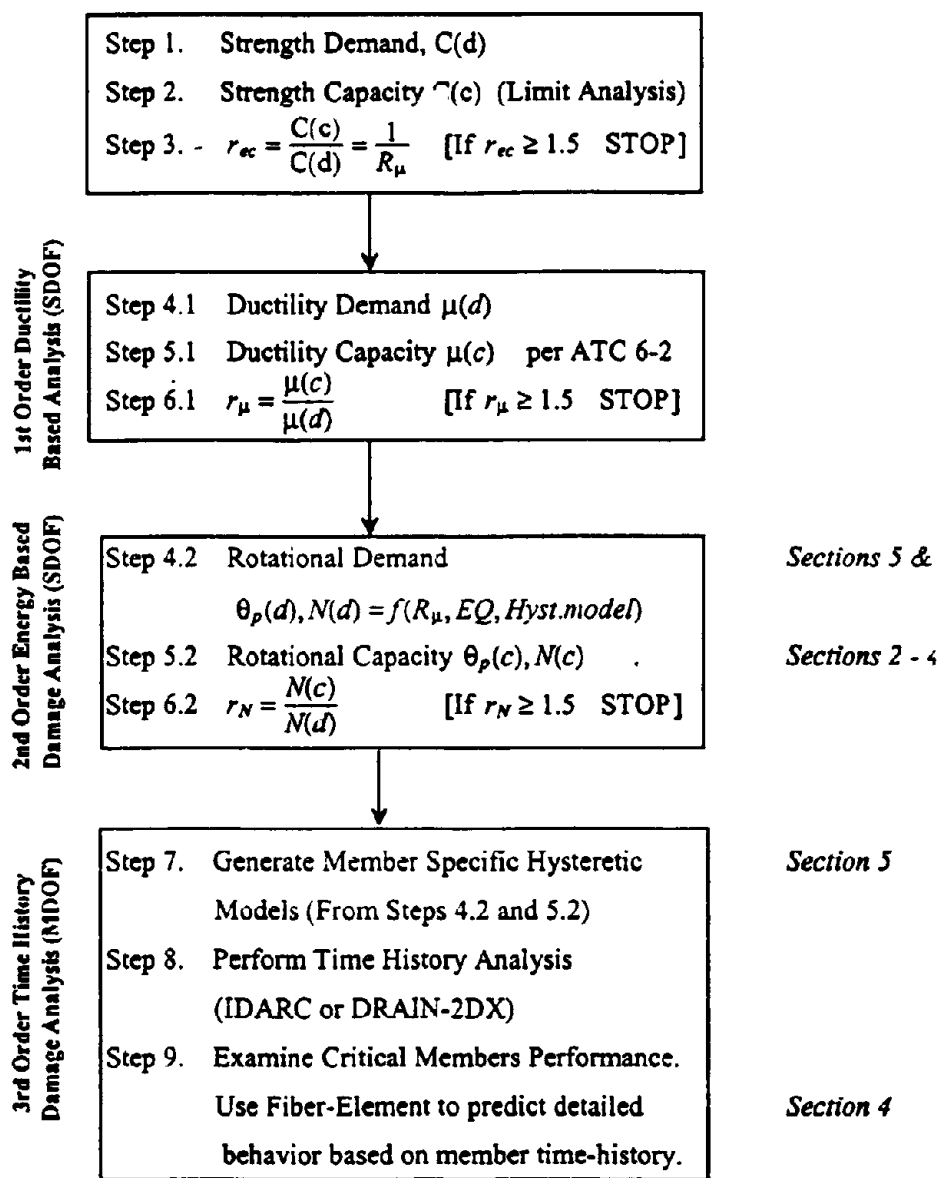


Fig. 1-1 Summary of Research Significance of this Study in the Context of a Seismic Evaluation Methodology.

1.3 Seismic Evaluation Methodologies

Herein a three level seismic evaluation methodology is proposed. The first is based on well-known concepts of ductility and uses limit analysis techniques from which *capacity/demand (C/D)* ratios are calculated for structural strength and ductility. This is called first-order approach as it does not concern itself with cyclic loading effects and is similar to the procedures given in ATC 6-2. The second is a new approach advanced herein, which is based on fatigue or damage concepts and is concerned with comparing energy absorption capacities with seismic energy demands. This is called a second-order approach, as it takes into account the earthquake duration and would be used when the results from a first-order analysis are in doubt. A third and more refined analysis level concerns a multi-degree of freedom system analysis, in which rational hysteretic models are implemented to determine non-linear structural/fatigue performance.

1.4 Scope of Present Investigation

Firstly, this investigation deals with the modeling of the hysteretic and fracture characteristics of reinforcing steel. The low cycle fatigue behavior of steel is modeled based on experimental data. The importance of this modeling is that it allows the prediction of the fatigue life of longitudinal bars in the context of a reinforced concrete member subjected to cyclic loading. Thus, this modeling allows the failure of a member due to low cycle fatigue to be predicted, which is predominant on well detailed beams and columns with low levels of axial load. Numerous examples are presented to show the capacity of the model to simulate both the stress-strain cyclic behavior and the fatigue fracture.

Secondly, this investigation deals with the modeling of the behavior of both confined and unconfined concrete subjected to cyclic compression and tension (Section 2). This is the first time any model has attempted to model cyclic behavior of concrete in both tension and compression. The need for such a model is more obvious when considering shear deformations where the tension capacity of reinforced steel plays an important role, as in the Modified Compression Field Theory (Collins and Mitchell, 1992), and the Softened Truss Model (Hsu, 1993).

Section 4 deals with the Fiber Elements modeling of the moment-curvature behavior of a concrete section and with the assessment of deformations. A cyclic strut-tie model is developed to assess shear deformations. This cyclic strut-tie model for shear deformation, which makes good use of the comprehensive constitutive models developed in sections 2 and 3, allows the behavior of shear dominated members to be simulated.

Finally, some conclusions and recommendations for further research are presented in the last section. This investigation has shed some light into the need for some well designed experiments to look into the behavior of some specific variables.

Section 2

Hysteretic and Damage Modeling of Steel Reinforcing Bars

2.1 Introduction

The hysteretic behavior of the reinforcing and prestressing steel bars influences the hysteretic behavior of a structural concrete member. Fracture of a reinforcing bar may also be defined as failure of the member itself. It is very important to thus model both the hysteretic and the fatigue properties of the reinforcing bars accurately. Tests performed by Kent and Park (1973), Ma et al. (1976) and Panthaki (1991) were used to calibrate the stress-strain model advanced herein. The degrading characteristic of steels with yield stresses ranging from 50 ksi to 120 ksi were studied, and damage relationships were incorporated into the model. The Menegotto-Pinto equation (1973) used by Mander et al. (1984) is used herein to represent the loading and unloading stress-strain relations.

2.2 Monotonic Stress-Strain Curve

Numerous tests have shown that the monotonic stress-strain curve for reinforcing steel can be described by three well defined branches. The corresponding relations for stress (f_s) and tangent modulus (E_t) after Mander et. al. (1984) are given as follows:

2.2.1 The Elastic Branch $0 \leq \epsilon_s \leq \epsilon_y$

$$f_s = E_s \epsilon_s \quad (2-1)$$

$$E_t = E_s \quad (2-2)$$

$$\text{where: } \epsilon_y = \frac{f_y}{E_s}$$

in which, ϵ_y = yield strain, f_y = yield stress, E_s = Elastic Modulus of Elasticity.

2.2.2 The Yield Plateau $\epsilon_y < \epsilon_s < \epsilon_{sh}$

$$f_s = f_y \quad (2-3)$$

$$E_t = 0 \quad (2-4)$$

in which, ϵ_{sh} = strain hardening strain.

2.2.3 Strain Hardened Branch $\epsilon_s \geq \epsilon_{sh}$

$$f_s = f_{su} + (f_y - f_{su}) \left| \frac{\epsilon_{su} - \epsilon_s}{\epsilon_{su} - \epsilon_{sh}} \right|^p \quad (2-5)$$

$$E_t = E_{sh} \text{sign} \left(\frac{\epsilon_{su} - \epsilon_s}{\epsilon_{su} - \epsilon_{sh}} \right) \left| \frac{f_{su} - f_s}{f_{su} - f_y} \right|^{(1-\frac{1}{p})} \quad (2-6)$$

where: $p = E_{sh} \frac{\epsilon_{su} - \epsilon_{sh}}{f_{su} - f_y}$

in which, ϵ_{su} is the strain at ultimate stress and f_{su} = ultimate (maximum) stress. These relations can be represented by a single equation as given in Eq. (2-45)

2.3 The Menegotto-Pinto Equation

The Menegotto-Pinto (1973) (M-P hereafter) is useful for describing a curve connecting two tangents with a variable radius of curvature at the intersection point of those two tangents, as shown in Fig. 2-1. The M-P equation is expressed as:

$$f_s = f_o + E_o(\epsilon_s - \epsilon_o) \left\{ Q + \frac{1-Q}{\left[1 + \left| E_o \frac{\epsilon_s - \epsilon_o}{f_{ch} - f_o} \right|^R \right]^{\frac{1}{R}}} \right\} \quad (2-7)$$

The tangent modulus at any point is given by:

$$E_t = \frac{\partial f_s}{\partial \epsilon_s} = E_{sec} - \frac{E_{sec} - QE_o}{1 + \left| E_o \frac{\epsilon_s - \epsilon_o}{f_{ch} - f_o} \right|^{-R}} \quad (2-8)$$

with a secant modulus connecting the origin coordinates (ϵ_o, f_o) and the coordinates of the point under consideration (ϵ_s, f_s) defined as:

$$E_{sec} = \frac{f_s - f_o}{\epsilon_s - \epsilon_o} \quad (2-9)$$

in which ϵ_s = steel strain, f_s = steel stress, ϵ_o = strain at initial point, f_o = stress at initial point, E_o = tangent modulus of elasticity at initial point, Q , R and f_{ch} are equation parameters to control the shape of the curve.

It should be noted that as it is presented, Eq. (2-7) has the following properties:

(1) a slope E_o at the starting coordinate (ϵ_o, f_o) , (2) it approaches the slope QE_o as $\epsilon_s \rightarrow \infty$. For computational tractability R needs to be limited to about 25. This essentially represents a bilinear curve given by a single equation.

To use this equation it is necessary to develop an algorithm to compute the parameters Q , f_{ch} and R . A procedure to compute these parameters is presented in the next section.

2.3.1 Computation of Parameters Q , f_{ch} and R

Let the denominator in the M-P equation be A such that,

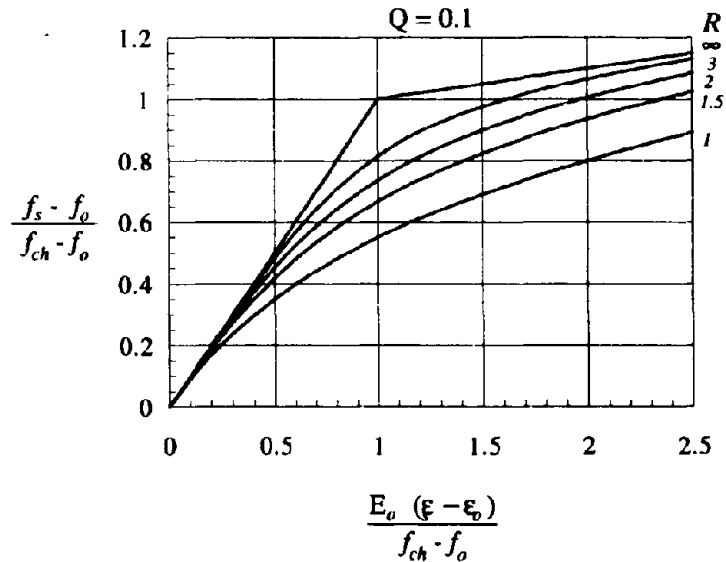


Fig. 2-1 The Menegotto-Pinto Equation

$$A = \left[1 + \left| E_o \frac{\epsilon_s - \epsilon_o}{f_{ch} - f_o} \right|^R \right]^{\frac{1}{R}} \quad (2-10)$$

The derivative of A is therefore:

$$\frac{dA}{d\epsilon_s} = \frac{A(1-A^{-R})}{\epsilon_s - \epsilon_o} \quad (2-11)$$

Eq. (2-7) can be expressed in terms of A as:

$$f_s = f_o + E_o(\epsilon_s - \epsilon_o) \left(Q + \frac{1-Q}{A} \right) \quad (2-12)$$

and then the derivative of f_s respect to ϵ_s gives a tangent modulus which is:

$$E_t = \frac{df_s}{d\epsilon_s} = E_o \left(Q + \frac{1-Q}{A} \right) - E_o \frac{1-Q}{A} \left(\frac{\epsilon_s - \epsilon_o}{A} \frac{dA}{d\epsilon_s} \right) \quad (2-13)$$

By substituting Eq. (2-11) into (2-13) and rearranging:

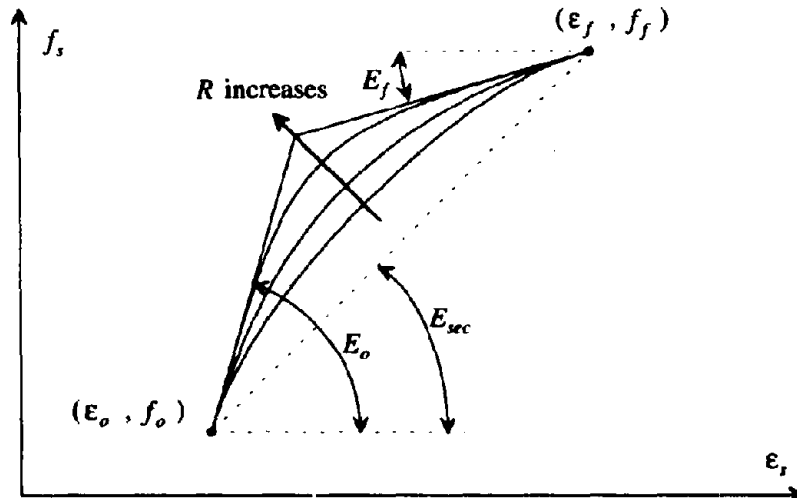


Fig. 2-2 Different Curves Having the Same Starting and Ending Properties

$$\frac{E_t}{E_o} = Q + \frac{1-Q}{A^{R+1}} \quad (2-14)$$

By evaluating this equation at $\epsilon_s = \epsilon_f$, and solving for Q ,

$$Q = \frac{\frac{E_f}{E_o} - A^{-(R+1)}}{1 - A^{-(R+1)}} \quad (2-15)$$

Solving for Q in Eq. (2-12),

$$Q = \frac{\frac{E_{sec}}{E_o} - A^{-1}}{1 - A^{-1}} \quad (2-16)$$

Eq. (2-15) was obtained from an equation related to the final slope (E_f), thus this equation guarantees that at the target point the slope condition is met $E_t(\epsilon_f) = E_f$. Eq. (2-16) was derived from the ordinate equation so, by satisfying this equation, the ordinate condition is met $f_s(\epsilon_f) = f_f$. To satisfy both conditions, it is necessary to equate both Eqs. (2-15) and (2-16).

$$E_f - E_{sec} \frac{1 - a^{R+1}}{1 - a} + E_o \frac{a(1 - a^R)}{1 - a} = 0 \quad (2-17)$$

where $a = A^{-1}$.

The solution procedure is as follows:

$$(1) E_{sec} = \frac{f_f - f_o}{\epsilon_f - \epsilon_o}$$

$$(2) R_{min} = \frac{E_f - E_{sec}}{E_{sec} - E_o}, \text{ the derivation of this expression is given in the next subsection}$$

2.3.2. It is not possible to reach the point (ϵ_f, f_f) with the slope E_f with a value of $R < R_{min}$. Evaluation of the M-P equation for the case of $R = R_{min}$ is only possible by taking the limit of the expression, so a value of R slightly greater than R_{min} has to be used, in order to apply the expression as it is shown in Eq. (2-7).

(3) If $R_{min} = 0$, it means that the three points are aligned, thus take $Q = 1$ and $f_{ch} = f_f$. The value of R need not to be modified.

$$(4) \text{ If } R \leq R_{min} \text{ then take } R = R_{min} + 0.01$$

(5) Solve for the value of a in the following expression:

$$E_f - E_{sec} \frac{1 - a^{R+1}}{1 - a} + E_o \frac{a(1 - a^R)}{1 - a} = 0 \quad (2-18)$$

To find the value of a the following procedure is used:

(a) Define a function $f(a)$ as:

$$f(a) = E_f - E_{sec} \frac{1 - a^{R+1}}{1 - a} + E_o \frac{a(1 - a^R)}{1 - a} \quad (2-19)$$

(b) Evaluate $f(1-\epsilon)$ and $f(\epsilon)$, where ϵ is a small value (≈ 0.01).

(c) If $f(1-\epsilon) * f(\epsilon) > 0$, no solution is found, so decrease the value of ϵ and repeat step (b).

(d) If $f(1-\epsilon) * f(\epsilon) \leq 0$ then a solution is found in this interval. The quadratically converging Newton-Raphson procedure can then be used to find the solution.

(e) Take as an initial estimate:

$$a_o = \frac{R_{min}}{R} \quad (2-20)$$

(f) If $f(a_o) * f(1-\epsilon) < 0$ then replace a_o by $\sqrt{a_o}$ until the inequality is false to ensure proper convergence. If this condition is not met the algorithm will find a solution outside the meaningful range.

(g) With a_o as an initial estimate the following recursive expression should be applied until convergence is met. It is important to note that the function $f(a)$ has a singularity at $a = 1$, so the value of Δa should be the smaller of $0.5(1 - a_o)$ and 0.001 .

$$a_{i+1} = a_i - \frac{2f(a_i) \Delta a}{f(a_i + \Delta a) - f(a_i - \Delta a)} \quad (2-21)$$

(8) After the value of a has been defined then,

$$b = \frac{(1 - a^R)^{\frac{1}{R}}}{a} \quad (2-22)$$

(9) The values of f_{ch} and Q are then calculated as:

$$f_{ch} = f_o + \frac{E_o}{b} (\epsilon_f - \epsilon_o) \quad (2-23)$$

$$Q = \frac{\frac{E_{sec}}{E_o} - a}{1 - a} \quad (2-24)$$

2.3.2 Menegotto-Pinto Equation Limiting Case

In step 2 of the procedure outlined above, a factor R_{min} was introduced. The derivation of that factor and the relation of the Menegotto-Pinto equation to a power equation is the subject of this subsection.

The Menegotto-Pinto equation can be expressed by:

$$y = y_o + E_o(x - x_o) \left[Q - \frac{1 - Q}{\left(1 + \left|E_o \frac{x - x_o}{y_{ch} - y_o}\right|^R\right)^{\frac{1}{R}}} \right] \quad (2-25)$$

If the curve is to pass through (x_f, y_f) , it can be rewritten as:

$$\frac{1}{E_o} \frac{y_f - y_o}{x_f - x_o} = \frac{E_{sec}}{E_o} = Q + \frac{1 - Q}{A} \quad (2-26)$$

and its derivative as:

$$\frac{E_f}{E_o} = Q + \frac{(1 - Q)}{A^{R+1}} \quad (2-27)$$

where:

$$A = \left(1 + \left|E_o \frac{x - x_o}{y_{ch} - y_o}\right|^R\right)^{\frac{1}{R}} \quad (2-28)$$

If,

$$a = A^{-1} \quad (2-29)$$

then by solving for Q in Eqs. (2-26) and 2-27), the following expression is obtained:

$$E_f - E_{sec} \frac{1 - a^{R+1}}{1 - a} + E_o \frac{a(1 - a^R)}{1 - a} = 0 \quad (2-30)$$

By solving for a in this equation, the parameters y_{ch} and Q are given by:

$$y_{ch} = y_o + E_o(x_f - x_o) \left(\frac{a}{(1 - a^R)^{\frac{1}{R}}} \right) \quad (2-31)$$

and,

$$Q = \frac{\frac{E_f}{E_o} - a^{R+1}}{1 - a^{R+1}} \quad (2-32)$$

Eq. (2-30) cannot be evaluated as it is written for $a = 1$, but it presents a limit. The limit value of the fraction in the second term is:

$$\lim_{a \rightarrow 1^-} \frac{1 - a^{R+1}}{1 - a} = R + 1 \quad (2-33)$$

while the other limit is:

$$\lim_{a \rightarrow 1^-} \frac{a(1 - a^R)}{1 - a} = R \quad (2-34)$$

So the limit for the equation when $a \rightarrow 1$ is:

$$E_f - E_{sec}(R + 1) + E_o R = 0 \quad (2-35)$$

Solving for R , the following equation for the critical value of R can be derived:

$$R_{cr} = \frac{E_f - E_{sec}}{E_{sec} - E_o} \quad (2-36)$$

This value, as can be shown numerically, represents the minimum value that R is to have, so that a solution to meet the conditions of both slope and ordinate value at the ending point. What is of interest now, is to know what the limit for the original equation would be. Both y_{ch} and Q tend to infinity as a tends to one. Eq. (2-25) can be expressed in terms of a as:

$$y = y_o + E_o(x - x_o)[m + Q(1 - m)] \quad (2-37)$$

where,

$$m = \frac{1}{\left[1 + \left| \frac{x-x_o}{x_f-x_o} \right|^R \frac{1-a^R}{a^R} \right]^{\frac{1}{R}}} \quad (2-38)$$

When $a \rightarrow 1$,

$$\lim_{a \rightarrow 1^-} m = 1 \quad (2-39)$$

The limit of $Q(1-m)$, is a complicated expression:

$$\lim_{a \rightarrow 1^-} Q(1-m) = \lim_{a \rightarrow 1^-} \frac{\frac{E_f}{E_o} - a^{R+1}}{1 - a^{R+1}} \left\{ 1 - \frac{1}{\left[1 + \left| \frac{x-x_o}{x_f-x_o} \right|^R \frac{1-a^R}{a^R} \right]^{\frac{1}{R}}} \right\} = \frac{\frac{E_f}{E_o} - 1}{R+1} \left| \frac{x-x_o}{x_f-x_o} \right|^R \quad (2-40)$$

So, Eq. (2-37) can be expressed as:

$$y = y_o + E_o(x-x_o) \left[1 + \frac{\frac{E_f}{E_o} - 1}{R+1} \left| \frac{x-x_o}{x_f-x_o} \right|^R \right] \quad (2-41)$$

The final form of the limiting case of the Menegotto-Pinto equation as:

$$y = y_o + E_o(x-x_o) + A(x-x_o)|x-x_o|^R \quad (2-42)$$

with,

$$R = \frac{E_f - E_{sec}}{E_{sec} - E_o} \quad (2-43)$$

and,

$$A = \frac{E_{sec} - E_o}{|x_f - x_o|^R} \quad (2-44)$$

Eq. (2-42) is dealt with in more detail in section 3.6.3. It is worth noting here that this equation represents the most "relaxed" of all the curves given by the M-P equation, but at the same time, the M-P equation cannot be evaluated for this case, as it is a limit expression.

2.4 Cyclic Properties of Reinforcing Steel

In this section a universally applicable cyclic stress-strain model is advanced for ordinary reinforcing and high strength prestressing bars. The model is composed of ten different rules, five for the tension side and five for the compression side. Each of the rules is described separately in the following sections.

2.4.1 Envelope Branches (Rules 1 and 2)

The envelope branches are defined by the monotonic stress-strain relation which is relocated and scaled to simulate strength degradation. The shape of the monotonic branch is kept intact, except that at the points of reversal a scale factor is calculated. This combined model ensures degradation within local cyclic, a phenomenon which has not been modeled before. The model was calibrated using experimental results given by Panthaki (1991). The stress-strain relation for the tension envelope curve can be expressed as a single expression by:

Rule 1 (Tension Envelope Branch)

$$f_s = \frac{E_s \epsilon_{ss}}{\left[1 + \left(\frac{E_s \epsilon_{ss}}{f_y^+}\right)^{10}\right]^{0.1}} + \frac{\text{sign}(\epsilon_{ss} - \epsilon_{sh}^+) + 1}{2} (f_{su}^+ - f_y^+) \left[1 - \left|\frac{\epsilon_{su}^+ - \epsilon_{ss}}{\epsilon_{su}^+ - \epsilon_{sh}^+}\right|^{p^+}\right] \quad (2-45a)$$

$$E_t = \frac{E_s}{\left[1 + \left(\frac{E_s \epsilon_{ss}}{f_y^+}\right)^{10}\right]^{1.1}} + \frac{\text{sign}(\epsilon_{ss} - \epsilon_{sh}^+) + 1}{2} \text{sign}(\epsilon_{su}^+ - \epsilon_{ss}) E_{sh}^+ \left|\frac{f_{su}^+ - f_s}{f_{su}^+ - f_y^+}\right|^{\frac{p^+ - 1}{p^+}} \quad (2-45b)$$

where:

$$\epsilon_{ss} = \epsilon_s - \epsilon_{om}^+ \quad (2-45c)$$

$$p^+ = E_{sh}^+ \frac{\epsilon_{su}^+ - \epsilon_{sh}^+}{f_{su}^+ - f_y^+} \quad (2-45d)$$

in which ϵ_{om}^+ = location of the tension envelope branch. Eq. (2-45) is shown plotted in Fig. 2-3. Also shown in this figure is the compression envelope branch defined in an analogous form as follows:

Rule 2 (Compression Envelope Branch)

$$f_s = \frac{E_s \epsilon_{ss}}{\left[1 + \left(\frac{E_s \epsilon_{ss}}{f_y^-}\right)^{10}\right]^{0.1}} + \frac{\text{sign}(\epsilon_{sh}^- - \epsilon_{ss}) + 1}{2} (f_{su}^- - f_y^-) \left[1 - \left|\frac{\epsilon_{su}^- - \epsilon_{ss}}{\epsilon_{su}^- - \epsilon_{sh}^-}\right|^{p^-}\right] \quad (2-46a)$$

$$E_t = \frac{E_s}{\left[1 + \left(\frac{E_s \epsilon_{ss}}{f_y^-}\right)^{10}\right]^{1.1}} + \frac{\text{sign}(\epsilon_{sh}^- - \epsilon_{ss}) + 1}{2} \text{sign}(\epsilon_{ss} - \epsilon_{su}^-) E_{sh}^- \left|\frac{f_{su}^- - f_s}{f_{su}^- - f_y^-}\right|^{\frac{p^- - 1}{p^-}} \quad (2-46b)$$

where:

$$\epsilon_{ss} = \epsilon_s - \epsilon_{om}^- \quad (2-46d)$$

$$p^- = E_{sh}^- \frac{\epsilon_{su}^- - \epsilon_{sh}^-}{f_{su}^- - f_y^-} \quad (2-46e)$$

in which ϵ_{om}^- = location of the compression envelope branch.

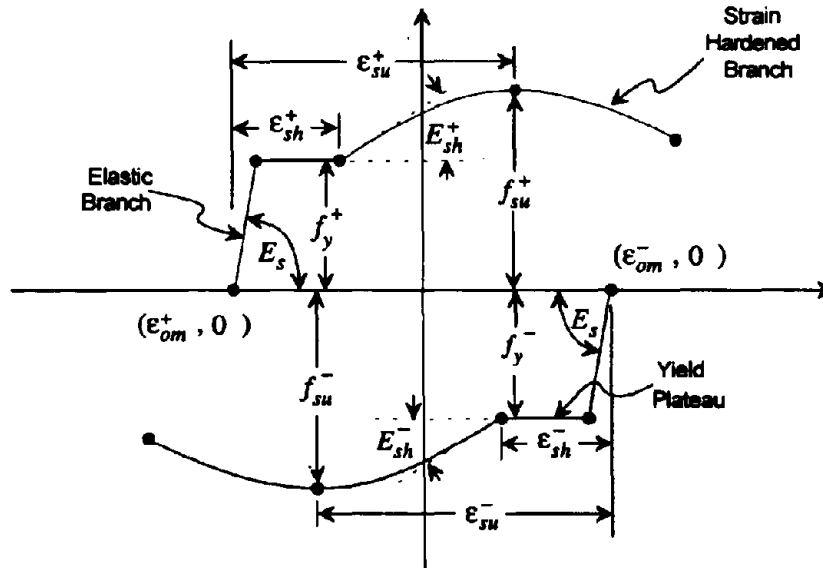


Fig. 2-3 Tension and Compression Envelope Curves

2.4.2 Reversal Branches (Rules 3 and 4)

When a reversal takes place on an envelope branch, a reversal curve connects this point of reversal with a target point on the opposite envelope. The curve that connects these two points will be referred to as a reversal branch. In general, reversal branches are completely defined by the extremum points: maximum excursion into the tension envelope branch ϵ_{\max} , and maximum excursion into the compression envelope branch ϵ_{\min} , (Fig. 2-6). If a reversal takes place from within the yield plateau on the tension envelope curve at a coordinate (ϵ_o^-, f_o^-) , with $f_o^- = f_y^+$, then ϵ_{\max} is defined as:

$$\epsilon_{\max} = \epsilon_o^- - \epsilon_{om}^+ \quad (2-47)$$

The target strain on the compressive envelope curve is calculated as:

$$\epsilon_{ta}^- = \epsilon_{om}^- + \epsilon_{\min} \quad (2-48)$$

where,

$$\epsilon_{\min} = \epsilon_y^- + p_r(\epsilon_{sh}^- - \epsilon_y^-) \quad (2-49)$$

and

$$\epsilon_{om}^- = \epsilon_o^- - \frac{f_o^-}{E_s} \quad (2-50)$$

with,

$$p_r = \frac{\epsilon_{\max} - \epsilon_y^+}{\epsilon_{sh}^+ - \epsilon_y^+} \quad (2-51)$$

While the target slope is given by:

$$E_{ta}^- = \frac{1}{\frac{1}{E_s} + p_r \left(\frac{1}{E_{sh}^-} - \frac{1}{E_s} \right)} \quad (2-52)$$

and the target stress if the yield stress on the compressive envelope branch (Fig. 2-5). In the case when the reversal takes place from the strain hardened curve of the tension envelope branch, then Eqs. (2-49) through (2-52) are modified as follows. The strain ϵ_{\min} is taken as the actual maximum excursion within the compressive envelope branch but,

$$|\epsilon_{\min}| > |\epsilon_{sh}^-| \quad (2-53)$$

The shifted origin abscissa for the compression envelope branch is calculated as:

$$\epsilon_{om}^- = \epsilon_a^- k_{rev} + \epsilon_b^-(1 - k_{rev}) \quad (2-54)$$

with:

$$\epsilon_a^+ = \epsilon_{om}^+ + \epsilon_{sh}^+ - \frac{f_y^+}{E_s} \quad (2-55)$$

$$\epsilon_b^+ = \epsilon_{om}^+ + \epsilon_{\max} - \frac{f_{\max}}{E_s} \quad (2-56)$$

in which k_{rev}^- is a factor to locate the compression envelope branch between the ϵ_a^+ and ϵ_b^+ as shown in Fig. 2-5, and was found to be:

$$k_{rev}^- = \exp\left(-\frac{\epsilon_{max}}{5000(\epsilon_y^+)^2}\right) \quad (2-57)$$

Finally the target stress and slope f_{ia}^- and E_{ia}^- are calculated using Eq. (2-46). Similarly, for the loading reversal branch, the shifted tension origin strain is given by:

$$\epsilon_{om}^+ = \epsilon_a^-(1 - k_{rev}^+) + \epsilon_b^+ k_{rev}^+ \quad (2-58)$$

with:

$$\epsilon_a^- = \epsilon_{om}^- + \epsilon_{sh}^- - \frac{f_y^-}{E_s} \quad (2-59)$$

$$\epsilon_b^- = \epsilon_{om}^- + \epsilon_{min}^- - \frac{f_{min}^-}{E_s} \quad (2-60)$$

where:

$$k_{rev}^+ = \exp\left(-\frac{|\epsilon_{min}^-|}{5000(\epsilon_y^-)^2}\right) \quad (2-61)$$

Then the target strain on the tension envelope branch is given by:

$$\epsilon_{ia}^+ = \epsilon_{om}^+ + \epsilon_{max} \quad (2-62)$$

In a similar way, the target stress f_{ia}^+ and slope E_{ia}^+ on the tension envelope branch is calculated using Eq. (2-45).

Experiments performed by Panthaki (1991) have shown that the initial Young's modulus at the point of reversal from the tension envelope branch (unloading) can be expressed as:

$$E_o^- = (1 - 3 \Delta\epsilon_a)E_s \quad (2-63)$$

While, for a reversal from the compression envelope branch (loading), the initial Young's modulus can be given by:

$$E_o^+ = (1 - \Delta\epsilon_a)E_s \quad (2-64)$$

The M-P parameter R was also found to be a function of the yield stress, that can be expressed as:

$$R^- = 16 \left(\frac{f_y}{E_s}\right)^{1/3} (1 - 10 \Delta\epsilon_a) \quad (2-65)$$

for the unloading branch, and

$$R^+ = 20 \left(\frac{f_y}{E_s} \right)^{1/3} (1 - 20 \Delta \epsilon_a) \quad (2-66)$$

where $\Delta \epsilon_a$ = strain amplitude for the cycle and E_o = initial Young's modulus for the reversal branch, as shown in Fig. 2-4. Analytical calibration of these variables are shown in Figs. 2-7 to 2-10 from experiments by Panthaki (1991), and Figs. 2-11 to 2-14 show some of the actual experimental loops that were used to fit the M-P equation.

The unloading and unloading branch are define as:

Rule 3 (Unloading Reversal Branch)

$$\begin{aligned} \epsilon_{a3} &= \epsilon_{om}^+ + \epsilon_{\max} \\ f_{a3} &= f_{\max} \\ E_{a3} &= E_o^- \\ \epsilon_{b3} &= \epsilon_{ia}^- \\ f_{b3} &= f_{ia}^- \\ E_{b3} &= E_{ia}^- \end{aligned} \quad (2-67)$$

The initial slope E_o^- and the Menegotto-Pinto equation parameter R^- are functions of the strain amplitude $\Delta \epsilon_a$ of the loop, Eqs. (2-63) and (2-65), which is defined as:

$$\Delta \epsilon_a = \frac{\epsilon_{b3} - \epsilon_{a3}}{2} \quad (2-68)$$

Rule 4 (Loading Reversal Branch)

$$\begin{aligned} \epsilon_{a4} &= \epsilon_{om}^- + \epsilon_{\min} \\ f_{a4} &= f_{\min} \\ E_{a4} &= E_o^+ \\ \epsilon_{b4} &= \epsilon_{ia}^+ \\ f_{b4} &= f_{ia}^+ \\ E_{b4} &= E_{ia}^+ \end{aligned} \quad (2-69)$$

where E_o^+ and R^+ are calculated using Eqs. (2-64) and (2-66), respectively, by having:

$$\Delta \epsilon_a = \left| \frac{\epsilon_{b4} - \epsilon_{a4}}{2} \right| \quad (2-70)$$

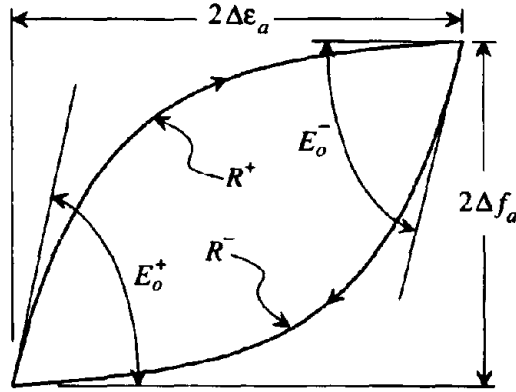


Fig. 2-4 Effect of the Strain Amplitude of the Reversal on the Equation Parameters

2.4.3 Returning Branches (Rules 5 and 6)

When partial unloading on the reversal unloading branch (rule 3) takes place, the reloading branch will be called loading returning branch (rule 5). An analogous branch will exist when a reversal takes place on the loading reversal branch (rule 4), and unloading is done through the unloading returning branch (rule 6), as shown in Fig. 2-15. At the occurrence of a reversal on rule 3, rule 5 will start and the target strain ϵ_{b5} is calculated as:

$$\epsilon_{b5} = \epsilon_{om}^+ + \epsilon_{max} + \Delta\epsilon_{re}^+ \quad (2-71)$$

with,

$$\Delta\epsilon_{re}^+ = \epsilon_{a3} - \epsilon_{a5} - \frac{f_y^+}{1.2 E_s} \quad (2-72a)$$

$$0 \leq \Delta\epsilon_{re}^+ \leq \frac{f_y^+}{3E_s} \quad (2-72b)$$

The target stress f_{b5} and slope E_{b5} are calculated by using Eq. (2-45). The initial Young's modulus $E_{a5} = E_o^+$ and parameter $R_5 = R^+$ are computed similarly by defining:

$$\Delta\epsilon_a = \frac{\epsilon_{b5} - \epsilon_{a5}}{2} \quad (2-73)$$

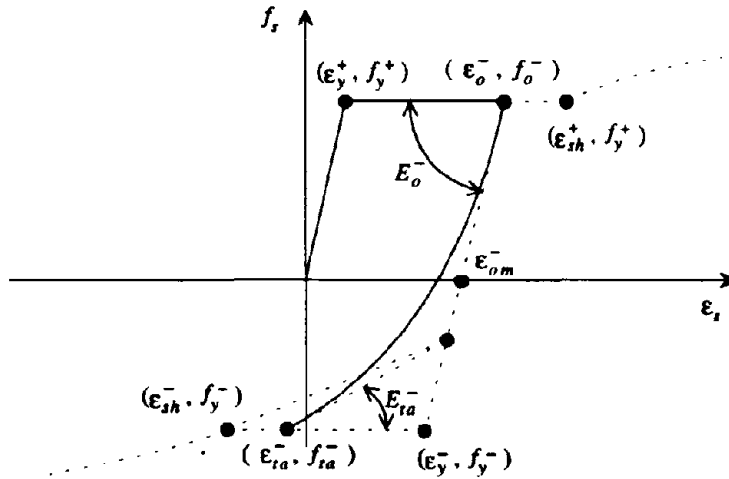


Fig. 2-5 Reversal From Yield Plateau

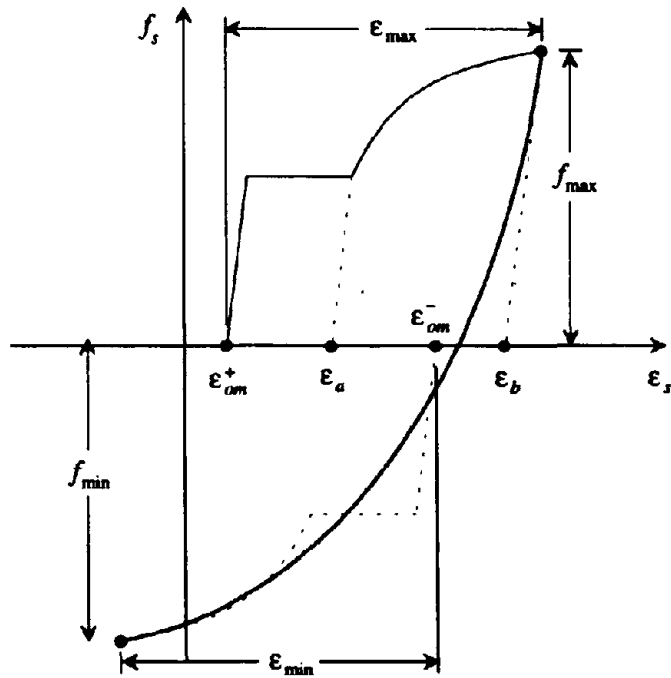


Fig. 2-6 Definition of the Reversal Unloading Branch

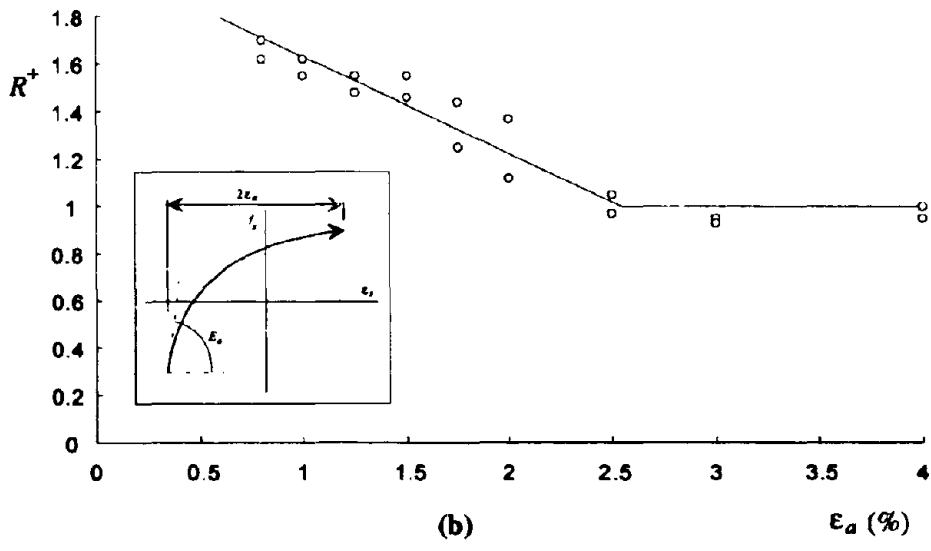
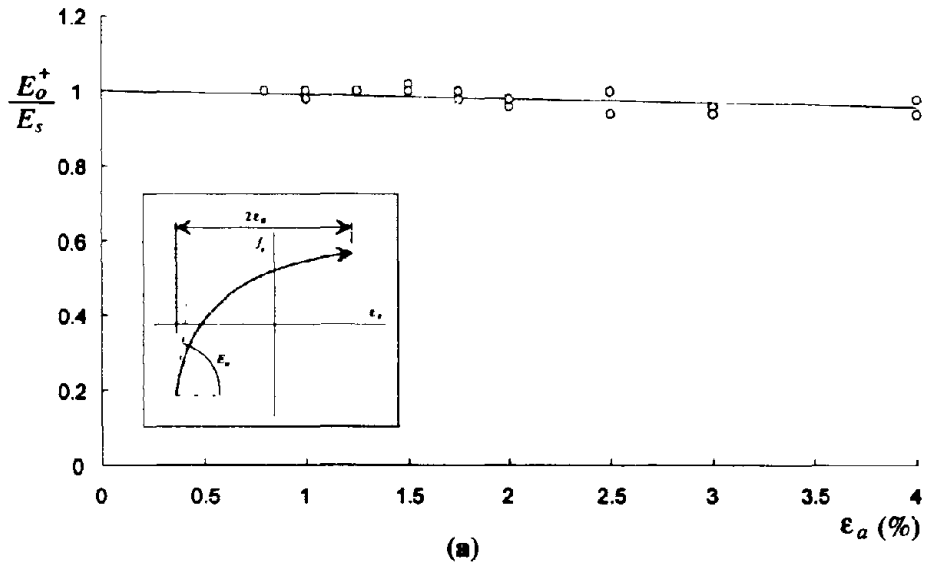


Fig. 2-7 Effect of the Strain Amplitude of Loop on the Initial Modulus and R Parameter for Reinforcing Bars ($f_y = 53$ ksi) (Loading)

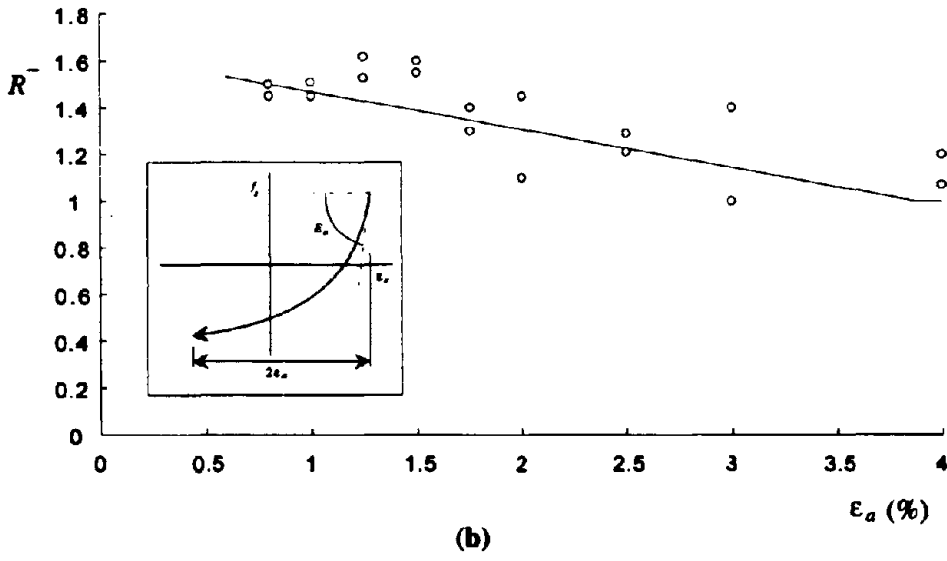
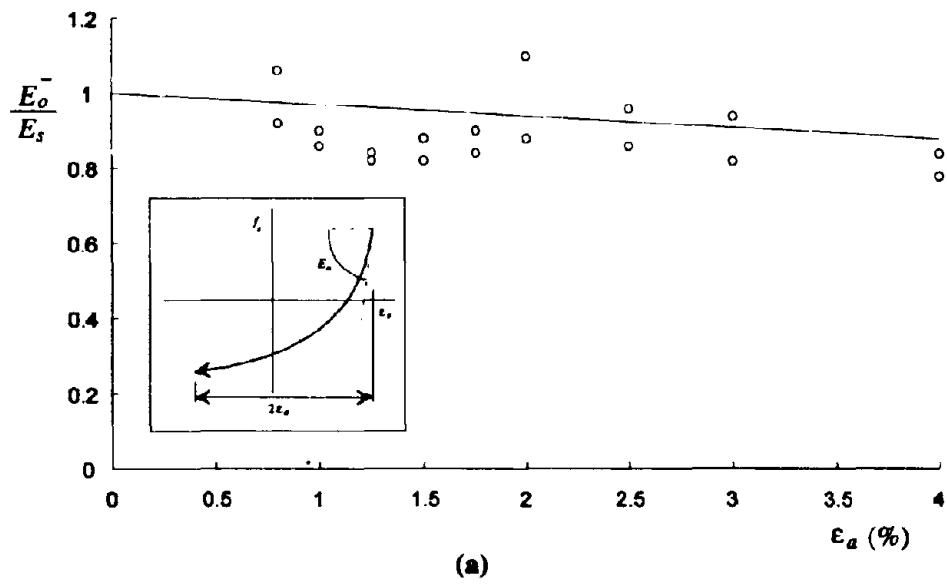
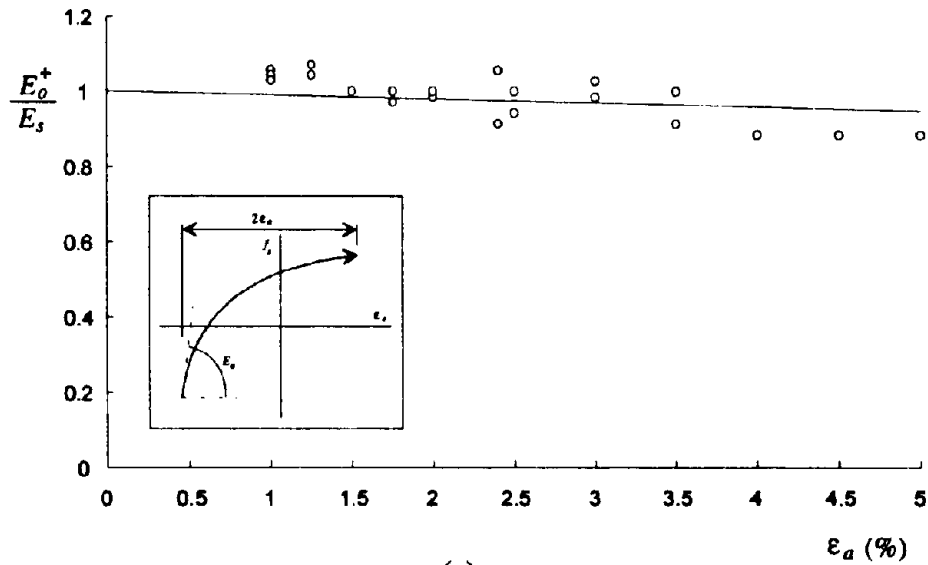
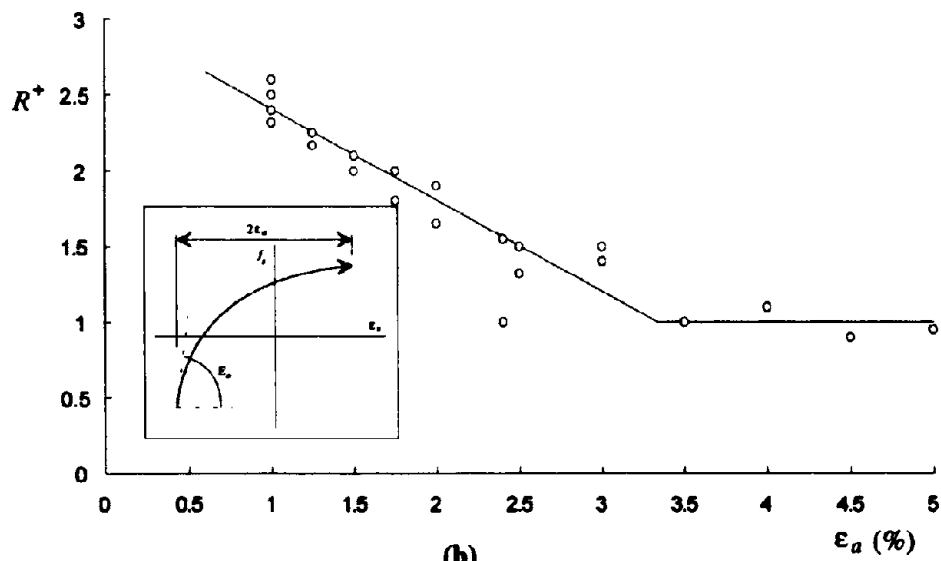


Fig. 2-8 Effect of the Strain Amplitude of Loop on the Initial Modulus and R Parameter for Reinforcing Bars ($f_y = 53$ ksi) (Unloading)

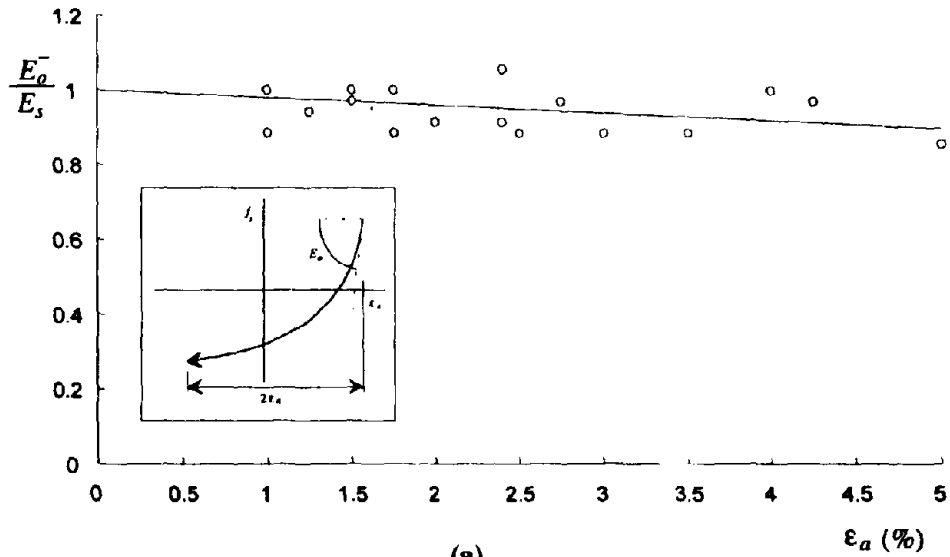


(a)

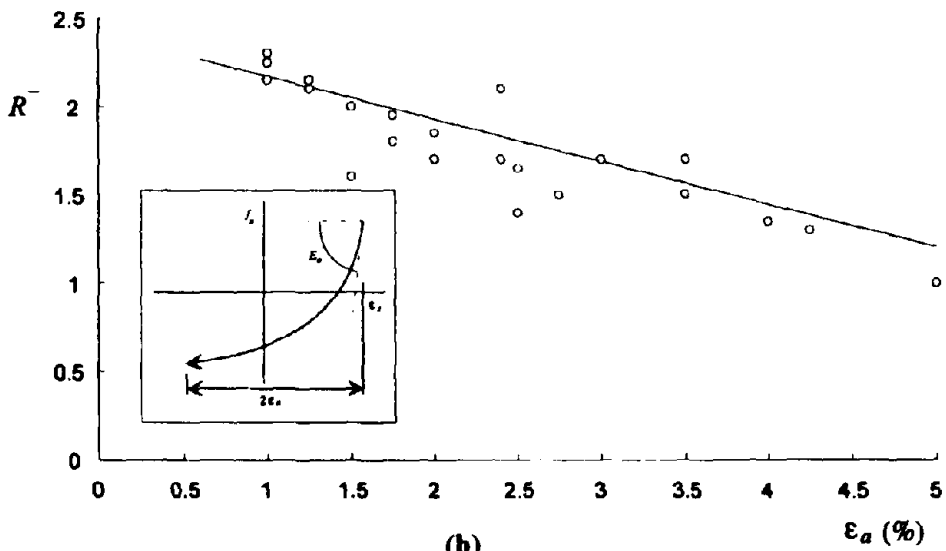


(b)

Fig. 2-9 Effect of the Strain Amplitude of Loop on the Initial Modulus and R Parameter for High Strength Bars ($f_y = 123$ ksi) (Loading)



(a)



(b)

Fig. 2-10 Effect of the Strain Amplitude of Loop on the Initial Modulus and R Parameter for High Strength Bars ($f_y = 123$ ksi) (Unloading)

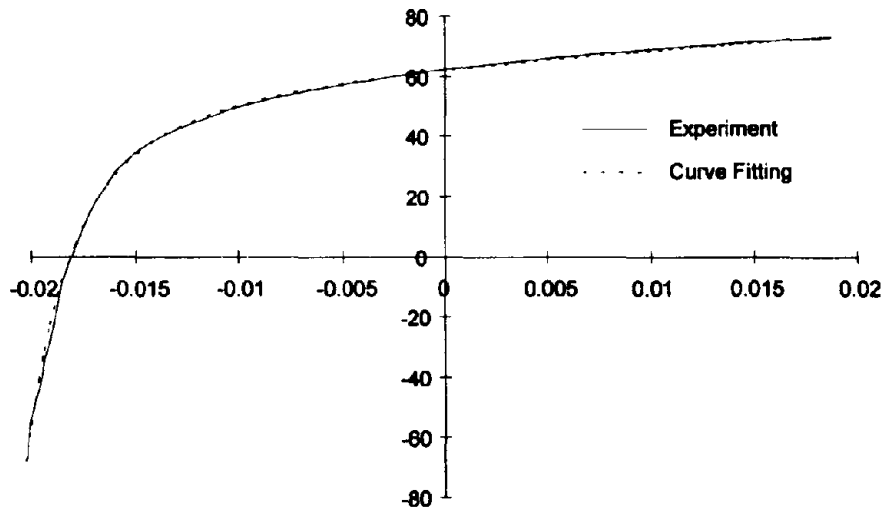


Fig. 2-11 Fitting of M-P Equation to a Loading Loop of Reinforcing Steel Bars ($f_y = 53$ ksi)

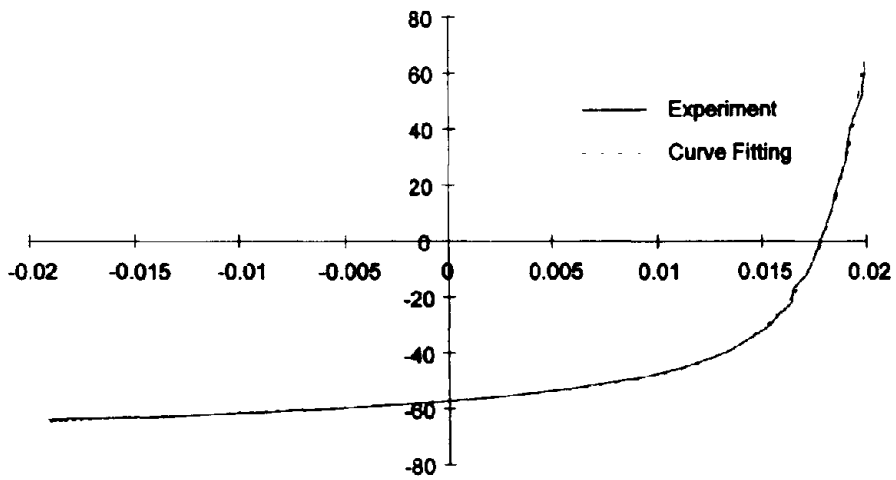


Fig. 2-12 Fitting of M-P Equation to an Unloading Loop of Reinforcing Steel Bars ($f_y = 53$ ksi)

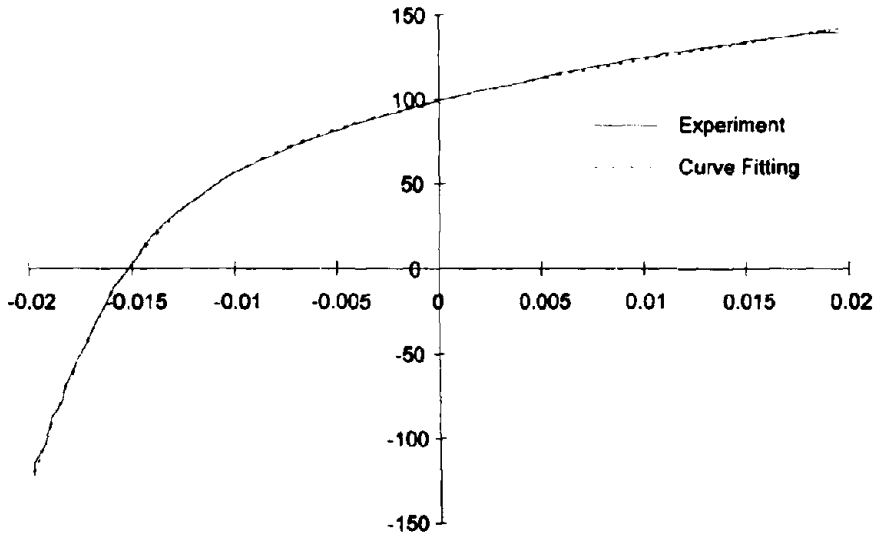


Fig. 2-13 Fitting of M-P Equation to a Loading Loop of High Strength Steel Bars ($f_y = 123$ ksi)

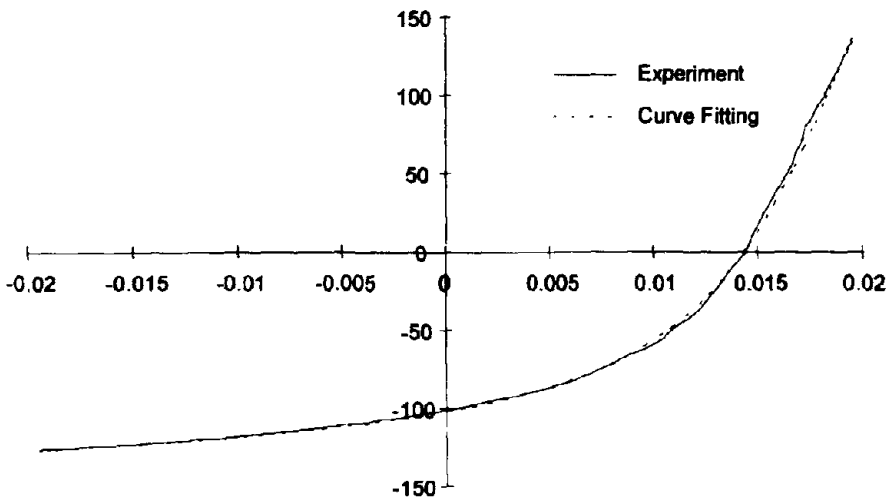


Fig. 2-14 Fitting of M-P Equation to an Unloading Loop of High Strength Steel Bars ($f_y = 123$ ksi)

In a similar way, a partial loading from the loading reversal branch (rule 4), which defines rule 6, is calculated as:

$$\epsilon_{b6} = \epsilon_{om}^- + \epsilon_{min} + \Delta\epsilon_{re} \quad (2-74)$$

with,

$$\Delta\epsilon_{re} = \epsilon_{a4} - \epsilon_{a6} - \frac{f_y^-}{1.2E_s} \quad (2-75a)$$

$$0 \geq \Delta\epsilon_{re} \geq \frac{f_y^-}{3E_s} \quad (2-75b)$$

2.4.4 First Transition Branches (Rules 7 and 8)

The curve followed after a reversal from an *envelope branch* curve has been named *reversal branch*, the one followed by a reversal from a reversal branch is called *the returning branch*. The curve then followed after a reversal from a returning branch is called *the first transition branch* and a reversal from this will lead to a *second transition branch*. These five types of curves are illustrated in Fig. 2-15. It should be noted that the reversal and the returning branches form a closed loop and the first and second transition branches cycle inside this loop.

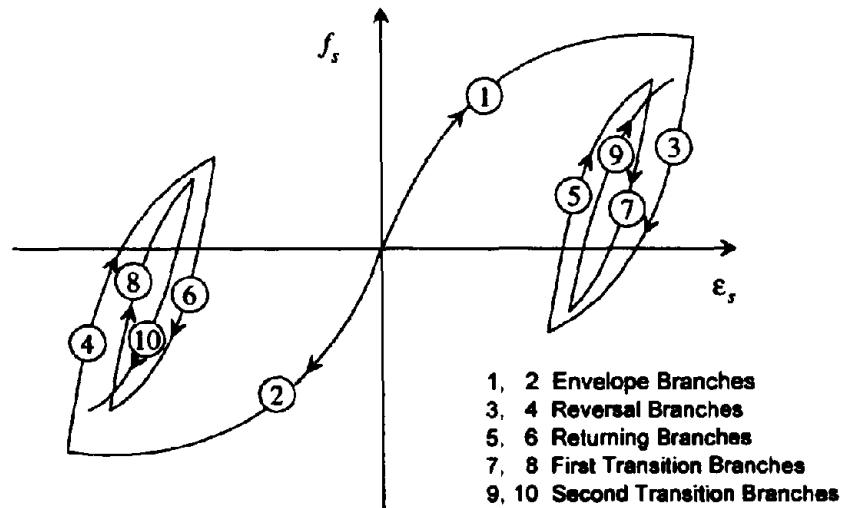


Fig. 2-15 Sequence of Partial Reversals

The target strain of rule 5 ϵ_{b5} is given in Eq. (2-71). This equation is different from the starting strain of rule 3 ϵ_{a3} , but if rule 5 would have reached the end, a reversal from this point would have been the starting point for rule 3 again. It means that in the case of a reversal from rule 5 (incomplete loading), a redefined rule 3 needs to be calculated. The starting strain for this redefined rule ought to be between the previous starting strain and the target strain of rule 5. By using a linear proportion,

$$\epsilon_{a3}^* = \epsilon_{b5} \frac{\epsilon_{a7} - \epsilon_{a5}}{\epsilon_{b5} - \epsilon_{a5}} + \epsilon_{a3} \frac{\epsilon_{b5} - \epsilon_{a7}}{\epsilon_{b5} - \epsilon_{a5}} \quad (2-76)$$

It can be noted that if the reversal happens when rule 5 has just started $\epsilon_{a7} = \epsilon_{a5}$, then from Eq. (2-76) $\epsilon_{a3}^* = \epsilon_{a3}$, what means that an "insinuation" of reversal occurred at rule 3, so the path followed should be on the unchanged rule 3. While if the reversal occurred at the end of rule 5 when $\epsilon_{a7} = \epsilon_{b5}$, that means it is already on the envelope branch and a reversal at this point should lead to rule 3, so $\epsilon_{a3}^* = \epsilon_{b5}$. Both extreme cases are satisfied by Eq. (2-76). Once the modified starting strain for rule 3 ϵ_{a3}^* has been obtained, the rule is completely defined as described in section 2.4.2.

The curve following a reversal from rule 5 is the first unloading transition curve (rule 7, Fig. 2-15), which target point is defined as:

$$\epsilon_{b7} = \epsilon_{a5} \quad (2-77)$$

Because every rule, except rule 1 and 2 (envelope branches), is defined at a reversal point, the initial coordinate is always the coordinate of the reversal point. The target stress f_{b7} and Young's modulus E_{b7} are calculated on the modified rule 3 at a strain ϵ_{b7} . The procedure to calculate rule 8, is exactly analogous. At a reversal from rule 6, a loading transition curve will connect the point of reversal with the modified reversal loading branch (rule 4). Where the modified starting strain for the modified rule 4 is given by:

$$\epsilon_{a4}^* = \epsilon_{b6} \frac{\epsilon_{a8} - \epsilon_{a6}}{\epsilon_{b6} - \epsilon_{a6}} + \epsilon_{a4} \frac{\epsilon_{b6} - \epsilon_{a8}}{\epsilon_{b6} - \epsilon_{a6}} \quad (2-78)$$

2.4.5 Second Transition Branches (Rules 9 and 10)

An incomplete transition from the returning branch to the reversal branch, a reversal on the first transition branch, is done through the second transition curve. The first transition curve

(rule 7 or 8) aims the reversal branch (rule 3 or 4), while the second transition branch (rule 9 or 10) aims the returning branch (rule 5 or 6). The relation among all the rules is shown diagrammatically in Fig. 2-16. Note that a rule can change to another rule either because a reversal took place or because it reached its target point.

The target point for the second transition branch is calculated in a way similar to that for first transition branch. A reversal at rule 7 will aim the loading returning branch (rule 5), thus the target strain for rule 9 is:

$$\epsilon_{b9} = \epsilon_{a7} \quad (2-79)$$

The target stress f_{b9} and slope E_{b9} are defined by the rule 5, as rule 9 is a transition branch to connect the point of reversal with the first loading transition branch (rule 5). Rule 10 is defined in the same way, when a reversal takes place on rule 8. In this case, the target strain $\epsilon_{b10} = \epsilon_{a8}$.

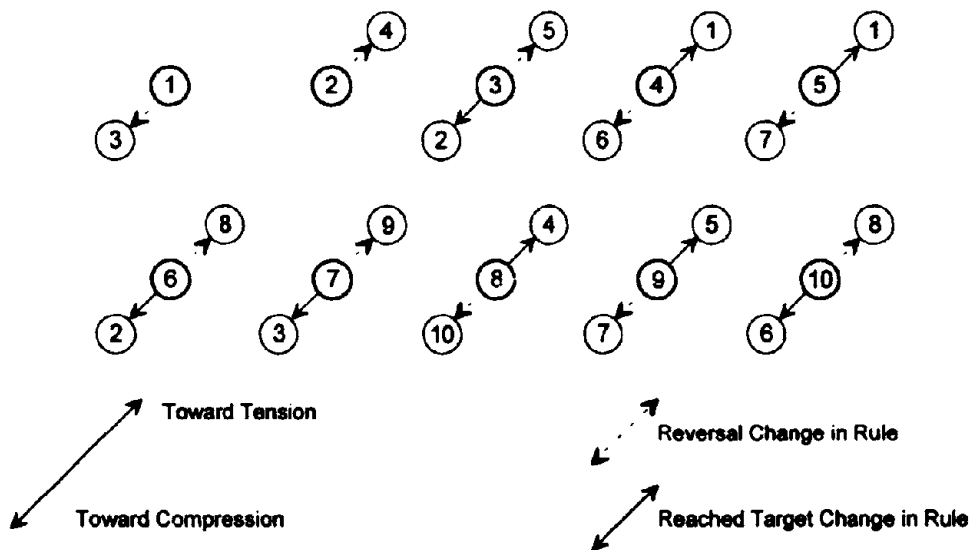


Fig. 2-16 Flow of Rules at Every Reversal and Target Strain

2.4.6 Strength Degradation

Degradation is taken into account by means of a scale factor. This scale factor is updated every time a reversal takes place. Degradation is directly associated with plastic deformation. The following proposed relationship proved to be applicable to both normal and high strength steel bars.

$$k_i = \left(\frac{\Delta f}{f_a} \right)_i = 1 - m_i \left(\frac{f_y}{E_s} \right)^{1/3} |19.5 \epsilon_p|^{2.5} \quad (2-81)$$

where:

$$\epsilon_p = \epsilon_a - \frac{f_a}{E_s} \quad (2-82)$$

in which m_i = factor that depends on the current scale factor, Δf = stress drop, ϵ_a = total strain amplitude, f_a = stress amplitude, ϵ_p = plastic strain amplitude, as shown in Fig. 2-17. The implementation of degradation through a scale factor ensures that degradation is considered all the time. Care has been taken to ensure that the model behaves smoothly under all kind of situations. Through a diagram like the one shown in Fig. 2-16 it is shown that every possible situation is considered. The model as defined before does not consider strength degradation, this is done by defining the stress as:

$$f_s = s_i f_{so} \quad (2-83)$$

with:

$$s_i = s_{i-1} k_i \quad (2-84)$$

$$m_i = 1 + \exp[-20.0(1 - s_i)] \quad (2-85)$$

where s_i is the scale factor that is modified at every reversal, m_i is a factor that amplifies degradation on the first reversals. It has been observed experimentally (Panthaki, 1991) that loop degradation tends to diminish with cycling, as shown in Fig. 2-19. As the material reaches incipient failure, degradation accelerates dramatically up to failure.

2.5 Stress-Strain Model Verification

Experimental data from Kent and Park, 1973; Ma, Bertero and Popov, 1976; and Panthaki, 1991, were used to test the model. Reasonable agreement was achieved. Results are shown in Figs. 2-20 to 2-34.

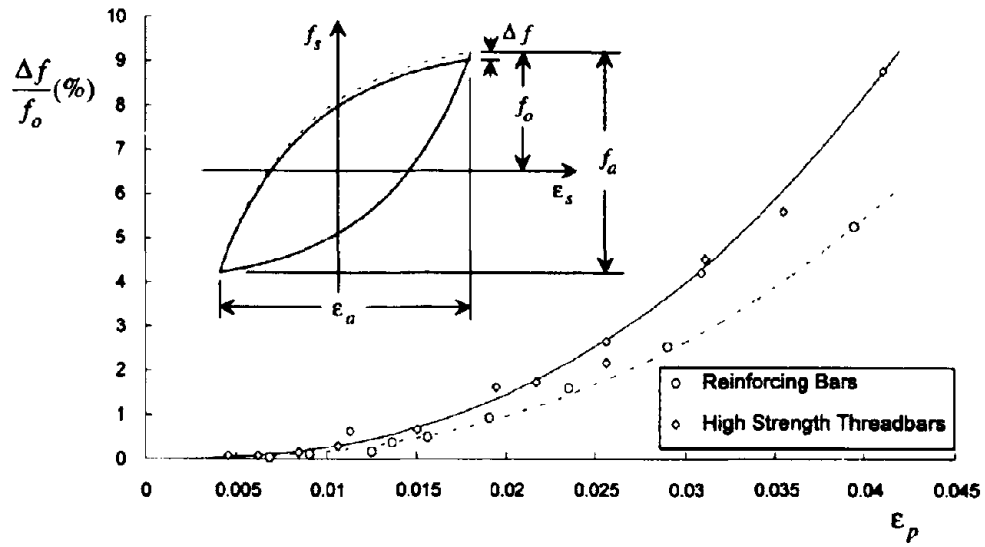


Fig. 2-17 Degradation of Reinforcing and High Strength Steel Bars

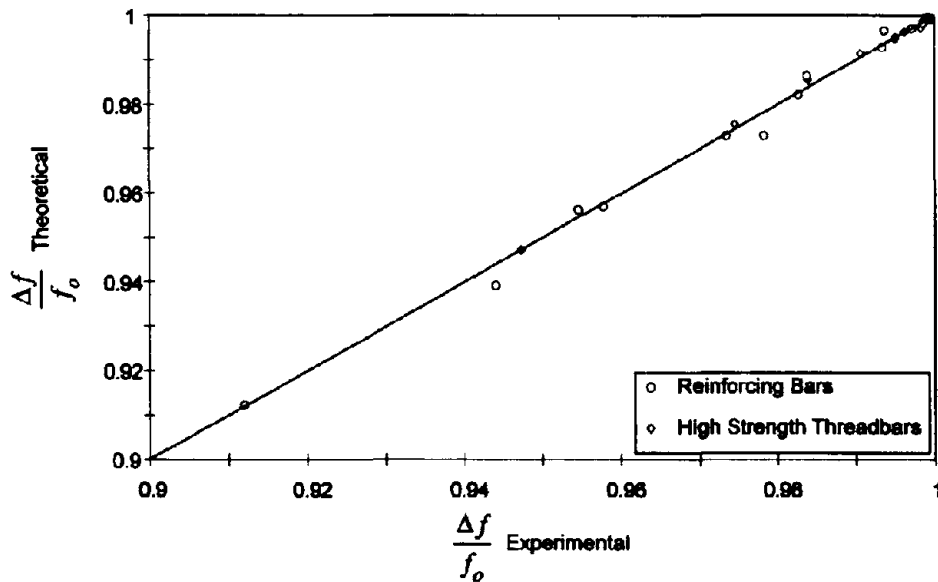


Fig. 2-18 Comparison of Degrading Model with Experimental Results

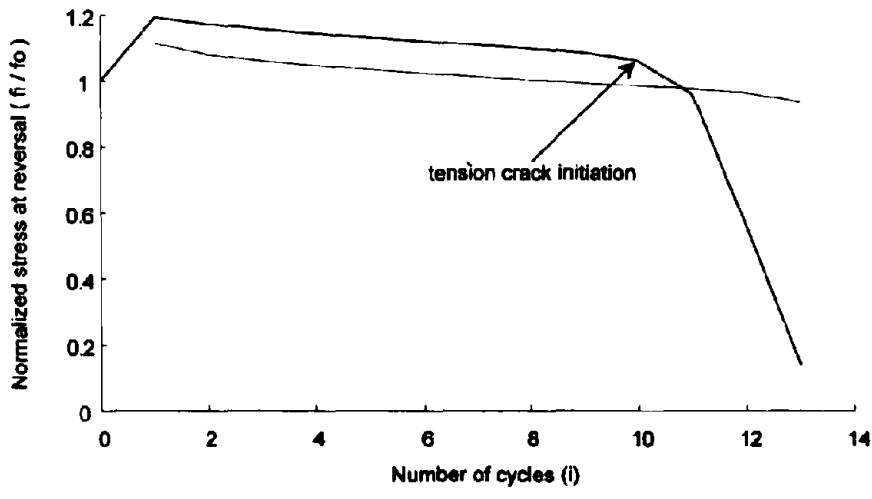
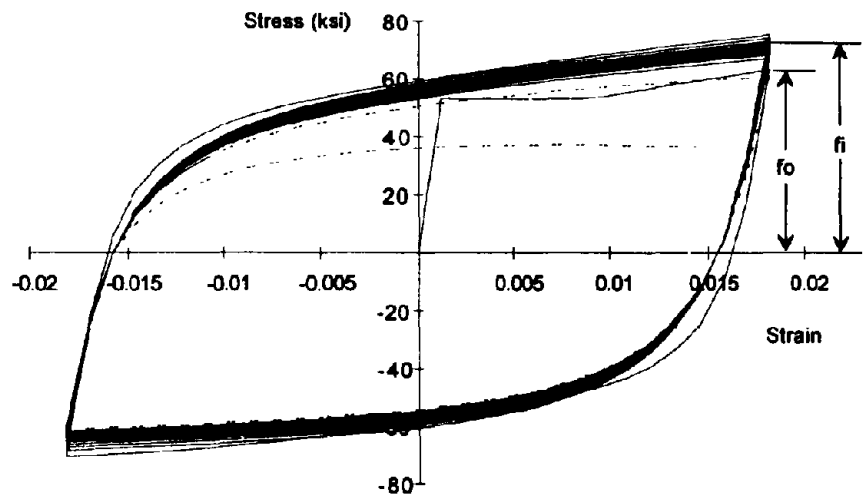


Fig. 2-19 Stress-Degradation Simulation and Fracture Prediction on Steel Bars

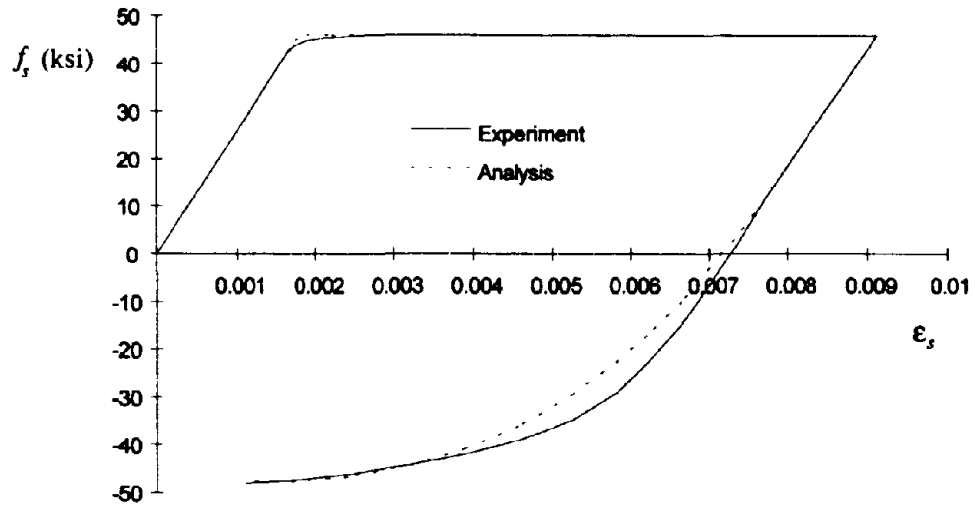


Fig. 2-20 Stress-Strain Experiment by Kent and Park (1973), Specimen 6

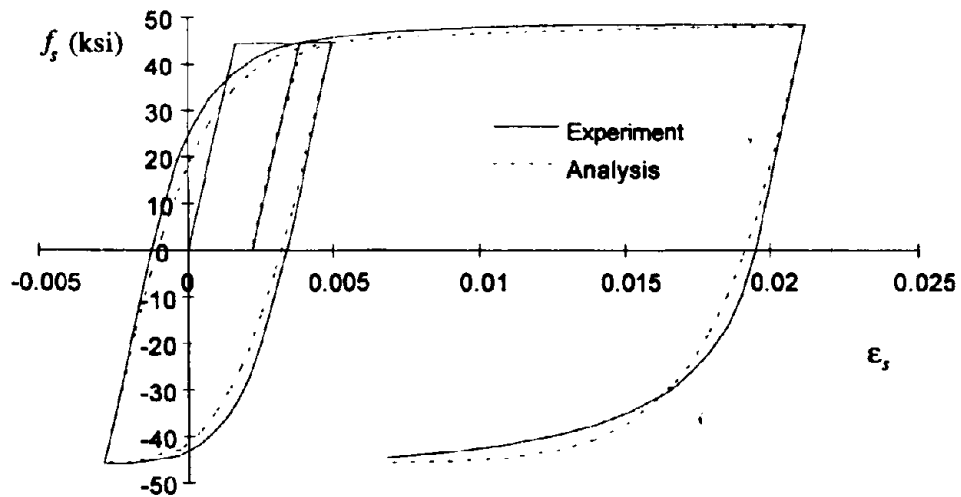


Fig. 2-21 Stress-Strain Experiment by Kent and Park (1973), Specimen 8

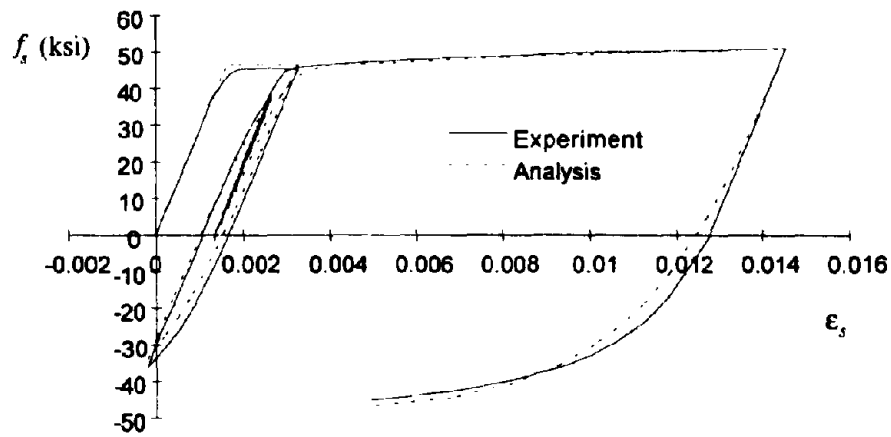


Fig. 2-22 Stress-Strain Experiment by Kent and Park (1973), Specimen 9

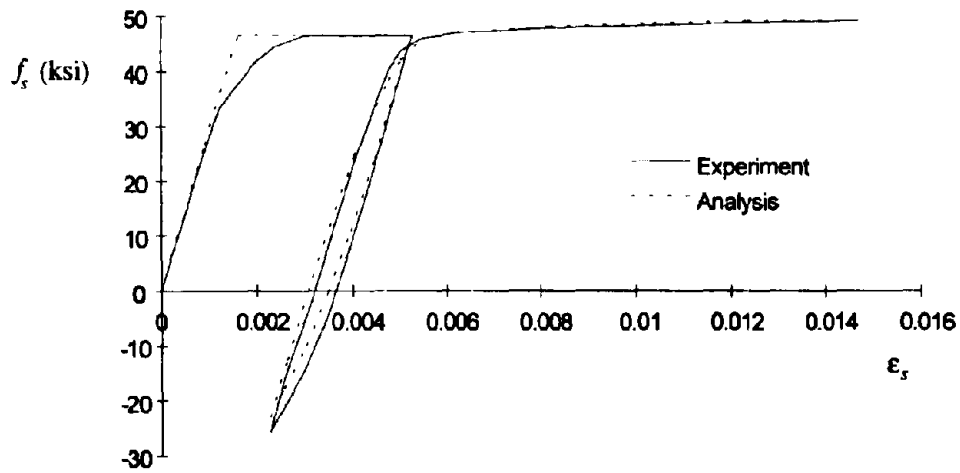


Fig. 2-23 Stress-Strain Experiment by Kent and Park (1973), Specimen 15

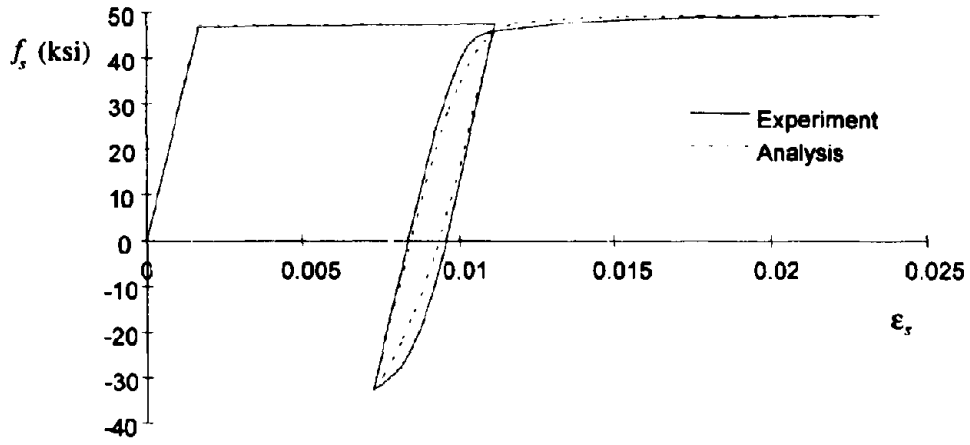


Fig. 2-24 Stress-Strain Experiment by Kent and Park (1973), Specimen 11

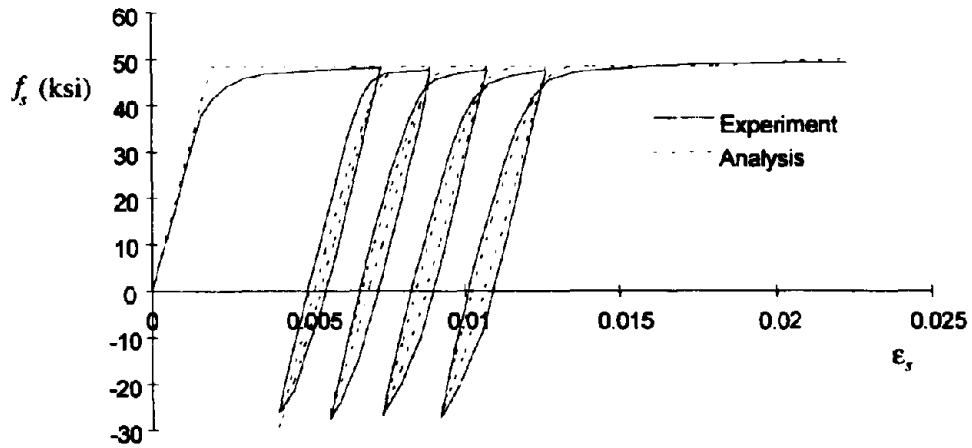


Fig. 2-25 Stress-Strain Experiment by Kent and Park (1973), Specimen 17

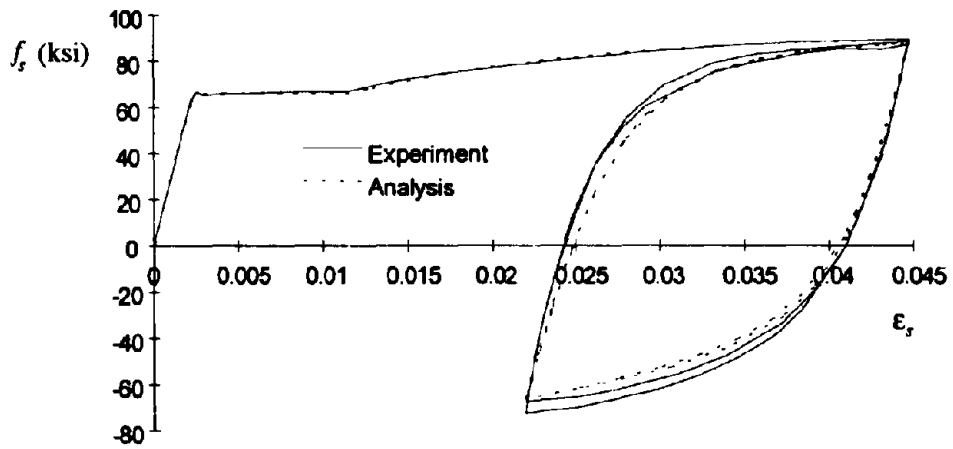


Fig. 2-26 Stress-Strain Experiment by Ma, Bertero and Popov (1976), Specimen 1

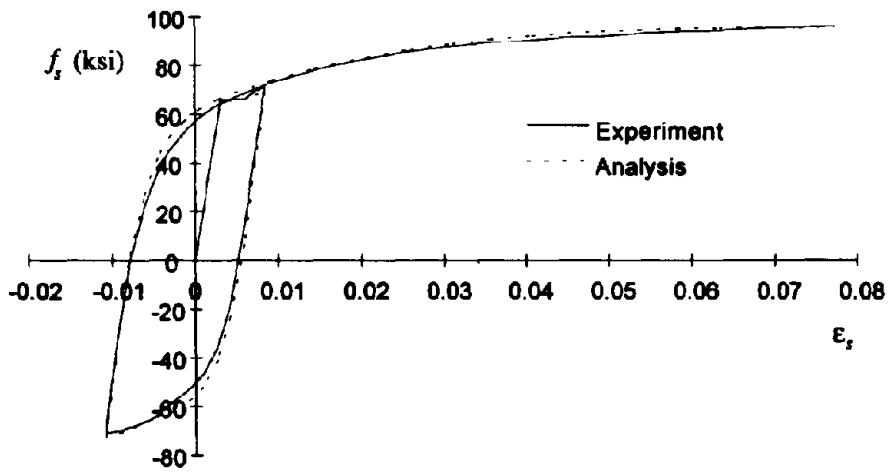


Fig. 2-27 Stress-Strain Experiment by Ma, Bertero and Popov (1976), Specimen 4

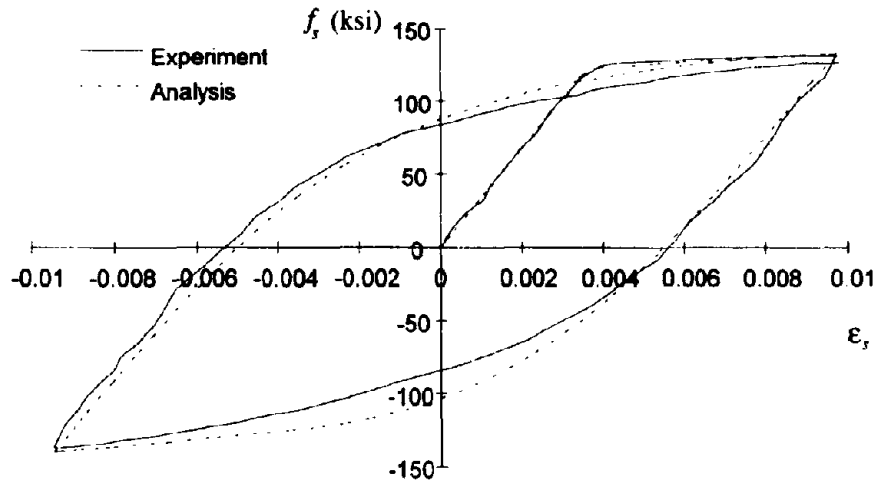


Fig. 2-28 Stress-Strain Experiment by Panthaki (1991), Specimen P2

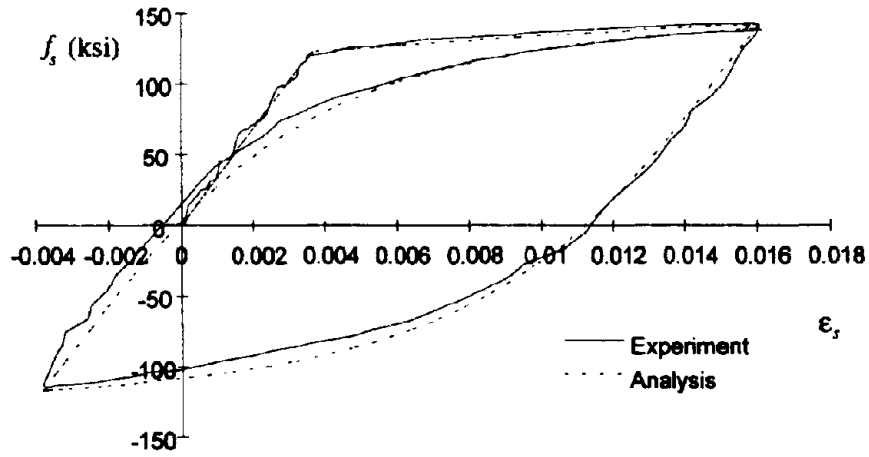


Fig. 2-29 Stress-Strain Experiment by Panthaki (1991), Specimen P3

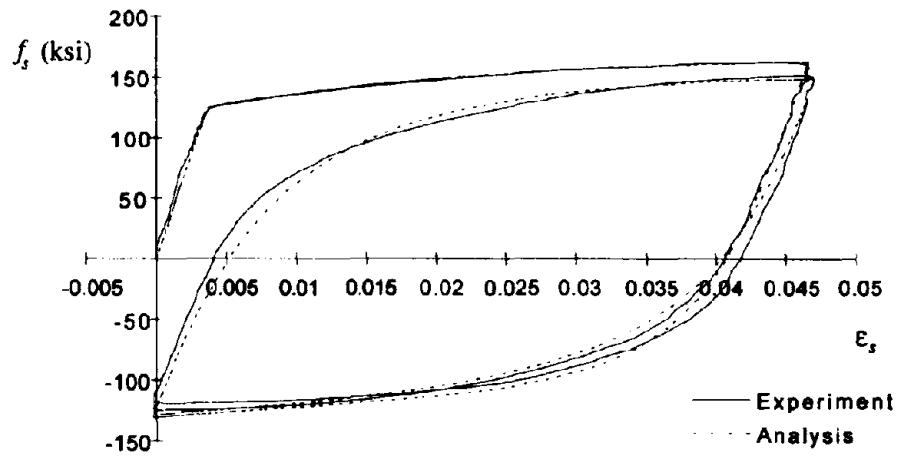


Fig. 2-30 Stress-Strain Experiment by Panthaki (1991), Specimen P16

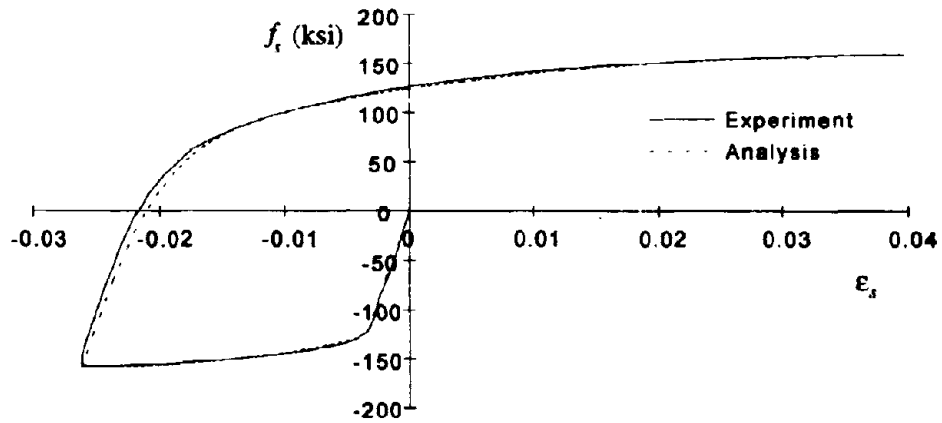


Fig. 2-31 Stress-Strain Experiment by Panthaki (1991), Specimen P19

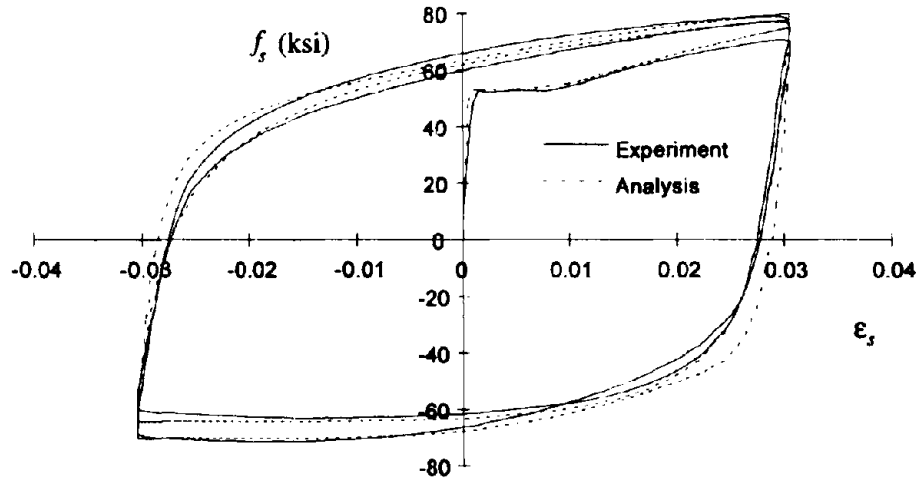


Fig. 2-32 Stress-Strain Experiment by Panthaki (1991), Specimen R1

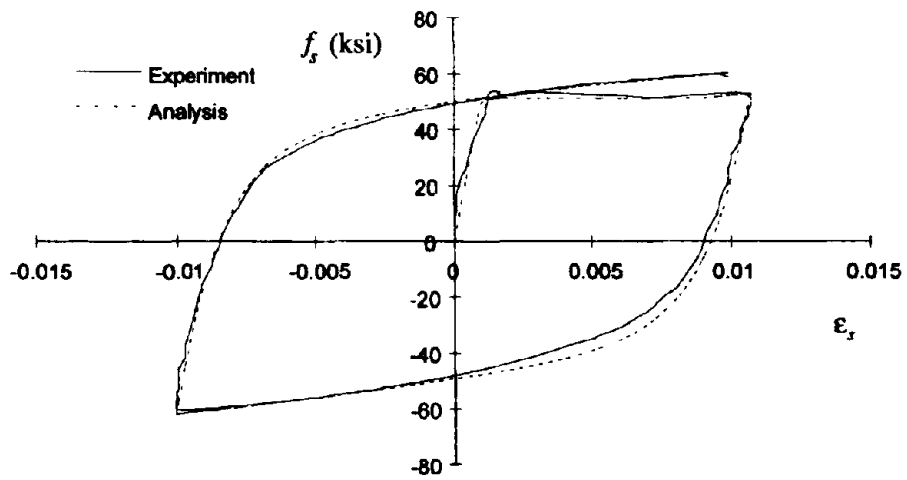


Fig. 2-33 Stress-Strain Experiment by Panthaki (1991), Specimen R4

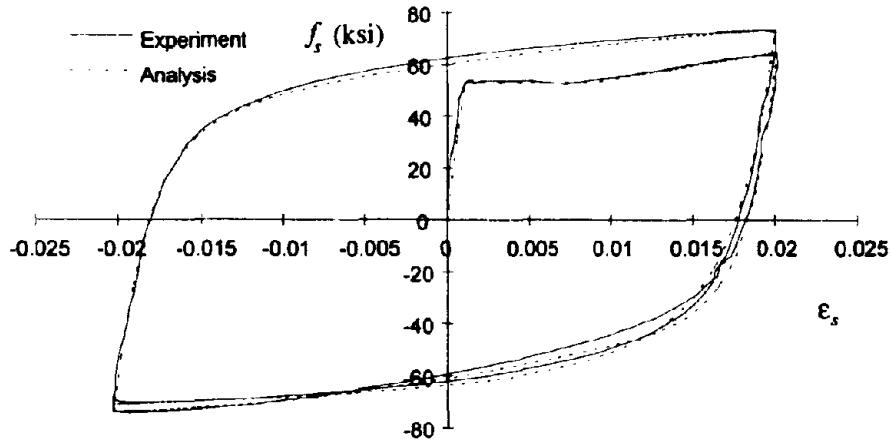


Fig. 2-34 Stress-Strain Experiment by Panthaki (1991), Specimen R5

2.6 Damage Modeling

The failure of a reinforced concrete member is intrinsically linked to the fracture of either the longitudinal reinforcing bars (Mander et al., 1992) or transverse reinforcement (Mander et al., 1984, 1988a, b). Thus, the prediction of steel fracture is an important aspect in the modeling of member behavior, particularly incipient failure.

The strain-life relation to estimate the life of a material is given by the Manson-Coffin (1955) equation expressed as:

$$\frac{\Delta \epsilon}{2} = \frac{\sigma'_f}{E} (2N_f)^b + \epsilon'_f (2N_f)^c \quad (2-86)$$

where $\Delta \epsilon$ = total strain amplitude, σ'_f = fatigue strength coefficient, b = fatigue strength exponent, E = Young's modulus, N_f = number of cycles to failure, ϵ'_f = fatigue ductility coefficient and c = fatigue ductility exponent.

The first term of the right hand side of Eq. (2-86) is known as the high cycle fatigue component while the second term is the low cycle fatigue component of the strain-life relation. In the case of earthquake loading, the members of a reinforced concrete structure can be subjected to inelastic deformations in which the steel reinforcing is subjected to large plastic reversals. In this case, the bar failure is predominantly due to low cycle fatigue, for which Eq. (2-86) can be simplified to (Koh and Stephens, 1991):

$$\frac{\Delta \epsilon}{2} = \epsilon'_f (2N_f)^c \quad (2-87)$$

which can be also be written as:

$$N_f = \frac{1}{2} \left(\frac{\Delta \epsilon}{2 \epsilon'_f} \right)^{-\frac{1}{c}} \quad (2-88)$$

A number of different theories has been suggested in the literature to describe the accumulation of partial fatigue damage. The Palmgren-Miner rule (Palmgren, 1924; Miner, 1945) is the simplest and still the most commonly used of all the cumulative damage models, it assumes a linear accumulation of damage that can be expressed as:

$$D_i = \frac{1}{N_f} \quad (2-89)$$

where D_i = damage for one cycle of a given amplitude $\Delta \epsilon$. The total damage accumulated is given by:

$$D = \sum D_i \quad (2-90)$$

Under random cycling, similar to what may be encountered in an earthquake, the problem of cycle counting and amplitude identification becomes cumbersome. The rain flow cycle counting method is one of the most popular methods used for this purpose. The method nevertheless becomes computationally cumbersome for long strain histories as it requires keeping track of the whole strain history for the problem. Other known cycle counting methods include the range pair counting, the peak counting, level crossing counting and range counting methods (Dowling, 1972). Once the cycles have been identified then a equivalent constant strain amplitude can be computed as:

$$\frac{D_{\text{variable}}}{D_{\text{constant}}} = \frac{\sum_{i=1}^n \left(\frac{\Delta \epsilon}{2} \right)_i^{-\frac{1}{c}}}{n \left(\frac{\Delta \epsilon}{2} \right)_e^{-\frac{1}{c}}} = 1 \quad (2-91)$$

thus,

$$\left(\frac{\Delta \epsilon}{2}\right)_e = \left[\frac{1}{n} \sum_{i=1}^n \left(\frac{\Delta \epsilon}{2}\right)_i^{-c} \right]^{-\frac{1}{c}} \quad (2-92)$$

Mander et al. (1992) have shown that for reinforcing bars and high strength threadbars c can be conservatively approximated as -0.5. Thus Eq. (2-92) becomes,

$$\left(\frac{\Delta \epsilon}{2}\right)_e = \left[\frac{1}{n} \sum_{i=1}^n \left(\frac{\Delta \epsilon}{2}\right)_i^2 \right]^{\frac{1}{2}} \quad (2-93)$$

It can readily be shown that if all the points are used rather than just the peaks,

$$\epsilon_{ae} = \frac{\Delta \epsilon_e}{2} = \sqrt{3} \epsilon_{STD} \quad (2-94)$$

where ϵ_{STD} is the standard deviation of the strain history response. The following procedure should be used to compute the standard deviation. At every new strain point, the average strain for the whole strain history is calculated by:

$$\bar{\epsilon} = \frac{\int \epsilon d|\epsilon|}{\int d|\epsilon|} = \frac{\frac{1}{2} \sum_{i=1}^n (\epsilon_i + \epsilon_{i-1}) |\epsilon_i - \epsilon_{i-1}|}{\sum_{i=1}^n |\epsilon_i - \epsilon_{i-1}|} \quad (2-95)$$

Thus the variance of the strain history is calculated by:

$$\epsilon_{STD}^2 = \frac{\int (\epsilon - \bar{\epsilon})^2 d|\epsilon|}{\int d|\epsilon|} = \frac{\frac{1}{3} \sum_{i=1}^n |\epsilon_i^3 - \epsilon_{i-1}^3|}{\sum_{i=1}^n |\epsilon_i - \epsilon_{i-1}|} - \bar{\epsilon}^2 \quad (2-96)$$

And the standard deviation is computed as the square root of the variance. Fig. 2-35 shows two examples of the results using the procedure outlined. Note that for the constant amplitude cycle, the standard deviation converges on the first complete cycle to a constant value. In the strain domain the shape of the wave is a triangle and thus,

$$\epsilon_{STD} = \frac{1}{\sqrt{3}} \left(\frac{\Delta \epsilon}{2}\right) = 0.577 \left(\frac{\Delta \epsilon}{2}\right) \quad (2-97)$$

An alternative way of computing the standard deviation is considering that the time history will resemble a sinusoidal movement. In this case, if the time steps are considered to be equally spaced, the standard deviation can be considered independently of the magnitude of the strain

changes, and it can be computed in a simple way, just by keeping the summation of strains. Thus, in the time domain the standard deviation is defined by:

$$\epsilon_{STD}^2 = \frac{\int (\epsilon - \bar{\epsilon})^2 dt}{\int dt} \quad (2-98)$$

As discrete data is to be used, Eq. (2-98) can be expressed as:

$$\epsilon_{STD}^2 = \frac{1}{n} \sum_{i=1}^n \epsilon_i^2 - \left(\frac{1}{n} \sum_{i=1}^n \epsilon_i \right)^2 \quad (2-99)$$

If all the points are used and not only the peaks, then:

$$\epsilon_{ae} = \left(\frac{\Delta \epsilon}{2} \right)_e = \sqrt{2} \epsilon_{STD} \quad (2-100)$$

The apparent contradiction between this equation and Eq. (2-94) should not be taken as such. The standard deviation computed in Eq. (2-94) is in the stress-strain domain and is dependent on the magnitude of the strain changes, while when Eq. (2-99) is used in the strain-time domain, it is assumed that the strain-time history shape resembles some form of harmonic loading. Sinusoidal waves are the time shape used in experiments and most structures will tend to show sinusoidal strain histories at its natural frequency.

An energy based cumulative damage model is proposed as:

$$D_i = \frac{\Delta W_i}{W_i(\epsilon_{ae})} \quad (2-101)$$

with,

$$\Delta W_i = \frac{1}{2} (f_i + f_{i-1})(\epsilon_i - \epsilon_{i-1}) \quad (2-102)$$

and

$$W_i(\epsilon_{ae}) = A(\epsilon_{ae})^B \quad (2-103)$$

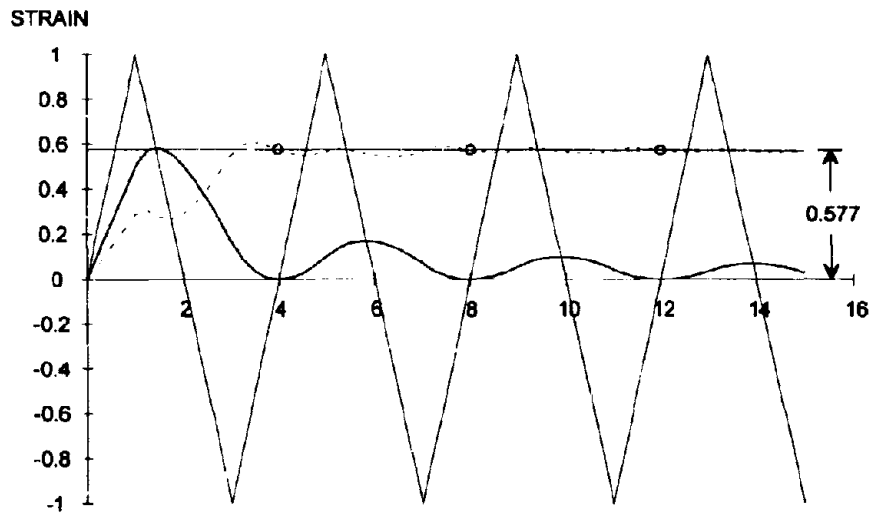
The experimental data obtained by Panthaki (1991) was reanalyzed and based on these analyses the following proposed values were obtained:

	A	B
Reinforcing Bars	1.22 (ksi)	-1.06
High Strength Prestressing Bars	1.09 (ksi)	-1.4

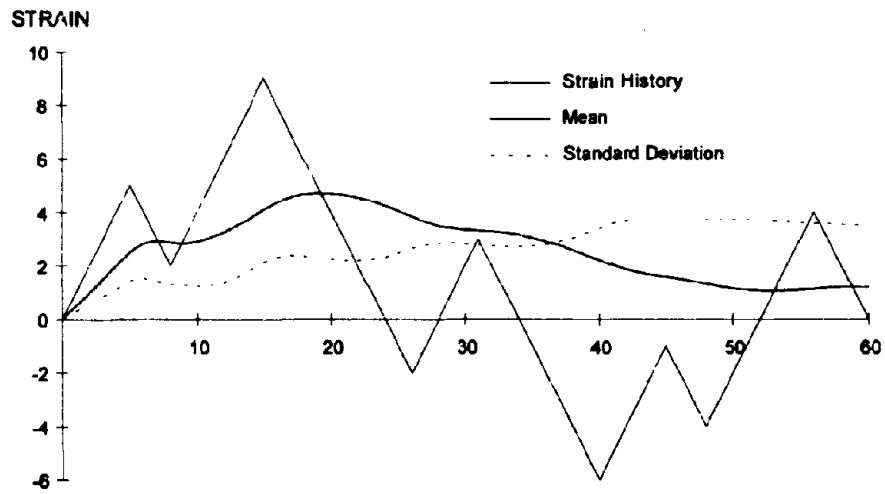
after which the following empirical equations are proposed:

$$A = \frac{E_s}{13400} (\epsilon_y)^{0.15} \quad (2-104)$$

$$B = -5.7(\epsilon_y)^{0.25} \quad (2-105)$$



(a) Constant Amplitude Cycles



(b) Variable Amplitude Cycles

Fig. 2-35 Determination of Equivalent Strain Amplitude

2.7 Damage Model Implementation and Verification

In Fig. 2-51 a comparison of the proposed damage model with experimental results from Panthaki (1991) is presented. The scattering in the experimental data can be modeled in terms of the deviation from the average result. An additional factor is used to simulate the effect of incipient failure upon the stress-strain behavior.

$$F_r = 0.5 \left[1 - \frac{u}{(1 + |u|^R)^{1/R}} \right] \quad (2-106)$$

This factor is used to simulate a normal distribution for which the parameter R was found to be approximately 3.27. This was obtained by minimizing the variance between both functions between $u = 0$ and $u = 3$.

The parameter u is a function of the damage index D_i and the standard deviation σ , and is defined as:

$$u = 2 \left(\frac{D_i - D_m}{\sigma} \right) \quad (2-106)$$

where, for tension stress,

$$D_m = 1 + \frac{\sigma}{2} \quad (2-107)$$

and for compression stress,

$$D_m = 1.2 + \frac{\sigma}{2} \quad (2-108)$$

while, for a single bar,

$$\sigma = 0.2 \quad (2-109)$$

and for multiple bars,

$$\sigma = 0.4 \quad (2-110)$$

To the knowledge of the writers, this is the first time that a model has tried to simulate this phenomenon. The incorporation of steel fracture simulation is a very important factor if the prediction of failure is desired. Fig. 2-51 shows how the model compares with experimental data, while Figs. 2-36 through 2-50 show individual comparisons at different strain amplitude tests.

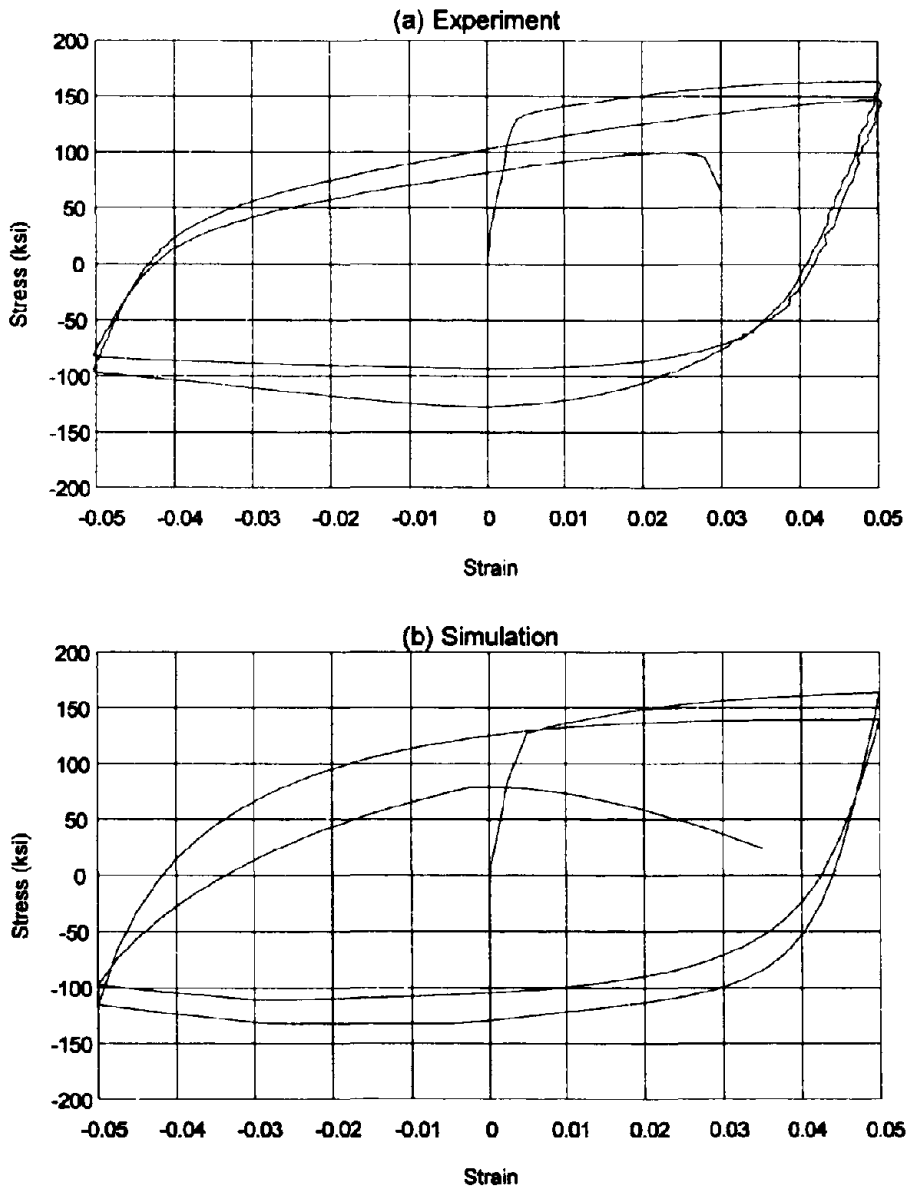


Fig. 2-36 High Strength Bar, Specimen P18 (Panthaki, 1991)

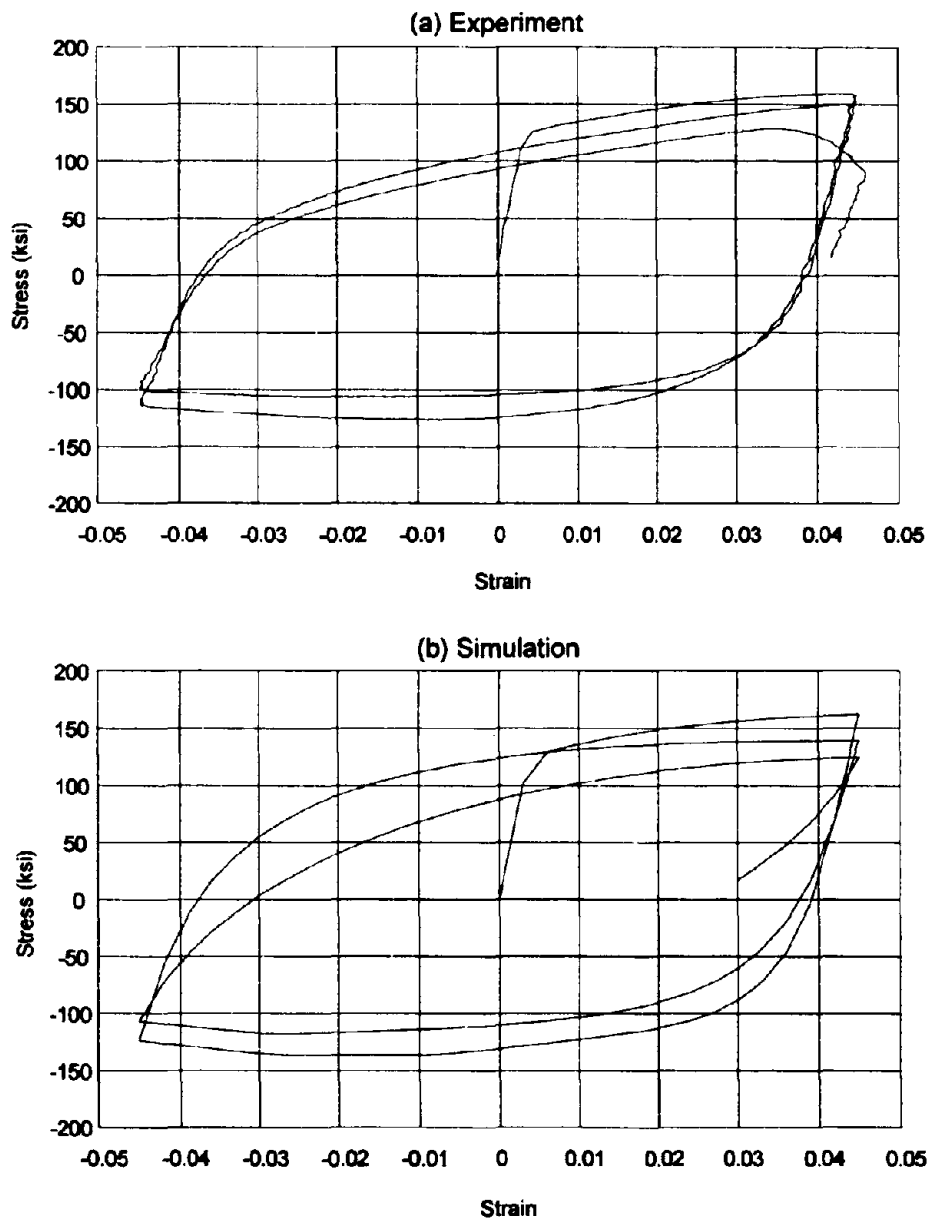


Fig. 2-37 High Strength Bar, Specimen P10

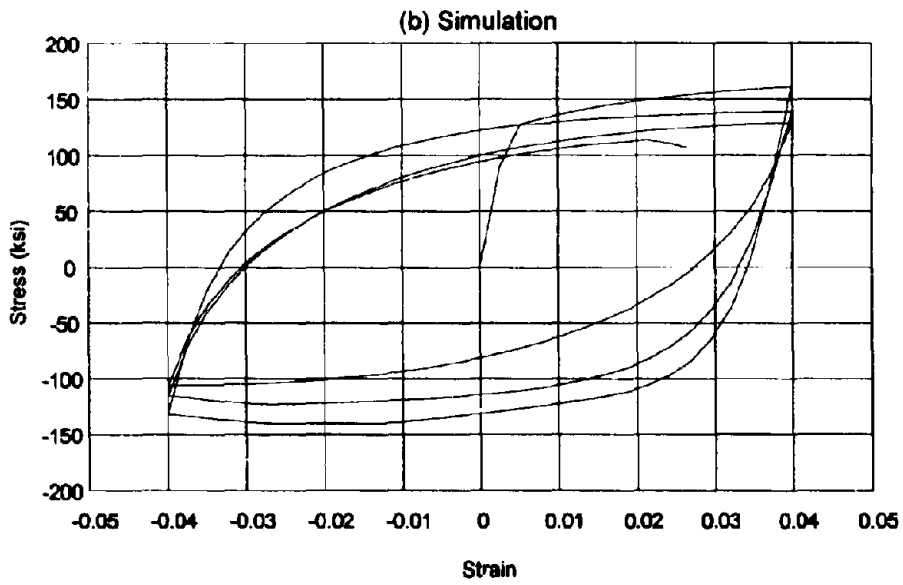
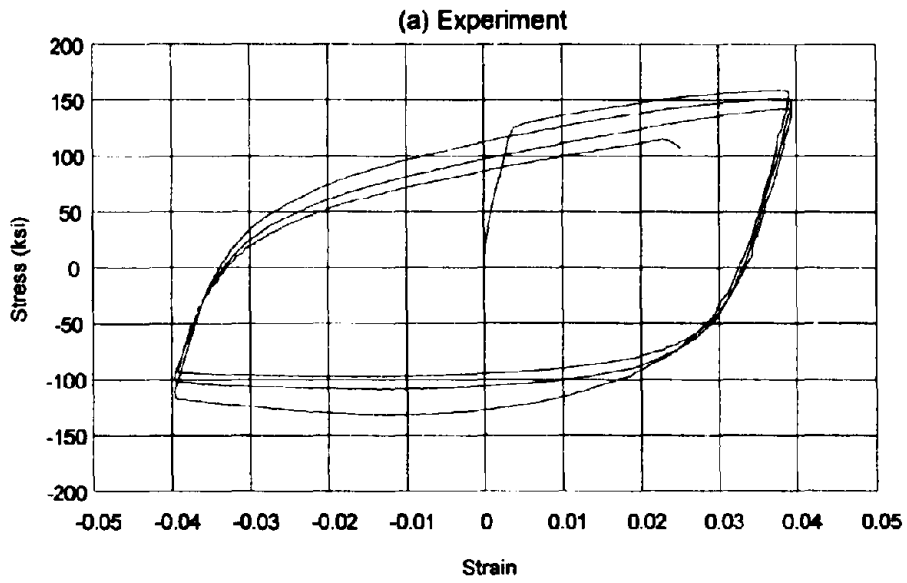


Fig. 2-38 High Strength Bar, Specimen P13

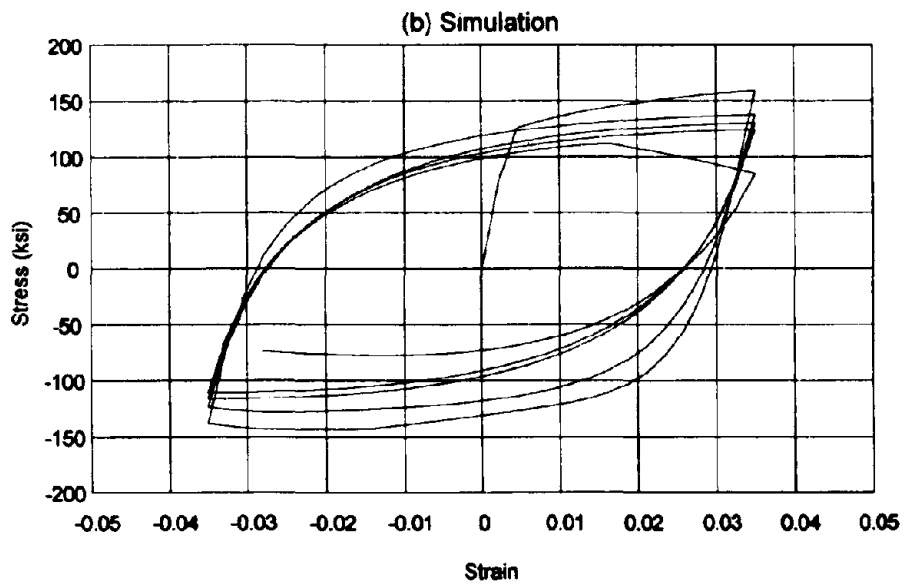
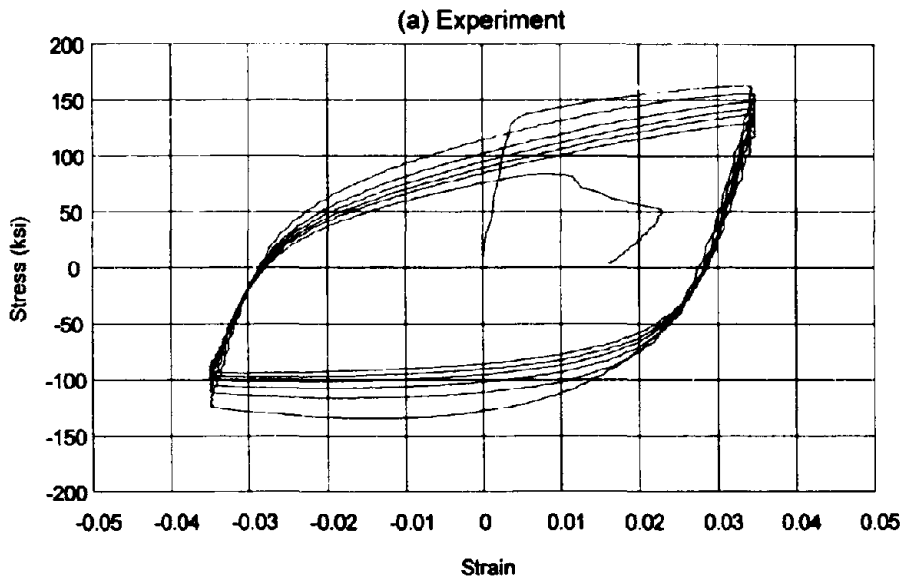


Fig. 2-39 High Strength Bar, Specimen P12

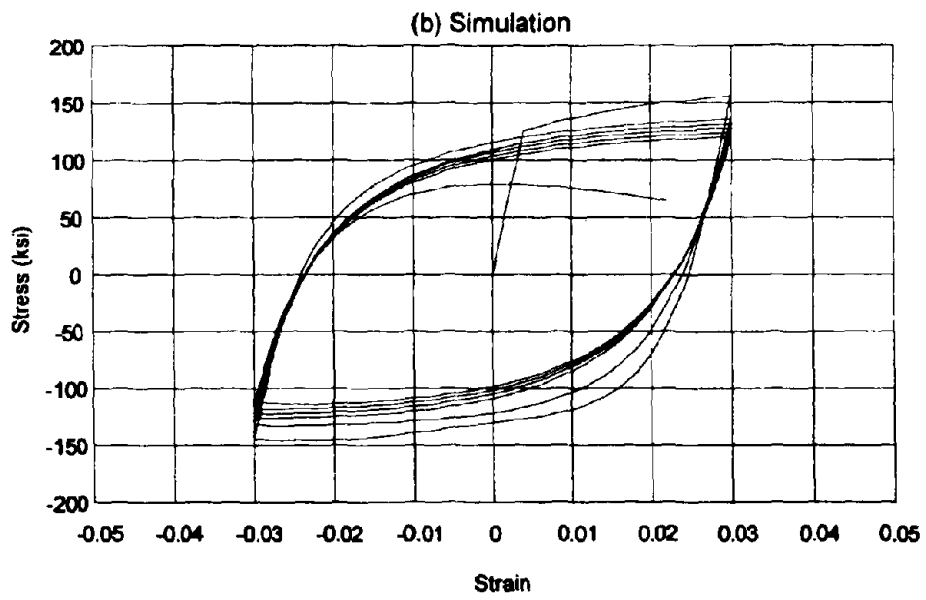
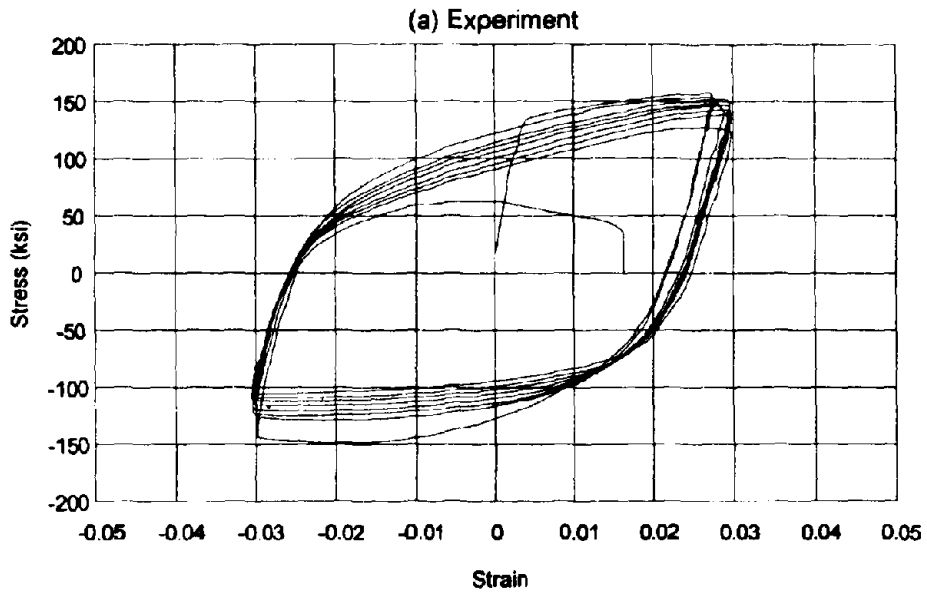


Fig. 2-40 High Strength Bar, Specimen P4

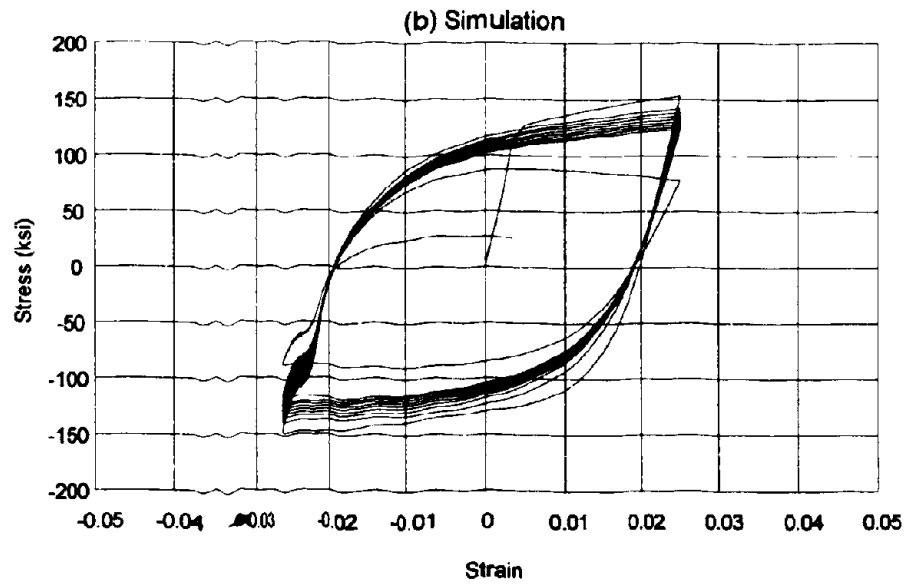
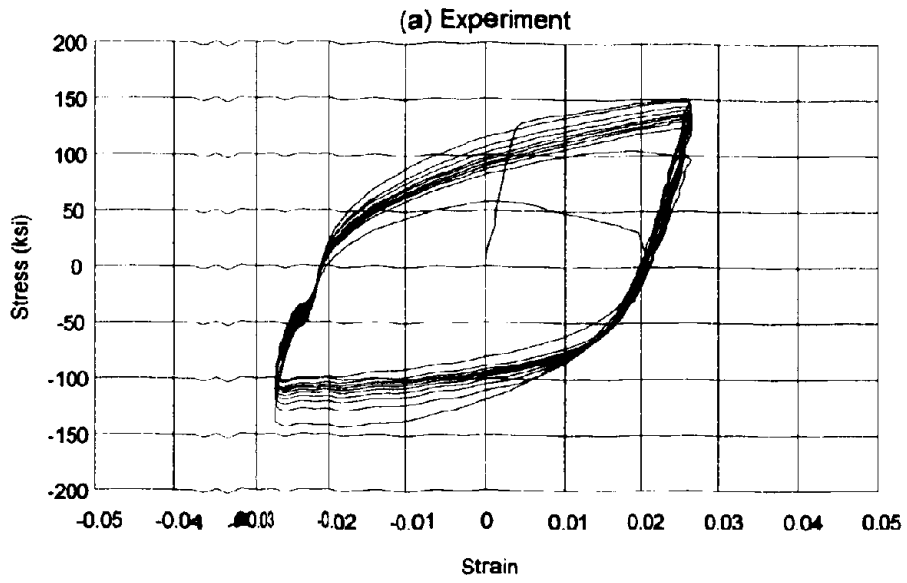


Fig. 2-41 High Strength Bar, Specimen P7

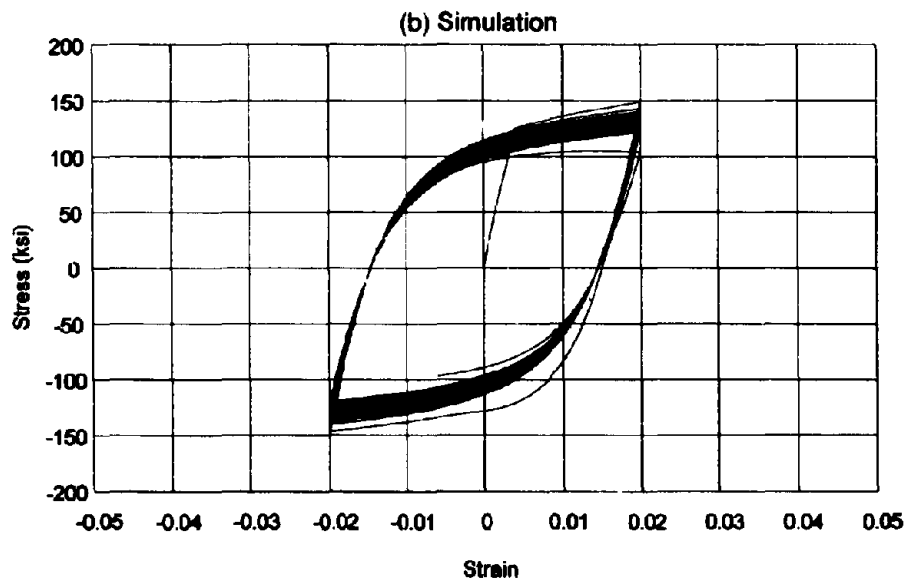
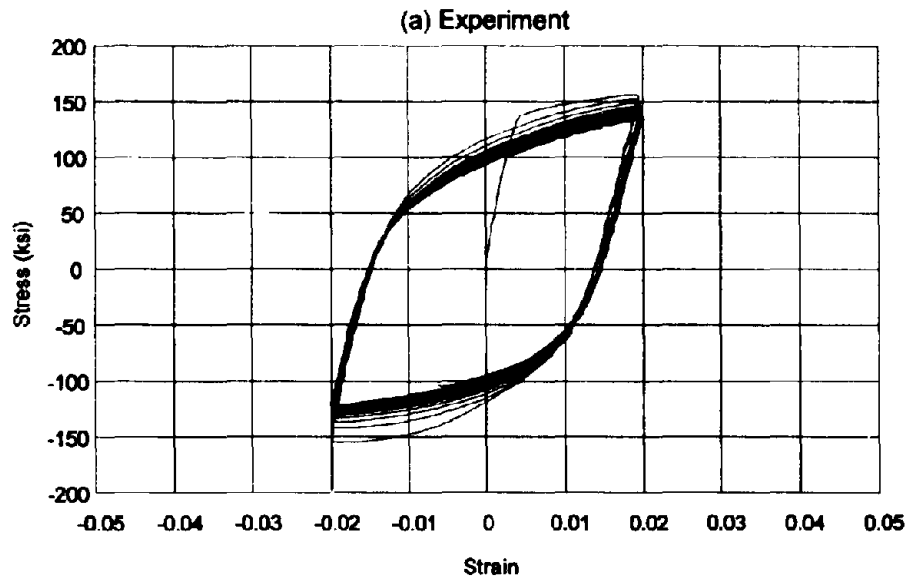


Fig. 2-42 High Strength Bar, Specimen P14

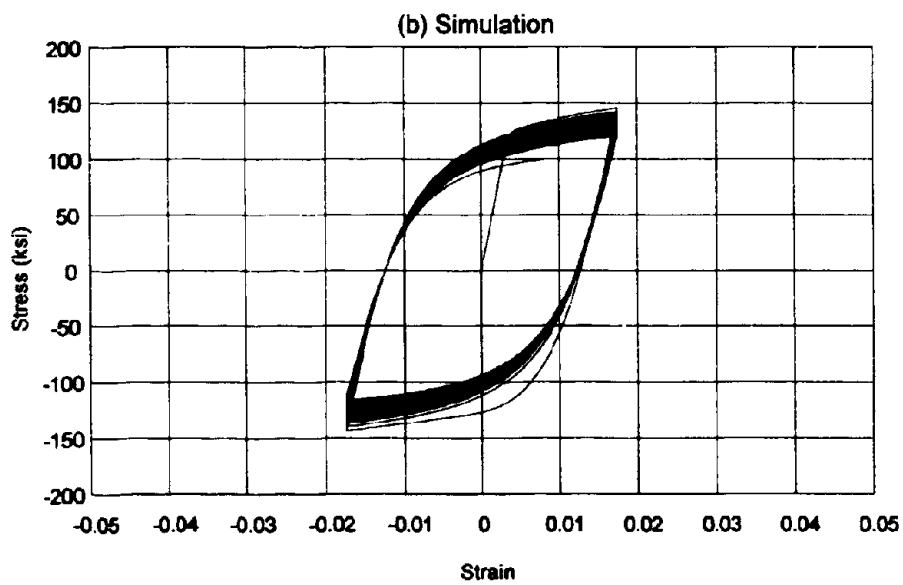
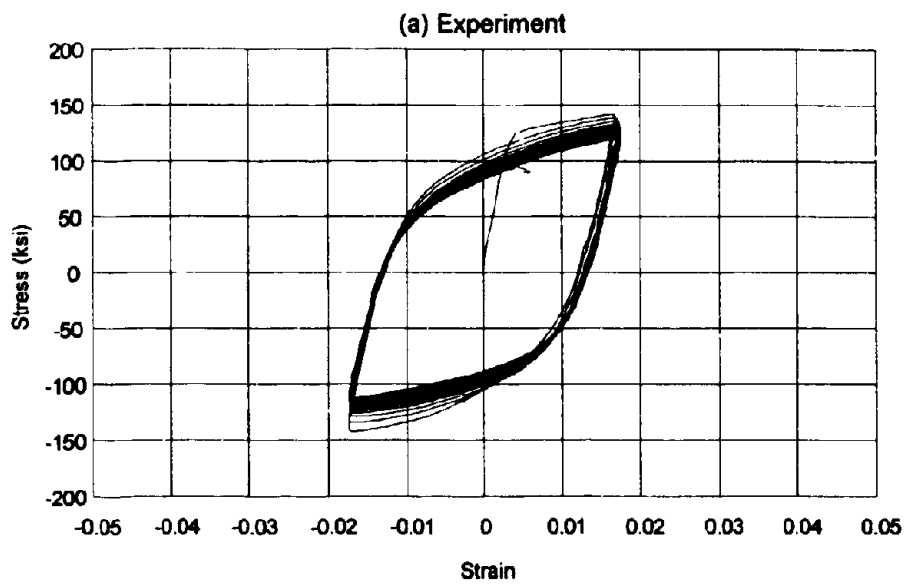


Fig. 2-43 High Strength Bar, Specimen P9

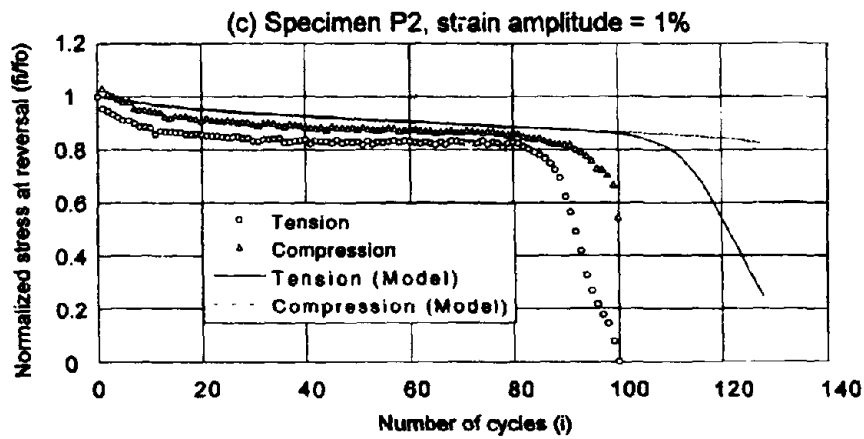
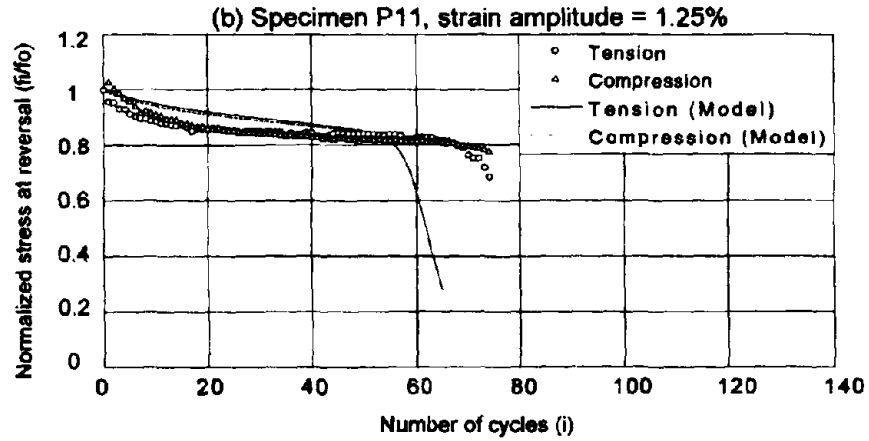
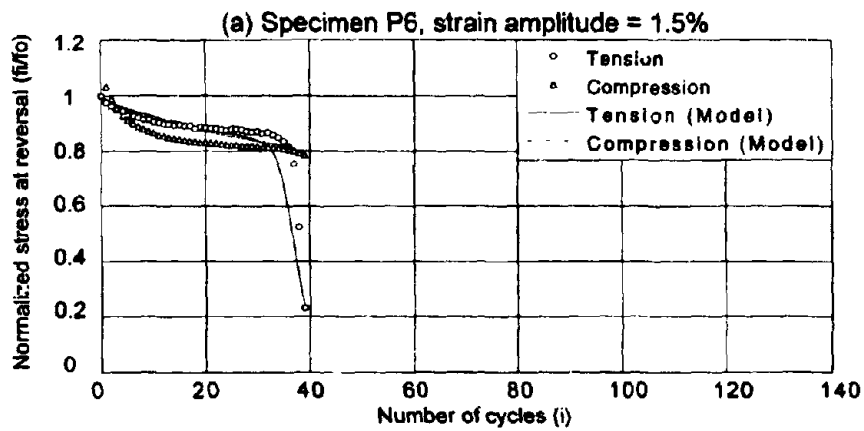


Fig. 2-44 High Strength Bars, Specimens P11, P2 and P3

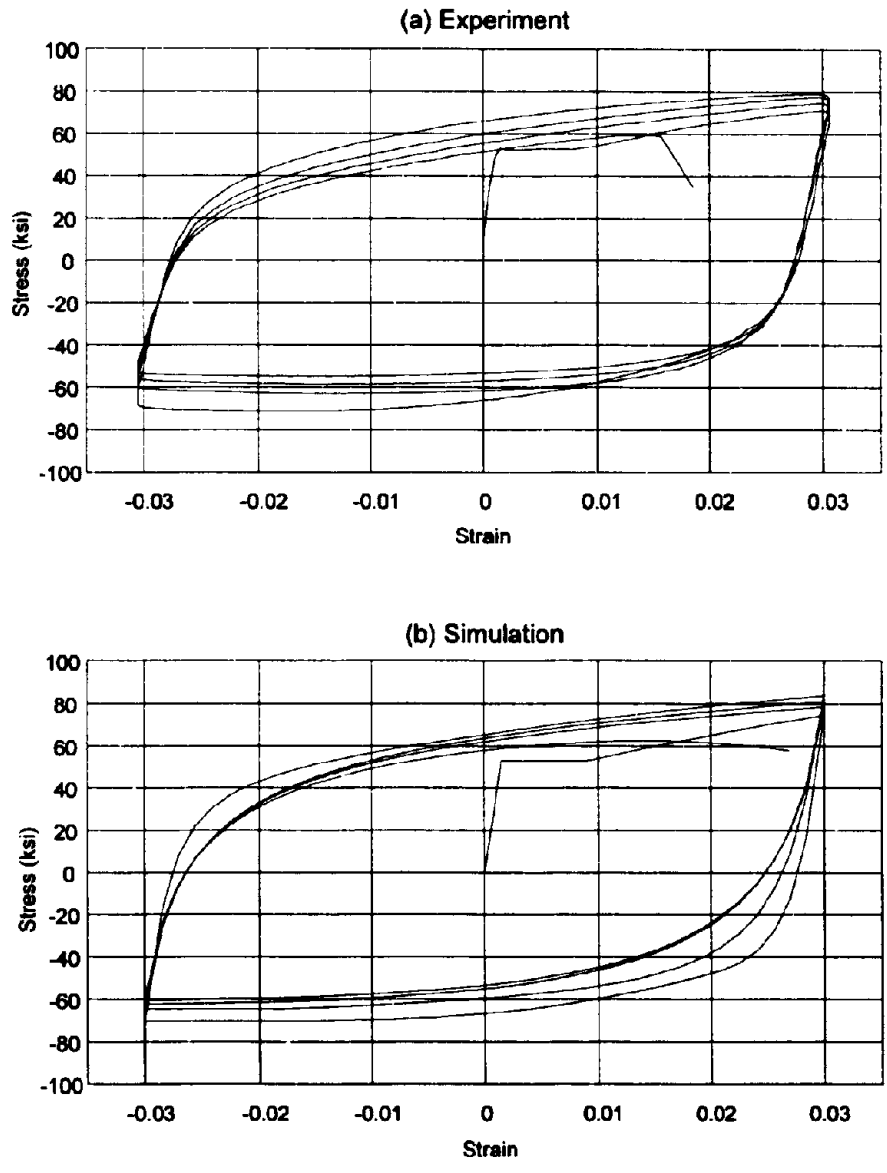


Fig. 2-45 Reinforcing Bar, Specimen R1

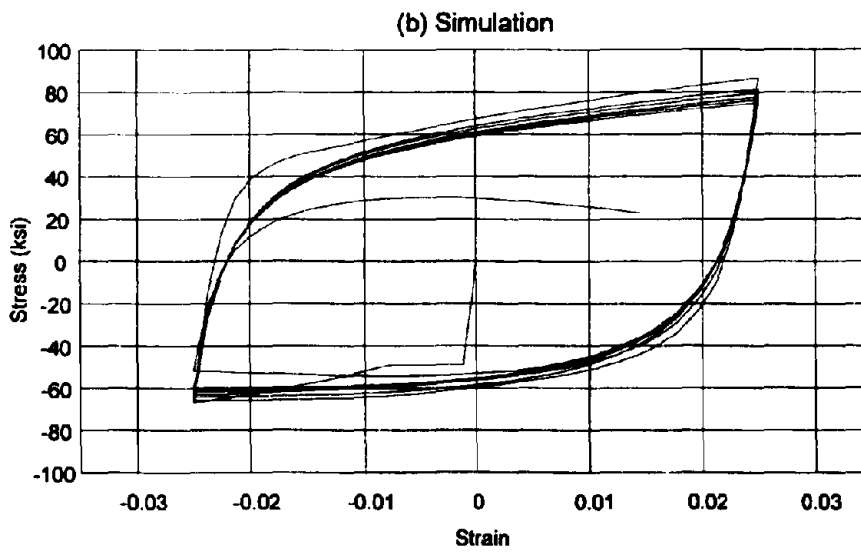
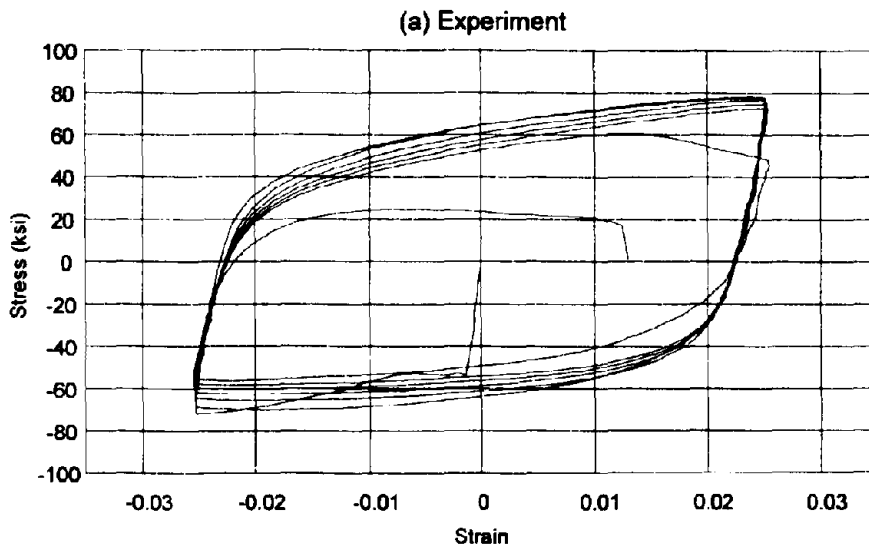


Fig. 2-46 Reinforcing Bar, Specimen R9

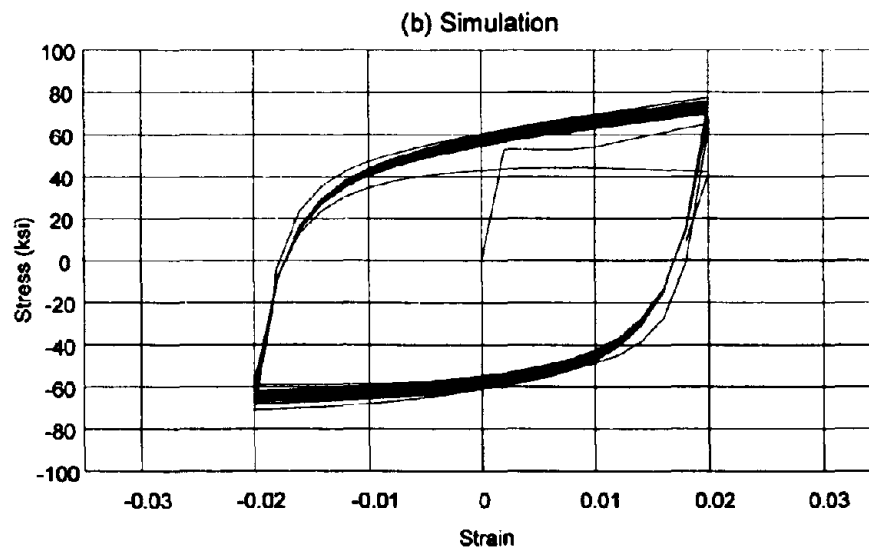
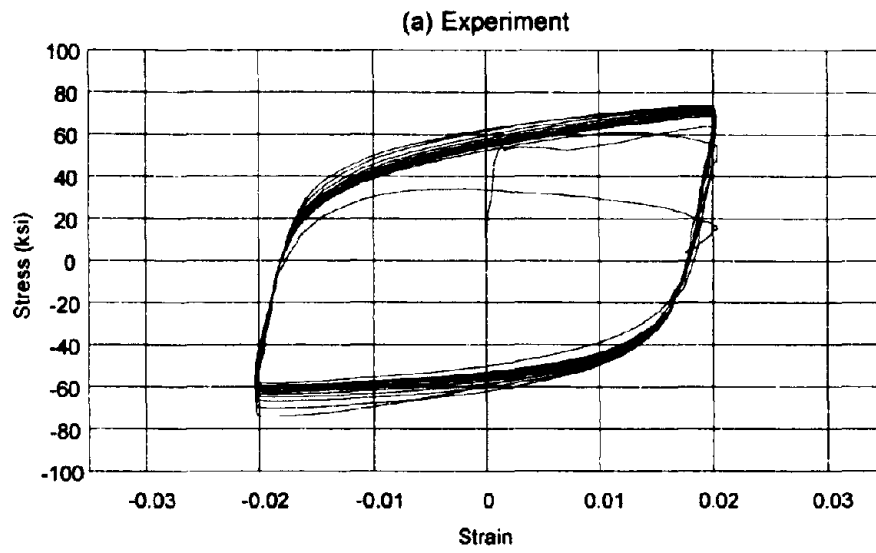


Fig. 2-47 Reinforcing Bar, Specimen R5

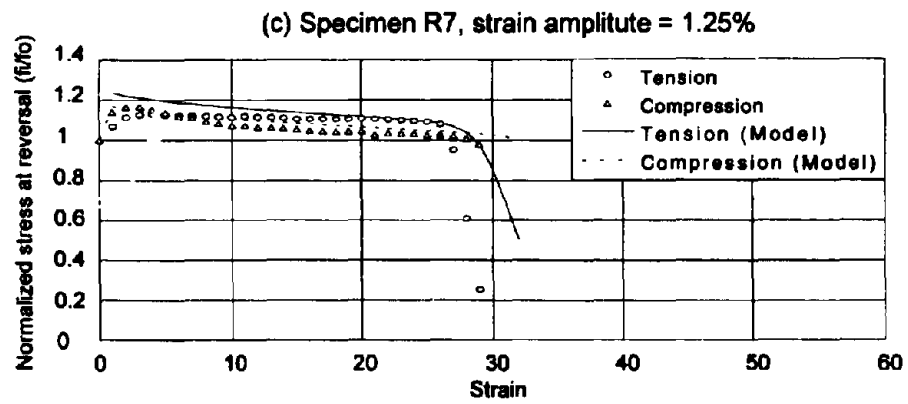
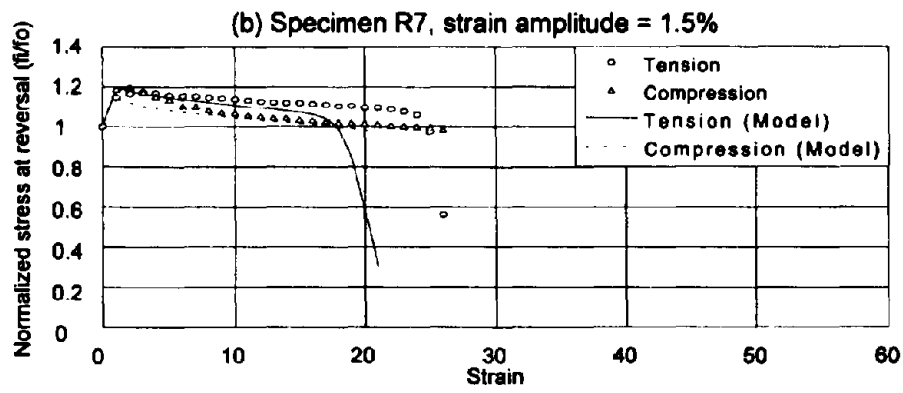
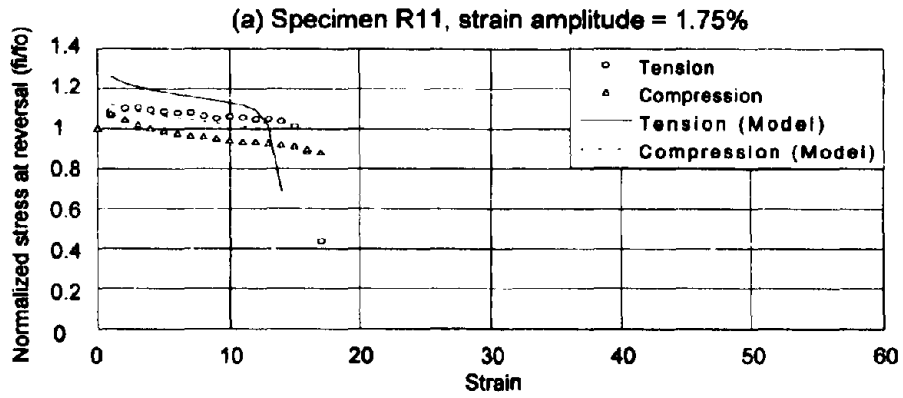


Fig. 2-48 Reinforcing Bars, Specimens R11, R7 and R10

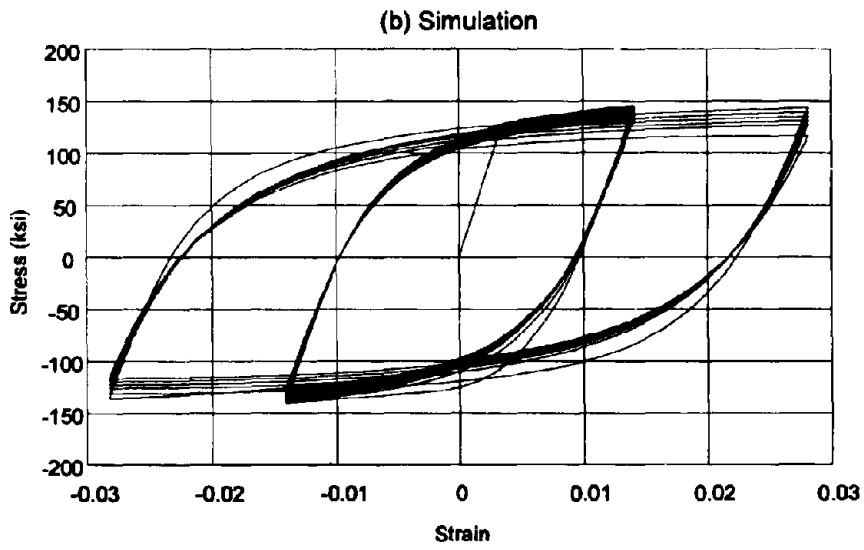
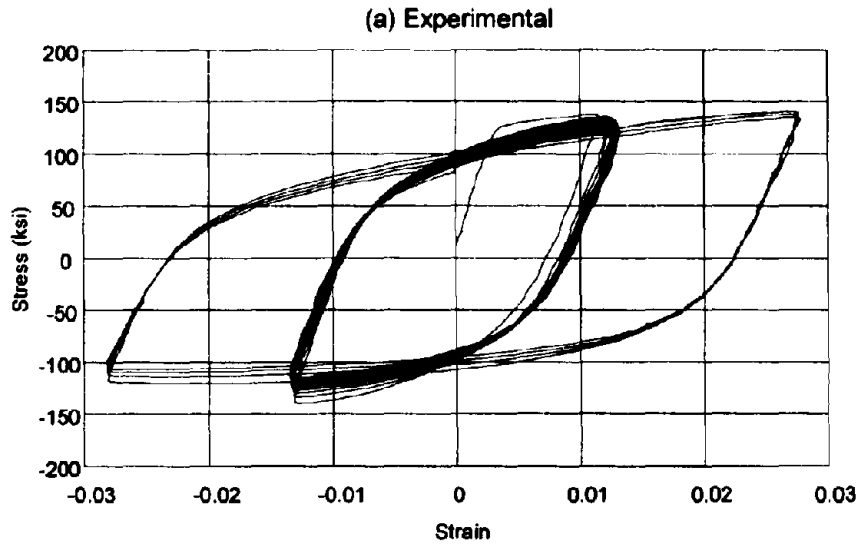


Fig. 2-49 High Strength Bar, Specimen P20, Low-High Step Test

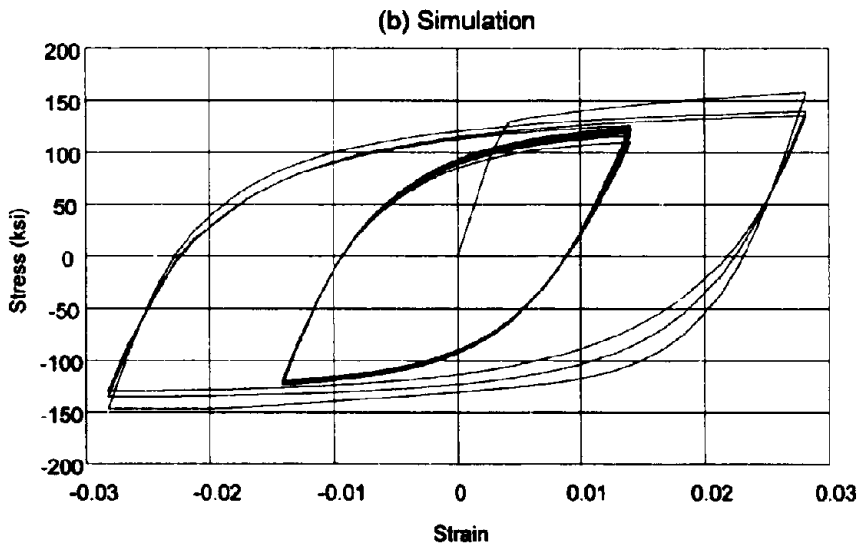
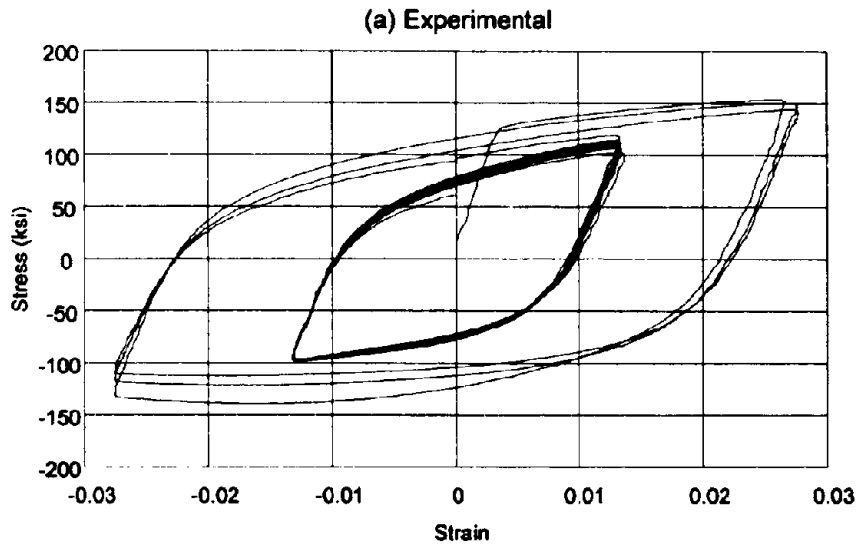


Fig. 2-50 High Strength Bar, Specimen P21, High-Low Step Test

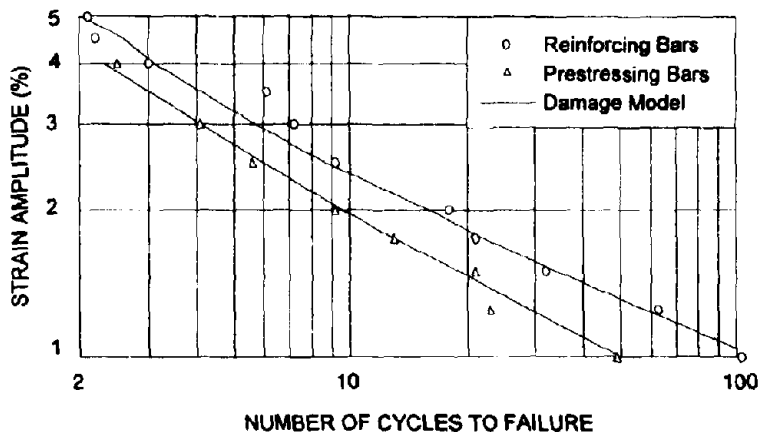


Fig. 2-51 Incipient Failure Prediction

2.8 Strain Rate Effects

It has been shown experimentally (Mander et al., 1984; Soroushian and Choi, 1987) that the rate of strain influences the stress-strain behavior of steel. Soroushian and Choi found that it affects the yield strength, the ultimate strength, the strain at the beginning of strain-hardening and ultimate strain. Their study showed that the effect of strain rate is different on different types of steel. The dynamic effect on the yield strength, as given by Soroushian and Choi, was found to be:

$$\frac{f'_y}{f_y} = (1.46 - 0.451 \times 10^{-6} f_y) + (0.0927 - 0.920 \times 10^{-6} f_y) \log_{10} |\dot{\epsilon}| \quad (2-111)$$

where f'_y = dynamic yield strength, f_y = quasi-static yield strength and $\dot{\epsilon}$ = strain rate in sec^{-1} .

Mander et al. found a simpler relationship expressed as a dynamic magnification factor given by:

$$D_s = 0.966 \left(1 + \left| \frac{\dot{\epsilon}}{5000} \right|^{1/6} \right) \quad (2-112)$$

where D_s = dynamic magnification factor.

2.9 Conclusions

The following conclusions can be drawn from this section:

- (1) A universally applicable model is presented which can simulate the hysteretic behavior of all types of steel. This is particularly important as steels of higher strength are being used today.
- (2) A method for assessing degradation was implemented. Previous models failed in simulating this phenomenon. This characteristic of the hysteretic behavior of steel is important as it also influences the degrading characteristics of a reinforced concrete member. Steel fracture leads to a sudden loss in strength and energy absorption capacity. Therefore reliable modeling of steel behavior is of paramount importance.
- (3) A step by step energy-based damage assessment methodology is presented. This is a simple alternative to the rain flow counting method to assess damage for random cycle behavior.
- (4) Numerous comparisons with experimental results show that both the hysteretic characteristics and prediction of fracture can be appropriately simulated by the models advanced herein.

Section 3

Modeling the Stress-Strain Cyclic Behavior of Concrete

3.1 Introduction

In the context of a computer program for the simulation of the cyclic behavior of concrete members, the implementation of all the hysteretic properties of confined and unconfined concrete becomes an important part. Many investigators have devoted their time to define experimentally and analytically the behavior of concrete.

In this section an advanced rule-based model, to simulate the hysteretic behavior of confined and unconfined concrete in both cyclic compression and tension for both ordinary as well as high strength concrete, is developed. Tension cyclic modeling is important when calculating deformations due to shear as in the Modified Compression Field Theory (Collins and Mitchell, 1991). The basic elements of a rule-based model are identified, which can be applied to any general purpose model. Fundamental ideas about the nature of degradation within partial looping is also dealt with; most models deal with degradation in terms of complete cycles without considering the event of incomplete cycles (as this is the normal type of experimental data available).

A reinforced concrete structure subjected to working loads might show cracking in some elements. Experimental tests (Yankelevsky and Reinhardt, 1987b) have shown that concrete in tension shows a cyclic behavior similar to that in compression. Thus, it was considered necessary to describe analytically the hysteretic behavior of concrete with excursions in both compression and tension. Particular emphasis has also been paid to the transition between opening and closing of cracked zones. This phenomenon has not been adequately addressed in previous models. Most existing models assume sudden crack closure with a rapid change in section modulus. Such a rapid change is not supported by experiments on lightly loaded columns.

The desirable characteristics of a general stress-strain relation for concrete are: (1) the slope at the origin is E_c , (2) it should show a peak at the point $(\epsilon'_{cc}, f'_{cc})$, (3) it should describe both the ascending and the descending parts of the concrete behavior and (4) it should have control over the descending (softening) branch. Control over the slope of the descending branch is important, because its shape is dependent on factors such as the degree of confinement and the strength of the concrete. Experiments have shown that for unconfined concrete, both the ascending and descending parts of the curve become steeper (Saenz, 1964). Tests have also shown that the slope of the descending branch curve for confined concrete can become very flat (Somes, 1970; Iyengar et al., 1970; Burdette, 1971; Kent and Park, 1971; Scott et al., 1982; Ahmad and Shah, 1982; Mander et al., 1988b).

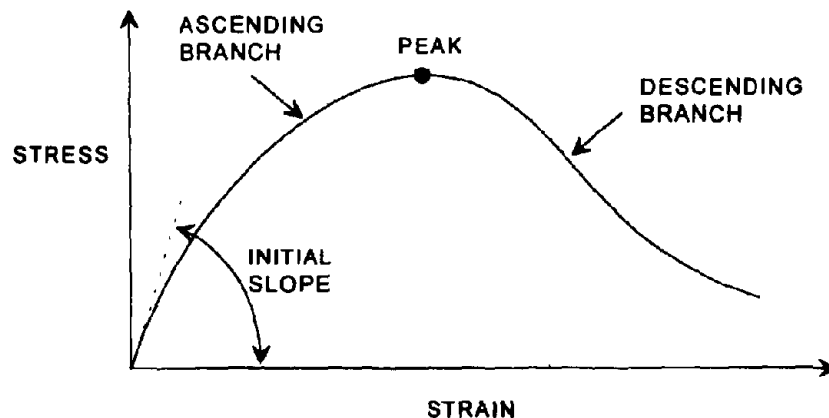


Fig. 3-1 Characteristics of the Stress-Strain Relation for Concrete

3.2 Review of Previous Work in Stress-Strain Relations for Concrete

3.2.1 Monotonic Compression Stress-Strain Equation

Historically, it has been commonly accepted that the envelope curve for the cyclic compressive behavior of confined and unconfined concrete is the monotonic compressive curve. To develop a suitable hysteretic model it is necessary to have a monotonic stress-strain curve to describe the envelope curve.

The properties of the monotonic stress-strain curve of concrete has been the subject of numerous papers. One of the first to proposed a formula to represent the stress-strain relationship in concrete was Bach (Smith and Young, 1955; Popovics, 1970). He presented a simple power function in the form:

$$y = kx^m \quad (3-1)$$

where,

$$y = \frac{f_c}{f'_{cc}}$$

$$x = \frac{\epsilon_c}{\epsilon'_{cc}}$$

in which ϵ_c = concrete strain, f_c = concrete stress, f'_{cc} = confined concrete strength (peak ordinate), ϵ'_{cc} = the corresponding strain (peak abscissa), k = constant determined by curve fitting, m = power with a value less than one.

The values of m recommended by Smith and Young (1955) where from 0.45 to 0.70, the higher values been for higher values of compressive strength. This equation is not appropriate to describe the monotonic behavior of concrete because: (1) it implies an infinite tangent at the origin, (2) it does not have a peak at $\epsilon_c = \epsilon'_{cc}$ and, (3) it does not have a descending branch, to describe the behavior after the peak stress has been reached. This equation is shown in Fig. 3-2.

Young (1960) analyzed three equations, all of which have descending parts at least in the neighborhood after the peak,

$$y = x[(n-2)x^2 - (2n-3)x + n] \quad (3-2)$$

$$y = xe^{(1-x)} \quad (3-3)$$

$$y = \sin\left(\frac{\pi}{2}x\right) \quad (3-4)$$

where, $n = \frac{E_c \epsilon'_{cc}}{f'_{cc}}$

in which E_c is the initial modulus of elasticity, x and y were defined in Eq. (3-1). Eqs. (3-3) and (3-4) have a fixed value of n , that is $n = e = 2.718$ and $n = \pi/2$, respectively. Eq. (3-2), on the other hand, can be adjusted by letting n have different values; this is shown in Fig. 3-3. Because Eq. (3-2) is a cubic polynomial it shows a local minimum that makes the equation unsuitable for values of n greater than about 2.4. Warner, 1969; and Al-Noury and

Chen, 1982, used this equation for the ascending branch, but they used a parabola for the descending branch.

Desayi and Krishnan (1964) proposed an equation in the form:

$$y = \frac{2x}{1+x^2} \quad (3-5)$$

This equation has a fixed value of $n = 2$. The shape of this equation after the peak has the correct tendency, and some generalizations of this equation were proposed afterward.

Kabaila (1964), discussing on the equation by Desayi and Krishnan, proposed a quartic polynomial relationship in the form:

$$y = 2.0x - 1.189x^2 + 0.1763x^3 + 0.0027x^4 \quad (3-6)$$

This equation also shows a fixed value of $n = 2$, and it has a minimum near $x = 3$, so the equation could only be used for values of x less than this value. The peak of this equation is not at $x = 1$, but rather at $x = 1.1333$. This type of equation could well fit an experiment but could not be used as a general equation.

Saenz (1964), also discussing on the equation proposed by Desayi and Krishnan, presents several other equations:

$$y = x(2-x) \quad (3-7)$$

This equation had been adopted by the European Concrete Committee and was used by many investigators to represent the ascending branch of the monotonic stress-strain curve. This parabola is a particular case of the cubic equation, Eq. (3-2), when the value of n is taken as 2.

Saenz also presents another two equations which generalize the equation proposed by Desayi and Krishnan, Eq.(3-5),

$$y = \frac{nx}{1+(n-2)x+x^2} \quad (3-8)$$

This equation has control of the initial tangent parameter n , by taking $n = 2$, it is reduced to Eq. (3-5). The behavior of this equation is presented in Fig. 3-4.

The second equation proposed by Saenz goes a step ahead, by allowing control over both the ascending and the descending branch. Control over the descending branch is

achieved by defining a point on the descending branch. The equation proposed, in the nomenclature used here, is expressed as:

$$y = \frac{nx}{1 + (R+n-2)x - (2R-1)x^2 + Rx^3} \quad (3-9)$$

where: $R = \frac{n(R_f - 1)}{(R_\epsilon - 1)^2} - \frac{1}{R_\epsilon}$

$$R_f = \frac{f'_{cc}}{f_f}$$

$$R_\epsilon = \frac{\epsilon_f}{\epsilon_o}$$

(ϵ_f, f_f) = a point on the descending branch of the curve.

This equation is presented in a very convenient form, because its parameters have physical meaning. The value of R is defined by a point on the descending branch of the curve. The behavior of this equation is presented in Fig. 3-6. When the value of R is taken as zero, Eq. (3-9) reduces to Eq. (3-8), and if in addition the value of n is set to two, it then reduces to the Desayi-Krishnan equation, Eq. (3-5).

Tulin and Gerstle (1964), also commenting on the Desayi-Krishnan equation proposed the equation:

$$y = \frac{3x}{2+x^3} \quad (3-10)$$

This equation is a particular case of Eq. (3-8) for a value of $n = 1.5$.

They also suggested a more general expression as:

$$y = \frac{(a+1)x}{a+x^r} \quad (3-11)$$

They stated that the constants a and r must be selected for best fit. They did not present any comments regarding how this fitting could be done, but it can be relatively easily be shown that if this equation is to have a peak at $x=1$, then r should be taken as $r = a + 1$ and it can be written in the following form.

$$y = \frac{rx}{r-1+x^r} \quad (3-12)$$

where $r = \frac{n}{n-1}$

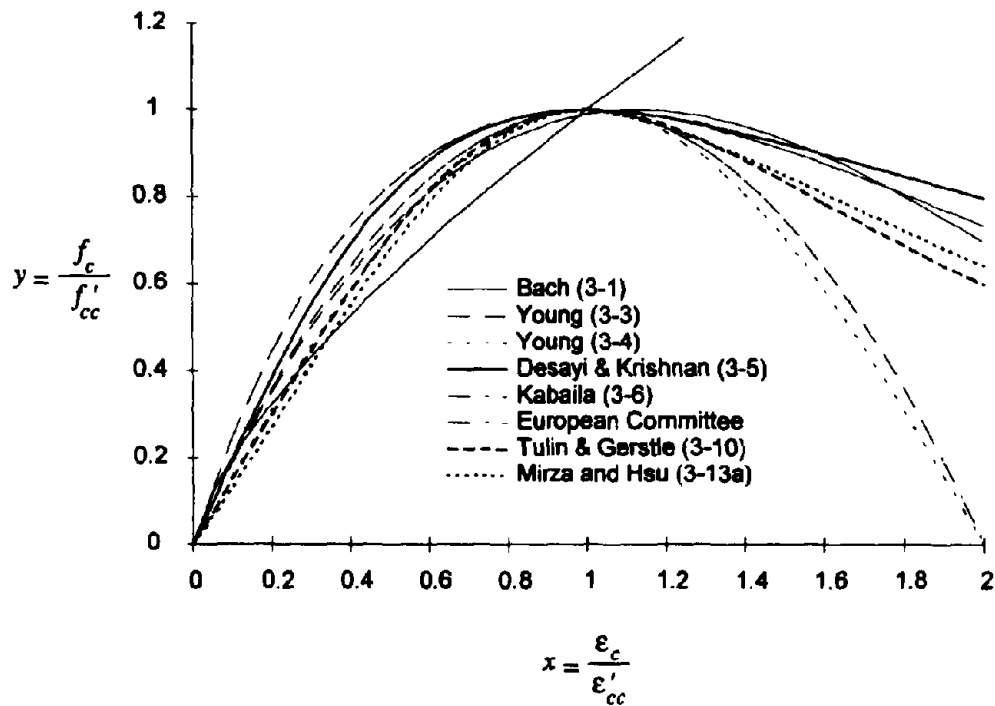


Fig. 3-2 Comparison of Different Stress-Strain Equations for Concrete

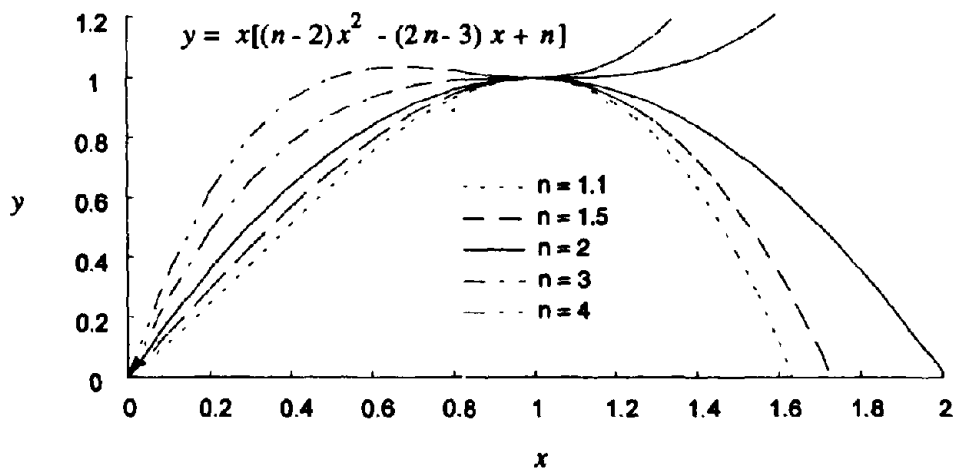


Fig. 3-3 Equation Suggested by Young (1960)

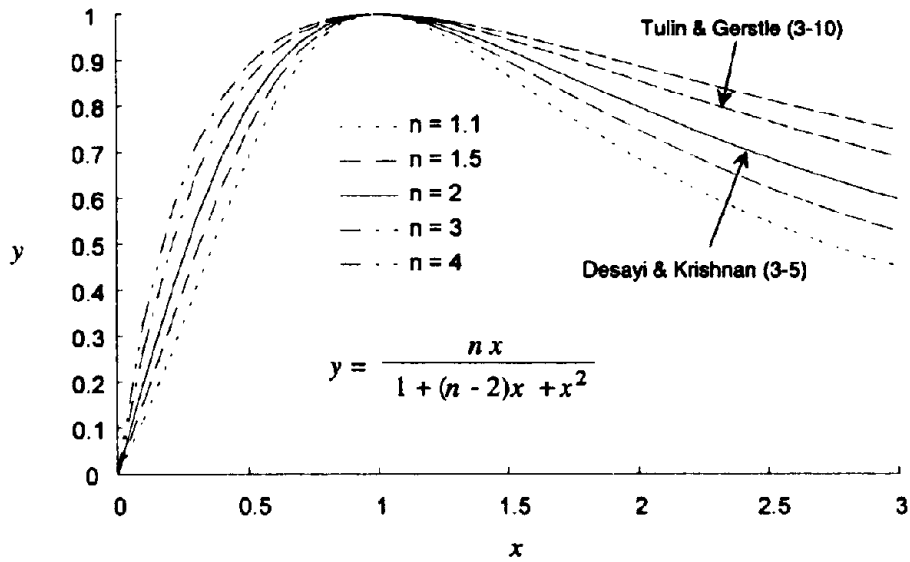


Fig. 3-4 Equation Suggested by Saenz (1964)

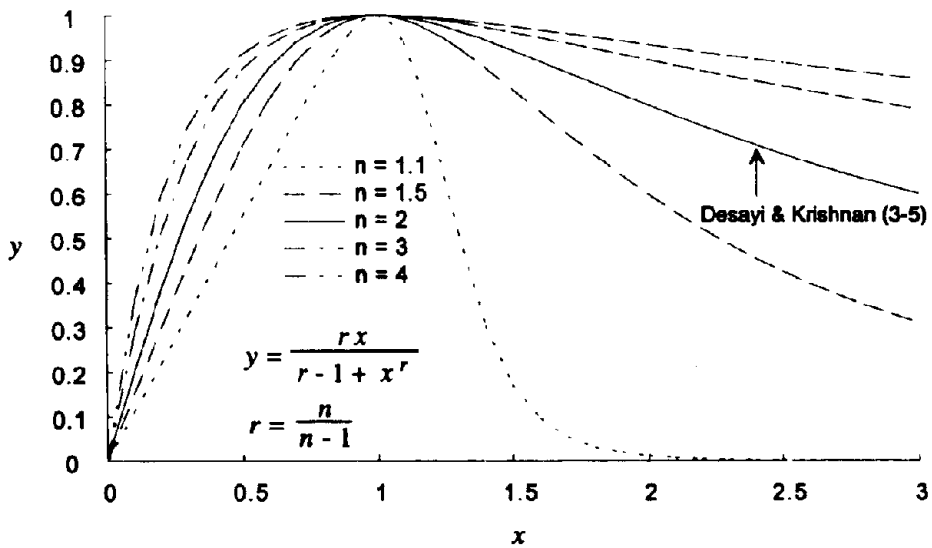


Fig. 3-5 Equation Proposed by Popovics (1973)

This equation known as Popovics' (1973) (Mander et al., 1988a; Carreira and Chu, 1985 and 1986a; Tsai, 1988) has proven to be very useful in describing the monotonic compressive stress-strain curve for concrete. This equation is shown in Fig. 3-5.

Mirza and Hsu (1969) used a relationship in the form:

$$y = \sin\left(\frac{\pi}{2}x\right) + 0.2x(x-1)(e^{1-x} - 1) \quad x \in [0, 1] \quad (3-13a)$$

$$y = 0.226 + 2.157x - 1.91x^2 + 0.596x^3 - 0.064x^4 \quad x \in (1, 3.4) \quad (3-13b)$$

This is a very complex relation and it does not possess control over the initial slope.

Sargin (taken from Ghosh, 1970) proposed a very general formulation, expressed in the notation used here:

$$y = \frac{nx + (D-1)x^2}{1 + (n-2)x + Dx^2} \quad (3-14)$$

where, D = factor controlling the slope of the descending branch.

This equation is another generalization of that by Saenz, Eq. (3-8). By taking D as one, Eq. (3-14) reduces to Eq. (3-8). This equation, as Eq. (3-9), also has control over the descending branch. This equation, nevertheless, can give negative values of stress, as can be seen if Fig. 3-7.

Fafitis and Shah (1985) proposed an equation of the form:

$$y = 1 - (1-x)^n \quad x \in [0, 1] \quad (3-15a)$$

$$y = e^{-a(x-1)^{1.15}} \quad x > 1 \quad (3-15b)$$

In this equation the value of a depends on the amount and spacing of transverse reinforcement.

A modification to the Popovics' relation, Eq. (3-12), was suggested by Thorenfeldt, Tomaszewicz and Jensen (Collins and Mitchell, 1991) in the form:

$$y = \frac{rx}{r-1+x^{rk}} \quad (3-16)$$

In this equation k takes a value of 1 for values of x less than 1 and values greater than 1 for values of x greater than 1. This means that by adjusting the value of k the descending branch can be made steeper. This approach can be used for unconfined concrete where for high values of concrete the descending branch becomes very steep, but could not be used for

the case of confined concrete where the descending branch needs to be flattened. This equation presents a slope discontinuity at the peak value and the value of k is not continuous.

Tsai (1988) recommended a generalized form of the Popovics' equation,

$$y = \frac{nx}{1 + \left(n - \frac{r}{r-1}\right)x + \frac{x^r}{r-1}} \quad (3-17)$$

where, r = factor to control the descending branch of the stress-strain relation. By taking $n = \frac{r}{r-1}$ Eq. (3-17) reduces to Popovics', Eq. (3-12), and by taking $r = 2$ it is reduced to Saenz', Eq. (3-8). The behavior of this equation is shown in Fig. 3-8.

The continuous equations reviewed can be classified in the following way:

(a) Equations to represent only the ascending branch:

- | | |
|----------------------|------------|
| (1) Bach | Eq.(3-1) |
| (2) Mirza and Hsu | Eq.(3-13a) |
| (3) Fafitis and Shah | Eq.(3-15a) |

(b) Equations to represent the ascending branch and the descending branch without having control on the initial slope:

- | | |
|-------------------------|-----------|
| (1) Young | Eq.(3-3) |
| (2) Young | Eq.(3-4) |
| (3) Desayi and Krishnan | Eq.(3-5) |
| (4) Kabaila | Eq.(3-6) |
| (5) Saenz | Eq.(3-7) |
| (6) Tulin and Gerstle | Eq.(3-10) |

(c) Equations to represent the ascending branch and the descending branch having control on the initial slope:

- | | |
|--------------|-----------|
| (1) Young | Eq.(3-2) |
| (2) Saenz | Eq.(3-8) |
| (3) Popovics | Eq.(3-12) |

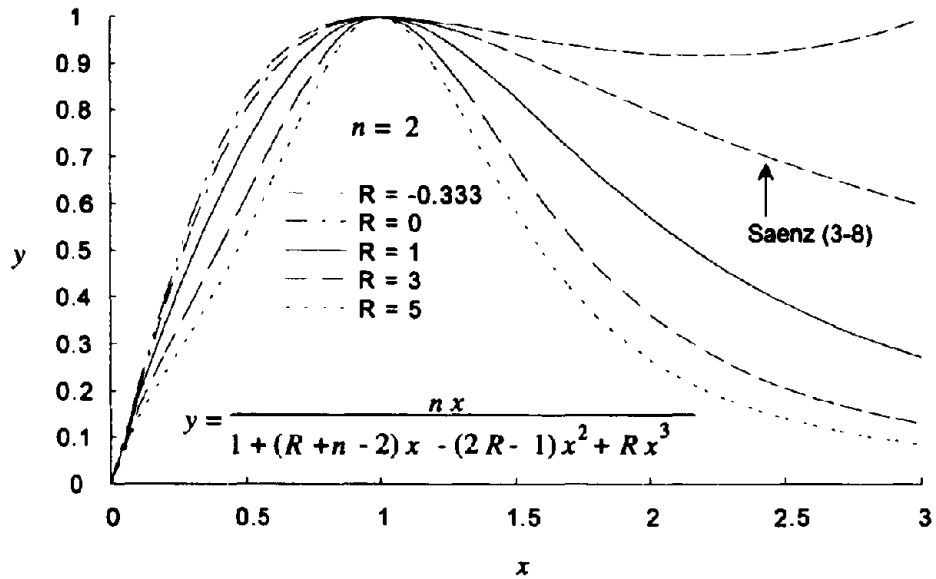


Fig. 3-6 Equation Suggested by Saenz (1964)

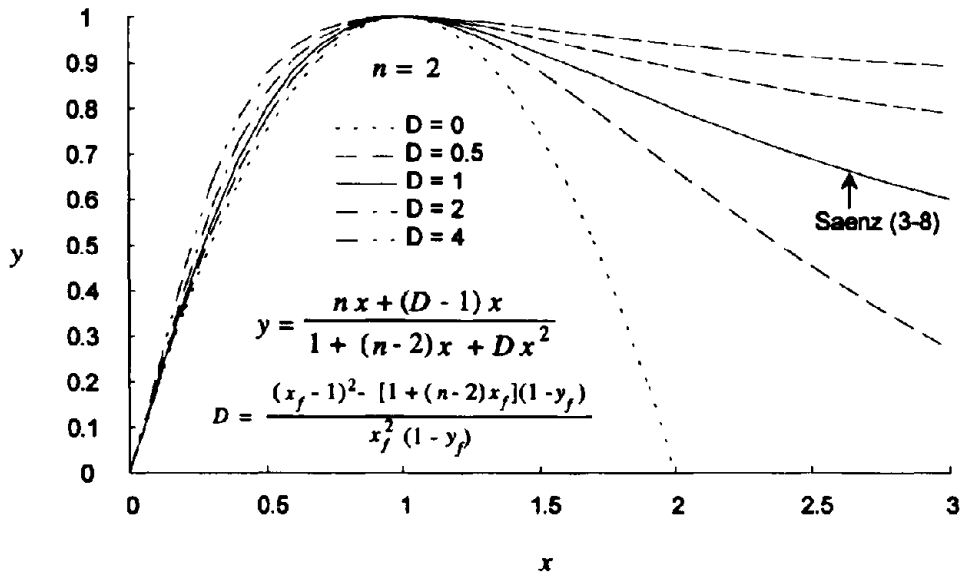


Fig. 3-7 Equation Suggested by Sargin (1968)

Tsai's Equation

$$y = \frac{nx}{1 + \left(n - \frac{r}{r-1}\right)x + \frac{x^r}{r-1}}$$

$$\frac{dy}{dx} = \frac{n(1-x^r)}{\left[1 + \left(n - \frac{r}{r-1}\right)x + \frac{x^r}{r-1}\right]^2}$$

$$\lim_{r \rightarrow 1} 1 + \left(n - \frac{r}{r-1}\right)x + \frac{x^r}{r-1} = 1 + (n-1)x + x \ln x$$

$$\lim_{x \rightarrow 0} x \ln x = 0$$

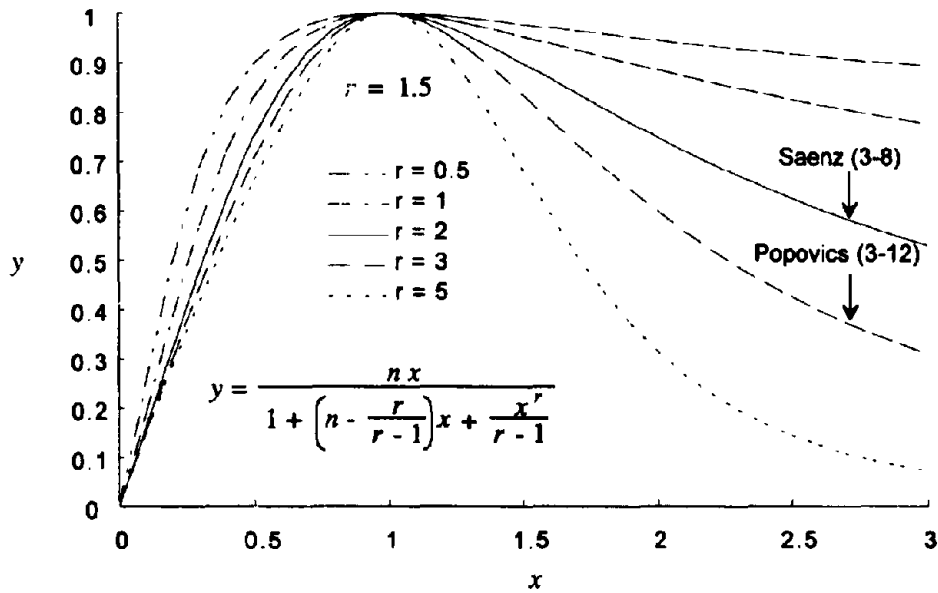


Fig. 3-8 Equation Proposed by Tsai (1988)

(d) Equations that have control on both the ascending branch (initial slope) and the descending branch:

(1) Saenz Eq.(3-9)

(2) Sargin Eq.(3-14)

(3) Tsai Eq.(3-17)

It should be noted that it is only Tsai's equation that gives reasonable control for all possibilities, whereas, as seen in Fig. 3-6, in Saenz's equation $y > 1$ under certain circumstances, and in Sargin's equation $y < 0$.

The equations of the last type are the most flexible and general, and by comparing their behavior it was concluded that Tsai's equation is the most suitable to represent the behavior of both confined and unconfined concrete.

$$y = \frac{nx}{1 + \left(n - \frac{r}{r-1}\right)x + \frac{x^r}{r-1}} \quad (3-17)$$

Furthermore, Mander's original concrete model (1988a) uses Popovics' equation which is really a special case of Tsai's equation. By adopting Tsai's equation and setting $n = \frac{r}{r-1}$, all of the standard data calibrated for Mander's confined concrete model can continue to be utilized. However, the advantage of using this new relationship gives the added flexibility of controlling the slope of the falling branch curve. This is particularly necessary for high strength concrete, and also when high strength transverse confining reinforcement is used. The model of Mander et al. (1988a) in its present form has difficulty coping with these two phenomena.

3.2.2 Initial Modulus of Elasticity

Several formulae for the modulus of elasticity have been proposed in the literature. Pauw (1960) reported several of these formulae. The first of these equations is the following:

$$E_c = 1,000f'_c \quad (3-18)$$

This equation was in the ACI building code before 1963. Although this equation has been used extensively because of its simplicity to represent the modulus of elasticity of normal strength concrete, it overestimates the value of E_c for high strength concrete.

An equation reported by Pauw which was proposed by the ACI-ASCE Committee 323 to estimate the value of E_c for normal strength concrete is:

$$E_c = 1,800,000 + 500f'_c \quad \text{psi} \quad (3-19)$$

$$E_c = 12,400 + 500f'_c \quad \text{MPa}$$

Another equation presented by Pauw which was proposed by Jensen in 1943, and is applicable only to normal strength concrete is:

$$E_c = \frac{6,000,000}{1 + \frac{2000}{f'_c}} \quad \text{psi} \quad (3-20)$$

$$E_c = \frac{41,000}{1 + \frac{14}{f'_c}} \quad \text{MPa}$$

The following linear relationship was developed by Lyse (Pauw, 1960), which is similar to Eq. (3-19).

$$E_c = 1,800,000 + 460f'_c \quad \text{psi} \quad (3-21)$$

$$E_c = 12,400 + 460f'_c \quad \text{MPa}$$

An equation proposed by Pauw (1960) that was adopted into the ACI building code since 1963, is applicable to both normal and lightweight concrete.

$$E_c = 33w^{1.5} \sqrt{f'_c} \quad (3-22)$$

in which f'_c is in *psi* and w in *pcf*.

For normal weight concrete, the ACI code assumes a weight of 145 *pcf* and proposes the following equation:

$$E_c = 57000 \sqrt{f'_c} \quad \text{psi} \quad (3-23)$$

$$E_c = 4,700 \sqrt{f'_c} \quad \text{MPa}$$

Pauw also presented another two formulae:

$$E_c = 13.82w^{1.79} f'_c{}^{0.44} \quad (3-24)$$

$$E_c = 158.1w^{1.51}f_c'^{0.30} \quad (3-25)$$

in which f_c' is in *psi* and w in *pcf*.

This last equation was obtained when excluding the data for concretes having a compressive strength less than 2000 *psi*. And according to the author it is believed to be more reliable than the one adopted by the ACI code. Note the smaller exponent.

Saenz (1964) suggested the following formula for the modulus of elasticity:

$$E_c = \frac{10^5 \sqrt{f_c'}}{1 + 0.006 \sqrt{f_c'}} \quad \text{psi}$$

$$E_c = \frac{8,300 \sqrt{f_c'}}{1 + 0.072 \sqrt{f_c'}} \quad \text{MPa} \quad (3-26)$$

Carrasquillo et al. (1981) recommended the following expression for normal weight concrete:

$$E_c = 40000 \sqrt{f_c'} + 1000000 \quad \text{psi}$$

$$E_c = 3300 \sqrt{f_c'} + 6900 \quad \text{MPa} \quad (3-27)$$

In more recent years, Klink (1985) has shown that the initial elastic modulus is greater than that calculated with Pauw's equation, Eq. (3-22). In addition, he showed that the elastic modulus varies across the section, being the smaller values for the points near the sides of the specimen. The equation Klink proposes is:

$$E_c = 14.6w^{1.75} \sqrt{f_c'} \quad (3-28)$$

in which f_c' is in *psi* and w in *pcf*. This equation gives values of E_c that are about 50 percent higher than those calculated for the other formulae, for normal weight concrete.

3.2.3 Strain at Peak Stress for Unconfined Concrete

The strain ϵ_c' corresponding to the maximum stress f_c' for unconfined concrete has been found to be a function of the maximum stress, although some authors have taken it as a constant value, normally 0.002 (Park and Paulay, 1975).

Saenz (1964) proposed a function in the form:

$$\epsilon_c' = (31.5 - f_c'^{0.25}) f_c'^{0.25} 10^{-5} \quad \text{psi}$$

$$\epsilon_c' = (14.3 - 29.4 f_c'^{0.25}) f_c'^{0.25} 10^{-5} \quad \text{MPa} \quad (3-29)$$

Popovics (1970) reviewed some other expressions:

$$\begin{aligned} \epsilon'_c &= 0.000546 + 2.56 \times 10^{-7} f'_c \quad \text{psi} \\ \text{(Ros)} \quad \epsilon'_c &= 0.000546 + 3.71 \times 10^{-5} f'_c \quad \text{MPa} \end{aligned} \quad (3-30)$$

$$\begin{aligned} \epsilon'_c &= \frac{f'_c}{680,000 + 260f'_c} \quad \text{psi} \\ \text{(Brandtzaeg)} \quad \epsilon'_c &= \frac{f'_c}{4,690 + 260f'_c} \quad \text{MPa} \end{aligned} \quad (3-31)$$

$$\begin{aligned} \epsilon'_c &= 3.7 \times 10^{-5} \sqrt{f'_c} \quad \text{psi} \\ \text{(Jager)} \quad \epsilon'_c &= 4.5 \times 10^{-4} \sqrt{f'_c} \quad \text{MPa} \end{aligned} \quad (3-32)$$

$$\begin{aligned} \epsilon'_c &= \frac{f'_c}{790,000 + 395f'_c} \quad \text{psi} \\ \text{(Hungarian Code)} \quad \epsilon'_c &= \frac{f'_c}{5,450 + 395f'_c} \quad \text{MPa} \end{aligned} \quad (3-33)$$

Carreira and Chu (1985) proposed an expression based on regression analysis:

$$\begin{aligned} \epsilon'_c &= (168 + 4.88 \times 10^{-3} f'_c) \times 10^{-5} \quad \text{psi} \\ \epsilon'_c &= (168 + 0.708 f'_c) \times 10^{-5} \quad \text{MPa} \end{aligned} \quad (3-34)$$

Sulayfani and Lamirault (1987) suggested the following expression:

$$\begin{aligned} \epsilon'_c &= 2.5 \times 10^{-4} f_c'^{0.246} \quad \text{psi} \\ \epsilon'_c &= 8.5 \times 10^{-4} f_c'^{0.246} \quad \text{MPa} \end{aligned} \quad (3-35)$$

It has been found that the observed strain at peak stress depends in factors such as humidity, rate of loading and age [Hughes and Gregory (1972); Dilger, Koch and Kowalczyk (1984); Soroushian, Choi and Alhamad (1986); Mander et al. (1984); Bischoff and Perry (1991)].

Popovics (1970) reviewed some other expressions:

$$\begin{aligned} \epsilon'_c &= 0.000546 + 2.56 \times 10^{-7} f'_c \quad \text{psi} \\ \epsilon'_c &= 0.000546 + 3.71 \times 10^{-5} f'_c \quad \text{MPa} \end{aligned} \quad (3-30)$$

$$\begin{aligned} \epsilon'_c &= \frac{f'_c}{680,000 + 260 f'_c} \quad \text{psi} \\ \epsilon'_c &= \frac{f'_c}{4,690 + 260 f'_c} \quad \text{MPa} \end{aligned} \quad (3-31)$$

$$\begin{aligned} \epsilon'_c &= 3.7 \times 10^{-5} \sqrt{f'_c} \quad \text{psi} \\ \epsilon'_c &= 4.5 \times 10^{-4} \sqrt{f'_c} \quad \text{MPa} \end{aligned} \quad (3-32)$$

$$\begin{aligned} \epsilon'_c &= \frac{f'_c}{790,000 + 395 f'_c} \quad \text{psi} \\ \epsilon'_c &= \frac{f'_c}{5,450 + 395 f'_c} \quad \text{MPa} \end{aligned} \quad (3-33)$$

Carreira and Chu (1985) proposed an expression based on regression analysis:

$$\begin{aligned} \epsilon'_c &= (168 + 4.88 \times 10^{-3} f'_c) \times 10^{-5} \quad \text{psi} \\ \epsilon'_c &= (168 + 0.708 f'_c) \times 10^{-5} \quad \text{MPa} \end{aligned} \quad (3-34)$$

Sulayfani and Lamirault (1987) suggested the following expression:

$$\begin{aligned} \epsilon'_c &= 2.5 \times 10^{-4} f_c'^{0.246} \quad \text{psi} \\ \epsilon'_c &= 8.5 \times 10^{-4} f_c'^{0.246} \quad \text{MPa} \end{aligned} \quad (3-35)$$

It has been found that the observed strain at peak stress depends in factors such as humidity, rate of loading and age [Hughes and Gregory (1972); Dilger, Koch and Kowalczyk (1984); Soroushian, Choi and Alhamad (1986); Mander et al. (1984); Bischoff and Perry (1991)].

3.2.4 Characteristic of the Descending Branch of the Monotonic Stress-Strain Curve for Unconfined Concrete

Popovics' equation, Eq. (3-12), has been used extensively in representing the complete stress-strain relationship for unconfined and confined concrete. The descending branch of this equation is very sensitive to the value of n (initial stiffness ratio), so if a good estimation of the descending branch is needed it is necessary to choose this value carefully, but by doing so the initial slope is not maintained. Another way of overcoming this problem has been to use a piecewise continuous curve [Eqs. (3-13) and (3-14)].

Kent and Park (1971) proposed a descending linear relationship passing through the point (ϵ_f, f_f) with:

$$\epsilon_f = \frac{3 + 0.002 f'_c}{f'_c - 1,000} \quad \text{psi} \quad (3-36a)$$

$$\epsilon_f = \frac{0.02 + 0.002 f'_c}{f'_c - 6.9} \quad \text{MPa} \quad (3-36b)$$

$$f_f = 0.5 f'_c$$

Sulayfani and Lamirault (1987) suggested a point on the descending curve as:

$$\epsilon_f = (1.68 - \frac{f'_c}{18,100}) \epsilon'_c \quad \text{psi} \quad (3-37a)$$

$$\epsilon_f = (1.68 - \frac{f'_c}{125}) \epsilon'_c \quad \text{MPa} \quad (3-37b)$$

$$f_f = 0.85 f'_c$$

Muguruma et al. (1991) suggested a linear relation for the descending branch that passes through the point (ϵ_f, f_f) :

$$\epsilon_f = 0.004 \quad (3-38a)$$

$$f_f = 0 \quad (3-38b)$$

Sakai et al. (1991) proposed a linear descending branch that passes through:

$$\epsilon_f = 0.005 \quad (3-39a)$$

$$f_f = 3.3 f'_c{}^{0.83} \quad \text{psi} \quad (3-39b)$$

$$f_f = 1.4 f'_c{}^{0.83} \quad \text{MPa}$$

Collins and Mitchell (1991) used a complete equation to model the descending branch.

$$f_c = \frac{rx}{r-1+x^{kr}} \quad (3-40a)$$

where:

$$r = .8 + \frac{f'_c}{2500} \text{ psi} \quad (3-40b)$$

$$r = .8 + \frac{f'_c}{17} \text{ MPa}$$

and,

$$k = 0.67 + \frac{f'_c}{9000} \text{ psi} \quad (3-40c)$$

$$k = 0.67 + \frac{f'_c}{62} \text{ MPa}$$

In the previous equation, the value of k is taken as 1 for the ascending branch and is calculated using Eq. (3-40c) for the descending branch. By using this procedure the continuity of the tangent elastic modulus is lost, as shown in Fig. 3-12.

Some other models have been presented by Wang et al. (1978), Popovics (1970) and Tsai (1988).

3.3 Recommended Complete Stress-Strain Curve for Unconfined Concrete

From the data reported by Klink (1985), the following expression for normal concrete can be derived:

$$w = 98.55 f'_c{}^{0.0489} \quad (3-41)$$

By combining Eqs. (3-25) and (3-41) an expression for the modulus of elasticity suitable for both normal and high strength concrete is obtained. The proposed equation is:

$$E_{0.45} = 162,000 f'_c{}^{3/8} \text{ psi} \quad (3-42)$$

$$E_{0.45} = 7,200 f'_c{}^{3/8} \text{ MPa}$$

This relationship is plotted in Fig. 3-9 and is compared with those mentioned previously, Eqs. (3-18) to (3-28).

In the previous equation, the modulus of elasticity has been named $E_{0.45}$ because it is defined as the secant modulus from the origin up to a stress of 45% of the concrete

strength. Mander et al. (1984) recommend an initial modulus of elasticity $E_c = 1.1 E_{0.45}$. In this study the initial elastic modulus was found to be between 10% and 18%, with an average of 15%, greater than the secant modulus. So the recommended initial modulus of elasticity is given as:

$$E_c = 185,000 f_c'^{3/8} \quad \text{psi} \quad (3-43)$$

$$E_c = 8,200 f_c'^{3/8} \quad \text{MPa}$$

Based on the data reported by Sulayfani and Lamirault (1987) the following simpler equation is proposed:

$$\epsilon_c' = \frac{f_c'^{1/4}}{4,000} \quad \text{psi} \quad (3-44)$$

$$\epsilon_c' = \frac{f_c'^{1/4}}{28} \quad \text{MPa}$$

which will also fit the data for high strength concrete presented by Muguruma et al. (1991). Thus, this equation may be used to represent the strain at peak stress for both normal and high strength concrete. Eq. (3-44) is plotted in Fig. 3-10 and compared with those mentioned previously, (Eqs. 3-29 to 3-35).

A simple explicit equation for the parameter r was adopted. The stress-strain curves obtained compared well with those suggested by Collins and Mitchell (1991). The proposed formula, for the descending branch, is given directly in terms of the parameter r of Tsai's equation, Eq. (3-17), as:

$$r = \frac{f_c'}{750} - 1.9 \quad \text{psi} \quad (3-45)$$

$$r = \frac{f_c'}{5.2} - 1.9 \quad \text{MPa}$$

In this section, a complete stress-strain curve for unconfined concrete is proposed. The equation to describe the monotonic compressive stress-strain curve for unconfined concrete is based on Tsai's equation:

$$y = \frac{nx}{1 + \left(n - \frac{r}{r-1}\right)x + \frac{x^r}{r-1}} \quad (3-46a)$$

where $x = \frac{\epsilon_c}{\epsilon_c'}$ and $y = \frac{f_c}{f_c'}$, n and r are parameters to control the shape of the curve.

The equation parameter n is defined by the initial modulus of elasticity, the concrete strength and the corresponding strain. The initial modulus of elasticity and peak strain as they were defined previously are given by:

$$E_c = 185,000 f_c'^{3/8} \quad \text{psi}$$

$$E_c = 8,200 f_c'^{3/8} \quad \text{Mpa}$$

and,

$$\epsilon_c' = \frac{f_c'^{1/4}}{4,000} \quad \text{psi}$$

$$\epsilon_c' = \frac{f_c'^{1/4}}{28} \quad \text{MPa}$$

Thus the parameter n is defined as:

$$n = \frac{E_c \epsilon_c'}{f_c'} = \frac{E_c}{E_{sec}} = \frac{46}{f_c'^{3/8}} \quad \text{psi} \quad (3-46b)$$

$$n = \frac{7.2}{f_c'^{3/8}} \quad \text{MPa}$$

The parameter r as it was defined previously in this section is given by:

$$r = \frac{f_c'}{750} - 1.9 \quad \text{psi} \quad (3-46c)$$

$$r = \frac{f_c'}{5.2} - 1.9 \quad \text{MPa}$$

The relation represented by Eqs. (3-46) is shown graphically in Fig. 3-11 for ordinary and high strength concrete up to 12000 psi . Analytical stress-strain relations given by Collins and Mitchell (1991) are presented in Fig. 3-12. In the equation used by them, a noncontinuous factor is used. The single equation used here has the advantage of being adaptable for both confined and unconfined concrete, as it allows the descending branch to shift either upward or downward, using the parameters n and r which are plotted in Fig. 3-13.

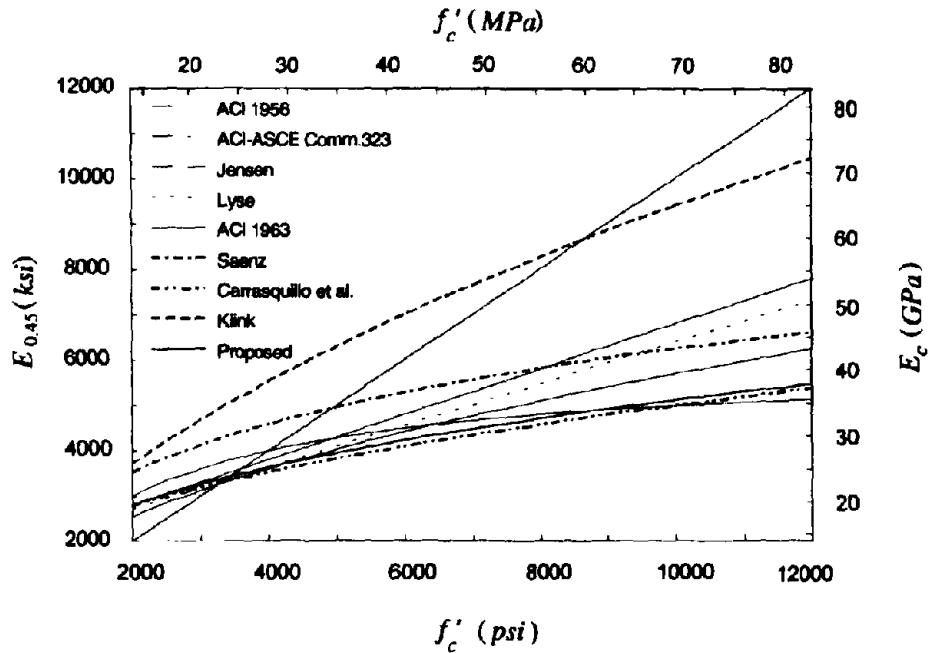


Fig. 3-9 Comparison of Different Equations for the Secant Modulus of Concrete

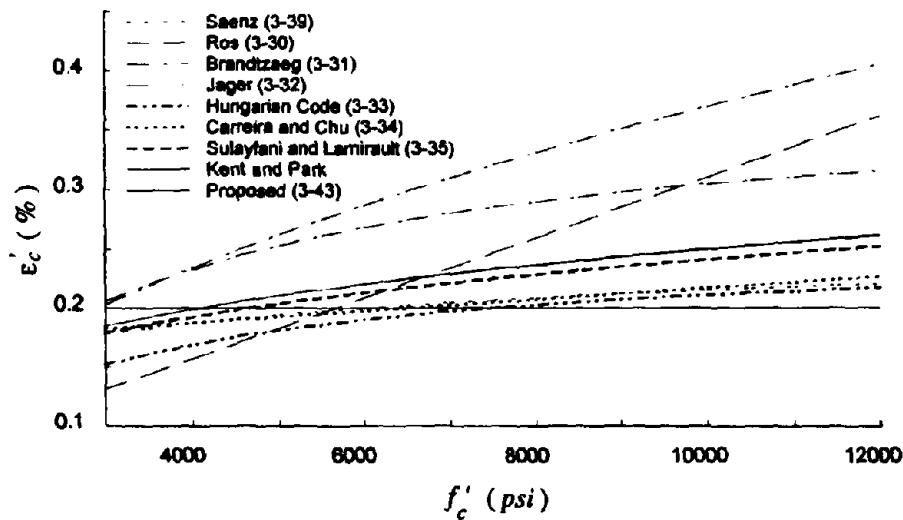


Fig. 3-10 Comparison of Different Equations for the Strain at Peak Stress

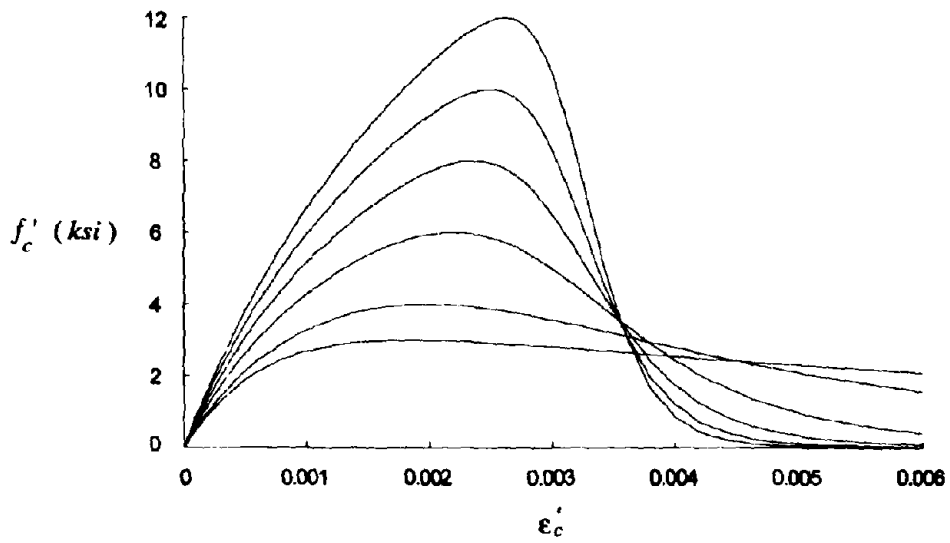


Fig. 3-11 Proposed Theoretical Stress-Strain Curves for Unconfined Concrete

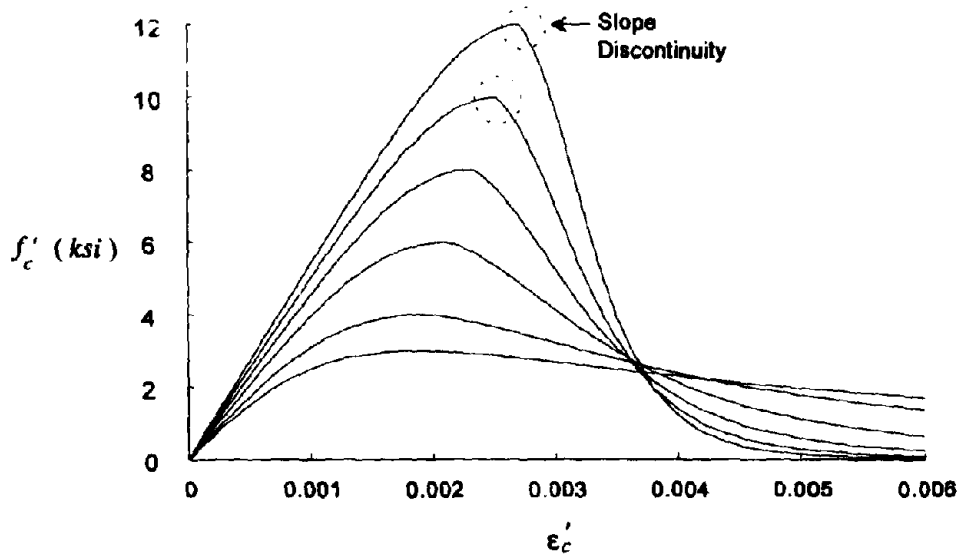


Fig. 3-12 Theoretical Stress-Strain Curves suggested by Collins and Mitchell

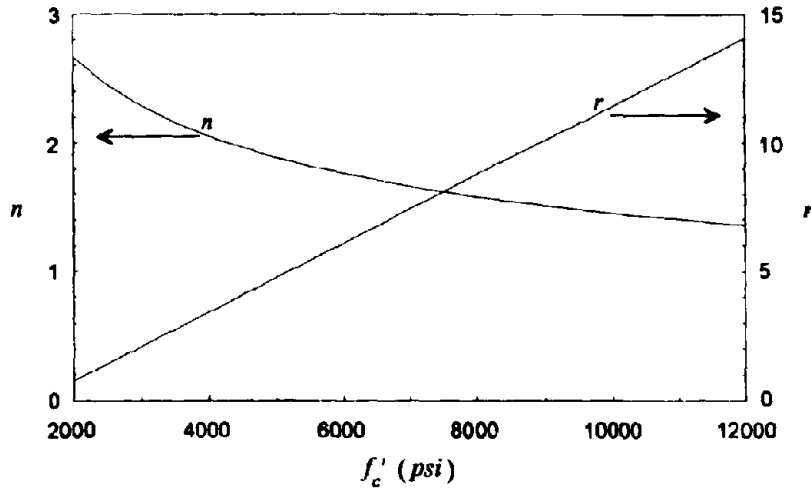


Fig. 3-13 Tsai's Equation Parameters for Unconfined Concrete

3.4 Confinement of Concrete

It has been shown by many investigators and is an accepted fact, that transverse reinforcement improves both the strength and the ductility of concrete. Several models have been put forward to describe this effect on the properties of confined concrete, and the mechanics of passive confinement by reinforcing steel has been explained successfully by Sheikh and Uzumeri (1980) for square sections with rectilinear hoops, and by Mander et al. (1988a) for all cases including rectangular sections with hoops and ties, and circular sections with either spirals or hoops.

The first attempts to describe the effect of confinement on the strength and ductility of concrete were empirical. Several authors proposed confinement models for rectangular and circular hoops. It was recognized that circular hoops provided better confinement than rectangular hoops. Generally, confinement models can be classified as hoop confinement models and material confinement models. The hoop confinement models are normally directed to describe the confinement mechanism within the context of a cross section, while the material confinement models try to explain the effect of biaxial or triaxial state of stresses on the ultimate strength of concrete.

3.4.1 Confinement Models

One of the first attempts to define the effect of confinement on the ultimate strength of concrete was made by Richart et al. (1928). They used *active hydrostatic fluid pressure* to confine concrete and proposed the following relationships

$$f'_{cc} = f'_c + k_1 f_l \quad (3-46a)$$

$$\epsilon'_{cc} = \epsilon'_c \left(1 + k_2 \frac{f_l}{f'_c} \right) \quad (3-46b)$$

Here, f'_{cc} and ϵ'_{cc} are the confined concrete strength and corresponding strain under the confining fluid pressure f_l , and f'_c and ϵ'_c are the unconfined concrete strength and corresponding strain. Factor k_1 was found to be 4.1 while $k_2 = 5 k_1$. Because of its simplicity, this equation has been widely applied, and was the basis of the confinement requirements for concrete columns in ACI-318 (Park and Paulay, 1975).

Balmer (1949) found the value of k_1 to vary between 4.5 and 7.0. He also used an *active hydrostatic fluid pressure* on standard size cylinders, which led him to suggest the following expression:

$$f'_{cc} = f'_c \left(1 + 9.175 \frac{f_l}{f'_c} \right)^{0.73} \quad (3-47)$$

Chan (1955) proposed a trilinear curve dependent on the volumetric ratio of the tie steel to concrete core to simulate the *passive confinement* of transverse *rectilinear ties*. He considered that this was the only variable affecting the strength and ductility of concrete confined, and that this was the first attempt to evaluate the effect of the passive confinement of transverse reinforcement upon the behavior of concrete under eccentric compression. He used specimens $6 \times 6 \times 11 \frac{1}{2}$ in. and $6 \times 3 \frac{5}{8} \times 52$ in.

Blume, Newmark and Corning (1961) proposed an expression for the strength enhancement due to *rectangular hoops*. Their equation used the result obtained by Richart et al. (1928), Eqs. (3-46), where the confining stress was considered to be given by:

$$f_l = 0.5 \left(\frac{2 A_{sh} f_{sh}}{a s} \right) \quad (3-48)$$

where the term a is the longer side of the rectangular concrete area enclosed by the hoop and f_{sh} is the stress in the hoop. While s is the hoop spacing and A_{sh} is the hoop cross sectional area. The reduced efficiency of the rectangular hoop in confining the core concrete was taken into account by introducing the preceding 0.5 factor, as shown by Iyengar et al. This is not a conservative assumption.

Roy and Sozen (1964) proposed a model in which the strength of concrete was not influenced by the degree of confinement. Their bilinear relation only considered an effect of passive confinement on the descending branch of the stress-strain relationship. This model was based on data obtained from *tests on prisms* (5 x 5 x 25 in). They considered a strain at peak stress of 0.002, and the ascending branch was taken linear. The obvious simplifications were to be refined by some authors afterward.

Soliman and Yu (1967) suggested a piecewise continuous curve composed of a parabola for the ascending branch, a horizontal plateau and a descending curve. Their equations were based on experimental data obtained for *rectangular* binders. They studied the effect of size, type and spacing of binders, shape of the cross-section and cover, then proposed an empirical model based on these variables.

$$f'_{cc} = f'_c (1 + 0.05 q'') \quad (3-49a)$$

with:
$$q'' = \left(1.4 \frac{A_{core}}{A_{gross}} - 0.45 \right) \frac{A_{sh}(s - s')}{A_{sh}s + 0.0028 B s} \quad (3-49b)$$

in which A_{core} = area of bound concrete under compression, A_{gross} = area of concrete under compression, s' = longitudinal spacing of transverse reinforcement, b_1 = breadth of bound concrete cross-section, d_1 = effective depth of bound concrete cross-section and $B = b_1$ or $0.7d_1$, whichever it the greater.

Iyengar, Desayi and Reddy (1970) developed some empirical expressions for circular and square spiral confinement, as well as for stirrup confinement.

The confinement pressure for *circular spiral hoops* proposed by Iyengar et al. was:

$$f_l = \frac{2A_{sh} f_{yh}}{d} \left(\frac{1}{s} - \frac{1}{s'} \right) \quad (3-50)$$

where s' is the least lateral dimension. It was assumed that a hoop spacing greater than the least lateral dimension produces no ductility or strength enhancement. This approach was also used by Soliman and Yu.

For *stirrups*, the confining pressure was found to be:

$$f_l = 0.174 \frac{2A_{sh} f_{yh}}{a} \left(\frac{1}{s} - \frac{1}{s'} \right) \quad (3-51)$$

where a was defined in Eq. (3-48). Note the preceding factor reflecting the less efficient confinement of rectilinear ties. Their experiments showed less efficiency for rectilinear ties than that assumed by Blume et al.

They also used a linear relation of the form proposed by Richart et al., Eqs. (3-46), where they found a value of $k_1 = 4.6$. The coefficient k_2 for spiral hoops was found to be $k_2 = 10 k_1$, and for rectilinear ties $k_2 = 8.8 k_1$.

Sargin (1971) proposed three equations to predict the ultimate strength and one equation to represent the corresponding strain. A continuous curve was proposed to represent stress-strain relationship, Eq. (3-14), where the parameters n and D were calibrated empirically from test results on *square* cross-sectional *prisms*.

Kent and Park (1971) presented a piecewise continuous model composed of an ascending parabola (similar to that proposed by Soliman and Yu), then a linear descending branch with a slope that depends on the amount of confinement and finally a sustained stress of $0.2 f'_c$. Their model did not reflect any strength enhancement due to the confinement steel. This model was later modified by Park, Priestley and Gill (1982) to include the effect of confinement upon the strength of concrete.

This model assumed a peak strain of 0.002 for unconfined concrete. In terms of the Richart et al. linear relationship Eqs. (3-46), Park et al. proposed the coefficients to be $k_1 = k_2 = 1$, and the equivalent confining pressure given by:

$$f_l = \rho_s f_{yh} \quad (3-52)$$

where ρ_s is the ratio of hoop reinforcement to volume of concrete core measured to outside of the hoops.

Leslie and Park (1974) proposed a model for the confinement of circular columns in which the ascending branch was composed of two parabolas. The descending branch was

composed of an inclined line with a slope $-Z$, it was assumed that concrete can sustain a stress of $0.2f'_c$ indefinitely, with:

$$Z = \frac{N}{f'_{cc}} \left(\frac{f'_c}{\rho_s f_y} \right)^{1.13} \quad N = \begin{cases} 15500 \text{ psi} \\ 107 \text{ MPa} \end{cases} \quad (3-53)$$

Vallenas, Bertero and Popov (1977) proposed a model similar to that by Kent and Park (1971) but the ascending branch reflects the effect of confinement. Instead of the parabola proposed by Kent and Park, they proposed an expression in which the initial slope can be specified. The coordinate of the peak proposed by Vallenas et al. is given by:

$$\epsilon'_{cc} = 0.0024 + 0.0005 \left(1 - 0.734 \frac{s}{h''} \right) \rho'' \frac{f_{yh}}{\sqrt{f'_c}} \quad (3-54a)$$

$$\frac{f'_{cc}}{f'_c} - 1 = 0.0091 \left(1 - 0.245 \frac{s}{h''} \right) \left(\rho'' + \frac{d''}{D} \rho \right) \frac{f_{yh}}{\sqrt{f'_c}} \quad (3-54b)$$

where ρ'' is the ratio of the total volume of confining transverse reinforcement to the volume of confined concrete, both only for the confined compressive zone of the beam cross section; ρ is the ratio of the cross-sectional area of the longitudinal bars to the total concrete area, both in the confined compressive zone, h'' is the average dimension of the compressive zone, defined by the expression $h'' = (h''_1 + h''_2) / 2$; where h''_1 and h''_2 are the dimensions of the compressive zone, measured to outside of the hoops; s is the hoop spacing, d'' is the nominal diameter of the transverse reinforcement and D is the nominal diameter of the reinforcing bars.

Priestley, Park and Potangaroa (1981) used an expression based on Richart's equation (1928), which is similar to that by Blume et al. The confining pressure for *spirally confined concrete* is assumed to be based on a uniformly distributed tube of steel:

$$f_l = \frac{2 A_{sp} f_{yh}}{d_s s_h} \quad (3-55)$$

Sheikh and Uzumeri (1982) proposed a rational model where the geometry of a square section and the rectilinear reinforcement distribution is directly taken into account. They then used experimental data to fit a proposed confining coefficient. The final equation suggested by them for *square cross-sections* is written as:

$$\frac{f'_{cc}}{f'_c} = 1.0 + \frac{2.73B^2}{P_{occ}} \left[\left(1 - \frac{nC^2}{5.5B^2} \right) \left(1 - \frac{s}{2B} \right)^2 \right] \sqrt{\rho_s f'_s} \quad (3-56)$$

where, $P_{occ} = 0.85 f'_c (B^2 - A_s)$, B = center to center distance of tie of square core, A_s = area of longitudinal steel, ρ_s = volumetric ratio of transverse steel, f'_s = stress in the lateral steel at the time of maximum resistance of confined concrete, C = center to center distance between longitudinal bars, s = center to center hoop spacing, n = number of bars on perimeter of core.

Ahmad and Shah (1982b) presented a model for the *confinement of spirally* reinforcement. Their model uses Sargin's equation, Eq. (3-13), and the parameters were determined by fitting experimental results. They proposed a confining pressure given by:

$$f_l = \frac{\rho_s f_{yh}}{2} \left(1 - \sqrt{\frac{s}{1.25 d_{cc}}} \right) \quad (3-57a)$$

$$\rho_s = \frac{\pi d_{sh}^2}{s d_{cc}} \quad (3-57b)$$

$$k_1 = \frac{6.61}{\sqrt{f'_c}} f_l^{0.04} \quad (3-57c)$$

$$k_2 = \frac{0.047}{(f'_c)^{1.2}} f_l^{0.19} \quad (3-57d)$$

Shah, Fafitis and Arnold (1988) suggested a model for *spirally confined concrete* similar to that by Ahmad and Shah. In their model the envelope curve is composed of two different equations, one for the ascending branch and another for the descending branch. The proposed confined concrete strength equations is:

$$f_{cc} = f'_c + \left(1.15 + \frac{3048}{f'_c} \right) f_r \quad (3-58a)$$

with,
$$f_r = \frac{2A_{sh}f_{yh}}{d} \left(\frac{1}{s} - \frac{1}{1.25d} \right) \quad (3-58b)$$

This model assumes that the effect of confinement disappears when the spacing is greater than about $0.25d$, where d is the column diameter. It should be noted that the experimental data on full size spirally confined columns reported by Mander et al. (1988b) show that this is an unrealistic implication.

Mander et al. (1988a) proposed an analytical model for confined concrete which used a plasticity based five parameter failure model after William and Warnke (1975) applied to a three dimensional (3D) hypoelastic constitutive model proposed by Elwi and Murray (1979). The equation used by Popovics, Eq. (3-11), was used to represent the stress-strain

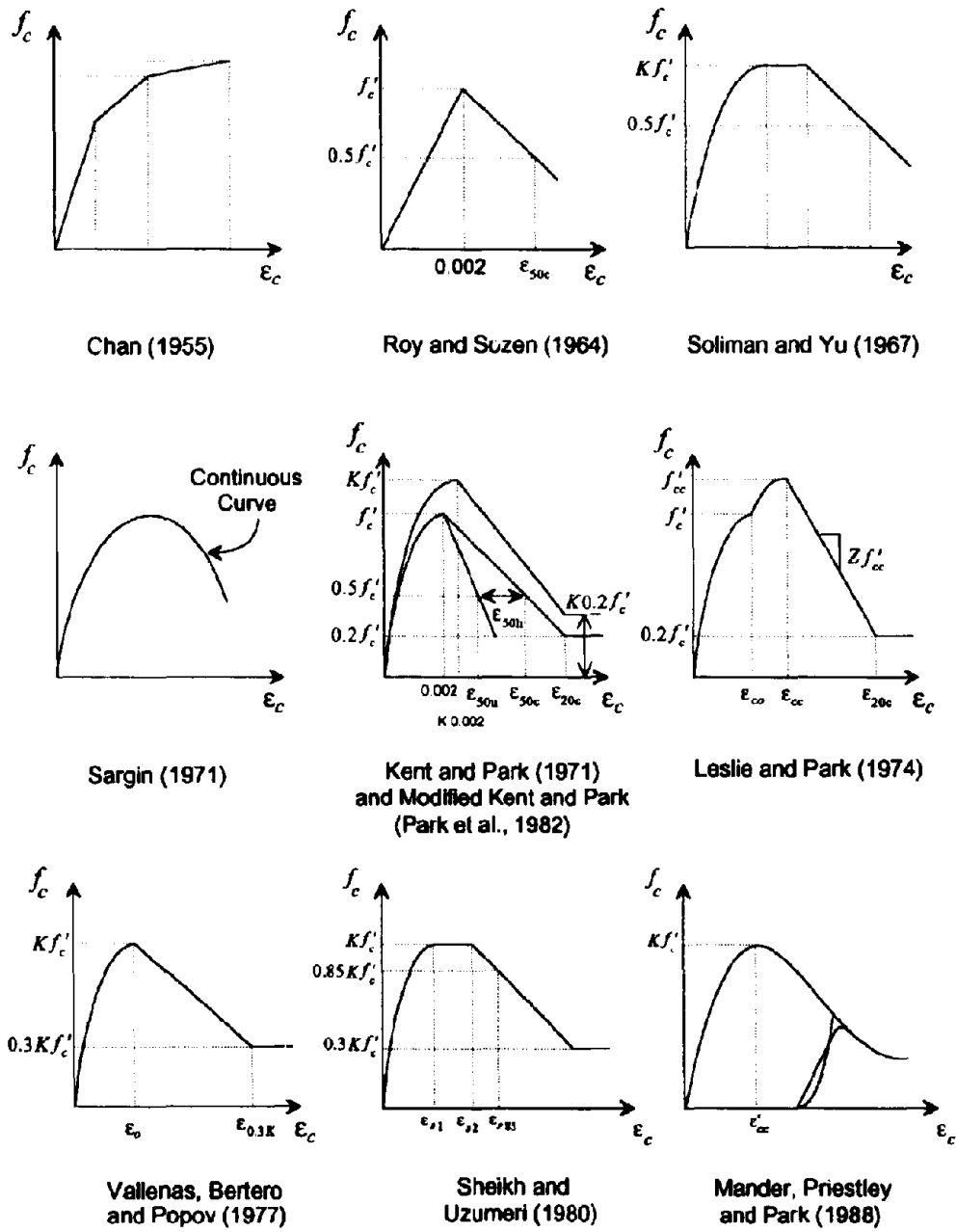


Fig. 3-14 Some Proposed Stress-Strain Curves for Confined Concrete

relationship. In this model the geometry of the section is taken into account by defining an effectively confined concrete core. This approach is an advanced version of the one used by Sheikh and Uzumeri (1982). The approach is applicable to any section shape (both rectangular and circular) and reinforcing type (rectilinear hoops, ties, and spirals or circular hoops). This model appears to be the only one that incorporates dynamic loading effects as well as cyclic loading. Details of the model are discussed below.

3.4.2 Confinement Mechanism

The lateral confining stresses are unevenly distributed along the depth of the compression zone (Soliman and Yu, 1967). The confining pressure comes from the transverse steel that is passively resisting the lateral expansion of the concrete subjected to compression. This confining action on the concrete makes it both stronger and more ductile. The most simple approach is to use empirical formulations to relate the confined strength and ductility to the unconfined properties of concrete. A more rational approach is to use a constitutive model to describe the effect of a multiaxial state of stress upon the ultimate strength of concrete. Many such models have been proposed in the literature, (Mills and Zimmerman, 1970; Liu, Nilson and Slate, 1972; Kupfer and Gerstle, 1973; Chen, A.C.T and Chen W.F., 1975; Darwin and Pecknold, 1977; Cedolin, Crutzen and Dei Poli, 1977; Ottosen, 1979; Kotsovos and Newman, 1979; Elwi and Murray, 1979; Bazant and Kim, 1979; Chen and Ting, 1980; Ahmad and Shah, 1982; Chuan-zhi, Zhen-hai and Xiu-qin, 1987).

3.4.2.1 Confinement of Circular Sections

The model proposed by Mander et al. (1988a) will be adopted herein, as it appears to be the only generalized model that is applicable to all section shapes. For circular section the effective lateral pressure is given by:

$$f_l = \frac{1}{2} k_e \rho_s f_s \quad (3-59)$$

with k_e is the confinement effectiveness coefficient defined by:

$$k_e = \frac{A_e}{A_{cc}} \quad (3-60)$$

The confining bars are assumed to yield by the time the maximum stress in the concrete is reached, in which case $f_s = f_{yh}$.

The effectively confined area shown in Fig. 3-15 can be calculated as:

$$A_e = \frac{\pi d_s^2}{4} \left(1 - 0.5 \frac{s'}{d_s}\right)^k \quad (3-61)$$

where d_s = diameter of circular or spiral hoops, s' = clear longitudinal spacing between spirals in which arching action of the concrete develops, the power k has a value of 2 for circular hoops and 1 for spirals (helix).

The concrete core area is calculated as:

$$A_{cc} = (1 - \rho_{cs}) \frac{\pi d_s^2}{4} \quad (3-62)$$

ρ_{cs} is the volumetric ratio of the transverse confining steel to the confined core given by:

$$\rho_{cs} = \frac{4A_{sh}}{s d_s} \quad (3-63)$$

ρ_{cl} is the volumetric ratio of the longitudinal steel in the confined core given by:

$$\rho_{cl} = \frac{A_{st}}{\pi d_s^2} \quad (3-64)$$

Thus, the final expression is given by:

$$f_i = \frac{\rho_s f_s \left(1 - 0.5 \frac{s'}{d_s}\right)^k}{2(1 - \rho_{cl})} \quad (3-65)$$

3.4.2.2 Confinement of Rectangular Sections

The effectively confined area for rectangular sections is shown in Fig. 3-15 and is given by:

$$A_e = \left(b_c d_c - \sum_{i=1}^n \frac{(w'_i)^2}{6}\right) \left(1 - 0.5 \frac{s'}{b_c}\right) \left(1 - 0.5 \frac{s'}{d_c}\right) \quad (3-66)$$

The concrete core area is given by:

$$A_{cc} = b_c d_c - A_{st} \quad (3-67)$$

The lateral confinement pressure for rectangular sections can have different values in each direction. In this case a general three dimensional state of stress is developed. The lateral pressure for each direction (x and y) is calculated as:

$$f_{lx} = k_e \rho_x f_{yh} \quad (3-68)$$

$$f_{ly} = k_e \rho_y f_{yh} \quad (3-69)$$

in which,

$$\rho_x = \frac{A_{sx}}{s d_c}$$

A_{sx} = total area of transverse reinforcement parallel to the x axis.

$$\rho_y = \frac{A_{sy}}{s b_c}$$

A_{sy} = total area of transverse reinforcement parallel to the y axis.

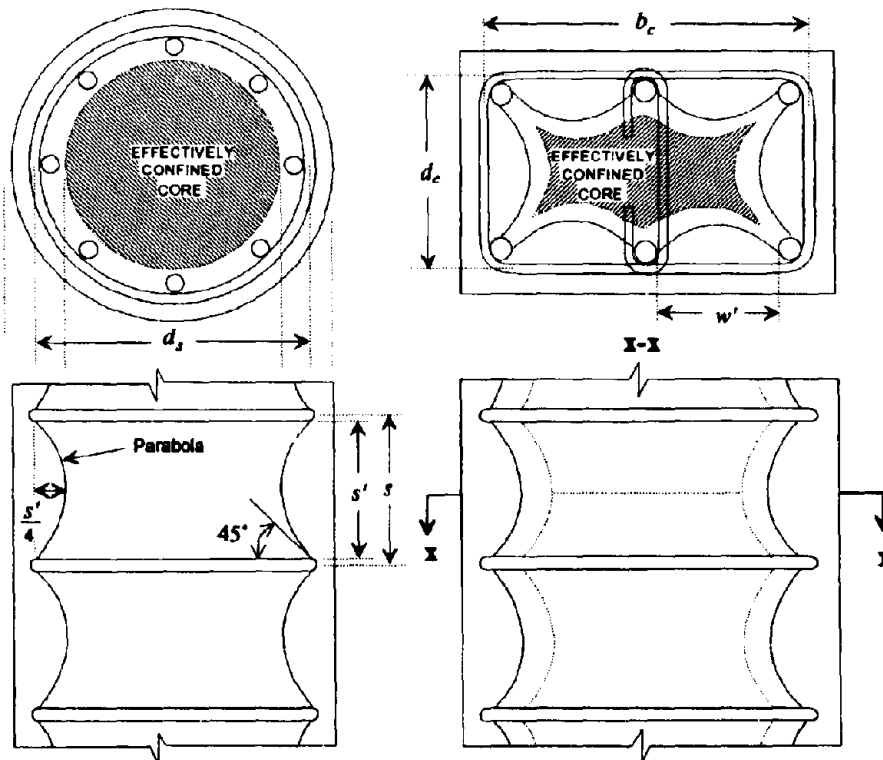


Fig. 3-15 Confinement Mechanism for Circular and Rectangular Cross Sections

3.4.3 Confinement Effect on Strength

The ultimate strength surface proposed by Mander et al. (1988a), led to a plot relating the confining pressure with the confined strength ratio. The procedure to find this value is rather complex and an iterative procedure has to be used. The results of this procedures were presented in a plot to obviate the lengthy calculations involved. In this section an approximate equation is proposed, that can be use to represent the failure surface proposed by Mander et al.

The equation proposed is:

$$K = \frac{f'_{cc}}{f'_c} = 1 + A\bar{x} \left(0.1 + \frac{0.9}{1 + B\bar{x}} \right) \quad (3-70a)$$

with:

$$\bar{x} = \frac{f'_{11} + f'_{22}}{2 f'_c} \quad (3-70b)$$

$$r = \frac{f'_{11}}{f'_{22}} \quad f'_{22} \geq f'_{11} \quad (3-70c)$$

$$A = 6.8886 - (0.6069 + 17.275r)e^{-4.989r} \quad (3-70d)$$

$$B = \frac{4.5}{\frac{5}{A}(0.9849 - 0.6306 e^{-3.8939r}) - 0.1} - 5 \quad (3-70e)$$

The comparison between the analytical results and the approximate equation presented above is shown in Fig.3-16.

This equation can be put in the form suggested by Richart et al. (1929):

$$f'_{cc} = f'_{co} + k_1 f_l \quad (3-71)$$

By taking f_l as the average of f_{11} and f_{22} , this can be rewritten as:

$$K = \frac{f'_{cc}}{f'_{co}} = 1 + k_1 \bar{x} \quad (3-72a)$$

with,

$$k_1 = A \left(0.1 + \frac{0.9}{1 + B\bar{x}} \right) \quad (3-72b)$$

For a symmetric triaxial state of stress $f_1 = f_{11} = f_{22}$, the analytical confinement coefficient K given by Mander et al. (1988a) is:

$$K = -1.254 + 2.254 \sqrt{1 + 7.94\bar{x}} - 2.0\bar{x} \quad (3-73)$$

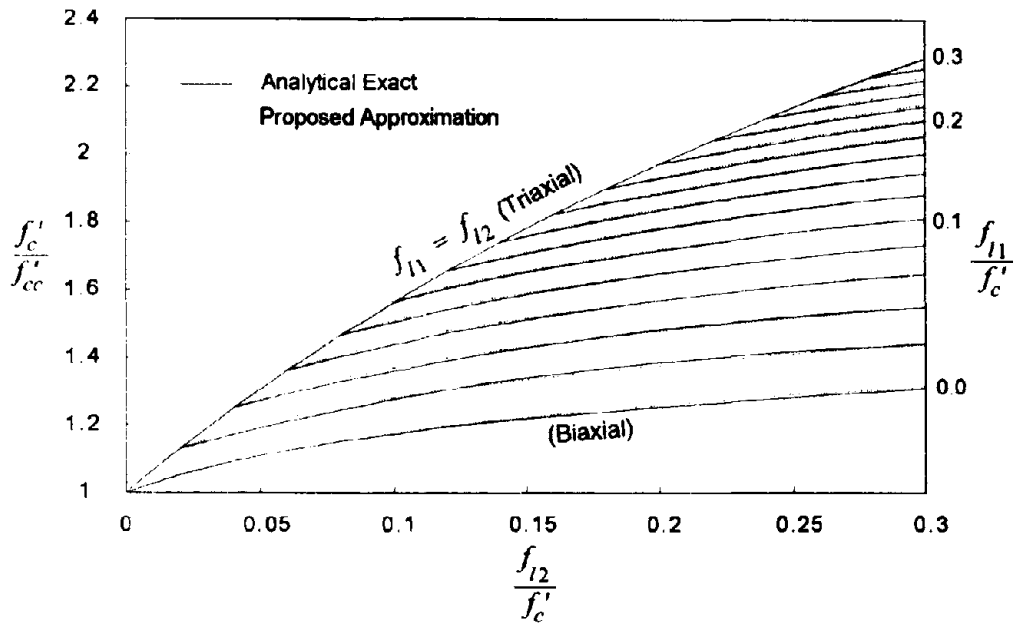


Fig. 3-16 Confined Concrete Strength Ratio

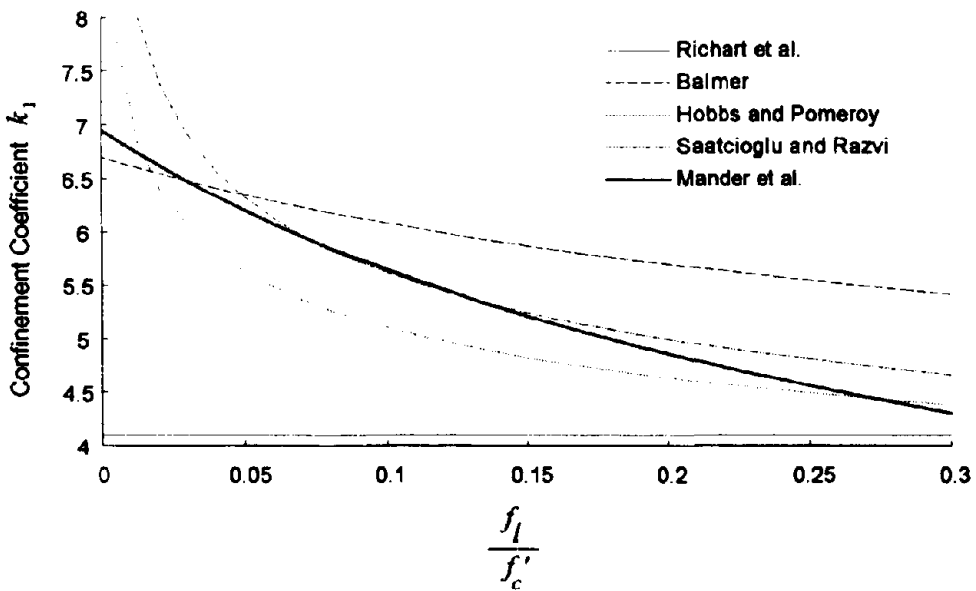


Fig. 3-17 Comparison of Different Models for Triaxial Confinement

By combining Eqs. (3-72a) and (3-73) the following equation is obtained:

$$k_1 = \frac{2.254 \left(\sqrt{1 + 7.94\bar{x}} - 1 \right) - 2.0\bar{x}}{\bar{x}} \quad (3-74)$$

Richart et al. (1929) found this value to be an average:

$$k_1 = 4.1 \quad (3-75)$$

While Balmer (1949) found a more complex relationship that can be expressed by:

$$k_1 = \frac{(1 + 9.175\bar{x})^{0.73} - 1}{\bar{x}} \quad (3-76)$$

Hobbs and Pomeroy (1974) suggested the following modification to the factor given by Richart et. al., to improve the accuracy for higher levels of confining pressure:

$$k_1 = 3.7\bar{x}^{-0.14} \quad (3-78)$$

Recently Saatcioglu and Razvi (1992) have proposed the following expression based on the data from Richart et al. (1929):

$$k_1 = 6.7(f_l)^{-0.17} \quad (3-79)$$

In the previous expression f_l is given in MPa. Assuming a concrete strength of approximately 30 MPa, the following expression is obtained:

$$k_1 = 3.8\bar{x}^{-0.17} \quad (3-80)$$

Eqs. (3-74) through (3-80) are compared in Fig. 3-17.

3.4.4 Confinement Effect on Ductility

When the concrete is subjected to high levels of compressive stress it expands laterally due to the Poisson effect. In a concrete column, this expansion forces the lateral hoops outward. The initial behavior of confined concrete should not be different to the unconfined behavior, because at low levels of axial load the stresses in the hoops are low, as is the confining pressure. The maximum stress is affected by the amount of confining hoops as is the strain at which this occurs. The shape of the descending branch of the stress-strain relationship is also affected. Richart et al. (1929) suggested an expression in the form:

$$\epsilon_{cc} = \epsilon_{co}(1 + k_2\bar{x}) \quad (3-81a)$$

with,

$$k_2 = 5k_1 \quad (3-81b)$$

This expression will be adopted herein because it has been confirmed experimentally by Balmer (1949), Mander et al. (1988b) and Saatcioglu et al. (1992). For high strength transverse steel Zahn et al. (1990) found the value of k_2 to be between 1.7 and 5 times k_1 , a value of 3 was used as an average.

3.4.5 Confinement Effect on the Descending Branch

Based on a series of tests performed previously by Mander et al. (1988b) at the University of Canterbury, the following empirical relationship for confined concrete is proposed:

$$\epsilon_f = 3\epsilon'_{cc} \quad (3-82a)$$

$$f_f = f'_{cc} - \Delta f_{cc} \quad (3-82b)$$

with,

$$\Delta f_{cc} = K \Delta f_c \left(\frac{0.8}{K^5} + 0.2 \right)$$

(3-82c)

and,

$$K = \frac{f'_{cc}}{f'_c}$$

(3-82d)

Where Δf_c is the stress drop for unconfined concrete for a strain $\epsilon_c = 3\epsilon'_c$, as shown in Fig. 3-19. The confined concrete strength (f'_{cc}) is calculated through Eq. (3-70a).

3.5 Concrete in Tension

An accurate estimation of the concrete strength and behavior is important as it is a main factor in the assessment of shear deformations and stresses by means of the Modified Compression Field Theory (Vecchio and Collins, 1986; Vecchio, 1989; Collins and Mitchell, 1991), or the Softened Truss Theory (Hsu, 1993). Cracking, which is governed by the tensile characteristics of concrete, is an important property of concrete, that affects its overall behavior.

The strength of concrete in direct tension can be estimated through the equation suggested by the ACI Committee 209 (ACI 209R-82):

$$f_t = g_1 \sqrt{w f'_c} \quad (3-83)$$

where w is the specific weight, that for normal weight concrete can be taken as 145 lb/ft^3 , the factor g_1 is approximate $1/3$. This equation gives rather conservative values for the tension strength of concrete, Carreira and Chu (1986a) recommend to take the g_1 between 0.45 and 0.55, which results in the equation:

$$f_t = 6 \sqrt{f'_c} \quad \text{psi} \quad (3-84)$$

$$f_t = 0.5 \sqrt{f'_c} \quad \text{MPa}$$

Collins and Mitchell (1991) recommend a lower value, for softened truss analysis:

$$f_t = 4 \sqrt{f'_c} \quad \text{psi} \quad (3-85)$$

$$f_t = 0.33 \sqrt{f'_c} \quad \text{MPa}$$

This formulation implicitly assumes that the average concrete stress between diagonal cracks is two-thirds of the maximum given by Eq. (3-84). The monotonic tensile stress strain relationship suggested by Vecchio and Collins (1986) is given by:

$$f_c = E_c \epsilon_c \quad |\epsilon_c| \leq \epsilon_t \quad (3-86)$$

$$f_c = \frac{\alpha_1 \alpha_2 f_t}{1 + \sqrt{500 \epsilon_t}} \quad |\epsilon_c| > \epsilon_t$$

in which f_t = concrete tension strength
 ϵ_t = strain at peak tension stress
 α_1, α_2 = factors accounting for bond characteristics of reinforcement and sustained or repeated loading respectively.

Hsu (1993) adopted a different relationship for the descending branch suggested by Tamai et al. (1988),

$$f_c = f_t \left(\frac{\epsilon_c}{\epsilon_t} \right)^{-0.4} \quad (3-87)$$

Barnard (1964) dealing with the brittle nature of concrete in tension wrote: "*Sudden rupture is not a property of a concrete specimen but is rather a consequence of the testing*"

conditions". With the use of stiff electrohydraulic-controlled testing machines, the complete stress-deformation behavior of concrete can be obtained. The shape of the monotonic tension stress-strain curve has been shown (Carreira and Chu, 1986a; Yankelevsky and Reinhardt, 1987b) to have a descending branch similar to that of monotonic compression. Carreira and Chu proposed the use of Popovics equation, but as shown before Tsai's equation is more general and flexible, so the monotonic tension stress-strain curve will be represented by the equation:

$$f_c = f_t \frac{nx}{1 + \left(n - \frac{r}{r-1}\right)x + \frac{x^r}{r-1}} \quad (3-88)$$

where, $x = \frac{\epsilon_c}{\epsilon_t}$, $n = \frac{E_c \epsilon_t}{f_t}$ and $r =$ parameter to control the shape of the descending branch.

It is worth noting that due to the fact that the observed tensile strength depends strongly on the testing conditions, experimental data on direct tensile strength tends to be more scattered than data for compression strength of plain concrete. Considerable data scattering for the descending branch of concrete in tension given by Vecchio and Collins (1986) makes the choice of any simple equation justifiable, thus Eq. (3-88) was suggested to be consistent with that of concrete in compression.

3.6 Compression Softening Effect

It has been found that transverse tensile strains substantially reduces the apparent strength and stiffness of concrete when compared with the uniaxial compression capacity (Vecchio and Collins, 1986). A number of investigators have addressed this phenomenon and proposed different constitutive relationships. In 1982 Vecchio and Collins proposed a modification of both the peak stress and the strain at peak stress by a factor β in the form:

$$\beta = \frac{1}{0.87 - 0.27 \frac{\epsilon_1}{\epsilon_2}} \quad (3-89a)$$

where ϵ_1 = principal tensile strain, and ϵ_2 = principal compression strain. The effect of this model is shown in Fig. 3-18a.

This model was later modified (Vecchio and Collins, 1986) to make it simpler for design purposes, as:

$$\beta = \frac{1}{0.80 + 0.34 \frac{\epsilon_1}{\epsilon_0}} \quad (3-89b)$$

where ϵ_0 = strain at peak stress for uniaxially loaded concrete.

Recently Vecchio and Collins (1993) have proposed two new improved models (Model A and Model B) to account for the softening effects. These new models were statistically calibrated using a much larger database. In Model A the softening factor is applied to both strength and strain and is given by:

$$\beta = \frac{1}{1 + K_c K_f} \quad (3-89c)$$

in which:

$$K_c = 0.35 \left(\frac{-\epsilon_1}{\epsilon_2} - 0.28 \right)^{0.80} \geq 1.0$$

$$K_f = 0.1825 \sqrt{f'_c} \geq 1.0$$

While for Model B the softening factor, applied to strength only, is given as:

$$\beta = \frac{1}{1 + K_c} \quad (3-89d)$$

in which:

$$K_c = 0.27 \left(\frac{\epsilon_1}{\epsilon_0} - 0.37 \right)$$

Vecchio and Collins (1993) also presented models proposed by other investigators:

Mikame et al. (1991), applied to strength only:

$$\beta = \frac{1}{0.27 + 0.96 \left(\frac{\epsilon_1}{\epsilon_0} \right)^{0.167}} \quad (3-89e)$$

Ueda et al. (1991):

$$\beta = \frac{1}{0.8 + 0.6(1000\epsilon_1 + 0.2)^{0.39}} \quad (3-89f)$$

Belarbi and Hsu (1991) have proposed different softening factors for strength and ductility which are functions of the principal tension strain, the orientation of the cracks respect to the reinforcement (θ) and the type of loading:

$$\beta_\sigma = \frac{0.9}{\sqrt{1 + K_\sigma \epsilon_1}} \quad (3-89g)$$

$$\beta_\epsilon = \frac{1}{\sqrt{1 + K_\epsilon \epsilon_1}} \quad (3-89h)$$

Proportional loading

$K_\sigma = 400; \quad \theta = 45^\circ, 90^\circ$

$K_\epsilon = 550; \quad \theta = 90^\circ$

$K_\epsilon = 160; \quad \theta = 45^\circ$

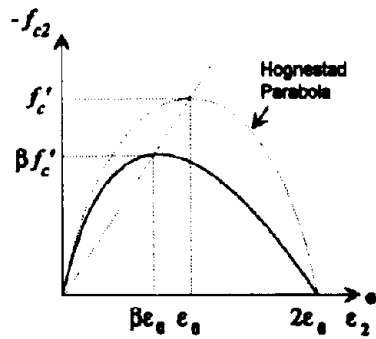
Sequential loading

$K_\sigma = 250; \quad \theta = 90^\circ$

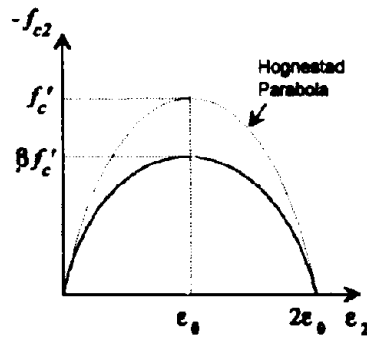
$K_\sigma = 400; \quad \theta = 45^\circ$

$K_\epsilon = 0; \quad \theta = 90^\circ$

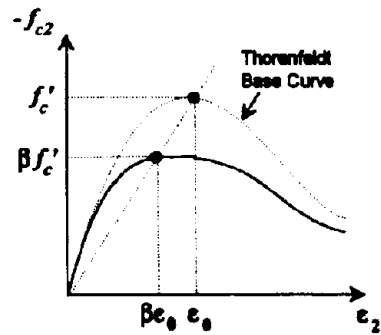
$K_\epsilon = 160; \quad \theta = 45^\circ$



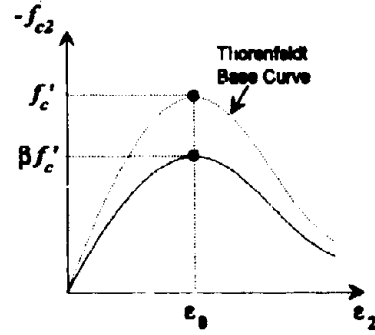
(a) 1982 Model



(b) 1986 Model



(c) Model A (1993)



(d) Model B (1993)

Fig. 3-18 Softening Models proposed by Vecchio and Collins (1982,1986, 1993)

Both Model A and Model B presented by Vecchio and Collins (1993) use the equation by Thorenfeldt et al. (Eq. 3-16) as the "base curve" shown in Figs. 3-18c,d. The Thorenfeldt's equation is identical to Popovics equation (Eq. 3-12) on the ascending branch, and Popovics equation behave similar to Tsai's equation (Eq. 3-17, Fig. 3-8) in this range. The equations for the softening parameter given by Vecchio and Collins (1993) were calibrated over the ascending branch, which in turn means that it would be justifiable to use Tsai's equation in conjunction with any of the softening parameters suggested by them.

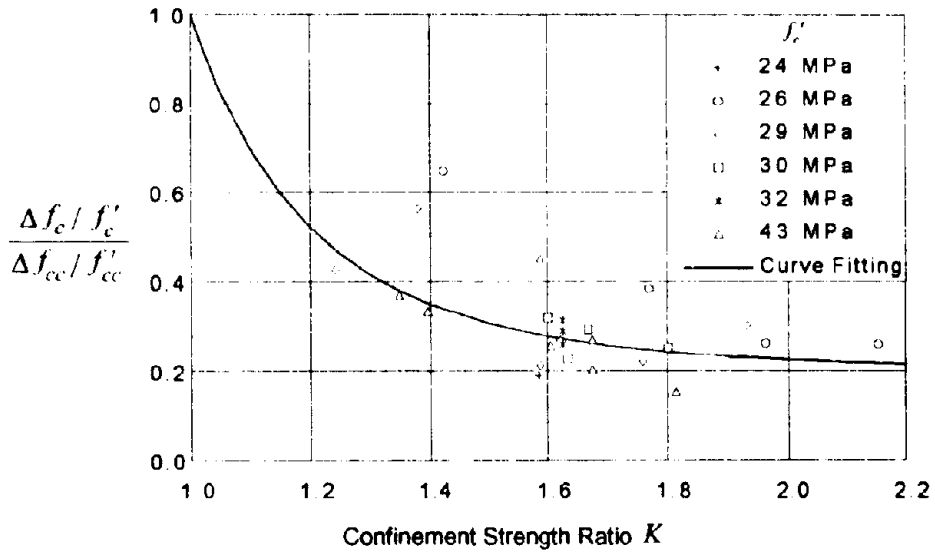
Vecchio and Collins (1993) also show that Models A and B are superior to all previous models, (Eqs. 3-89e to 3-89h), with Model A being only marginally better than Model B. In the present study Model B is adopted for computational simplicity.

3.7 Dynamic Effects on Concrete Behavior

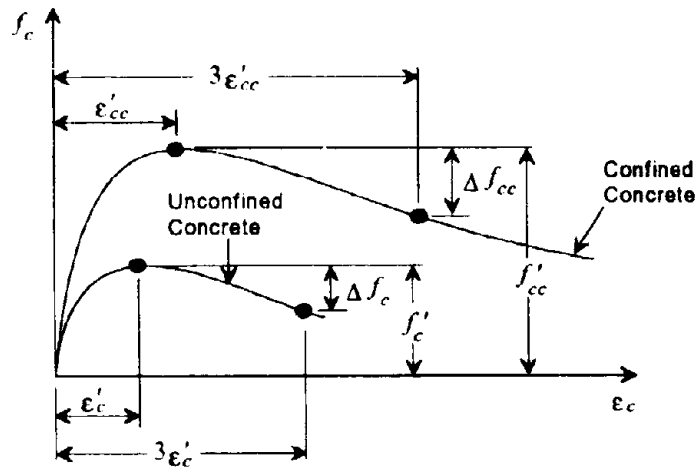
Most dynamic tests on concrete found in literature have been performed on plain concrete cylinders or small reinforced concrete models. The dynamic effect on full size reinforced concrete members was studied by Mander et al. (1988a) leading to the following proposed strength magnification factor:

$$D_f = \frac{f'_{cd}}{f'_c} = \frac{1 + \left| \frac{\dot{\epsilon}}{0.035(f'_c)^2} \right|^{1/6}}{1 + \left| \frac{0.00001}{0.035(f'_c)^2} \right|^{1/6}} \quad (3-90)$$

where f'_{cd} = dynamic concrete strength, f'_c = quasi static concrete strength and $\dot{\epsilon}$ = strain rate in sec^{-1} .



(a)



(b)

Fig. 3-19 Falling Branch for Confined Concrete

3.8 Modeling Hysteretic Behavior

Some general observations are described in this section with respect to the basic behavior of concrete which dictate the characteristics of a rule based hysteretic model.

3.8.1 Basic Components of a Hysteretic Model

Three basic components can be identified in the hysteretic behavior of any material or structural element. These are shown diagrammatically in Fig. 3-20 and described below.

(1) Envelope curves: can be fixed or relocatable, can also be of constant amplitude or scaleable. These curves are the "back bones" of the general hysteretic behavior. Shifting and scaling is used to simulate degradation. Degradation can also be simulated, not by shifting the entire curve, but by shifting the returning point. This means that the point of return to an envelope curve is different to the point where the last reversal occurred from.

(2) Connecting curves: are the connection between the envelope curves. There can be several points of inflection in these curves, as it is used to represent pinching (crack closure), and other softening or hardening phenomena within the material or structural element. Normally more than one equation has to be used to represent this kind of curve.

(3) Transition curves: When a reversal from a connecting curve takes place a transition curve has to be used to make the transition to the connecting curve that goes in the opposite direction. If the transition curve is taken directly to the envelope curve, the model can become unstable, presenting unwanted shifting under local looping (common on most applications).

The terms positive and negative used in the diagram do not refer to the sign of the ordinate but to the direction of the abscissa change, in other words, the direction of displacement in the positive or negative direction.

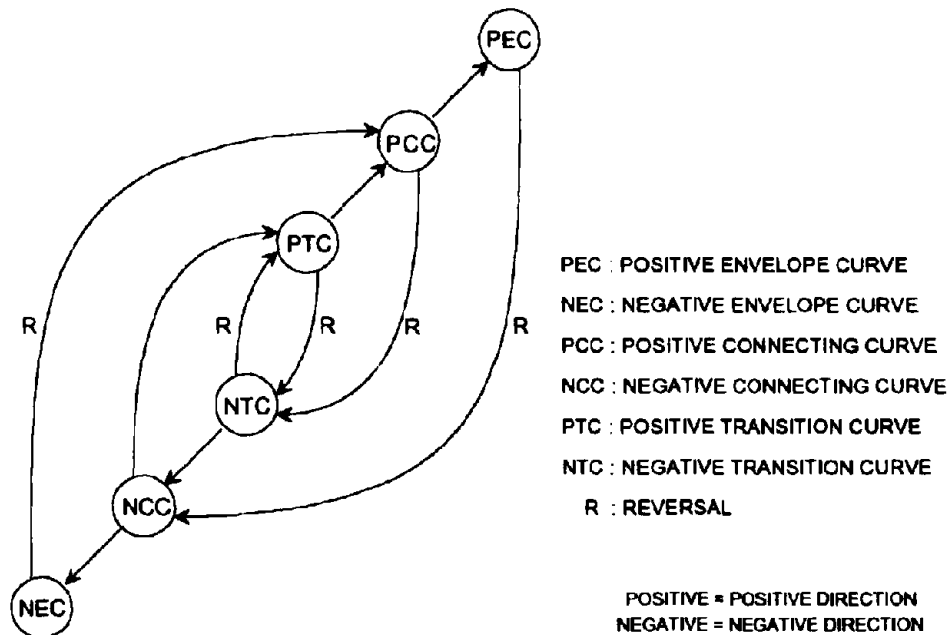


Fig. 3-20 Relationship Between Curves in a Rule-Based Model

3.8.2 A General Approach to Assessing Degradation Within Partial Looping in a Rule-Based Hysteretic Model

A rule-based hysteretic model has normally two ways of assessing degradation. The first method uses a shifting of the origin of the envelope curve or of the returning point on it, the second one uses a scaling variable to reduce the amplitude of the envelope curve. Most models are calibrated to assess complete loop degradation, normally related to the way in which experiments are performed, but in some cases they lack the ability for assessing local loop degradation. In this section a general procedure directed to assess local looping degradation is advanced.

Let (x_{un}, y_{un}) be an *unloading point* on the *positive envelope curve* where a reversal has occurred. Also let (x_w, y_w) be the *target point* on the *negative envelope curve*, which is

completely defined by the reversal point and the previous history of the hysteretic behavior. Finally, let (x_{re}, y_{re}) be a *returning point* on the positive envelope curve, again this point should be completely defined by the target point and the previous history, as shown in Fig. 3-21.

3.8.2.1 First partial reversal

The unloading curve connects the unloading point (x_{un}, y_{un}) with the target point (x_{ta}, y_{ta}) , should the unloading have been complete, the total displacement undergone would be:

$$\sum |\Delta x|_0 = x_{un} - x_{ta} + x_{re} - x_{ta} = x_{un} + x_{re} - 2x_{ta} \quad (3-91a)$$

In the case of an incomplete unloading, Fig. 3-22, the total displacement is:

$$\sum |\Delta x|_1 = x_{un} - x_{ro} + x_{rel} - x_{ro} = x_{un} + x_{rel} - 2x_{ro} \quad (3-91b)$$

A factor k_1 can be defined as:

$$k_1 = \frac{\sum |\Delta x|_1}{\sum |\Delta x|_0} \quad (3-92)$$

It can be clearly seen that when this factor is zero the actual total displacement is zero, which means that no degradation is needed because there was no movement at all. At the other extreme, when the factor has a value of one, the degrading function should take the reloading curve to the returning point. The actual mapping of the intermediate cases can take any monotonic shape, a linear mapping being the logical choice, unless it can be calibrated with actual experimental data. This can result in having to solve a non-linear system of equations, as the factor k_1 that defines the returning point abscissa is a function of the modified returning point itself.

If the degrading function for a complete cycle has the form of a shifting displacement on the positive envelope curve, then an explicit solution can be given. Let Δx_0 be this function, such that the returning point abscissa can be calculated as:

$$x_{re} = x_{un} + \Delta x_0 \quad (3-93)$$

Then Eq. (3-91a) becomes:

$$\Sigma |\Delta x|_0 = 2(x_{un} - x_{ia}) + \Delta x_0 \quad (3-94)$$

The transformed displacement increment Δx_1 for an incomplete unloading is defined such that the modified returning point can be calculated by:

$$x_{rel} = x_{un} + \Delta x_1 \quad (3-95)$$

Thus, Eq. (3-91b) becomes.

$$\Sigma |\Delta x|_1 = 2(x_{un} - x_{ro}) + \Delta x_1 \quad (3-96)$$

A linear proportionality of displacement increments will result in:

$$\frac{\Delta x_1}{\Sigma |x|_1} = \frac{\Delta x_0}{\Sigma |x|_0} \quad (3-97)$$

By substituting Eqs. (3-94) and (3-95) into (3-97) and performing algebraic manipulations,

$$\Delta x_1 = \frac{x_{un} - x_{ro}}{x_{un} - x_{ia}} \Delta x_0 \quad (3-98)$$

Once the modified displacement has been calculated then the modified returning point can be calculated by using Eq. (3-95). As a general case this point is defined by solving the equations that define the returning point uniquely, by applying a mapping function as previously described.

3.8.2.2 Partial reloading

In the case of a total reloading from an incomplete unloading, the reloading curve will reach the positive envelope curve at the modified returning point (x_{rel}, y_{rel}) . An unloading from this point would aim at a new target point (x_{ia1}, y_{ia1}) which should be a function of the returning point (x_{rel}, y_{rel}) . If on the other hand an incomplete reloading takes place, the target point (x_{ia1}, y_{ia1}) needs to be modified. This can be done by defining a new unloading point (x_{un2}, y_{un2}) .

The displacement for a total reloading from the point of reloading (x_{ro}, y_{ro}) to the returning point (x_{rel}, y_{rel}) is:

$$\Sigma |x|_2 = x_{rel} - x_{ro} \quad (3-99)$$

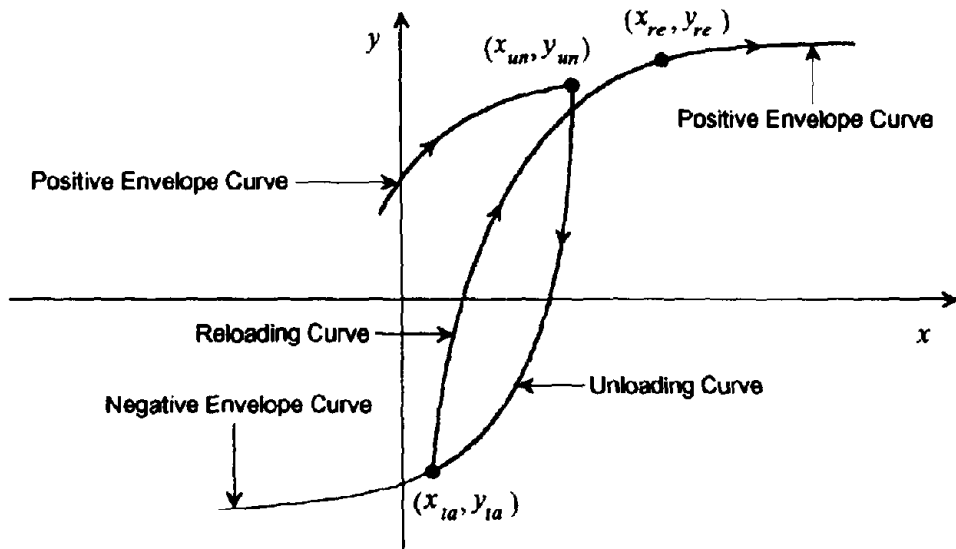


Fig. 3-21 Target Point and Reloading Point in a Complete Reversal

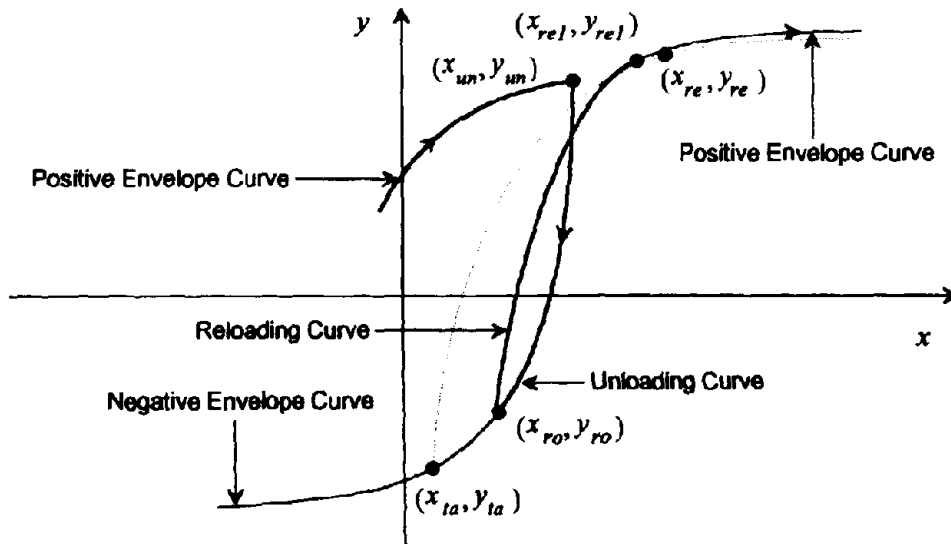


Fig. 3-22 Reloading from a Partial Unloading

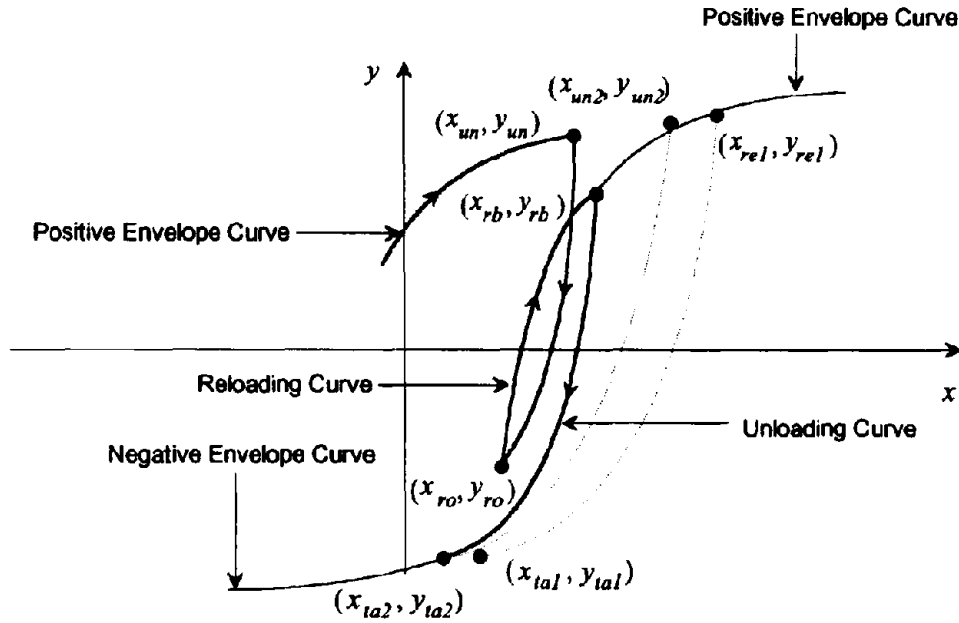


Fig. 3-23 Unloading from a Partial Reloading

When an incomplete reloading occurs, and the unloading takes place from (x_{rb}, y_{rb}) , then the total displacement from the reloading point (x_{ro}, y_{ro}) is:

$$\Sigma|\Delta x|_3 = x_{rb} - x_{ro} \quad (3-100)$$

By linear proportionality of the displacement increments:

$$\frac{\Delta x_2}{\Sigma|\Delta x|_3} = \frac{\Delta x_1}{\Sigma|\Delta x|_2} \quad (3-101)$$

By replacing Eqs. (3-99) and (3-100) into Eq. (3-101):

$$\Delta x_2 = \frac{x_{rb} - x_{ro}}{x_{rel} - x_{ro}} \Delta x_1 \quad (3-102)$$

This displacement increment still refers to the unloading point abscissa x_{un} , thus:

$$x_{un2} = x_{un} + \Delta x_2 \quad (3-103)$$

It should be noticed that if no displacement takes place from the reloading point $x_{rb} = x_{ro}$, then the displacement increment Δx_2 is zero which is correct, meaning that the target point is the original one. At this point the previous unloading abscissa is substituted by that calculated in Eq. (3-103). The next step is then to look at a partial unloading again.

3.8.2.3 Partial Unloading from a Partial Reloading

The new unloading point (x_{un2}, y_{un2}) calculated in Eq. (3-103) defines a target point (x_{ia2}, y_{ia2}) and returning point (x_{re2}, y_{re2}) , just as the unloading from the positive envelope curve. The difference is that now the starting point is not at the unloading point (x_{un2}, y_{un2}) but at the point of reversal (x_{rb}, y_{rb}) .

Because the unloading point has been replaced by the new unloading point, the "2" can be dropped from all the definitions. Thus, the displacement increment to reach the returning point is:

$$\Delta x_0 = x_{re2} - x_{un2} = x_{re} - x_{un} \quad (3-104)$$

Eq. (3-91a) has to be modified to include the new starting point:

$$\Sigma|\Delta x|_0 = x_{rb} - x_{ia2} + x_{re2} - x_{ia2} = x_{rb} + x_{un} - 2x_{ia} + \Delta x_0 \quad (3-105)$$

In case of an incomplete unloading from (x_{rb}, y_{rb}) at the reloading point (x_{ro}, y_{ro}) , a new displacement increment has to be defined.

$$\Delta x_1 = x_{re1} - x_{un} \quad (3-106)$$

The total displacement to reach the modified returning point (x_{re1}, y_{re1}) is:

$$\Sigma|\Delta x|_1 = x_{rb} - x_{ro} + x_{re3} - x_{ro} = x_{rb} + x_{un} - 2x_{ro} + \Delta x_1 \quad (3-107)$$

Finally by applying linear proportionality,

$$\Delta x_1 = \frac{x_{rb} + x_{un} - 2x_{ro}}{x_{rb} + x_{un} - 2x_{ia}} \Delta x_0 \quad (3-108)$$

This is the general form of Eq. (3-98). Any other parameter that depends on the unloading point can then be modified accordingly.

The application of the procedure just described can be summarized as follows:

- (1) At the point of unloading (x_{un}) from the envelope curve calculate:
 - (a) The target point (x_{ta})
 - (b) The displacement increment to reach the returning point (Δx_0)
- (2) Make $x_{rb} = x_{un}$
- (3) In case of a partial unloading (x_{ro}) use Eq. (3-108) to calculate the returning point (x_{rel})
- (4) In case of a partial reloading (x_{rb}) use Eq. (3-102) to calculate a new unloading point (x_{un}) and calculate:
 - (a) The target point (x_{ta})
 - (b) The displacement increment to reach the returning point (Δx_0)
- (5) Repeat from step (3).

The procedure was developed in terms of abscissas, and could have been described in terms of the ordinates, but in some cases the hysteretic behavior observed is not monotonically increasing but it can present peaks which can in turn represent ambiguities. This would make the ordinate an unsuitable variable to use. Another approach could be the use of energy (area under the curve) which is a more rational approach, but this approach requires much more computation, for sometimes the area has to be calculated numerically.

3.8.3 A Smooth Transition Curve for Mathematical Modeling

The need for a transition curve in mathematical modeling has led some researchers to propose various equations. Perhaps the most notable of all is the Ramberg-Osgood equation

Osgood (1935). A kind of inverse form of the R-O equation is the equation proposed by Menegotto and Pinto (1973), which has also been used extensively. Although useful, these equations are not simple to use when applied to certain problems, and normally require a degree of iteration to compute their control parameters.

A general equation that starts from an initial point (x_o, y_o) with an slope E_o and ends up at a final point (x_f, y_f) with a slope E_f is needed. A cubic polynomial of the form:

$$y = ax^3 + bx^2 + cx + d \quad (3-109)$$

can be fitted to satisfy the conditions presented, but as it is known a cubic polynomial might present a change of curvature, what means that it may not represent a monotonic transition. The curvature is related to the second derivative, which in this case would be a linear equation, that has to cross the x axis at some point. An equation that does not present this kind of change in curvature is needed. The proposed algebraic equation has the general form:

$$y = y_o + E_o(x - x_o) + A(x - x_o)^B \quad (3-110)$$

By taking derivative,

$$y' = E_o + AB(x - x_o)^{B-1} \quad (3-111)$$

If it is now assumed that the factor B has a value greater than 1, otherwise the first derivative would be indeterminate at $x = x_o$. Thus,

$$y'(x_o) = E_o \quad (3-112)$$

The derivative at the final point should be E_f , then:

$$y'(x_f) = E_f = E_o + AB(x_f - x_o)^{B-1} \quad (3-113)$$

Also,

$$AB(x_f - x_o)^{B-1} = E_f - E_o \quad (3-114)$$

By evaluating the ordinate at the final point,

$$y_f = y_o + E_o(x_f - x_o) + A(x_f - x_o)^B \quad (3-115)$$

Or,

$$A(x_f - x_o)^{B-1} = \frac{y_f - y_o}{x_f - x_o} - E_o = E_{sec} - E_o \quad (3-116)$$

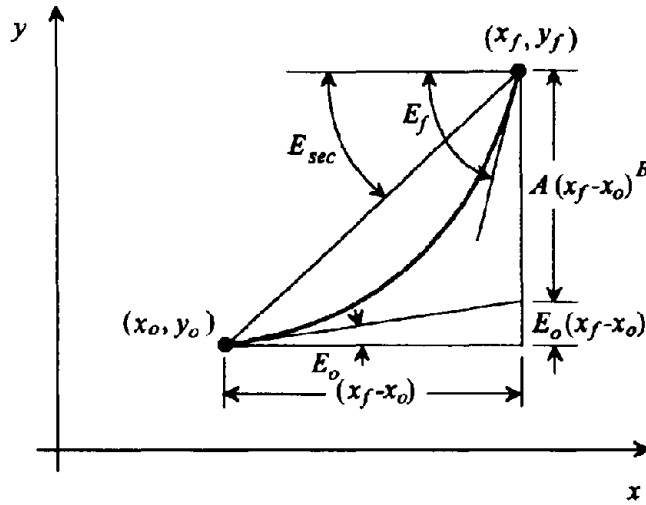


Fig. 3-24 A Smooth Transition Curve

By dividing Eqs. (3-114) by (3-116),

$$B = \frac{E_f - E_o}{E_{sec} - E_o} \quad (3-117)$$

Finally,

$$A = \frac{E_{sec} - E_o}{(x_f - x_o)^{B-1}} \quad (3-118)$$

where,

$$E_{sec} = \frac{y_f - y_o}{x_f - x_o} \quad (3-119)$$

In a more general form, the final expression is given as:

$$y = y_o + (x - x_o)[E_o + A|x - x_o|^R] \quad (3-120)$$

$$y' = E_o + A(R+1)|x - x_o|^{R-1} \quad (3-121)$$

where,

$$R = \frac{E_f - E_{sec}}{E_{sec} - E_o} \quad (3-122)$$

$$A = \frac{E_{sec} - E_o}{|x_f - x_o|^{R-1}} \quad (3-123)$$

and E_{sec} is given by Eq. (3-119).

3.9 Cyclic Properties of Confined and Unconfined Concrete

The monotonic curve forms the envelope for the stress-strain cyclic behavior. This was shown experimentally by Sinha, Gerstle and Tulin (1964) ; and Karsan and Jirsa (1969) and modeled by Mander et al. (1988a) for unconfined concrete in cyclic compression. For the case of confined concrete Mander et al. (1988b) also performed tests and validated their model (1988a). Experiments by Gopalaratnam and Shah (1985); and Yankelevsky and Reinhardt (1987b) have shown that this is also the case for concrete in cyclic tension.

3.9.1 Compression Envelope Curve (Rules 1 and 5)

The compression envelope curve is defined by the initial slope E_c , the peak coordinate $(\epsilon'_{cc}, f'_{cc})$, Tsai's equation r factor and a factor $x_{cr}^- > 1$ to define the spalling strain.

Both the compression and tension envelope curves can be written in non-dimensional form by the use of the following equations:

$$y(x) = \frac{nx}{D(x)} \quad (3-124)$$

$$z(x) = \frac{(1-x^r)}{[D(x)]^2} \quad (3-125)$$

where,

$$\begin{aligned} D(x) &= 1 + \left(n - \frac{r}{r-1}\right)x + \frac{x^r}{r-1} & r \neq 1 \\ &= 1 + (n - 1 + \ln x)x & r = 1 \end{aligned} \quad (3-126)$$

Let n and x be defined as:

$$x^- = \left| \frac{\epsilon_c}{\epsilon'_{cc}} \right| \quad (3-127)$$

$$n^- = \left| \frac{E_c \epsilon'_{cc}}{f'_{cc}} \right| \quad (3-128)$$

The spalling non-dimensional strain can be calculated by:

$$x_{sp} = x_{cr}^- - \frac{y(x_{cr}^-)}{n^- z(x_{cr}^-)} \quad (3-129)$$

where ϵ_c = concrete strain, f_c^- = concrete stress on the compression envelop, ϵ'_{cc} = concrete strain at peak confined stress, f'_{cc} = confined concrete strength, E_c = concrete initial Young modulus, x^- = non-dimensional strain on the compression envelope, x^-_{cr} = non-dimensional critical strain on the compression envelope curve. This strain is used to define a tangent line up to the spalling strain. x_{sp} = non-dimensional spalling strain, $y(x)$ = non-dimensional stress function, $z(x)$ = non-dimensional tangent modulus function, f_c = stress in concrete, E_t = tangent modulus, n^- = n value for the compression curve, assumed to be the same as that of unconfined concrete.

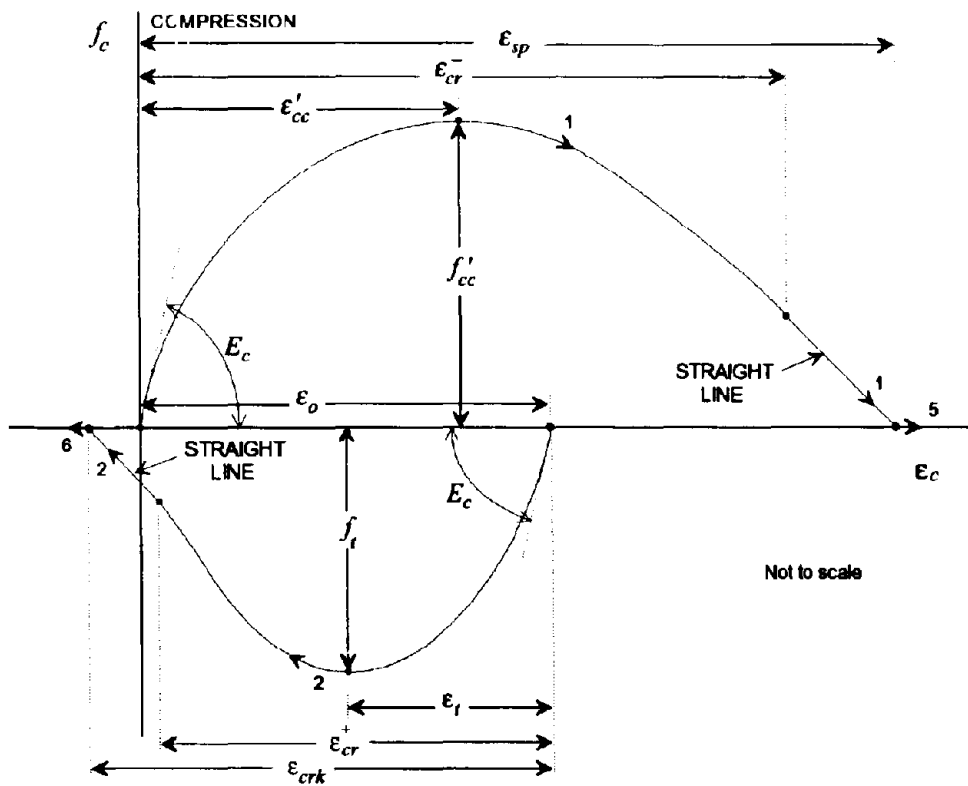


Fig. 3-25 Tension and Compression Envelope Curves

The stress and the tangent Young modulus at any given strain on the envelope compression curve are defined by:

$$f_c = f_c^-(x^-) \quad (3-130)$$

$$E_t = E_t^-(x^-)$$

where $f_c^-(x^-)$ and $E_t^-(x^-)$ are defined as:

(a) For $x^- < x_{cr}^-$ (Tsai's equation) (Rule 1):

$$f_c^- = f_{cc}' y(x^-) \quad (3-131)$$

$$E_t^- = E_c z(x^-) \quad (3-132)$$

(b) For $x_{cr}^- \leq x^- \leq x_{sp}$ (Straight Line) (Rule 1):

$$f_c^- = f_{cc}' [y(x_{cr}^-) + n^- z(x_{cr}^-) (x^- - x_{cr}^-)] \quad (3-133)$$

$$E_t^- = E_c z(x_{cr}^-) \quad (3-134)$$

(c) For $x^- > x_{cr}^-$ (Spalled) (Rule 5):

$$f_c^- = E_t^- = 0 \quad (3-135)$$

Once the concrete is considered to have spalled the stresses are zero from that moment on. Confined concrete can be considered not to spall, in such a case a large value of x_{cr}^- should be defined. Note that the minus superscript is considered to refer to the compression side of the stress-strain behavior.

3.9.2 Tension Envelope Curve (Rules 2 and 6)

The shape of the tension envelope curve is the same as that of the compression envelope curve. This curve is shifted to a new origin ϵ_o as it is explained later in this section. The non-dimensional parameters n and x given by:

$$x^+ = \left| \frac{\epsilon_c - \epsilon_o}{\epsilon_t} \right| \quad (3-136)$$

$$n^+ = \frac{E_c f_t}{\epsilon_t} \quad (3-137)$$

The cracking non-dimensional cracking strain is given by:

$$x_{crk}^+ = x_{cr}^+ - \frac{y(x_{cr}^+)}{n^+ z(x_{cr}^+)} \quad (3-138)$$

where ϵ_t = strain at peak tension stress, f_t = concrete tension strength, x^+ = non-dimensional strain in the tension envelope curve, n^+ = n value for the tension envelope curve, x_{cr}^+ = critical strain on the tension envelope curve. This factor is used to defined the cracking strain. The stress and tangent modulus for any given strain on the tension envelope curve are similarly defined as:

$$f_c = f_c^+(x^+) \quad (3-139)$$

$$E_t = E_t^+(x^+)$$

where $f_c^+(x^+)$ and $E_t^+(x^+)$ are defined as:

(a) For $x^+ < x_{cr}^+$ (Rule 2):

$$f_c^+ = f_t y(x^+) \quad (3-140)$$

$$E_t^+ = E_c z(x^+) \quad (3-141)$$

(b) For $x_{cr}^+ \leq x^+ \leq x_{crk}^+$ (Rule 2):

$$f_c^+ = f_t [y(x_{cr}^+) + n^+ z(x_{cr}^+) (x^+ - x_{cr}^+)] \quad (3-142)$$

$$E_t^+ = E_c z(x_{cr}^+) \quad (3-143)$$

(c) For $x^+ > x_{cr}^+$ (Cracked) (Rule 6):

$$f_c^+ = E_t^+ = 0 \quad (3-144)$$

Where functions y and z are defined by Eqs. (3-124) and (3-125). When the concrete has cracked it is considered to no longer resist any tension stress, as a result of crack opening, but on the other hand a gradual crack closure is considered to take place.

3.9.3 Pre-Cracking Unloading and Reloading Curves

The basic elements of the unloading and reloading curves are dealt with in this section. Every rule is represented by a smooth curve that starts at a starting point with a given slope and ends up at a target point with an ending slope, and the equation used to represent the transition is the one derived in section 3.7.3. In terms of stresses and strains:

$$f_c = f_t + (\epsilon_c - \epsilon_t) [E_t + A |\epsilon_c - \epsilon_t|^R] \quad (3-145)$$

$$E_t = \frac{\partial f_c}{\partial \epsilon_c} = E_t + A(R+1) |\epsilon_c - \epsilon_t|^R \quad (3-146)$$

in which,

$$R = \frac{E_F - E_{SEC}}{E_{SEC} - E_I} \quad (3-147)$$

$$A = \frac{E_{SEC} - E_I}{|\epsilon_F - \epsilon_I|^R} \quad (3-148)$$

with,
$$E_{SEC} = \frac{f_F - f_I}{\epsilon_F - \epsilon_I} \quad (3-149)$$

where "f" is stress, "ε" is strain, "E" is tangent or secant modulus, "c" means concrete, "I" initial, "F" final, "SEC" secant, "t" tangential and "R" and "A" are equation parameters.

To define the cyclic properties of concrete, statistical regression analyses were performed on the experimental data from Sinha, Gerstle and Tulin (1964), Karsan and Jirsa (1969), Spooner and Dougill (1975), Okamoto (1976) and Tanigawa (1979). The model parameters looked for are shown in Fig. 3-26, and the results of the analysis were:

$$E_{sec}^- = E_c \left(\frac{\left| \frac{f_{un}^-}{E_c \epsilon_{cc}'} \right| + 0.57}{\left| \frac{\epsilon_{un}^-}{\epsilon_{cc}'} \right| + 0.57} \right) \quad (3-150)$$

$$E_{pl}^- = 0.1 E_c \exp \left(-2 \left| \frac{\epsilon_{un}^-}{\epsilon_{cc}'} \right| \right) \quad (3-151)$$

$$\Delta f^- = 0.09 f_{un}^- \sqrt{\left| \frac{\epsilon_{un}^-}{\epsilon_{cc}'} \right|} \quad (3-152)$$

$$\Delta \epsilon^- = \frac{\epsilon_{un}^-}{1.15 + 2.75 \left| \frac{\epsilon_{un}^-}{\epsilon_{cc}'} \right|} \quad (3-153)$$

The derived variables are then:

$$\epsilon_{pl}^- = \epsilon_{un}^- - \frac{f_{un}^-}{E_{sec}^-} \quad (3-154)$$

$$f_{new}^- = f_{un}^- - \Delta f^- \quad (3-155)$$

$$E_{new}^- = \frac{f_{new}^-}{\epsilon_{un}^- - \epsilon_{pl}^-} \quad (3-156)$$

$$\epsilon_{re}^- = \epsilon_{un}^- + \Delta \epsilon^- \quad (3-157)$$

$$f_{re}^- = f^- \left(\left| \frac{\epsilon_{re}^-}{\epsilon_{cc}'} \right| \right) \quad (3-158)$$

$$E_{re}^- = E^- \left(\left| \frac{\epsilon_{re}^-}{\epsilon_{cc}'} \right| \right) \quad (3-159)$$

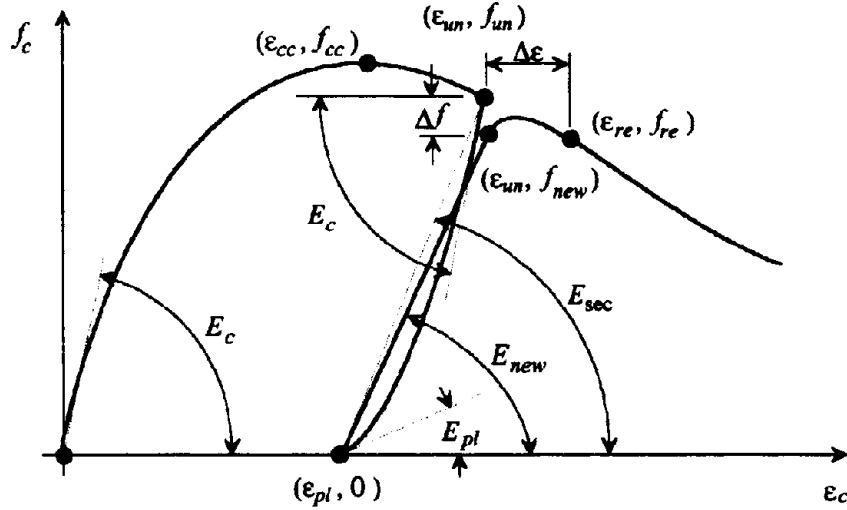


Fig. 3-26 Cyclic Compression Characteristics of Concrete

For cyclic behavior of concrete in tension, some of the properties defined in equations (3-150) through (3-159) required modification. The hysteretic parameters for cyclic tension are given by:

$$E_{sec}^+ = E_c \left(\frac{\left| \frac{f_{un}^+}{E_c \epsilon_t} \right| + 0.67}{\left| \frac{\epsilon_{un}^+ - \epsilon_o}{\epsilon_t} \right| + 0.67} \right) \quad (3-160)$$

$$E_{pl}^+ = \frac{E_c}{\left| \frac{\epsilon_{un}^+ - \epsilon_o}{\epsilon_t} \right|^{1.1} + 1} \quad (3-161)$$

$$\Delta f^+ = 0.15 f_{un}^+ \quad (3-162)$$

$$\Delta \epsilon^+ = 0.22 \epsilon_{un}^+ \quad (3-163)$$

Similarly,

$$\epsilon_{pl}^+ = \epsilon_{un}^+ - \frac{f_{un}^+}{E_{sec}^+} \quad (3-164)$$

$$f_{new}^+ = f_{un}^+ - \Delta f^+ \quad (3-165)$$

$$E_{new}^+ = \frac{f_{new}^+}{\epsilon_{un}^+ - \epsilon_{pl}^+} \quad (3-166)$$

$$\epsilon_{re}^+ = \epsilon_{un}^+ + \Delta\epsilon^+ \quad (3-167)$$

$$f_{re}^+ = f^+ \left(\left| \frac{\epsilon_{re}^+ - \epsilon_o}{\epsilon_t} \right| \right) \quad (3-168)$$

$$E_{re}^+ = E^+ \left(\left| \frac{\epsilon_{re}^+ - \epsilon_o}{\epsilon_t} \right| \right) \quad (3-169)$$

where ϵ_{un} = unloading strain from an envelope curve, f_{un} = unloading stress, ϵ_{pl} = plastic strain, E_{pl} = tangent modulus when the stress is released, f_{new} = new stress at the unloading strain, E_{new} = tangent modulus at the new stress point, ϵ_{re} = strain at the returning point to the envelope curve, f_{re} = stress at the returning point, E_{re} = tangent modulus at the returning point.

A reversal from the compression envelope curve is done through rules 3, 9 and 8 as shown. The variables that define this reversal curve are calculated as follows:

- (1) Calculate the compression strain ductility as:

$$x_u^- = \left| \frac{\epsilon_{un}^-}{\epsilon_{cc}^-} \right| \quad (3-170)$$

- (2) Calculate the tension strain ductility,

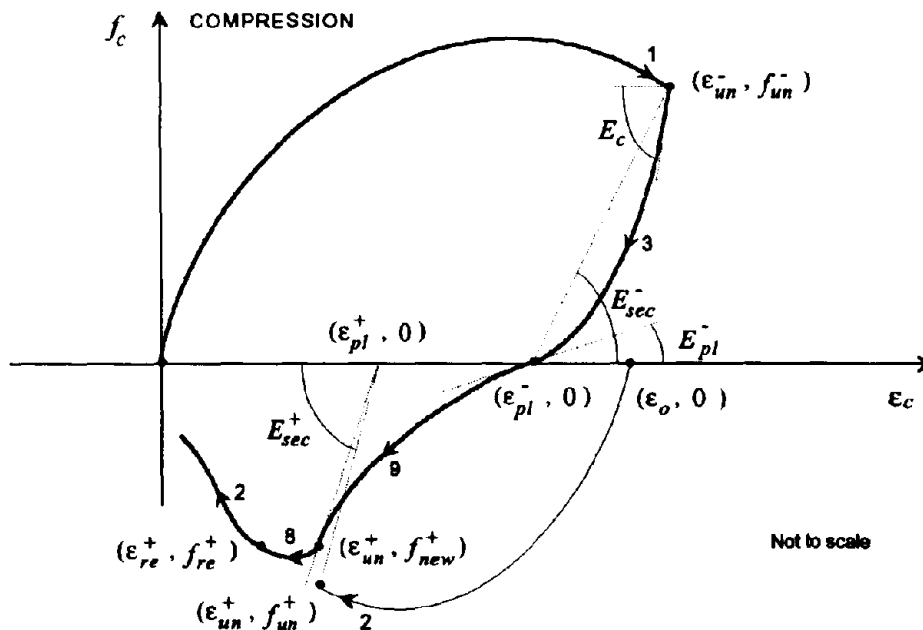


Fig. 3-27 Complete Unloading Branch

$$x_u^+ = \left| \frac{\epsilon_{un}^+ - \epsilon_o}{\epsilon_t} \right| \quad (3-171)$$

(3) If $x_u^+ < x_u^-$ then:

$$x_u^+ = x_u^-$$

$$\epsilon_o = 0$$

$$\epsilon_{un}^+ = x_u^+ \epsilon_t$$

$$f_{un}^+ = f_c^+(x_u^+) \text{ using Eq. (3-139)}$$

(4) Calculate

$$\Delta \epsilon_o = \frac{2 f_{un}^+}{E_{sec}^+ + E_{pl}^-} \quad (3-172)$$

(5) Finally,

$$\epsilon_o = \epsilon_{pl}^- + \Delta \epsilon_o - x_u^+ \epsilon_t \quad (3-173)$$

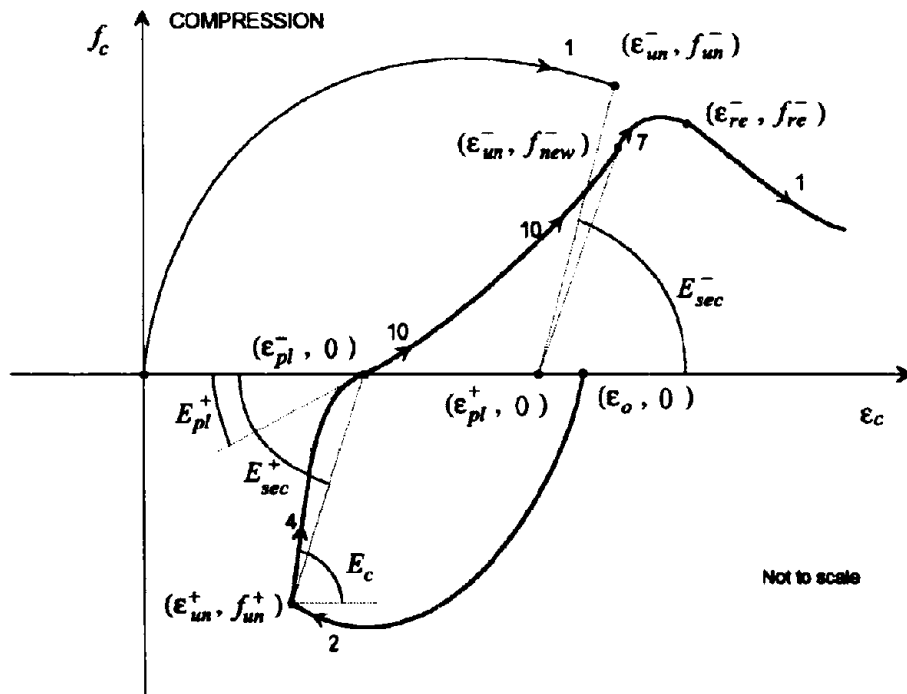


Fig. 3-28 Complete Loading Branch

and,

$$\epsilon_{un}^+ = x_M^+ \epsilon_I + \epsilon_o \quad (3-174)$$

The rules parameters for the connecting curve for a reversal from the compression envelope curve are defined by:

$$\begin{array}{l} \text{Rule 3} \\ \epsilon_I = \epsilon_{un}^- \\ f_I = f_{un}^- \\ E_I = E_c \\ \epsilon_F = \epsilon_{pl}^- \\ f_F = 0 \\ E_F = E_{pl}^- \end{array} \quad (3-175)$$

$$\begin{array}{l} \text{Rule 9} \\ \epsilon_I = \epsilon_{pl}^- \\ f_I = 0 \\ E_I = E_{pl}^- \\ \epsilon_F = \epsilon_{un}^+ \\ f_F = f_{new}^+ \\ E_F = E_{new}^+ \end{array} \quad (3-176)$$

$$\begin{array}{l} \text{Rule 8} \\ \epsilon_I = \epsilon_{un}^+ \\ f_I = f_{new}^+ \\ E_I = E_{new}^+ \\ \epsilon_F = \epsilon_{re}^+ \\ f_F = f_{re}^+ \\ E_F = E_{re}^+ \end{array} \quad (3-177)$$

Similarly, for a reversal from the tension envelope curve:

$$\begin{array}{l} \text{Rule 4} \\ \epsilon_I = \epsilon_{un}^+ \\ f_I = f_{un}^+ \\ E_I = E_c \\ \epsilon_F = \epsilon_{pl}^+ \\ f_F = 0 \\ E_F = E_{pl}^+ \end{array} \quad (3-178)$$

$$\begin{array}{l} \text{Rule 10} \\ \epsilon_I = \epsilon_{pl}^+ \\ f_I = 0 \\ E_I = E_{pl}^+ \\ \epsilon_F = \epsilon_{un}^- \\ f_F = f_{new}^- \\ E_F = E_{new}^- \end{array} \quad (3-179)$$

$$\begin{aligned}
 \epsilon_I &= \epsilon_{un}^- \\
 f_I &= f_{new}^- \\
 E_I &= E_{new}^- \\
 \epsilon_F &= \epsilon_{re}^- \\
 f_F &= f_{re}^- \\
 E_F &= E_{re}^-
 \end{aligned}
 \tag{3-180}$$

Rule 7

3.9.4 Post-Cracking Unloading and Reloading Curves

After complete cracking is considered to have occurred, no tension capacity is assumed to exist, so the tension side of the hysteresis behavior will also not exist. The after unloading (rule 3), the crack will open (rule 6); when the direction of loading reverses, gradual crack closure takes place (rule 13).

$$\begin{aligned}
 \epsilon_I &= \epsilon_r \\
 f_I &= 0 \\
 E_I &= 0 \\
 \epsilon_F &= \epsilon_{un}^- \\
 f_F &= f_{new}^- \\
 E_F &= E_{new}^-
 \end{aligned}
 \tag{3-181}$$

Rule 13

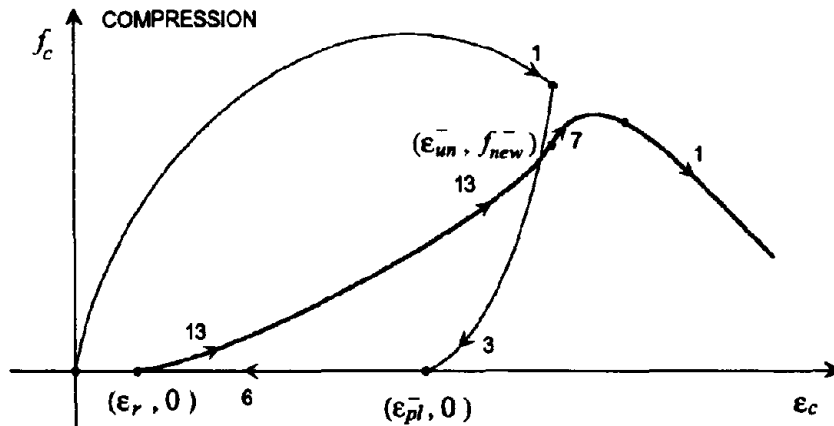


Fig. 3-29 Loading and Unloading Curve after Cracking

3.9.5 Pre-Cracking Transition Curves

When a partial loading or unloading within any of the connecting curve occurs, a transition curve is used. Rules 3, 4, 9 and 10 are connecting curves, so each one will be considered individually. When a reversal from rule 3 takes place, f_{new}^- needs to be changed, the new stress ordinate is called f_{re}^- ; and the returning point coordinate $(\epsilon_{re}^-, f_{re}^-)$ are also changed to $(\epsilon_{re}^-, f_{re}^-)$. The modified expressions are:

$$f_{new}^- = f_{un}^- - \Delta f^- \frac{\epsilon_{un}^- - \epsilon_{ro}^-}{\epsilon_{un}^- - \epsilon_{pl}^-} \quad (3-182)$$

$$E_{new}^- = \frac{f_{new}^- - f_{ro}^-}{\epsilon_{un}^- - \epsilon_{ro}^-} \quad (3-183)$$

$$\epsilon_{re}^- = \epsilon_{un}^- + \Delta \epsilon^- \frac{\epsilon_{un}^- - \epsilon_{ro}^-}{\epsilon_{un}^- - \epsilon_{pl}^-} \quad (3-184)$$

$$f_{re}^- = f^-(\epsilon_{re}^-) \quad (3-185)$$

$$E_{re}^- = E^- \left(\left| \frac{\epsilon_{re}^-}{\epsilon_{cc}^-} \right| \right) \quad (3-186)$$

The curve modified Rule 7 is thus given as:

Rule7*

$$|\epsilon_{ro}^-| \leq |\epsilon_c| \leq |\epsilon_{un}^-|$$

$$\begin{aligned} \epsilon_I &= \epsilon_{ro}^- \\ f_I &= f_{ro}^- \\ E_I &= E_c \\ \epsilon_F &= \epsilon_{un}^- \\ f_F &= f_{new}^- \\ E_F &= E_{new}^- \end{aligned} \quad (3-187)$$

$$|\epsilon_{un}^-| < |\epsilon_c| < |\epsilon_{re}^-|$$

$$\begin{aligned} \epsilon_I &= \epsilon_{un}^- \\ f_I &= f_{new}^- \\ E_I &= E_{new}^- \\ \epsilon_F &= \epsilon_{re}^- \\ f_F &= f_{re}^- \\ E_F &= E_{re}^- \end{aligned} \quad (3-188)$$

Similarly for a reversal from rule 4, the modified rule 8 is given as:

Rule 8*

$$\begin{aligned}
 &|\epsilon_{ro}^+ - \epsilon_o| \leq |\epsilon_c - \epsilon_o| \leq |\epsilon_{un}^+ - \epsilon_o| & \begin{aligned} \epsilon_I &= \epsilon_{ro}^+ \\ f_I &= f_{ro}^+ \\ E_I &= E_c \\ \epsilon_F &= \epsilon_{un}^+ \\ f_F &= f_{new}^+ \\ E_F &= E_{new}^+ \end{aligned} & (3-189)
 \end{aligned}$$

$$\begin{aligned}
 &|\epsilon_{un}^+ - \epsilon_o| < |\epsilon_c - \epsilon_o| < |\epsilon_{re}^+ - \epsilon_o| & \begin{aligned} \epsilon_I &= \epsilon_{un}^+ \\ f_I &= f_{new}^+ \\ E_I &= E_{new}^+ \\ \epsilon_F &= \epsilon_{re}^+ \\ f_F &= f_{re}^+ \\ E_F &= E_{re}^+ \end{aligned} & (3-190)
 \end{aligned}$$

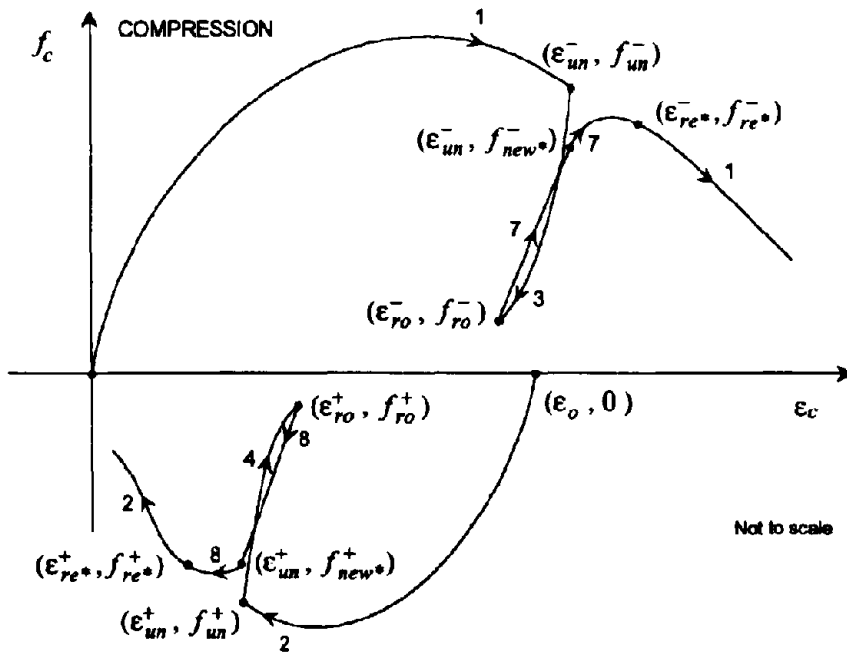


Fig. 3-30 Partial Unloading Curves for Tension and Compression

where:

$$f_{new}^+ = f_{un}^+ - \Delta f^+ \frac{\epsilon_{un}^+ - \epsilon_{ro}^+}{\epsilon_{un}^+ - \epsilon_{pl}^+}$$

(3-191)

$$E_{new}^+ = \frac{f_{new}^+ - f_{ro}^+}{\epsilon_{un}^+ - \epsilon_{ro}^+} \quad (3-192)$$

$$\epsilon_{re}^+ = \epsilon_{un}^+ + \Delta \epsilon^+ \frac{\epsilon_{un}^+ - \epsilon_{ro}^+}{\epsilon_{un}^+ - \epsilon_{pl}^+} \quad (3-193)$$

$$f_{re}^+ = f^+ \left(\left| \frac{\epsilon_{re}^+ - \epsilon_o}{\epsilon_t} \right| \right) \quad (3-194)$$

$$E_{re}^+ = E^+ \left(\left| \frac{\epsilon_{re}^+ - \epsilon_o}{\epsilon_t} \right| \right) \quad (3-195)$$

A reversal from rule 9 at the point $A (\epsilon_a, f_a)$ will target the point $B (\epsilon_b, f_b)$ through rule 11, an incomplete loading on rule 11 will target the point $A (\epsilon_a, f_a)$ again through rule 12. The relation between A and B is computed through the relation:

$$\frac{\epsilon_a - \epsilon_{pl}^-}{\epsilon_{un}^+ - \epsilon_{pl}^-} = \frac{\epsilon_{un}^- - \epsilon_b}{\epsilon_{un}^- - \epsilon_{pl}^+} \quad (3-196)$$

Rule 11

$$\begin{aligned} \epsilon_t &= \epsilon_r \\ f_t &= f_r \\ E_t &= E_c \\ \epsilon_F &= \epsilon_b \\ f_F &= f_b \\ E_F &= E_t(\epsilon_b) \end{aligned} \quad (3-197)$$

Rule 12

$$\begin{aligned} \epsilon_t &= \epsilon_r \\ f_t &= f_r \\ E_t &= E_c \\ \epsilon_F &= \epsilon_a \\ f_F &= f_a \\ E_F &= E_t(\epsilon_a) \end{aligned} \quad (3-198)$$

where (ϵ_r, f_r) is the last reversal coordinate.

3.9.6 Post-Cracking Transition Curves

After cracking, the tension envelope curve is zero, and the connecting compression curve becomes rule 13. A reversal from rule 13 at coordinate (ϵ_a, f_a) targets the horizontal axis at strain ϵ_b , which is calculated by:

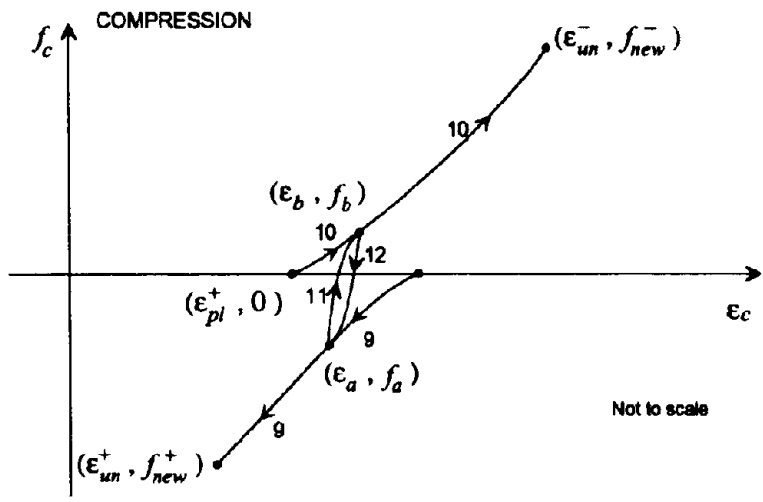


Fig. 3-31 Transition Curves (Before Cracking)

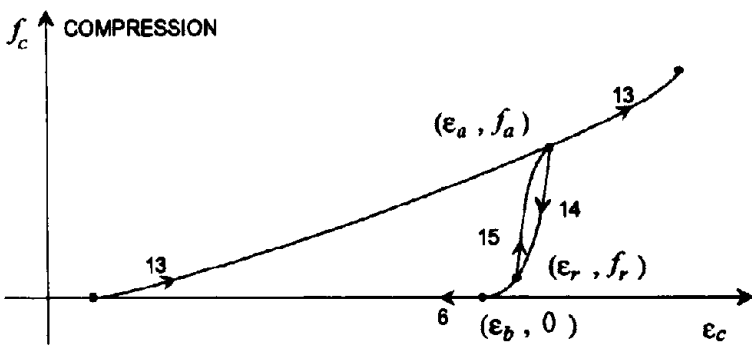


Fig. 3-32 Transition Curves (After Cracking)

$$\epsilon_b = \epsilon_a - \frac{f_a}{E_{mc}^-} \quad (3-199)$$

Rule 14

$$\begin{aligned} \epsilon_I &= \epsilon_r \\ f_I &= f_r \\ E_I &= E_c \\ \epsilon_F &= \epsilon_b \\ f_F &= 0 \\ E_F &= 0 \end{aligned} \quad (3-200)$$

Rule 15

$$\begin{aligned} \epsilon_I &= \epsilon_r \\ f_I &= f_r \\ E_I &= E_c \\ \epsilon_F &= \epsilon_a \\ f_F &= f_a \\ E_F &= E_t(\epsilon_a) \end{aligned} \quad (3-201)$$

where, again (ϵ_r, f_r) is the coordinate at last reversal.

Fig. 3-33 summarizes the relation among the rules of the model just presented. The tension side has been exaggerated for purposes of clarity.

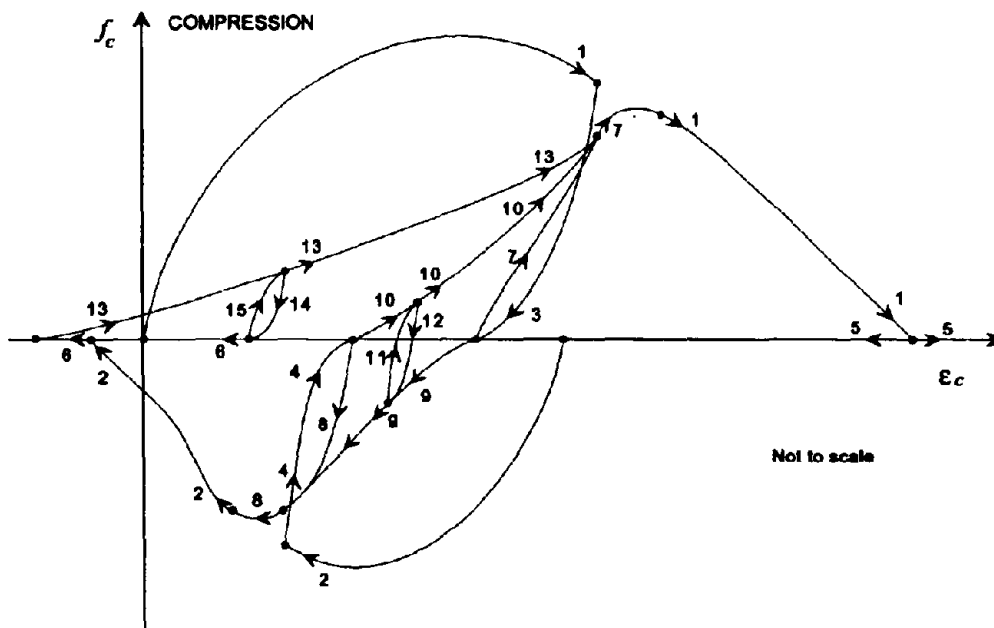


Fig. 3-33 Relationship Among the Model Rules

3.10 Model Verification

A subroutine ACONCRETE was implemented for use in a computer program. Results from the model are shown in Figs. 3-34 to 3-38 for unconfined concrete. Experimental data from Sinha, Gerstle and Tulin (1964), Karsan and Jirsa (1960), Okamoto et al. (1976), and Tanigawa et al. (1979) for cyclic compression, were used to test the model. Fig. 3-39 presents Yankelevsky and Reinhardt (1987b) experimental data for cyclic tension with small incursions into compression, while Figs. 3-40 and 3-41 show the application of the model to the Mander et al. (1988b) experimental data for confined concrete in cyclic compression. Finally Fig. 3-42 shows how the tension branch of the model compares with the equations given by Collins and Mitchell, Eq. (3-86); and by Hsu, Eq. (3-87). It is to be noted that no previous model (Mander et al., 1988a; Yankelevsky and Reinhardt, 1987a) could describe the cyclic behavior of concrete in both tension and compression.

3.11 Damage Analysis

The ultimate rotation capacity at a plastic hinge is a function of the ultimate concrete compressive strain ϵ_{cu} . Early experimental work led to empirical equations for ϵ_{cu} , (Park and Paulay, 1975). More recently, Scott et al. (1982) have proposed that the ultimate compressive strain be defined by the first hoop fracture. Mander et al. (1984, 1988a) proposed a rational method for the prediction of the first hoop fracture based on an energy approach. In this method the energy stored in the hoop is considered to give the additional energy absorption capacity to the confined concrete. An energy analysis within the core area (A_{cc}) is as follows:

The strain energy capacity of unconfined concrete U_{co} is given by:

$$U_{co} = A_{cc} \int_0^{\epsilon_{spall}} f_c d\epsilon \quad (3-202)$$

where ϵ_{spall} = spalling strain of unconfined concrete. As the stress-strain relationship for unconfined concrete is known, the integral term can be calculated by numerically integrating

this expression. A good approximation to the volumetric strain energy capacity of plain unconfined concrete was found by Mander et al. (1984) to be given by:

$$\int_0^{\epsilon_{spall}} f_c d\epsilon = \begin{matrix} 0.205 \sqrt{f'_c} & \text{psi} \\ 0.017 \sqrt{f'_c} & \text{MPa} \end{matrix} \quad (3-203)$$

The fracture strain energy of hoop reinforcement is calculated as:

$$U_{sh} = \rho_{sh} A_{cc} \int_0^{\epsilon_{sf}} \epsilon_s d\epsilon_s \quad (3-204)$$

where ρ_{sh} = volumetric transverse steel content relative to the concrete core; f_s and ϵ_s = stress and strain in transverse reinforcement; ϵ_{sf} = fracture strain of transverse reinforcement. The volumetric fracture strain energy was found by Mander et al. (1984) to be a constant for all types of reinforcing steel and independent of bar size, that can be taken as:

$$\int_0^{\epsilon_{sf}} f_s d\epsilon_s = \begin{matrix} 16 \text{ ksi} \\ 110 \text{ MPa} \end{matrix} \pm 10\% \quad (3-205)$$

The energy balance theory assumes that the energy to fracture the transverse reinforcement comes from the difference in strain energy capacity between the confined and unconfined concrete ($U_{cc} - U_{co}$), plus an additional energy to maintain yield in the longitudinal steel in compression (U_{sc}). Thus,

$$U_{sf} = U_{cc} - U_{co} + U_{sc} \quad (3-206)$$

with

$$U_{sc} = \rho_{cc} A_{cc} \int_0^{\epsilon_{cu}} f_{sl} d\epsilon_c \quad (3-207)$$

and

$$U_{cc} = A_{cc} \int_0^{\epsilon_{cu}} f_{cc} d\epsilon_c \quad (3-208)$$

in which, ρ_{cc} = volumetric longitudinal steel content relative to the core concrete, f_{sl} = stress on the longitudinal stress bars, f_{cc} = stress on the confined concrete and ϵ_{cu} = strain at fracture (ultimate strain on core concrete).

For eccentric loading, the energy balance theory can be readily applied by assigning a participation factor to the core concrete and to every steel layer. This participation factor is the proportion of energy absorption in compression that is taken by the critical crossie. This

approach was developed and validated by Mander et al. (1988a, b) and has been adopted herein.

3.12 Conclusions

The following conclusions can be drawn from this section:

1. It has been demonstrated that the equation proposed by Tsai is the most effective in describing the shape of the monotonic behavior of concrete both in compression and tension. Other equations may give anomalies in behavior. Tsai's equation can be used for both confined and unconfined concrete. This equation is a generalized form of that by Popovics, requiring four control parameters: ϵ'_{cc} , f'_{cc} , E_c and r . The fourth parameter controls the falling branch curve. This is considered important when modeling the behavior of high strength concrete or when high strength steel is used to confine the concrete.

2. The confinement model developed by Mander et al. (1984, 1988a,b), applicable to any general cross-sectional shape, can be further simplified by the use of the given approximate equation.

3. Calibration of parameters in both confined and unconfined concrete led to some empirical equations that can be further enhanced as more experimental data become available.

4. The general components of a rule-based model are identified, and suggestions to ensure a consistent behavior were presented.

5. The mathematical description of degradation has been examined, and a general model to describe it is proposed.

6. A mathematical expression to join two slopes is proposed.

7. A model to describe the behavior of concrete in both cyclic tension and compression is proposed. To the knowledge of the authors, this is the first time a model to represent the hysteretic behavior in both tension and compression of confined and unconfined concrete is proposed. The model proved to be effective in describing the hysteretic behavior of confined and unconfined concrete, subjected to both compression cyclic loading and tension cyclic loading. As more experimental data becomes available for cyclic tension, better equation validation/calibration may be possible. No experiments to relate cyclic combined tension and compression have been done to this date, except for that by Yankelevsky and Reinhardt (1987b) for tension cyclic loading with small incursions into compression. It is necessary to have this kind of experimental data to calibrate the model more reliably, and is considered essential for robust deterministic damage assessments of members governed by cyclic flexure-shear effects.

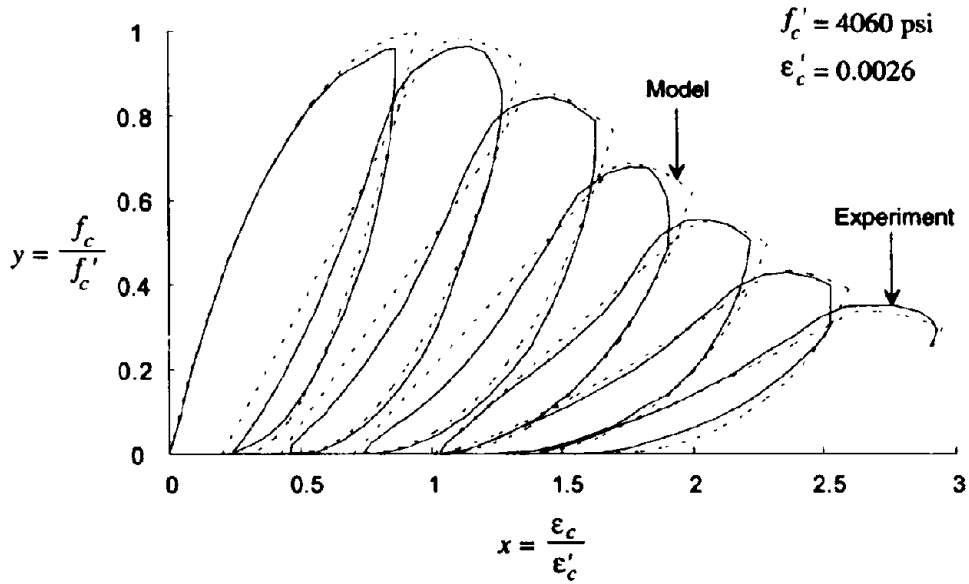


Fig. 3-34 Unconfined Cyclic Compression Test by Sinha, Gerstle and Tulin (1964)

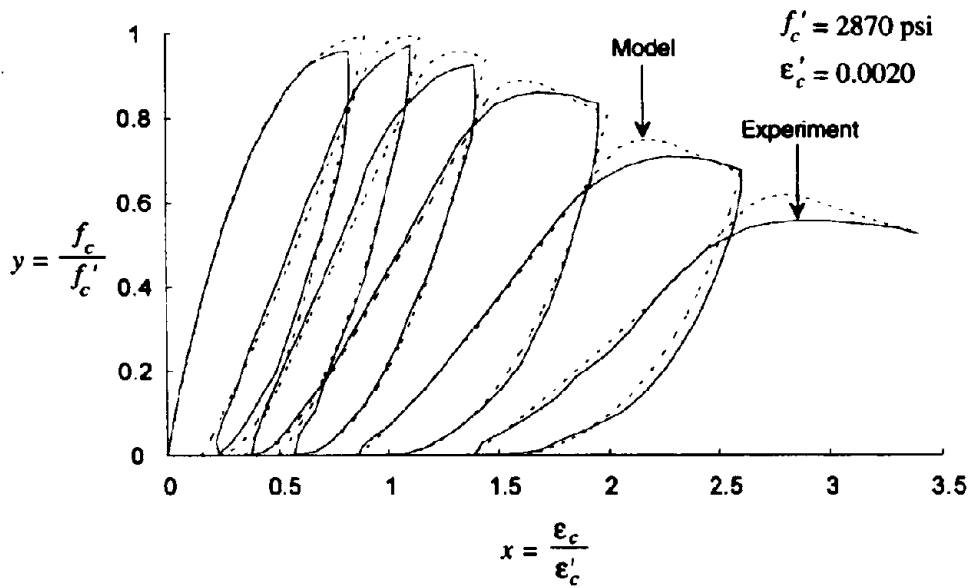


Fig. 3-35 Unconfined Cyclic Compression Test by Karsan and Jirsa (1969)

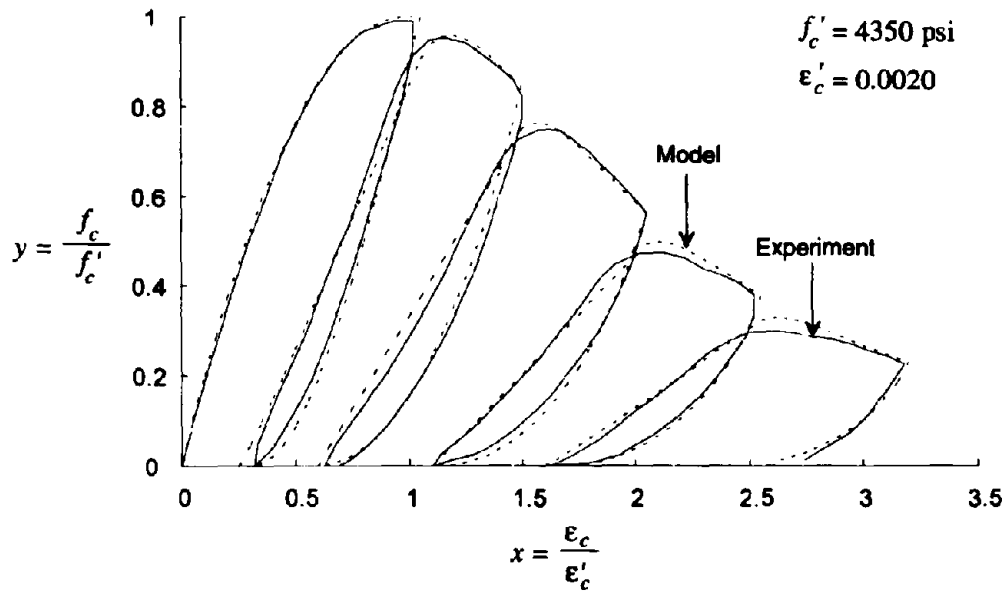


Fig. 3-36 Unconfined Cyclic Compression Test by Okamoto (1976)

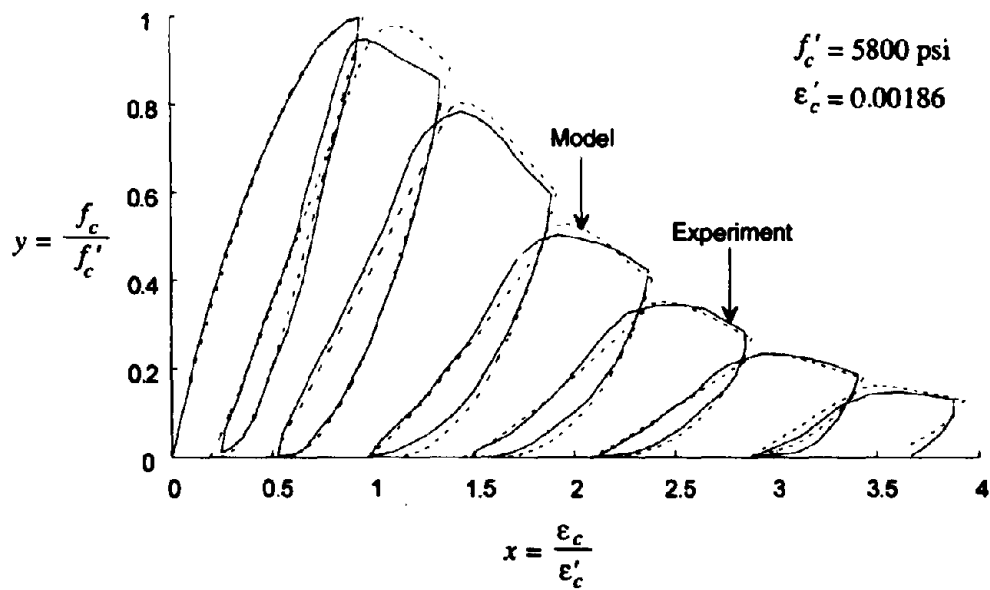


Fig. 3-37 Unconfined Cyclic Compression Test by Okamoto (1976)

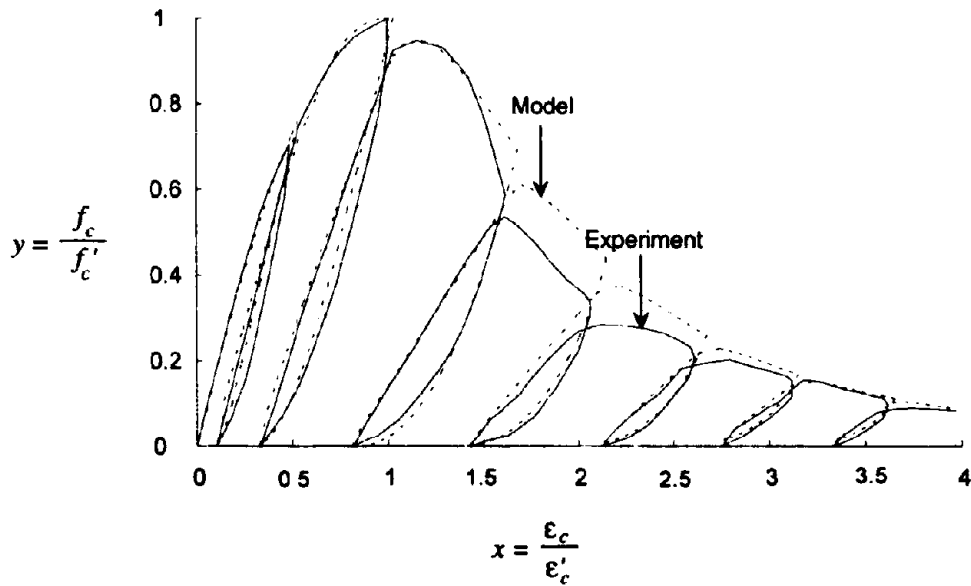


Fig. 3-38 Unconfined Cyclic Compression Test by Tanigawa (1979)

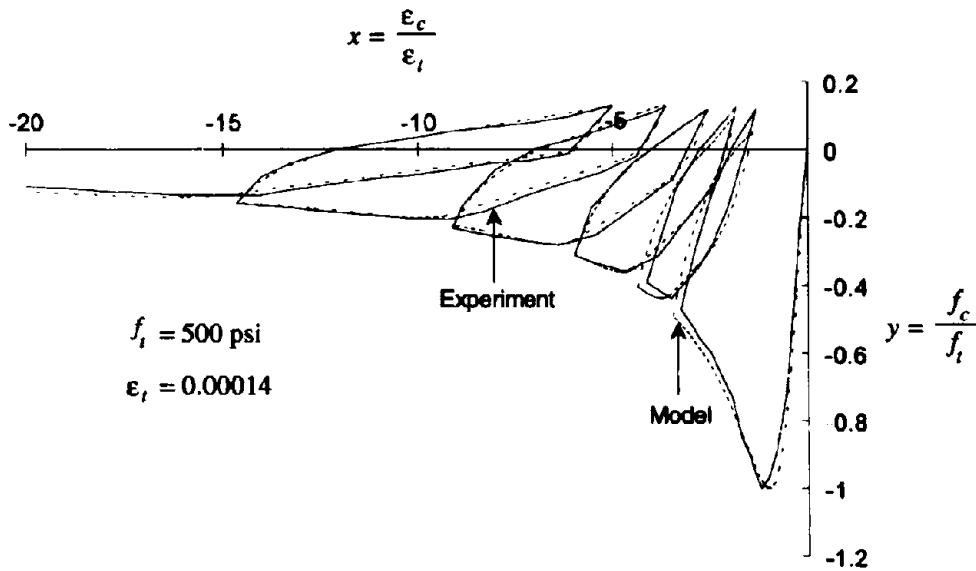


Fig. 3-39 Cyclic Tension Test by Yankelevsky and Reinhardt (1987)

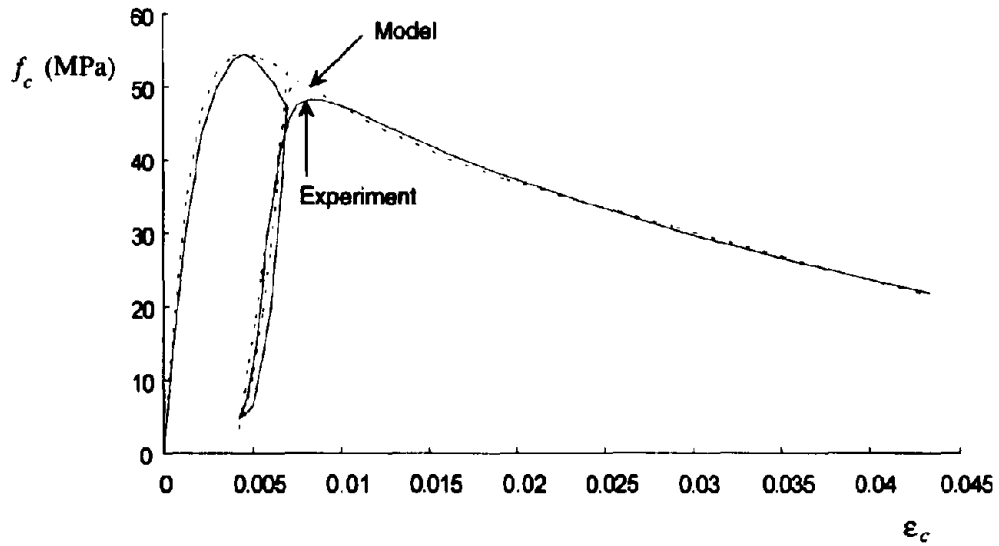


Fig. 3-40 Confined Concrete Cyclic Test by Mander et al. (1984)

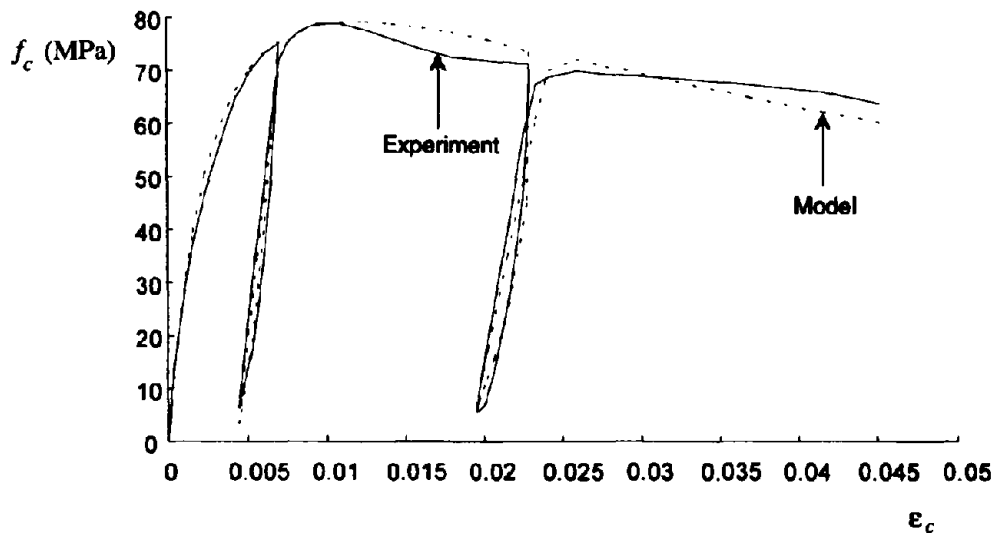


Fig. 3-41 Confined Concrete Cyclic Test by Mander et al. (1984)

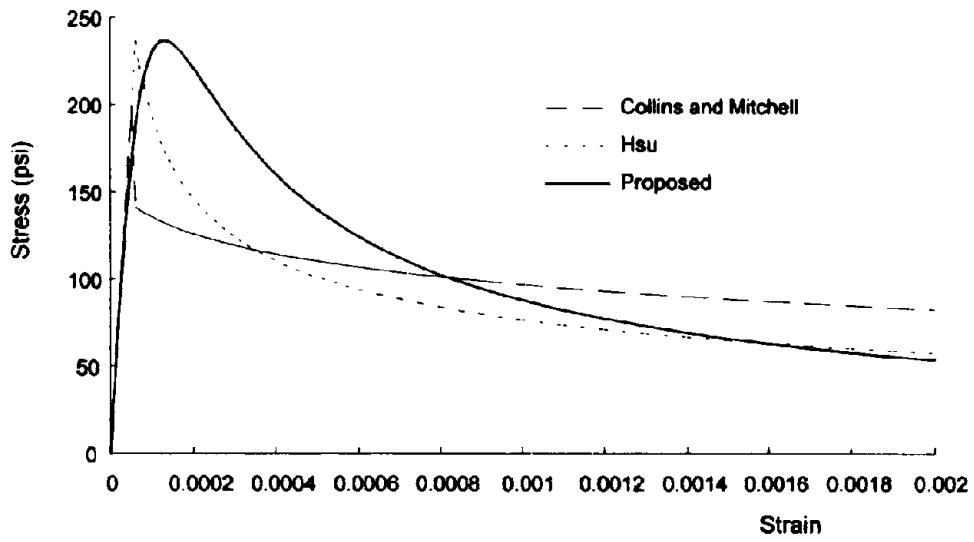


Fig. 3-42 Comparison of the Proposed Tension Branch Equation with other Analytical Equations.

Section 4

Damage Modeling of Reinforced Concrete Columns using Fiber-Element Analysis

4.1 Introduction

A computer program RC-COLA was developed to obtain the moment-curvature and force-displacement response of structural concrete columns under reversed cyclic flexure and axial force. The main objective of the program as part of this investigation is to develop an advanced micro-model analysis program to perform simulated experiments. Experimental simulation can be used as the input data for the calibration of macro-models that are commonly used in general purpose non-linear dynamic analysis programs such as IDARC and DRAIN-2DX. So far, the fine tuning of macro-model parameters have been based capriciously on the user choice. This arbitrary choice of model parameters generates some skepticism regarding the validity of such analyses. This problem will be addressed later in the next section. The present section develops, from first principles, a biaxial "fiber" analysis. Herein the term "Fiber-Element Analysis" is coined to refer to the entire computational procedure.

4.2 Moment-Curvature Analysis for Uniaxial Bending

The strain profile is assumed to follow Bernoulli's assumption that plane sections remain plane, thus the strain at any fiber is given by:

$$\epsilon = \epsilon_o + \phi(y - y_o) \quad (4-1)$$

where ϵ_o = strain at the centroid, y_o = ordinate of the origin, ϵ = strain at any ordinate y . For a given centroidal origin, if no bond slip is assumed to occur, the strain in the concrete and the reinforcing bars will be the same, both being determined from Eq. (4-1).

The axial force and the moment at a given section can be readily calculated as:

$$P = \int_{A_g} f_c dA + \sum_i (f_{si} - f_{ci}) A_{si} \quad (4-2)$$

$$M = \int_{A_g} (y - y_o) f_c dA + \sum_i (y_{si} - y_o) (f_{si} - f_{ci}) A_{si} \quad (4-3a)$$

$$M = \int_{A_g} y f_c dA + \sum_i y_{si} (f_{si} - f_{ci}) A_{si} - y_o P \quad (4-3b)$$

where, P = axial load, M = moment about the centroid, A_g = gross area, f_c = concrete stress function, i = index to refer to the i th layer of steel, f_{si} = steel stress, f_{ci} = concrete stress, A_{si} = area of steel, y_{si} = ordinate. Note that the origin can be located anywhere, to make the formulation general.

It is important to note that for a zero axial load section the neutral axis coincides with the centroid of the transformed section, and as the behavior goes into the inelastic zone, the centroid shifts. When no axial load is present the point about which the moment is defined is irrelevant. But in the presence of axial load, the point about which the moment is defined is important. For symmetric sections the geometric centroid is the obvious choice, but for asymmetric sections two definitions are possible: (1) location of the neutral axis in the absence of axial load, as mentioned before, this location shifts; (2) plastic centroid, which is defined for a constant strain at the material strength capacities.

If the centroidal strain ϵ_o and curvature ϕ are known the axial force P and moment M can be directly calculated by using Eqs. (4-2) and (4-3). But normally the inverse problem, in which ϵ_o and ϕ are to be determined from known values of P and M , or a mixed problem is encountered. In this case some degree of iteration may be needed to find the solution. The Newton-Raphson algorithm can be utilized for this purpose as follows:

$$\begin{Bmatrix} \epsilon_{o\ i+1} \\ \phi_{i+1} \end{Bmatrix} = \begin{Bmatrix} \epsilon_{o\ i} \\ \phi_i \end{Bmatrix} + \begin{Bmatrix} \Delta\epsilon_{o\ i} \\ \Delta\phi_i \end{Bmatrix} \quad (4-4)$$

where the incremental strain $\Delta\epsilon_{o\ i}$ and curvature $\Delta\phi_i$ are determined from

$$\begin{Bmatrix} \Delta P_i \\ \Delta M_i \end{Bmatrix} = \begin{bmatrix} \frac{\partial P}{\partial \epsilon_o} & \frac{\partial P}{\partial \phi} \\ \frac{\partial M}{\partial \epsilon_o} & \frac{\partial M}{\partial \phi} \end{bmatrix}_i \begin{Bmatrix} \Delta\epsilon_{o\ i} \\ \Delta\phi_i \end{Bmatrix} \quad (4-5)$$

in which ΔP_i and ΔM_i are the incremental forces needed to reach the specified forces P and M from the state of stresses i at the section.

The first element of the Jacobian matrix, $\frac{\partial P}{\partial \epsilon_o}$, can be calculated as follows:

$$\frac{\partial P}{\partial \epsilon_o} = \frac{\partial}{\partial \epsilon_o} \int_{A_s} f_c dA + \frac{\partial}{\partial \epsilon_o} \sum_i (f_{si} - f_{ci}) A_{si} \quad (4-6)$$

$$\frac{\partial P}{\partial \epsilon_o} = \int_{A_s} \frac{\partial f_c}{\partial \epsilon} \frac{\partial \epsilon}{\partial \epsilon_o} dA + \sum_i \left(\frac{\partial f_{si}}{\partial \epsilon} - \frac{\partial f_{ci}}{\partial \epsilon} \right) \frac{\partial \epsilon}{\partial \epsilon_o} A_{si} \quad (4-7)$$

where in Eq. (4-7) the chain rule of derivation was applied. From Eq.(4-1)

$$\frac{\partial \epsilon}{\partial \epsilon_o} = 1 \quad (4-8)$$

By definition the tangent modulus of elasticity for concrete is defined as:

$$E_{tc} = \frac{\partial f_c}{\partial \epsilon} \quad (4-9)$$

and for steel, at layer i ,

$$E_{tsi} = \frac{\partial f_{si}}{\partial \epsilon} \quad (4-10)$$

Both are calculated at a specified strain, thus finally

$$EA = \frac{\partial P}{\partial \epsilon_o} = \int_{A_s} E_{tc} dA + \sum_i (E_{tsi} - E_{tci}) A_{si} \quad (4-11)$$

where EA is the instantaneous effective axial stiffness.

The off-diagonal terms $\frac{\partial P}{\partial \phi}$ and $\frac{\partial M}{\partial \epsilon_o}$ are equal, what results in a symmetrical stiffness matrix. These terms are calculated as follows:

$$\frac{\partial P}{\partial \phi} = \frac{\partial}{\partial \phi} \int_{A_s} f_c dA + \frac{\partial}{\partial \phi} \sum_i (f_{si} - f_{ci}) A_{si} \quad (4-12)$$

$$\frac{\partial P}{\partial \phi} = \int_{A_s} \frac{\partial f_c}{\partial \epsilon} \frac{\partial \epsilon}{\partial \phi} dA + \sum_i \left(\frac{\partial f_{si}}{\partial \epsilon} - \frac{\partial f_{ci}}{\partial \epsilon} \right) \frac{\partial \epsilon}{\partial \phi} A_{si} \quad (4-13)$$

and from Eq. (4-1)

$$\frac{\partial \epsilon}{\partial \phi} = y - y_o \quad (4-14)$$

Thus,

$$\frac{\partial P}{\partial \phi} = \int_{A_s} E_{tc} (y - y_o) dA + \sum_i (E_{tsi} - E_{tci}) (y_{si} - y_o) A_{si} \quad (4-15)$$

Finally, by rearranging,

$$EZ = \frac{\partial P}{\partial \phi} = \frac{\partial M}{\partial \epsilon_o} = \int_{A_c} y E_{tc} dA + \sum_i y_{si} (E_{tsi} - E_{tci}) A_{si} - y_o EA \quad (4-16)$$

The flexural rigidity can be determined in the same way as

$$\frac{\partial M}{\partial \phi} = \int_{A_c} y E_{tc} (y - y_o) dA + \int_i y_{si} (E_{tsi} - E_{tci}) (y_{si} - y_o) A_{si} - y_o EZ \quad (4-17)$$

$$\frac{\partial M}{\partial \phi} = \int_{A_c} y^2 E_{tc} dA + \sum_i y_{si}^2 (E_{tsi} - E_{tci}) A_{si} - y_o \left[\int_{A_c} y E_{tc} dA + \sum_i y_{si} (E_{tsi} - E_{tci}) A_{si} \right] - y_o EZ \quad (4-18)$$

The expression in brackets in Eq. (4-18) can be found from Eq. (4-16) to be

$$\int_{A_c} y E_{tc} dA + \sum_i y_{si} (E_{tsi} - E_{tci}) A_{si} = EZ + y_o EA \quad (4-19)$$

By substituting Eq. (4-19) into Eq. (4-18),

$$EI = \frac{\partial M}{\partial \phi} = \int_{A_c} y^2 E_{tc} dA + \sum_i y_{si}^2 (E_{tsi} - E_{tci}) A_{si} - 2y_o EZ - y_o^2 EA \quad (4-20)$$

Summarizing:

$$P = \int_{A_c} f_c dA + \sum_i (f_{si} - f_{ci}) A_{si} \quad (4-21a)$$

$$M = \int_{A_c} y f_c dA + \sum_i y_{si} (f_{si} - f_{ci}) A_{si} - y_o P \quad (4-21b)$$

$$EA = \int_{A_c} E_{tc} dA + \sum_i (E_{tsi} - E_{tci}) A_{si} \quad (4-21c)$$

$$EZ = \int_{A_c} y E_{tc} dA + \sum_i y_{si} (E_{tsi} - E_{tci}) A_{si} - y_o EA \quad (4-21d)$$

$$EI = \int_{A_c} y^2 E_{tc} dA + \sum_i y_{si}^2 (E_{tsi} - E_{tci}) A_{si} - 2y_o EZ - y_o^2 EA \quad (4-21e)$$

In all the equations listed above, an integral over the area has to be calculated. These integrals represent the concrete component. Numerically these integrals can be calculated through the following procedure.

All the integral terms in Eqs. (4-21) are particular cases of the more general equation:

$$\int_{A_x} y^n f dA = \int_h y^n f b dy \quad (4-22)$$

in this equation, f represents either f_c or E_{ϵ} , and b is a function representing the width of the cross-section. This integral can be accurately computed by subdividing the cross-section into smaller fibers (strips), as:

$$\int_{A_x} y^n f dA = \sum_j \int_{h_j} y^n f b dy \quad (4-23)$$

where h_j is the height of the strip j (see Fig. 4-1).

In terms of , each fiber contribution can be computed by:

$$\int_{h_j} f b dy = \int_0^{h_j} f b d\xi \quad (4-24)$$

$$\int_{h_j} y f b dy = \int_0^{h_j} (y_{oj} + \xi) f b d\xi = \int_0^{h_j} \xi f b d\xi + y_{oj} \int_{h_j} f b dy \quad (4-25)$$

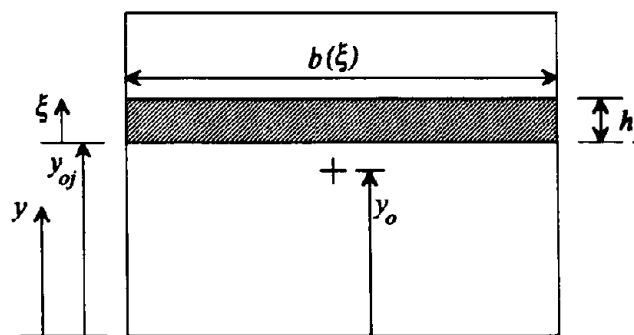


Fig. 4-1 Definition of Global and Local Coordinates

$$\begin{aligned}
\int_{h_j} y^2 f b dy &= \int_0^{h_j} (y_{oj} + \xi)^2 f b d\xi = \int_0^{h_j} \xi^2 f b d\xi + 2y_{oj} \int_0^{h_j} \xi f b d\xi + y_{oj}^2 \int_0^{h_j} f b d\xi \\
&= \int_0^{h_j} \xi^2 f b d\xi + 2y_{oj} \int_{h_j} y f b dy - y_{oj}^2 \int_{h_j} f b dy
\end{aligned} \tag{4-26}$$

Note that integrals over dy are in global coordinates while those over $d\xi$ are in local coordinates (see Fig. 4-1). For any given strip the integrals can be computed to any desired degree of accuracy. If parabolic behavior is assumed for f and b then:

$$f = A + B\xi + C\xi^2 \tag{4-27a}$$

$$b = D + E\xi + F\xi^2 \tag{4-27b}$$

and by evaluating the functions at equal intervals Δy

$$f_0 = A \tag{4-28a}$$

$$f_1 = A + B\Delta y + C(\Delta y)^2 \tag{4-28b}$$

$$f_2 = A + 2B\Delta y + 4C(\Delta y)^2 \tag{4-28c}$$

also,

$$b_0 = D \tag{4-29a}$$

$$b_1 = D + E\Delta y + F(\Delta y)^2 \tag{4-29b}$$

$$b_2 = D + 2E\Delta y + 4F(\Delta y)^2 \tag{4-29c}$$

Thus by solving for A, B and C in Eq. (4-28)

$$A = f_0 \tag{4-30a}$$

$$B\Delta y = -\frac{3}{2}f_0 + 2f_1 - \frac{1}{2}f_2 \tag{4-30b}$$

$$C(\Delta y)^2 = \frac{1}{2}f_0 - f_1 + \frac{1}{2}f_2 \tag{4-30c}$$

Similarly,

$$B_0 = D = b_0 \tag{4-31a}$$

$$B_1 = E\Delta y = -\frac{3}{2}b_0 + 2b_1 - \frac{1}{2}b_2 \tag{4-31b}$$

$$B_2 = F(\Delta y)^2 = \frac{1}{2}b_0 - b_1 + \frac{1}{2}b_2 \tag{4-31c}$$

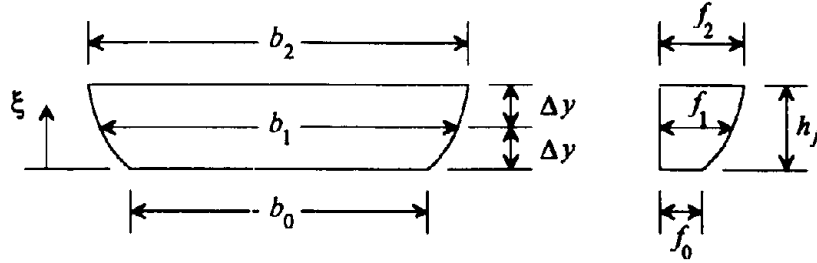


Fig. 4-2 Definition of Variables on a Fiber Element

By applying Eqs. (4-30) and (4-31) to Eqs. (4-27) and then evaluating the integrals, the following result was obtained:

$$\int_0^{h_j} \xi^n f b d\xi = \Delta y^{n+1} y \sum_{k=0}^2 \frac{2^{n+1+k}}{(n+1+k)(n+2+k)(n+3+k)} [(-n+1-k)f_0 + 4(n+1+k)f_1 + (n+1+k)^2 f_2] B_k \quad (4-32)$$

Thus

$$\int_0^{h_j} f b d\xi = \Delta y \left[\frac{1}{3}(f_0 + 4f_1 + f_2)B_0 + \frac{1}{6}(8f_1 + 4f_2)B_1 + \frac{2}{15}(-f_0 + 12f_1 + 9f_2)B_2 \right] \quad (4-33a)$$

or

$$\int_0^{h_j} f b d\xi = \Delta y \left[\frac{1}{3}(f_0 + 4f_1 + f_2)b_0 + \frac{1}{3}(2f_1 + f_2)(-3b_0 + 4b_1 - b_2) + \frac{1}{15}(-f_0 + 12f_1 + 9f_2)(b_0 - 2b_1 + b_2) \right] \quad (4-33b)$$

Also,

$$\int_0^{h_j} \xi f b d\xi = (\Delta y)^2 \left[\frac{2}{3}(2f_1 + f_2)b_0 + \frac{1}{15}(-f_0 + 12f_1 + 9f_2)(-3b_0 + 4b_1 - b_2) + \frac{2}{15}(-f_0 + 8f_1 + 8f_2)(b_0 - 2b_1 + b_2) \right] \quad (4-34)$$

and

$$\int_0^{h_j} \xi^2 f b d\xi = (\Delta y)^3 \left[\frac{2}{15}(-f_0 + 12f_1 + 9f_2)b_0 + \frac{2}{15}(-f_0 + 8f_1 + 8f_2)(-3b_0 + 4b_1 - b_2) + \frac{8}{105}(-3f_0 + 20f_1 + 25f_2)(b_0 - 2b_1 + b_2) \right] \quad (4-35)$$

Lack of convergence normally comes from the shape of the stress function and not from the geometry of the cross-section, so to simplify the integration formulae, it was assumed that the cross-section had a linear variation profile, instead of a quadratic. The simplified equations are then:

$$\int_0^{h_j} f b d\xi = \Delta y \left[\frac{1}{3}(f_0 + 4f_1 + f_2)b_0 + \frac{1}{3}(2f_1 + f_2)(b_2 - b_0) \right] \quad (4-36)$$

$$\int_0^{h_j} \xi f b d\xi = (\Delta y)^2 \left[\frac{2}{3}(2f_1 + f_2)b_0 + \frac{1}{15}(-f_0 + 12f_1 + 9f_2)(b_2 - b_0) \right] \quad (4-37)$$

$$\int_0^{h_j} \xi^2 f b d\xi = (\Delta y)^3 \left[\frac{2}{15}(-f_0 + 12f_1 + 9f_2) + \frac{2}{15}(-f_0 + 8f_1 + 8f_2)(b_2 - b_0) \right] \quad (4-38)$$

And for the case of a constant width cross-section these equations can be further simplified to:

$$\int_0^{h_j} f b d\xi = \frac{1}{3} \Delta y (f_0 + 4f_1 + f_2) b_0 \quad (4-39)$$

$$\int_0^{h_j} \xi f b d\xi = \frac{2}{3} (\Delta y)^2 (2f_1 + f_2) b_0 \quad (4-40)$$

$$\int_0^{h_j} \xi^2 f b d\xi = \frac{2}{15} (\Delta y)^3 (-f_0 + 12f_1 + 9f_2) b_0 \quad (4-41)$$

Eq. (4-39) can be easily identified as Simpson's rule of numerical integration.

The procedure to evaluate the concrete components on Eqs. (4-21) is as follows. The concrete section is divided into discrete fiber elements of confined and unconfined concrete. For each of these fibers the starting and ending width is specified b_0 and b_2 the concrete stress (f_c) for the starting, middle and ending ordinate is computed (f_{c0} , f_{c1} and f_{c2}); the tangential Young's modulus (E_{tc}) is also computed at these locations (E_{tc0} , E_{tc1} and E_{tc2}). The starting ordinate of the element (y_{oi}) and the half-height (Δy) are also identified. Then the global axis integrals for the element are computed as:

$$\Delta P_c = \Delta y \left[\frac{1}{3}(f_{c0} + 4f_{c1} + f_{c2})b_0 + \frac{1}{3}(2f_{c1} + f_{c2})(b_2 - b_0) \right] \quad (4-42)$$

$$\Delta M_o = (\Delta y)^2 \left[\frac{2}{3}(2f_{c1} + f_{c2})b_0 + \frac{1}{15}(-f_{c0} + 12f_{c1} + 9f_{c2})(b_2 - b_0) \right] + y_{oi} \Delta P_c \quad (4-43)$$

$$\Delta EA_c = \Delta y \left[\frac{1}{3}(E_{tc0} + 4E_{tc1} + E_{tc2})b_0 + \frac{1}{3}(2E_{tc1} + E_{tc2})(b_2 - b_0) \right] \quad (4-44)$$

$$\Delta EZ_c = (\Delta y)^2 \left[\frac{2}{3}(2E_{tc1} + E_{tc2})b_0 + \frac{1}{15}(-E_{tc0} + 12E_{tc1} + 9E_{tc2})(b_2 - b_0) \right] + y_{oi} \Delta EA_c \quad (4-45)$$

$$\Delta EI_c = (\Delta y)^3 \left[\frac{2}{15}(-E_{tc0} + 12E_{tc1} + 9E_{tc2})b_0 + \frac{2}{15}(-E_{tc0} + 8E_{tc1} + 8E_{tc2})(b_2 - b_0) \right] + 2y_{oi} \Delta EZ_c - y_{oi}^2 \Delta EA_c \quad (4-46)$$

The total axial force, bending moment and stiffness are then given by:

$$P = \sum_{i=1}^{ne} \Delta P_{ci} + \sum_{j=1}^{ns} (f_{sj} - f_{cj}) A_{sj} \quad (4-47)$$

$$M = \sum_{i=1}^{ne} \Delta M_{ci} + \sum_{j=1}^{ns} y_{si} (f_{sj} - f_{cj}) A_{sj} - y_o P \quad (4-48)$$

$$EA = \sum_{i=1}^{ne} \Delta EA_{ci} + \sum_{j=1}^{ns} (E_{tsj} - E_{tcj}) A_{sj} \quad (4-49)$$

$$EZ = \sum_{i=1}^{ne} \Delta EZ_{ci} + \sum_{j=1}^{ns} y_{sj} (E_{tsj} - E_{tcj}) A_{sj} - y_o EA \quad (4-50)$$

$$EI = \sum_{i=1}^{ne} \Delta EI_{ci} + \sum_{j=1}^{ns} y_{sj}^2 (E_{tsj} - E_{tcj}) A_{sj} - 2y_o EZ - y_o^2 EA \quad (4-51)$$

4-3 Moment-Curvature Analysis for Biaxial Bending

The same basic concepts outlined in the previous sub-section can be applied to the case of biaxial bending. The longitudinal strain at any point on the cross-section is given by:

$$\varepsilon = \varepsilon_o + \phi_x (y - y_o) - \phi_y (x - x_o) \quad (4-53)$$

The axial force is then given by

$$P = \iint_{A_s} f_c dA + \sum_j (f_{sj} - f_{cj}) A_{sj} \quad (4-54)$$

$$M_x = \iint_{A_s} y f_c dA + \sum_j y_{sj} (f_{sj} - f_{cj}) A_{sj} - y_o P \quad (4-55)$$

$$M_y = - \iint_{A_s} x f_c dA - \sum_j x_{sj} (f_{sj} - f_{cj}) A_{sj} + x_o P \quad (4-56)$$

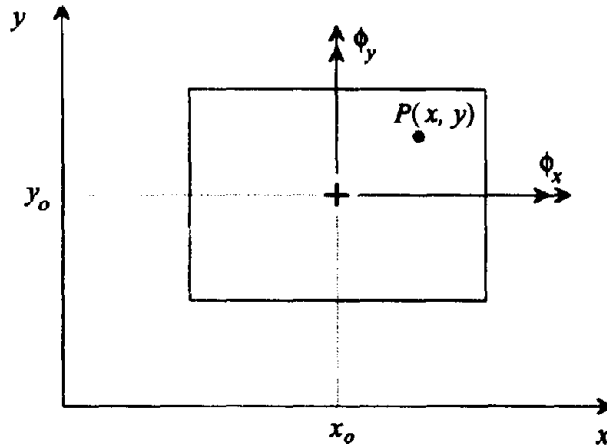


Fig. 4-3 Definition of Variables for Biaxial Bending

For a given centroidal strain (ϵ_o) and curvatures (ϕ_x and ϕ_y), the equations are in explicit form and therefore the axial force P and moments (M_x and M_y) can be readily related. The inverse problem (P , M_x and M_y specified) requires iteration to compute (ϵ_o , ϕ_x and ϕ_y). As in the case of uniaxial bending, the Newton-Raphson procedure can be applied. Incremental deformations are related to incremental forces through a stiffness matrix given by:

$$\begin{Bmatrix} \Delta P \\ \Delta M_x \\ \Delta M_y \end{Bmatrix} = \begin{bmatrix} EA & EZ_x & EZ_y \\ EZ_x & EI_x & EI_{xy} \\ EZ_y & EI_{xy} & EI_y \end{bmatrix} \begin{Bmatrix} \Delta \epsilon_o \\ \Delta \phi_x \\ \Delta \phi_y \end{Bmatrix} \quad (4-57)$$

with,

$$EA = \frac{\partial P}{\partial \epsilon_o} = \iint_{A_s} E_{ic} dA + \sum_j (E_{ij} - E_{icj}) A_{sj} \quad (4-58)$$

$$EZ_x = \frac{\partial P}{\partial \phi_x} = \frac{\partial M_x}{\partial \epsilon_o} = \iint_{A_s} y E_{ic} dA + \sum_j y_{sj} (E_{ij} - E_{icj}) A_{sj} - y_o EA \quad (4-59)$$

$$EZ_y = \frac{\partial P}{\partial \phi_y} = \frac{\partial M_y}{\partial \epsilon_o} = -\iint_{A_s} x E_{tc} dA - \sum_j x_{sj} (E_{tsj} - E_{tcj}) A_{sj} + x_o EA \quad (4-60)$$

$$EI_x = \frac{\partial M_x}{\partial \phi_x} = \iint_{A_s} y^2 E_{tc} dA + \sum_j y_{sj}^2 (E_{tsj} - E_{tcj}) A_{sj} - 2y_o EZ_x - y_o^2 EA \quad (4-61)$$

$$EI_y = \frac{\partial M_y}{\partial \phi_y} = \iint_{A_s} x^2 E_{tc} dA + \sum_j x_{sj}^2 (E_{tsj} - E_{tcj}) A_{sj} + 2x_o EZ_y - x_o^2 EA \quad (4-62)$$

$$EI_{xy} = \frac{\partial M_x}{\partial \phi_y} = \frac{\partial M_y}{\partial \phi_x} = -\iint_{A_s} xy E_{tc} dA - \sum_j x_{sj} y_{sj} (E_{tsj} - E_{tcj}) A_{sj} + x_o EZ_x - y_o EZ_y + x_o y_o EA \quad (4-63)$$

The formulation specified in Eqs. (4-54) through (4-63) have only two assumptions implicit in them: (1) Plane sections remain plane, Eq.(4-53); (2) The area locations occupied by the steel reinforcement is very small compared to the concrete area, so that no integration is necessary and all the properties can be expressed by summations. The concrete components in these equations, nevertheless, need to be approximated by some integration technique.

For rectangular sections, an explicit formulation can be given. It is proposed that the cross-section be divided in a matrix mesh of fibers as shown in Fig. 4-4a. Each rectangular fiber element had a midpoint node, as shown in Fig. 4-4b. A parabolic interpolation function can be chosen as:

$$f = f_o + B\eta + C\xi + D\eta\xi + E\eta^2 + F\xi^2 \quad (4-64)$$

with

$$B\Delta x = C\Delta y = -\frac{3}{2}f_o + 2f_3 - \frac{1}{2}f_4 \quad (4-65)$$

$$D\Delta x\Delta y = f_o - f_1 - f_2 + f_4 \quad (4-66)$$

$$E(\Delta x)^2 = \frac{1}{2}f_o + f_1 - 2f_3 + \frac{1}{2}f_4 \quad (4-67)$$

$$F(\Delta y)^2 = \frac{1}{2}f_o + f_2 - 2f_3 + \frac{1}{2}f_4 \quad (4-68)$$

where η and ξ are the x and y local coordinates axis, that are related to the global coordinates axis through:

$$\eta = x - x_{oi} \quad (4-69)$$

$$\xi = y - y_{oi} \quad (4-70)$$

where x_{oi} and y_{oi} are the coordinates of the lower left corner of the element, and should not be confused with the coordinates of the centroid. In terms of local coordinates, each fiber element contribution to the integrals can be computed as:

$$\iint_{A_e} f dA = \int_0^{\Delta x} \int_0^{\Delta y} f d\eta d\xi \quad (4-71)$$

$$\iint_{A_e} y f dA = \int_0^{\Delta x} \int_0^{\Delta y} (y_{oi} + \xi) f d\eta d\xi = \int_0^{\Delta x} \int_0^{\Delta y} \xi f d\eta d\xi + y_{oi} \iint_{\Delta A} f dA \quad (4-72)$$

$$\iint_{A_e} x f dA = \int_0^{\Delta x} \int_0^{\Delta y} (x_{oi} + \eta) f d\eta d\xi = \int_0^{\Delta x} \int_0^{\Delta y} \eta f d\eta d\xi + x_{oi} \iint_{\Delta A} f dA \quad (4-73)$$

Similarly

$$\iint_{\Delta A} x y f dA = \int_0^{\Delta x} \int_0^{\Delta y} \eta \xi f d\eta d\xi + x_{oi} \iint_{\Delta A} y f dA + y_{oi} \iint_{\Delta A} x f dA - x_{oi} y_{oi} \iint_{\Delta A} f dA \quad (4-74)$$

$$\iint_{\Delta A} x^2 f dA = \int_0^{\Delta x} \int_0^{\Delta y} \eta^2 f d\eta d\xi + 2x_{oi} \iint_{\Delta A} x f dA - x_{oi}^2 \iint_{\Delta A} f dA \quad (4-75)$$

$$\iint_{\Delta A} y^2 f dA = \int_0^{\Delta x} \int_0^{\Delta y} \xi^2 f d\eta d\xi + 2y_{oi} \iint_{\Delta A} y f dA - y_{oi}^2 \iint_{\Delta A} f dA \quad (4-76)$$

The numerical integration of the interpolation function Eq. (4-64) can be computed in terms of the node values (f_o, f_1, f_2, f_3 and f_4), resulting:

$$\int_0^{\Delta x} \int_0^{\Delta y} \eta^m \xi^n f d\eta d\xi = (\Delta x)^{m+1} (\Delta y)^{n+1} \sum_{k=0}^4 a_k f_k \quad (4-77)$$

where

$$a_o = \frac{1}{(m+1)(n+1)} \left[\frac{1}{(m+2)(m+3)} + \frac{1}{(n+2)(n+3)} \right] - \frac{1}{2(m+2)(n+2)} \left(\frac{1}{m+1} + \frac{1}{n+1} \right) \quad (4-78a)$$

$$a_1 = \frac{1}{(m+3)(n+1)} - \frac{1}{(m+2)(n+2)} \quad (4-78b)$$

$$a_2 = \frac{1}{(m+1)(n+3)} - \frac{1}{(m+2)(n+2)} \quad (4-78c)$$

$$a_3 = \frac{2}{(m+1)(n+2)(n+3)} + \frac{2}{(m+2)(m+3)(n+1)} \quad (4-78d)$$

$$a_4 = \frac{1}{(m+2)(n+2)} - \frac{1}{4} a_3 \quad (4-78e)$$

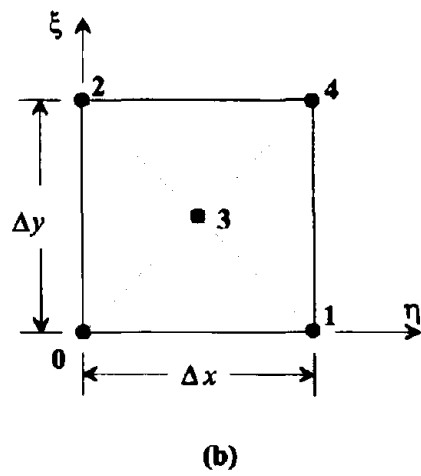
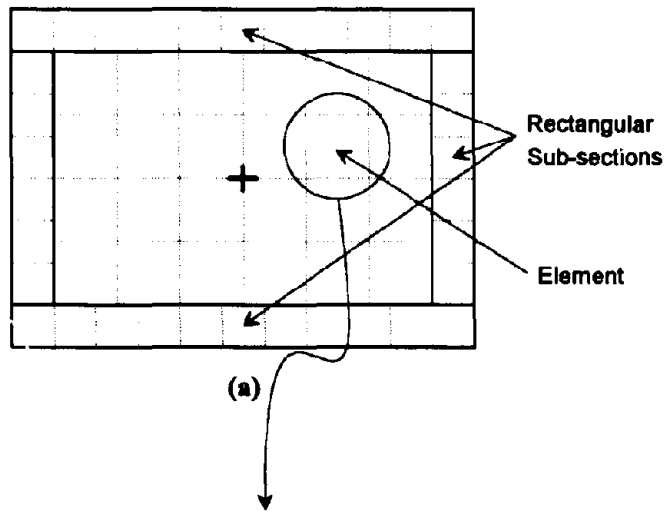


Fig. 4-4 Element Node Numbering

Then by giving m and n the appropriate values :

for $m=0$ and $n=0$:

$$\int_0^{\Delta x} \int_0^{\Delta y} f d\eta d\xi = \frac{1}{12} \Delta x \Delta y (f_0 + f_1 + f_2 + 8f_3 + f_4) \quad (4-79)$$

for $m=1$ and $n=0$:

$$\int_0^{\Delta x} \int_0^{\Delta y} \eta f d\eta d\xi = \frac{1}{12} (\Delta x)^2 \Delta y (f_1 + 4f_3 + f_4) \quad (4-80)$$

for $m=0$ and $n=1$:

$$\int_0^{\Delta x} \int_0^{\Delta y} \xi f d\eta d\xi = \frac{1}{12} \Delta x (\Delta y)^2 (f_2 + 4f_3 + f_4) \quad (4-81)$$

for $m=1$ and $n=1$:

$$\int_0^{\Delta x} \int_0^{\Delta y} \eta \xi f d\eta d\xi = \frac{1}{72} (\Delta x)^2 (\Delta y)^2 (-f_0 + f_1 + f_2 + 12f_3 + 5f_4) \quad (4-82)$$

for $m=2$ and $n=0$:

$$\int_0^{\Delta x} \int_0^{\Delta y} \eta^2 f d\eta d\xi = \frac{1}{360} (\Delta x)^3 \Delta y (-4f_0 + 27f_1 - 5f_2 + 76f_3 + 26f_4) \quad (4-83)$$

and, for $m=0$ and $n=2$:

$$\int_0^{\Delta x} \int_0^{\Delta y} \xi^2 f d\eta d\xi = \frac{1}{360} \Delta x (\Delta y)^3 (-4f_0 - 5f_1 + 27f_2 + 76f_3 + 26f_4) \quad (4-84)$$

The procedure to evaluate the forces (P , M_x and M_y) and stiffness (EA , EZ_x , EZ_y , EI_{xy} , I_x and I_y) is summarized as follows.

(1) The geometry of the discretized cross-section is known. For every element the size (Δx and Δy) and coordinate of the lower-left node (x_{oi} , y_{oi}) are known. The position and area of reinforcing bars is also specified (x_{sj} , y_{sj}), A_{sj} .

(2) From Bernoulli's assumption, the strain at every node can be readily computed, for a given centroidal strain (ϵ_o) and curvatures (ϕ_x , ϕ_y), by using Eq. (4-53).

(3) The stress (f_s) and tangential Young's modulus (E_{ts}) can be computed by knowing the strain and previous history using an appropriate constitutive model. Thus, for every element

f_{c0i} , f_{c1i} , f_{c2i} , f_{c3i} , f_{c4i} , f_{sc0i} , f_{sc1i} , f_{sc2i} , f_{sc3i} and f_{sc4i} are known.

(4) The strain at bar location is calculated, and by using constitutive models for concrete and steel the stresses and tangential Young's modulus are calculated (f_{sj} , f_{tj} , E_{tsj} , E_{tj}).

(5) The concrete components for each element are defined by:

$$\Delta P_i = \frac{1}{12} \Delta x \Delta y (f_{c0} + f_{c1} + f_{c2} + 8f_{c3} + f_{c4}) \quad (4-85)$$

$$\Delta M_{xi} = \frac{1}{12} \Delta x (\Delta y)^2 (f_{c2} + 4f_{c3} + f_{c4}) + y_{oi} \Delta P_i \quad (4-86)$$

$$\Delta M_{yi} = \frac{1}{12} (\Delta x)^2 \Delta y (f_{c1} + 4f_{c3} + f_{c4}) + x_{oi} \Delta P_i \quad (4-87)$$

$$\Delta EA_i = \frac{1}{12} \Delta x \Delta y (E_{tc0} + E_{tc1} + E_{tc2} + 8E_{tc3} + E_{tc4}) \quad (4-88)$$

$$\Delta EZ_{xi} = \frac{1}{12} \Delta x (\Delta y)^2 (E_{tc2} + 4E_{tc3} + E_{tc4}) + y_{oi} \Delta EA_i \quad (4-89)$$

$$\Delta EZ_{yi} = \frac{1}{12} (\Delta x)^2 \Delta y (E_{tc1} + 4E_{tc3} + E_{tc4}) + x_{oi} \Delta EA_i \quad (4-90)$$

$$\Delta EI_{xi} = \frac{1}{360} \Delta x (\Delta y)^3 (-4E_{tc0} - 5E_{tc1} + 27E_{tc2} + 76E_{tc3} + 26E_{tc4}) + 2y_{oi} \Delta EZ_{xi} - y_{oi}^2 \Delta EA_i \quad (4-91)$$

$$\Delta EI_{yi} = \frac{1}{360} (\Delta x)^3 \Delta y (-4E_{tc0} + 27E_{tc1} - 5E_{tc2} + 76E_{tc3} + 26E_{tc4}) + 2x_{oi} \Delta EZ_{yi} - x_{oi}^2 \Delta EA_i \quad (4-92)$$

$$\Delta EI_{xyi} = \frac{1}{72} (\Delta x \Delta y)^2 (-E_{tc0} + E_{tc1} + E_{tc2} + 12E_{tc3} + 5E_{tc4}) + x_{oi} \Delta EZ_{xi} + y_{oi} \Delta EZ_{yi} - x_{oi} y_{oi} \Delta EA_i \quad (4-93)$$

(6) Finally the total forces and stiffness for the cross-section are given by

$$P = \sum_{i=1}^{ne} \Delta P_i + \sum_{j=1}^{ns} (f_{sj} - f_{cj}) A_{sj} \quad (4-94)$$

$$M_x = \sum_{i=1}^{ne} \Delta M_{xi} + \sum_{j=1}^{ns} y_{sj} (f_{sj} - f_{cj}) A_{sj} - y_o P \quad (4-95)$$

$$M_y = -\sum_{i=1}^{ne} \Delta M_{yi} - \sum_{j=1}^{ns} x_{sj} (f_{sj} - f_{cj}) A_{sj} + x_o P \quad (4-96)$$

$$EA = \sum_{i=1}^{ne} \Delta EA_i + \sum_{j=1}^{ns} (E_{tsj} - E_{tcj}) A_{sj} \quad (4-97)$$

$$EZ_x = \sum_{i=1}^{ne} \Delta EZ_{xi} + \sum_{j=1}^{ns} y_{sj} (E_{tsj} - E_{tcj}) A_{sj} - y_o EA \quad (4-98)$$

$$EZ_y = -\sum_{i=1}^{ne} \Delta EZ_{yi} - \sum_{j=1}^{ns} x_{sj} (E_{tsj} - E_{tcj}) A_{sj} + x_o EA \quad (4-99)$$

$$EI_x = \sum_{i=1}^{ne} \Delta EI_{xi} + \sum_{j=1}^{ns} y_{sj}^2 (E_{tsj} - E_{tcj}) A_{sj} - 2y_o EZ_x - y_o^2 EA \quad (4-100)$$

$$EI_y = \sum_{i=1}^{ne} \Delta EI_{yi} + \sum_{j=1}^{ns} x_{sj}^2 (E_{tsj} - E_{tcj}) A_{sj} + 2x_o EZ_y - x_o^2 EA \quad (4-101)$$

$$EI_{xy} = -\sum_{i=1}^{ne} \Delta EI_{xyi} - \sum_{j=1}^{ns} x_{sj} y_{sj} (E_{tsj} - E_{tcj}) A_{sj} + x_o EZ_x - y_o EZ_y + x_o y_o EA \quad (4-102)$$

4.4 Force-Displacement Analysis

In the previous sections a procedure to obtain the moment-curvature relationship for uniaxial as well as biaxial bending was presented. This section presents a methodology by which deformation can be assessed. The total deformation Δ can be expressed in terms of its various components as:

$$\Delta = \Delta_e + \Delta_p + \Delta_{se} + \Delta_{sp} \quad (4-103)$$

where Δ_e is the elastic flexure deformation, Δ_p is the plastic flexure deformation, Δ_{se} is the elastic shear deformation and Δ_{sp} is the inelastic shear deformation. In what follows is a description of each of these components of displacement follows.

4.4.1 Elastic Flexural Deformation

The flexural deformation on a column can be found by taking first moments of the curvature diagram.

$$\Delta = \int_0^L x \phi(x) dx \quad (4-104)$$

If the moments in the column are caused by a concentrated shear force applied at the top, as shown in Fig. 4-5, then the moment at any distance x from the top can be found to be:

$$M_x = \frac{M_L}{L} x \quad (4-105)$$

where L is the length of the column and M_L is the maximum moment.

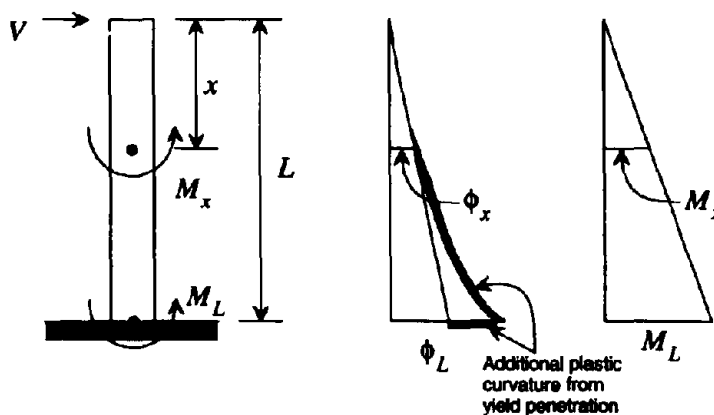


Fig. 4-5 Flexural Deformation on a Column

Thus, the relationship given in Eq.(4-104) can be expressed as:

$$\Delta = \left(\frac{L}{M_L}\right)^2 \int_0^{M_L} M \phi(M) dM \quad (4-106)$$

As discrete points on the moment-curvature relationship are calculated, the integral above can be computed numerically as:

$$\Delta = \frac{1}{6} \left(\frac{L}{M_L}\right)^2 \sum_{j=1}^n (M_j - M_{j-1}) [\phi_j (2M_j + M_{j-1}) + \phi_{j-1} (M_j + 2M_{j-1})] \quad (4-107)$$

For inelastic deformations it is necessary to calculate the elastic and plastic components separately. Mander et al. (1984) proposed to express the elastic components in terms of an effective stiffness calculated at first yield, given by:

$$EI_{eff} = \frac{M_y L^2}{3\Delta_y} \quad (4-108)$$

where Δ_y is the yield displacement calculated from Eq. (4-107) when the moment at the base causes a longitudinal bar to yield; and M_y is the moment at first yielding. Thus for deformations beyond the elastic limit, the elastic flexural deformation is calculated as:

$$\Delta_e = \phi_e \frac{L^2}{3} = \frac{ML^2}{3EI_{eff}} \quad (4-109)$$

4.4.2 Plastic Flexural Deformation

Based on study of experimental distribution of curvatures, Mander et al. (1984) proposed a parabolic distribution of plastic curvature. This is adopted herein to assess plastic deformations. The procedure is as follows:

(a) The magnitude of the plastic curvature (ϕ_p) at the critical section is given by:

$$\phi_p = (\phi - \phi_e) \quad (4-110)$$

where ϕ_e is the elastic curvature from Eq. (4-109) above.

(b) The length of the plastic curvature distribution L_{pc} is given by:

$$L_{pc} = L - L \left| \frac{M_y}{M_{max}} \right| \quad (4-111)$$

where M_{max} is the maximum moment.

(c) Some additional plastic curvature from penetration of the yielding of longitudinal reinforcement is accounted for by defining an empirical length of yield penetration as:

$$L_{py} = 6.35\sqrt{d_b} \quad (in) \quad (4-112)$$

$$L_{py} = 32\sqrt{d_b} \quad (mm)$$

where d_b is the longitudinal bar diameter.

(d) The plastic rotation, θ_p , of the column is calculated as:

$$\theta_p = \phi_p \left(\frac{1}{3}L_{pc} + L_{py} \right) \quad (4-113)$$

(e) Finally, the plastic deformation is given by:

$$\Delta_p = \theta_p \left(L - \frac{1}{4}L_{pc} \right) \quad (4-114)$$

4.4.3 Elastic Shear Deformation

Two methods are considered herein for the assessment of shear deformations. The first method considers deformations for the elastic and cracked stages, when the member has not yielded. The procedure outlined by Park and Paulay (1975) to assess elastic shear deformations was used to calculate the shear deformations for the elastic and cracked zones. The second method uses a proposed Equivalent Truss Method which has been found appropriate to assess cyclic inelastic shear deformations.

In what follows is an explanation of the procedure.

(a) Prior to cracking the shear deformation can be computed as:

$$\Delta_{se} = \frac{V}{K_{ve}}L \quad (4-115)$$

where V is the applied shear and K_{ve} is the shear stiffness given by:

$$K_{ve} = \frac{0.4E_cA_g}{f} \quad (4-116)$$

in which the factor 0.4 assumes that the Poisson ratio for concrete is $\nu = 0.25$ and $G = 0.4E_c$, A_g is the area that contributes to shear stiffness, and f is a form factor. For rectangular

cross-sections $f = 1.2$, and for T, I and hollow sections $f = 1$. At this stage of uncracked behavior the member shows a much greater shear stiffness compared to the cracked stage.

(b) When cracking exists over a length smaller than the hinge zone but no yield has occurred:

$$\Delta_{se} = VL \left[\frac{1}{K_{ve}} \frac{M_{cr}}{M_{max}} + \frac{1}{K_{vh}} \left(1 - \frac{M_{cr}}{M_{max}} \right) \right] \quad (4-117)$$

where M_{cr} is the cracking moment and K_{vh} is the post-cracking shear stiffness within the plastic hinge region.

The post-cracking elastic shear stiffness is related to the inclination of cracks and is calculated by the expression given by Park and Paulay (1975):

$$K_v = \frac{\rho_v \sin^4 \theta \sin^4 \beta (\cot \theta + \cot \beta)}{\sin^4 \theta + n \rho_v \sin^4 \beta} E_s b_w d \quad (4-118)$$

where θ is the angle of inclination of the cracks respect to the longitudinal axis, β is the angle of inclination of the stirrups, normally $\beta = 90^\circ$. E_s is the modulus of elasticity of the hoop reinforcement, $n = \frac{E_s}{E_c}$ is the modular ratio, E_c is the modulus of elasticity of concrete, and ρ_v is the volumetric ratio of hoop reinforcement calculated by:

$$\rho_v = \frac{A_v}{s b_w} \quad (4-119)$$

in which A_v is the total area of hoop steel, b_w is the width of the concrete web and s is the hoop spacing.

For transverse reinforcement with $\beta = 90^\circ$, Eq. (4-118) can be simplified to:

$$K_{v\theta} = \frac{b_w d \cot \theta}{\frac{1}{E_s \rho_v} + \frac{1}{E_c \sin^4 \theta}} \quad (4-120)$$

(c) When cracking extends beyond the hinge region then the shear deformation is given by:

$$\Delta_{se} = VL \left[\frac{1}{K_{ve}} \frac{M_{cr}}{M_{max}} + \frac{1}{K_{vh}} \frac{L_h}{L} + \frac{1}{K_{vc}} \left(1 - \frac{M_{cr}}{M_{max}} - \frac{L_h}{L} \right) \right] \quad (4-121)$$

where K_{vh} is the shear stiffness within the hinge region calculated by using Eq. (4-120) for the hoop spacing s_h within the hinge region, while K_{vc} is the shear stiffness outside the hinge region calculated for a hoop spacing s_u of the unconfined zone.

4.4.4 Inelastic Shear Deformation

For squat columns the amount of shear deformation can be significant. Under cyclic loading some plastic shear deformation may be present, particularly for existing gravity load designed bridge columns that possess only the nominal minimum amount of transverse reinforcement. Thus to correctly assess these plastic shear deformations a suitable model is needed. Both the Modified Compression Field Theory, MCFT, (Collins and Mitchell, 1991) and the Softened Truss Model, STM, (Hsu, 1993) deal with the problem of inelastic shear deformations, but as they were developed are suitable only for monotonic loading of membrane type elements. Both models are what Hsu (1993) calls rotating angle models, as at every stage the inclination of cracks is calculated assuming that they coincide with the principal axis. This approach has shown good accuracy with experimental results, as some of its variables are calibrated with experimental data.

In the context of a Fiber Element program for cyclic loading, a more straight forward constant crack angle model has been developed, which takes into account the tension capacity of reinforced concrete that has been incorporated in both the MCFT and the STM. When examining experimental performance of columns tested by Mander et al. (1984, 1993) and Ang et al. (1987) it is evident that after cracking the inclination of the cracks remains unchanged, but they generally grow in length and width as ductility amplitudes increase. It is thus felt that the model presented in this section that assumes a fixed angle is realistic for columns members.

The procedure to assess shear deformation in the case of shear dominated members is described below.

Four defined shear zones are identified as shown in Fig. 4-6. Three of the zones are elastic, which means that they are independent of the strain history and that the deformations are proportional to the shear force applied. This does not mean that the shear displacement is linear, because as cracking progresses upward, the length over which the different shear stiffnesses apply is changed.

(1) *Elastic Uncracked Zone* : the length of this zone can be calculated by:

$$L_e = L \left| \frac{M_{cr}}{M_{max}} \right| \quad (4-122)$$

Over this zone the shear stiffness is K_{ve} which is given by Eq. (4-115).

(2) *Elastic Cracked Zone Outside the Hinge Region* : if cracking has extended beyond the hinge zone, the length of this zone is calculated as $L_{crc} = L_{cr} - L_h$, otherwise it is taken as zero. The stiffness prevalent in this zone K_{vc} is governed by the spacing provided outside the hinge region, which is calculated by using Eq. (4-120). The cracked length is given by:

$$L_{cr} = L - L_e \quad (4-123)$$

(3) *Cracked Zone Within the Hinge Region* : the shear stiffness K_{vh} within this region is defined by the hinge hoop spacing and calculated by Eq. (4-120). The length of this zone is given by $L_{crh} = L_h - L_{pc}$ or by $L_{crh} = L_{cr} - L_{pc}$ if cracking has not extended outside the hinge region. The yielded zone length L_{pc} is given by Eq. (4-111).

(4) *Yielded Zone* : within this zone shear is considered to behave inelastically, thus the deformation is history dependent and may not be proportional to the current shear being applied. A shear deformation γ is calculated using a Cyclic Inelastic Strut-Tie (CIST) model developed in the next sub-section.

The elastic shear deformation is thus given by:

$$\Delta_{se} = V \left(\frac{L_e}{K_{ve}} + \frac{L_{crc}}{K_{vc}} + \frac{L_{crh}}{K_{vh}} \right) \quad (4-124)$$

while, the inelastic shear deformation is calculated by:

$$\Delta_{sp} = \gamma L_{pc} \quad (4-125)$$

4.4.4.1 Proposed Cyclic Inelastic Strut-Tie (CIST) Model for Shear Deformations

The determination of inelastic shear deformations has been one of the most elusive subjects on reinforced concrete. Recently the Modified Compression Field Theory (Collins and Mitchell, 1991) and the Softened Truss Model (Hsu, 1993) have gathered a lot of attention as rational means of assessing shear deformations. Nevertheless, these models have only been developed for membrane type elements under monotonic shear. In this subsection a straight forward model is presented which is applicable not only to monotonic shear but for cyclic inelastic shear as well.

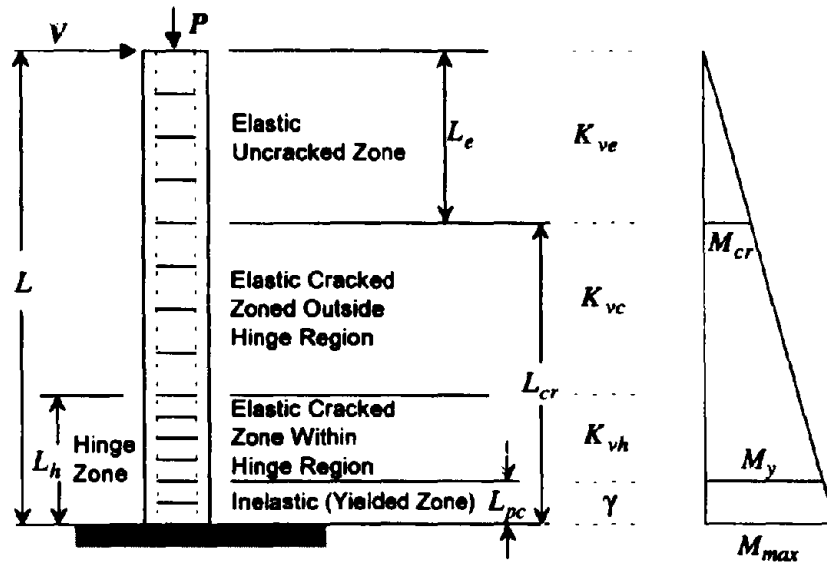


Fig. 4-6 Shear Deformation on a Column

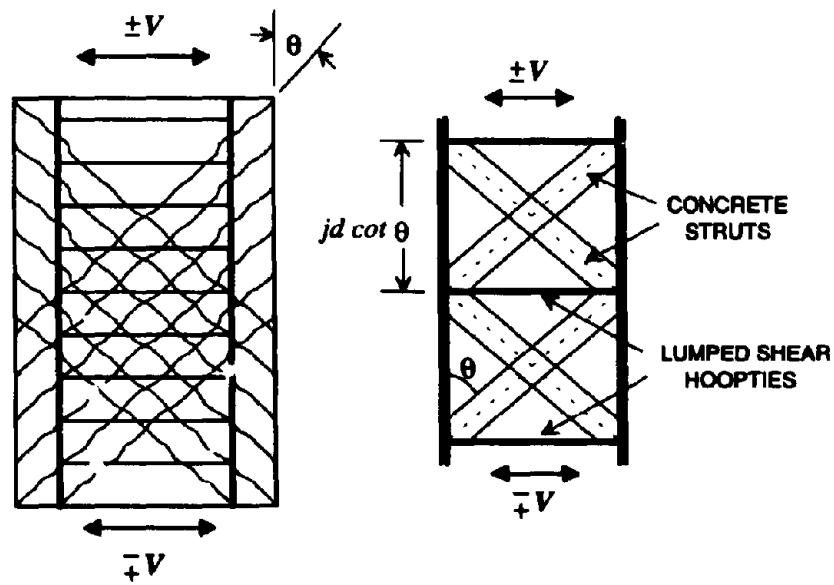
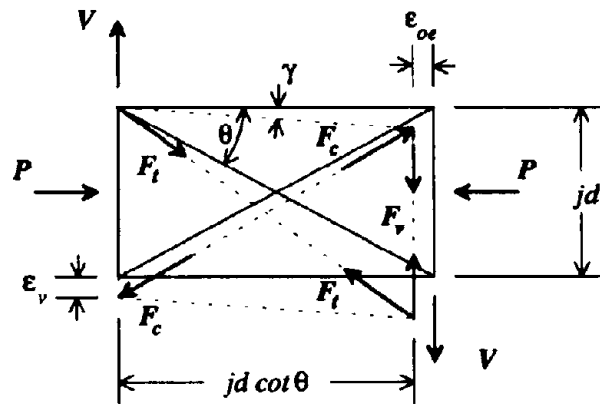
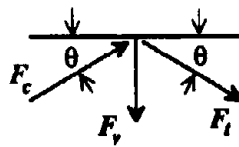


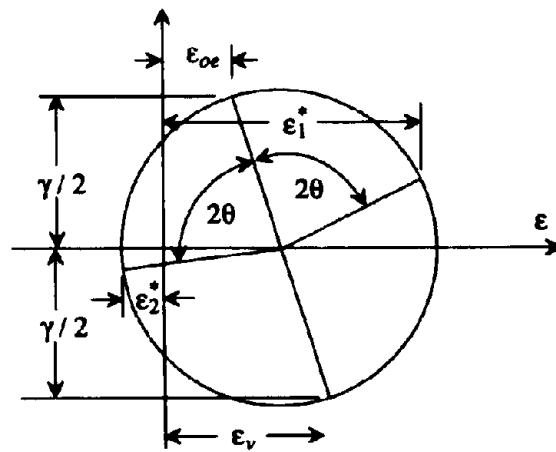
Fig. 4-7 Equivalent Strut-Tie Model for Shear Deformations



(a)

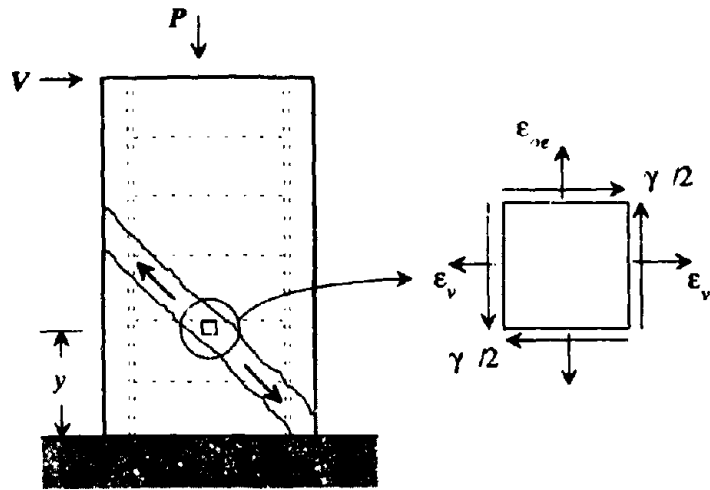


(b)

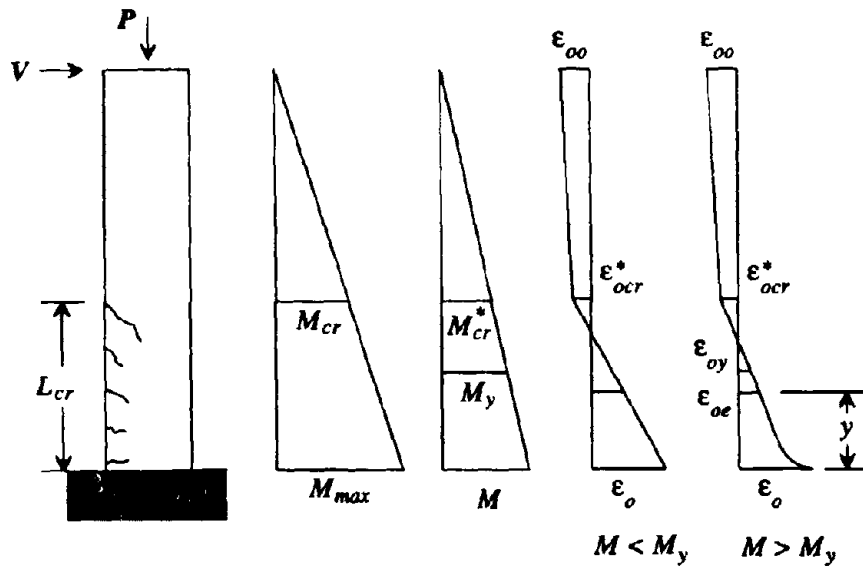


(c)

Fig. 4-8 Equilibrium and Strain Transformation in the Cyclic Inelastic Strut-Tie Shear Model



(a)



(b)

Fig. 4-9 Definition of Average Longitudinal Strain on Shear Concrete Strut

It is assumed that the angle of inclination of the cracks remains constant after cracking. This assumption, as mentioned earlier, is supported by experimental evidence. The concrete model developed in Section 3 is particularly appropriate for the CIST model, as it can model the stress-strain cyclic behavior of the concrete struts in both tension and compression. Of special importance in this model is the modeling of gradual crack closure. An equilibrium of external forces in Fig. 4-8a leads to,

$$V = (F_c + F_t) \sin \theta \quad (4-126)$$

Whereas, an equilibrium of internal forces in Fig. 4-8b gives,

$$F_v = (F_c - F_t) \sin \theta \quad (4-127)$$

where F_c = compressive force in the concrete strut, F_t = tensile force in the concrete tie, F_v = force on the steel hoop and θ = inclination of cracks. The forces in the concrete and steel are given by:

$$F_c = f_c A_w \cos \theta = f_c j d b_w \cos \theta \quad (4-128a)$$

$$F_t = f_t A_w \cos \theta = f_t j d b_w \cos \theta \quad (4-128b)$$

$$F_v = f_{sv} A_{sv} \frac{j d \cot \theta}{s} \quad (4-129)$$

in which f_c = compressive stress in the concrete strut, f_t = tensile stress on the concrete tie, f_{sv} = stress on the hoopties, $A_w = j d b_w$ = concrete shear area, A_{sv} = area of transverse steel resisting shear, and s = hoop spacing. It is to be noted that $A_w \cos \theta$ is the shear area perpendicular to the concrete strut, whereas $A_{sv} \frac{j d \cot \theta}{s}$ is the lumped area of transverse reinforcement. By combining Eqs. (4-126) through (4-129) and rearranging, the following expression is obtained:

$$V = A_{sv} f_{sv} \frac{j d}{s} \cot \theta + f_t j d b_w \cot \theta (2 \sin^2 \theta) \quad (4-130)$$

These equations can be compared with that of the MCFT (Collins and Mitchell, 1991),

$$V = A_{sv} f_{sv} \frac{j d}{s} \cot \theta + f_t j d b_w \cot \theta \quad (4-131)$$

It can be seen that Eqs. (4-130) and (4-131) agree when the inclination angle $\theta = 45^\circ$. For other angles the error = $1 - 2 \sin^2 \theta$, e.g. if $\theta = 30^\circ$, error = 0.5 = 50% of the concrete tension contribution. The term that corresponds to the tension capacity of concrete, is normally small compared to the steel component, which makes Eq. (4-130) a good approximation. The

simplicity introduced by this approximation is well worth it, as it will be shown in the following subsection.

Fig. 4-8c shows the relation between the strains in the longitudinal/transverse direction and the strains in the struts. The tensile strain in the concrete tie ϵ_1^* is calculated as:

$$\epsilon_1^* = \epsilon_{oe} \cos^2 \theta + \epsilon_v \sin^2 \theta + \gamma \sin \theta \cos \theta \quad (4-132)$$

whereas the compressive strain on the concrete strut is:

$$\epsilon_2^* = \epsilon_{oe} \cos^2 \theta + \epsilon_v \sin^2 \theta - \gamma \sin \theta \cos \theta \quad (4-133)$$

in which ϵ_{oe} = average longitudinal strain on the concrete struts, ϵ_v = strain on the transverse hoops and γ = shear distortion.

The relation between the stresses and strains is given by the constitutive models,

$$f_1^* = f_c(\epsilon_1^*) \quad (4-134)$$

$$f_2^* = f_c(\epsilon_2^*, \epsilon_1^*) \quad (4-135)$$

$$f_{sv} = f_v(\epsilon_v) \quad (4-136)$$

in which f_c and f_v represent the constitutive relations for concrete and steel respectively. Note that in Eqs. (4-132) to (4-136) the nomenclature has been changed. The asterisk * means that they do not represent the true principal strains or stresses, as the MCFT and the STM assume.

The concrete is modeled in four struts, two for unconfined concrete and two for confined concrete, in both directions. Although, in the preceding paragraphs the struts and ties have been referred to as compressive and tensile elements, they actually alternate between struts and ties as the member is being subjected to cyclic loading.

The implementation of the model in the context of a column analysis program is given in the following steps:

A. Moment-Curvature Analysis

(a.1) Take a curvature ϕ for which the analysis is going to be performed.

(a.2) Assume a centroidal strain ϵ_o . The assumption of this strain may be based on an incremental analysis estimation, if previous steps of the analysis are known.

(a.3) Perform a section analysis to calculate the axial force P and moment M at the critical section according to procedure described in subsection 4.2.

(a.4) If the axial load P does not satisfy the external axial load applied, then repeat steps 2 and 3 until convergence is satisfied. Increasing the value of ϵ_c increases the axial load value, unless crushing of the concrete occurs. It is possible, that for high values of axial load, or high values of curvature deformation, no centroidal strain could be found to satisfy equilibrium. This means that the section may not be able to sustain that axial load anymore, at this point the analysis can be stopped.

B. Flexure Deformations

(b.1) Once the axial load and moment has been defined, the flexural deformations Δ_c and Δ_p can be calculated according to the procedure given in subsection 4.4.1 and 4.4.2.

(b.2) If no $P\Delta$ effect is being considered, the shear force is calculated as:

$$V = \frac{M}{L} \quad (4-137)$$

in which L = length of column to the point of contraflexure. In the case where $P\Delta$ is being considered, a first approximation the deflection may be taken as $\Delta = \Delta_c + \Delta_p$, as the shear deformations are not known at this stage. The shear force can then be calculated as:

$$V = \frac{M + \beta P\Delta}{L + \alpha\beta\Delta} \quad (4-138)$$

where β = proportion of $P\Delta$ considered, which depends on geometric characteristics of the problem; α = is the fraction of the shear force which is added to the axial load. This last factor is used on a variable axial load problem, as encountered on external columns in a frame or multi-column pier seat. In Eq. (4-138) the moment at the critical cross-section is considered to be:

$$M = VL - \beta P\Delta \quad (4-139)$$

in which the negative sign implies that the axial load P is positive in tension.

C. Shear Deformations

The elastic shear deformation Δ_{se} can be calculated by the procedure given in subsections 4.4.3 and 4.4.4. To calculate the inelastic shear deformation the procedure given in the following steps is used. These steps summarize the proposed CIST model.

(c.1) The average longitudinal strain ϵ_{oe} for the concrete struts can be computed as depicted in Fig. 4-9.

(i) The distance from the critical cross-section to the location of the average longitudinal strain y is taken as the lesser of $\frac{1}{2}L_{cr}$ and $\frac{1}{2}jd \cot \theta$.

(ii) If $M \leq M_y$ then,

$$\epsilon_{oe} = \epsilon_o + (\epsilon_{ocr}^* - \epsilon_o) \frac{y}{L_{cr}} \quad (4-140)$$

in which, ϵ_{ocr}^* is the centroidal strain at the limit of the cracked section of the column, that can be calculated as:

$$\epsilon_{ocr}^* = \epsilon_{oo} + (\epsilon_{ocr} - \epsilon_{oo}) \left| \frac{M_{cr}^*}{M_{cr}} \right| \quad (4-141)$$

where M_{cr}^* = moment at the commencement of cracked section, that is calculated as:

$$M_{cr}^* = M \frac{L - L_{cr}}{L_{cr}} \quad (4-142)$$

in which L_{cr} is the length of the cracked section, which is defined by Eq. (4-123).

(iii) If $M > M_y$ then ϵ_{oe} is given by:

$$\epsilon_{oe} = \epsilon_{ocr}^* + (\epsilon_{oy} - \epsilon_{ocr}^*) \frac{L_{cr} - y}{L_{cr} - L_y} \quad \text{for } y \geq L_y \quad (4-143)$$

or,

$$\epsilon_{oe} = \epsilon_{oy} + (\epsilon_o - \epsilon_{oy}) \left(\frac{L_y - y}{L_y} \right)^2 \quad \text{for } y < L_y \quad (4-144)$$

where,

$$L_y = L \left(1 - \frac{M_y}{M} \right) \quad (4-145)$$

in which ϵ_{oy} is the centroidal strain at the location of the yield moment (Fig. 4-9b).

(c.2) Assume a value of the shear distortion γ , which may be based on previous steps of the analysis.

(c.3) Assume a transverse strain ϵ_v ,

(c.4) Calculate the stress in the transverse steel, Eq. (4-136).

(c.5) Calculate the strains in the concrete struts and ties Eqs. (4-132) and (4-133).

(c.6) Calculate the stresses on the concrete struts and ties through the constitutive model, Eqs. (4-134) and (4-135). The stresses should be computed for both the confined and unconfined concrete.

(c.7) Compute the force components,

$$F_{cc1} = f_{cc}^*(\epsilon_1^*) jdb_{wc} \cos \theta \quad (4-146)$$

$$F_{co1} = f_{co}^*(\epsilon_1^*) jdb_{wo} \cos \theta \quad (4-147)$$

$$F_{cc2} = f_{cc}^*(\epsilon_2^*) jdb_{wc} \cos \theta \quad (4-148)$$

$$F_{co2} = f_{co}^*(\epsilon_2^*) jdb_{wo} \cos \theta \quad (4-149)$$

$$F_v = A_{sv} f_{sv} \frac{jdb}{s} \cot \theta \quad (4-150)$$

where jdb_{wo} and jdb_{wc} are the unconfined and confined shear area respectively.

(c.8) Check internal equilibrium,

$$|F_v + (F_{cc1} + F_{co1} + F_{cc2} + F_{co2}) \sin \theta| \leq \textit{tolerance} \quad (4-151)$$

If the equilibrium requirement is not met, repeat from step (c.3).

(c.9) Calculate shear force,

$$V = (F_{cc1} + F_{co1} - F_{cc2} - F_{co2}) \sin \theta \quad (4-152)$$

If the shear force calculated in Eq. (4-152) is not equal, within a given tolerance, to the shear force given by Eq. (4-138), then the value shear distortion γ needs to be adjusted, and the procedure is repeated from step (c.2).

Once convergence has being satisfied, the shear distortion angle γ is used to find the inelastic shear deflection,

$$\Delta_{sp} = \gamma L_{pc} \quad (4-153)$$

D. Total Deflection

The total deflection on the columns is:

$$\Delta = \Delta_e + \Delta_p + \Delta_{se} + \Delta_{sp} \quad (4-154)$$

If the $P\Delta$ effect is being considered then the shear force needs to be adjusted by using the total deflection Δ in Eq. (4-138), and the whole procedure is to be repeated from step c.2.

This procedure account for both $P\Delta$ and variable axial load effect. Of special importance in this procedure is a robust algorithm to solve the different variables at certain steps. Iterations are needed to calculate the centroidal strain ϵ_o , the transverse strain ϵ_v , and the shear distortion γ . The strategy to solve for these variables includes the following:

(1) Secant Method is used as a first option. This method is used, because of it higher order of convergence near the solution, and because the solution is not bracketed. To

guarantee the stability a maximum step is defined, as the method can get out of bounds if the derivative of the function gets small. The best solution is always stored, in case the method does not converge.

(2) If at any given iteration, it is found that a solution exists between two points, then the method of solution switches to a Regula Falsi approach, as this ensures a solution.

(3) If convergence is not found, then as an alternative, a somewhat slower algorithm will try to bracket the solution. During every trial value, the best solution is always being kept track of. It is possible that by specifying too small a tolerance, no convergence can be achieved, in which case the best solution is returned. If the bracketing routine is successful in finding a range in which the solution is located, then a Regula Falsi method is applied to find the solution.

(4) Because of numerical round-off errors it is always necessary to use a counter to avoid an endless loop.

This method of solution has proven to be effective to give the numerical procedure good stability, which is particularly important, as so many calculations are being performed.

4.4.4.2 Crack Inclination Angle

The assessment of inelastic shear deformation within the plastic hinge region implies that the fixed angle CIST model has an influence only after the section is fully cracked. To ensure a tractable solution, limit analysis is adopted herein to define the crack inclination angle. Limit analyses can define three possible shear failure modes in membrane type elements (Marti and Meyboom, 1992):

(1) Yielding of both reinforcements, concrete does not crush. Thus,

$$f_s = f_y \quad (4-155)$$

$$f_v = f_{vy} \quad (4-156)$$

$$f_c = f'_{ce} \quad (4-157)$$

in which f_s, f_y = stress and yield stress of longitudinal reinforcing steel, f_v, f_{yv} = stress and yield stress of transverse reinforcement, f_c, f'_{ce} = stress and effective concrete strength of concrete. In membrane type elements where there is little or no confinement the effective concrete strength may be lower than the uniaxial strength of plain concrete due to the softening effect of tension in the perpendicular direction (Collins and Mitchell, 1991). In this investigation, the effective concrete strength will be taken as the uniaxial strength of plain concrete, as the confinement effect at the base of a column tends to compensate for the softening effect. The inclination of the principal compressive strain for this case is calculated by:

$$\tan \theta = \sqrt{\frac{\rho_{sv} f_{yv}}{\rho_s f_y}} \quad (4-158)$$

in which

$$\rho_s = \frac{A_{st}}{j d b_w} \quad (4-159)$$

and

$$\rho_{sv} = \frac{A_{sv}}{s b_w} \quad (4-160)$$

and the applied shear stress is given by,

$$\tau_u = \sqrt{(\rho_s \rho_{sv} f_y f_{yv})} \quad (4-161)$$

(2) Yielding of reinforcement in weak (transverse) direction, concrete crushes and reinforcement in strong direction remains elastic. In this case,

$$\sin \theta = \sqrt{\frac{\rho_{sv} f_{yv}}{f'_c}} \quad (4-162)$$

and,

$$\tau_u = \sqrt{(f'_c - \rho_{sv} f_{yv}) \rho_{sv} f_{yv}} \quad (4-163)$$

(3) Concrete crushes and both reinforcements remain elastic. For this case,

$$\theta = 45^\circ \quad (4-164)$$

and

$$\tau_u = \frac{1}{2} f'_c \quad (4-165)$$

Note that this implies that the element is being subjected to pure shear. To find the governing mode, the lowest value of τ_u is taken, and its corresponding inclination angle. Nevertheless, the crack inclination is not to be taken less than a minimum which is given by,

$$\tan \theta_{\min} = \frac{jd}{2L} \quad (4-166)$$

which is dictated by the rocking effect as described by Mander et al. (1993). In this analysis it is to be noted that the fixed angle assumed by the model is taken as the inclination angle of the principal compressive stress at failure. Analyses by Collins and Mitchell (1991) indicate that this angle does not change significantly after yielding.

4.5 Validation of Fiber-Element Model

A computer program UB-COLA was developed to simulate the cyclic behavior of a reinforced concrete column. The program incorporates the CIST model for shear deformations. The concrete model advanced in Section 3, which incorporates the simulation of concrete in both tension and compression cyclic behavior, and the simulation of gradual crack closure, for confined and unconfined concrete, was incorporated into the program. The energy balance theory developed by Mander et al. (1988) for the prediction of first hoop fracture was also implemented, which makes the program capable of predicting failure by hoop fracture. The steel model developed in section 2, which incorporates local cyclic degradation and the proposed fatigue model, was also incorporated. Thus the program is able to simulate longitudinal bar fracture. Finally, the inelastic cyclic shear model presented in this section was implemented into the program to simulate more accurately the cyclic behavior of shear critical columns.

Two column specimens tested by Aycardi et al. (1992) were chosen to compare the fiber element model against; these are Specimens 2 and 4. The prismatic columns had a 4 x 4 in. cross-section embedded into a 20 x 9 x 8 in. reinforced concrete base. The distance from the column base up to the point of application of the lateral load was 21 in. The longitudinal reinforcement consisted of four D4 bars (0.225 in. diameter, with an area of 0.04 in²). The transverse reinforcement consisted of a 0.12 in. diameter smooth round wire (#11 gage) spaced at 4 in., with a cover of 0.5 in. measured to the centerline of the hoop. The steel and concrete properties are given in Tables 4-1 and 4-2, respectively.

Table 4-1 Experimental Steel Properties , Aycardi et al. (1992)

Steel Type	f_y (ksi)	E_s (ksi)	ϵ_{sh}	E_{sh} (ksi)	f_{su} (ksi)	ϵ_{su}	ϵ_{sf}
D4	65	31050	0.026	750	73	0.107	0.15
#11 Gage	56	29800	0.014	450	70	0.14	-

Table 4-2 Experimental Concrete Properties, Aycardi et al. (1992)

f'_{co} (ksi)	E_c (ksi)	ϵ'_{co}	ϵ_{spall}	r
4.35	4280	0.0023	0.02	2.44

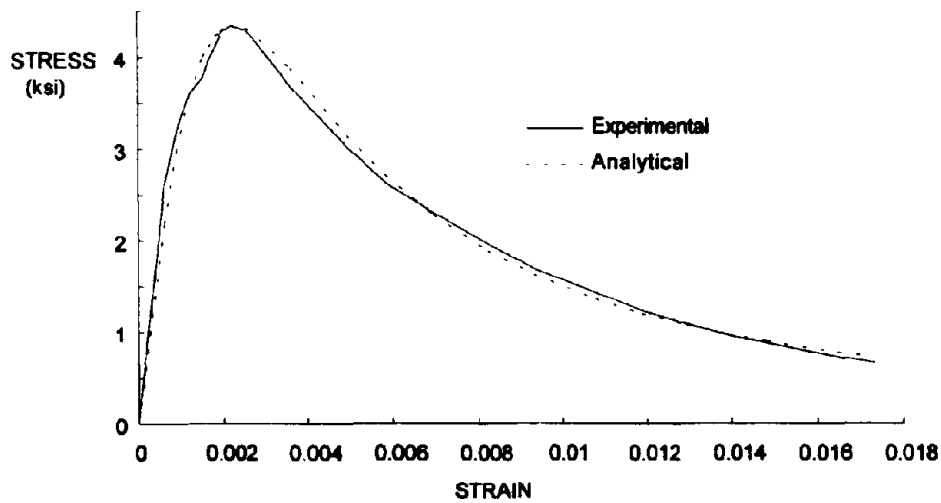


Fig. 4-10 Comparison of the Analytical Stress-Strain Relationship with the Experimental Behavior of Plain Concrete from Aycardi et al. (1992) for Specimens 2 and 4.

Specimen 2 was tested with a constant axial load of 21.2 kips resulting in a load ratio of $\frac{P}{f'_c A_g} = 0.30$. Whereas specimen 4 was tested with a variable axial load where $P = 6.95 + 2V$ (kips), which results in a load ratio of $\frac{P}{f'_c A_g} = 0.10$. These may be considered typical building columns. The columns were tested at incremental cycle amplitudes of $\pm 0.25\%$, $\pm 0.5\%$, $\pm 1\%$, $\pm 2\%$, $\pm 3\%$, $\pm 4\%$ and $\pm 5\%$ drift, with 2 complete cycles at every drift step. Both the analytical model given by Mander et al. (1984) and the UB-COLA model are successful in predicting the force-displacement relationship for a columns with high level of axial load (Fig. 4-12), whereas the proposed model gives better results for low level of axial load due to the gradual crack closure incorporated in it (Fig. 4-11).

Three ductile hollow reinforced concrete columns (Columns A, C and D) tested by Mander et al. (1984) are also compared with the fiber element model. The columns had a height of 3.2 m and a square cross section of 750 mm with 120 mm thick walls, containing sixty 10 mm Grade 275 deformed bars (D10) as longitudinal reinforcement giving a volumetric ratio of 0.0155. The longitudinal reinforcement was distributed uniformly around each face with a cover of 20 mm. The specimens contained different arrangements of transverse steel in the plastic hinge zone. The cyclic testing consisted of two complete cycles at each displacement ductility factor of $\mu = \pm 2, \pm 4, \pm 6$ and ± 8 . Column A had a low axial load $P = 0.1 f'_c A_g$ and minimum (antibuckling) steel. Column C had a moderate axial load $P = 0.3 f'_c A_g$ and confining steel, whereas Column D had a moderate level of axial load and minimum steel. For a detailed description of the specimens refer to Mander et al. (1984).

Of particular interest in this investigation is the capability of the model to simulate different failure modes. After Column A had been tested at the specified displacement ductility factors, the specimen was subjected to 40 dynamic cycles up to fracture of the longitudinal bars. The present model predicted a fracture of the longitudinal reinforcement after 31 cycles, as shown in Fig. 4-14. It may be noted that the present formulation improves the simulation of gradual crack closure. Of special importance is the degree of detail that the

present formulation was capable of simulating, especially concrete failure in Column C, Fig. 4-15. Fig. 4-16 shows the experimental behavior (Fig. 4.16a) compared to the original model of Mander et al. (1984) (Fig 4.16b) with the proposed model using the UB-COLA program (Fig. 4.16c). Both models predicted the overall behavior quite well as neither shear nor crack closure concerns dominate in this column.

Finally, a shear critical column was chosen to show the capability of the CIST model to accurately simulate cyclic inelastic shear behavior. A full size cap-to-column connection of a shear critical bridge pier tested by Mander et al. (1993) was tested under reverse cyclic loading. It should be noted that in this test, the cyclic inelastic shear behavior was assessed, which allows the comparison of the proposed analytical model with actual experimental behavior. The pier had an average square cross section of 910 mm of side. The longitudinal reinforcement consisted of 16 #7 bars enclosed by single perimeter hoops at 305 mm centers. The concrete strength was found to be 7.4 ksi (51 MPa). A detailed description of the specimen is found in Mander et al. (1993). Figs. 4-17 shows the analytical prediction and the experimental behavior of the shear critical column. Note how the CIST model was able to accurately simulate the inelastic shear behavior. The fiber model proposed by Mander et al. (1984) was incapable of simulating this shear behavior, as it is based on an elastic shear model.

4.6 Conclusions

In this section, a Fiber Element approach has been presented which can simulate the hysteretic behavior of a reinforced concrete column. Equations for uniaxial bending with quadratically varying dimensions and quadratically varying stress functions were presented. These higher order elements can both improve convergence and reduce the number of elements required. Equations for a five node rectangular element for biaxial bending were also presented, although no implementation of such a model has been included, as no biaxial experiments with curvature assessment was found in the literature. It is necessary to

investigate the biaxial interaction of cracking and yielding to support any assumption to assess deformations in a biaxially loaded column.

The cyclic inelastic strut-tie (CIST) model presented, was successfully applied to simulate the shear hysteretic behavior. The fatigue damage model presented in Section 2 predicted a failure by hoop fracture after 31 cycles, compared to 40 cycles found experimentally. The simulation of gradual crack closure can improve the hysteretic shape on columns with low levels of axial load, as compared with previous models with sudden crack closure. With the implementation of robust algorithms for solving for different variables in the procedure presented, the program presented a very stable performance. It is important to mention that during the implementation of the program, care must be taken to ensure numerical stability during the evaluation of the different equations as underflow or overflow may occur, particularly when small reversals are attempted by the solving algorithms.

Finally, it is worth making some comparative comments on the program COLUMN (Mander, et al. 1984) and the program developed in this study, UB-COLA. It is evident that the differences are often small between the two programs, especially for moderate levels of axial load ($P > 0.25f'_cA_g$) where crack closure and shear deformations are not of particular concern. The original program COLUMN was written to predict the performance of well detailed capacity designed bridge columns in which the transverse shear reinforcement is not expected to yield. For such columns that program performs satisfactorily - although it cannot predict a steel fatigue failure.

The new program UB-COLA, was specifically designed to handle issues pertaining to concrete failure, inelastic shear deformations, steel fatigue and gradual crack closure - all features of poorly detailed existing columns. The program can also handle new columns with high strength concrete and steel.

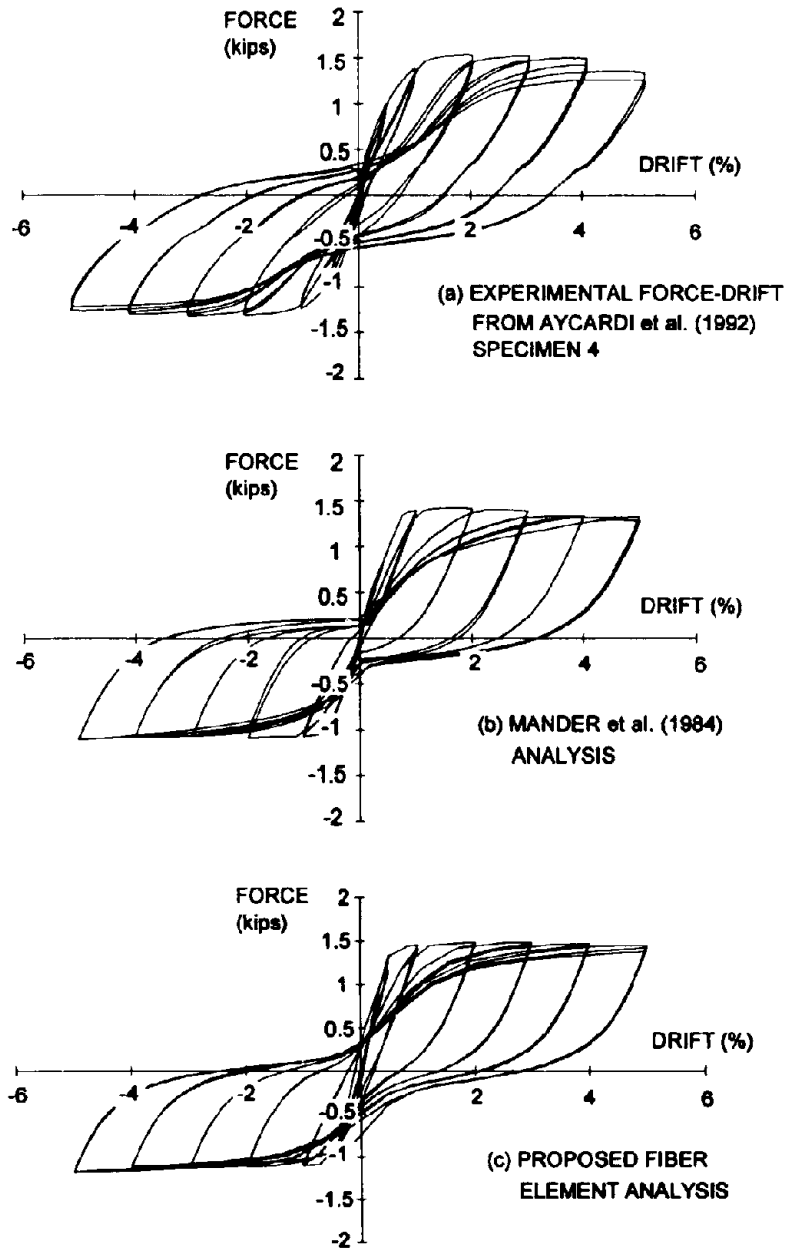


Fig. 4-11 Comparison of Proposed Fiber Element Model with Experimental Results from Aycardi et al. (1992) Specimen 4, $P = 0.10 f'_c A_g$.

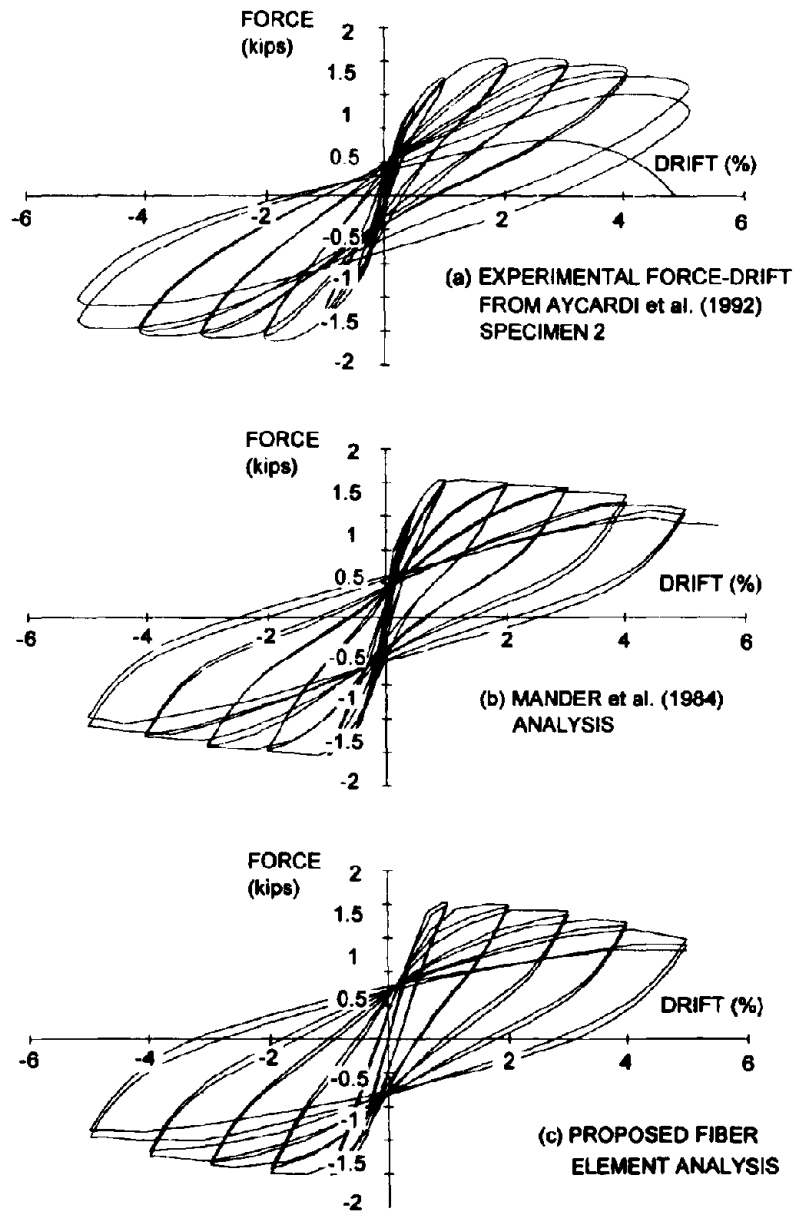


Fig. 4-12 Comparison of Proposed Fiber Element Analysis with Experimental Results from Aycardi et al. (1992) Specimen 2, $P = 0.30 f_c' A_g$.

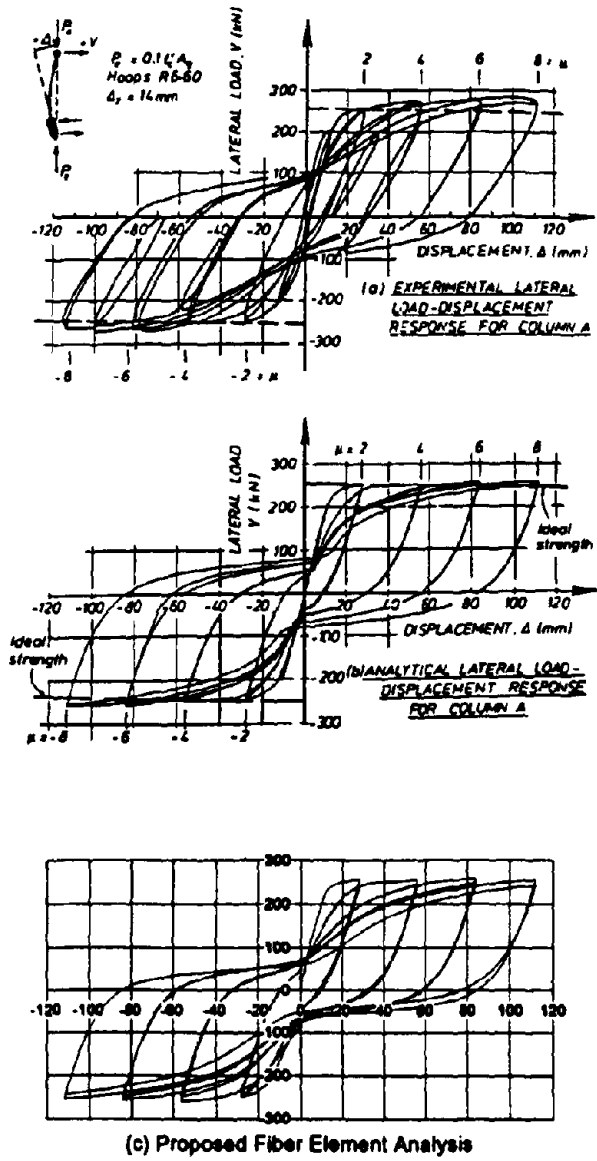
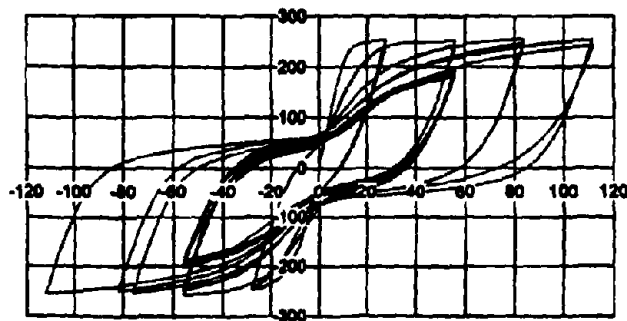
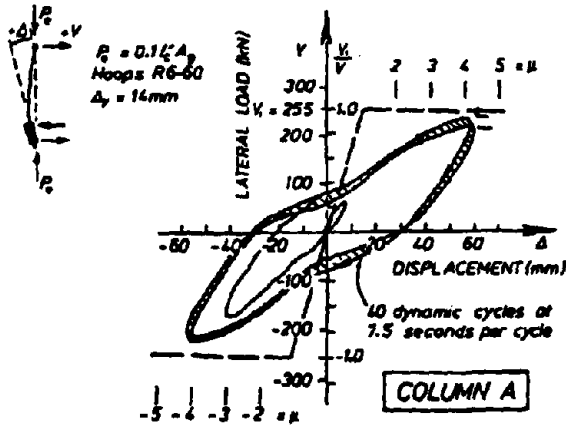
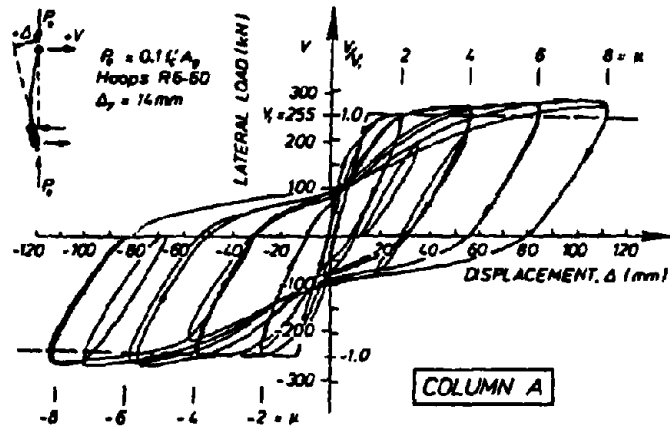
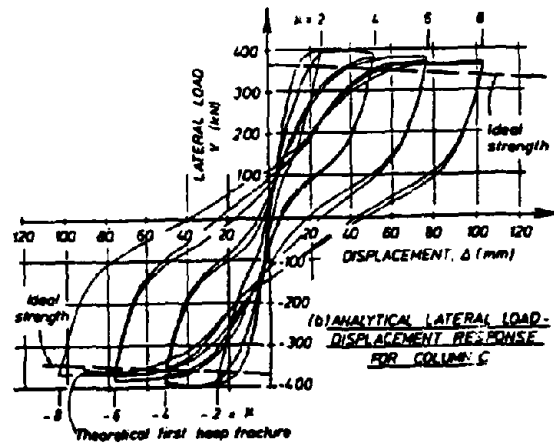
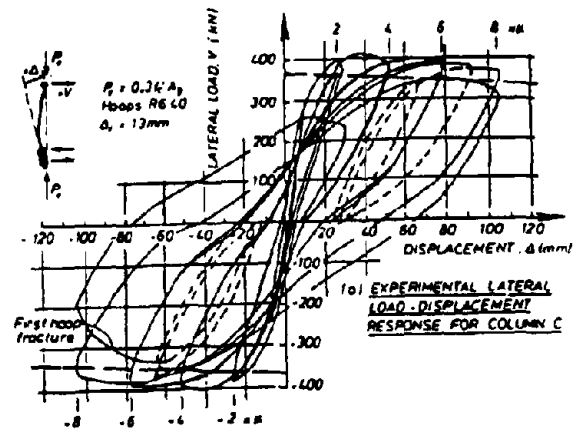


Fig. 4-13 Comparison of Proposed Fiber Element Analysis with Experimental and Analytical Results from Mander et al. (1984) Column A.



(c) Proposed Fiber Element Analysis

Fig. 4-14 Prediction of Low Cycle Fatigue Fracture of Longitudinal Bars For Column A.



(c) Proposed Fiber Element Analysis

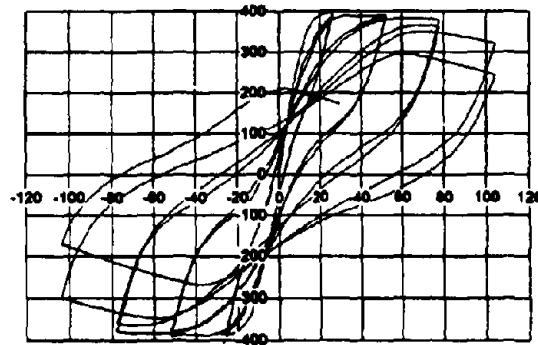


Fig. 4-15 Comparison of Proposed Fiber Element Analysis with Experimental and Analytical Results from Mander et al. (1984) Column C

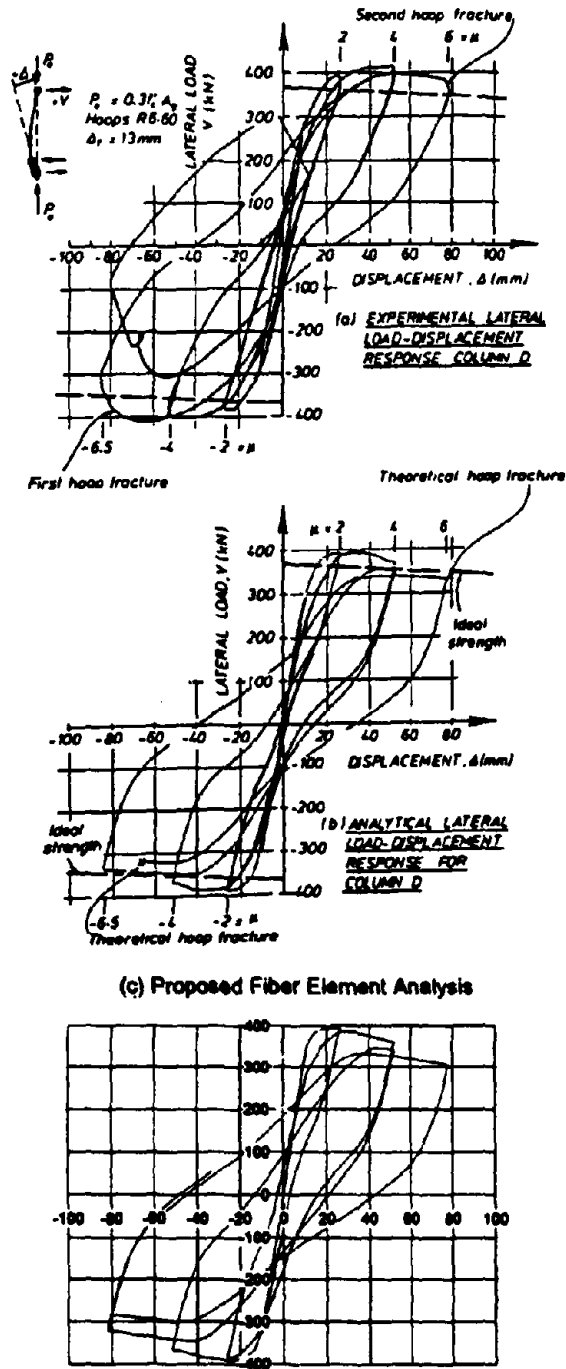
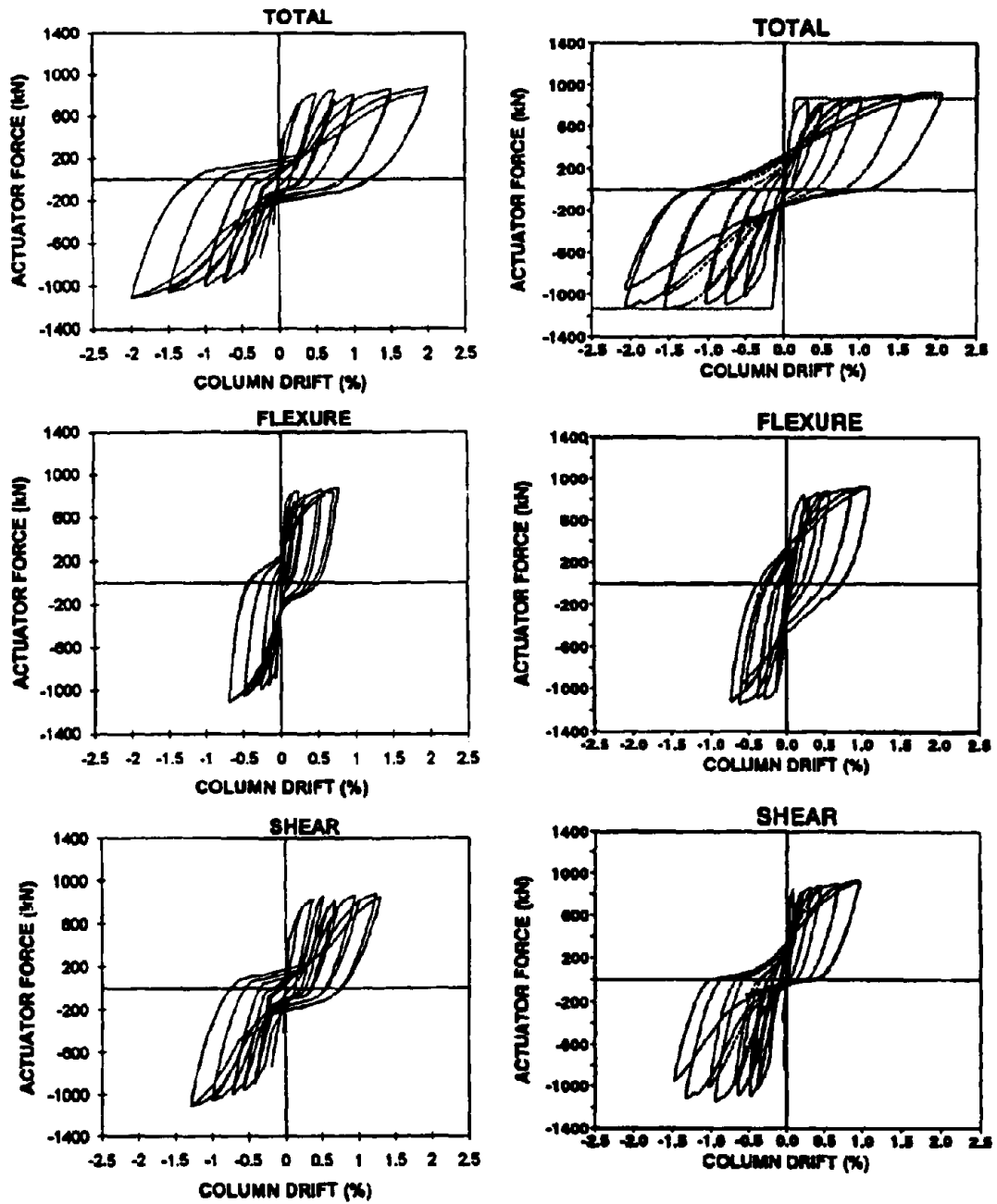


Fig. 4-16 Comparison of Proposed Fiber Element Analysis with Experimental and Analytical Results from Mander et al. (1984) Column D



ANALYTICAL
EXPERIMENTAL

**Fig. 4-17 Analytical Simulation of a Full Size Shear Critical Bridge Pier
Tested by Mander et al. (1993)**

Section 5

Summary, Conclusions and Recommendations

5.1 Summary

This study has been concerned with the computational modeling of energy absorption (fatigue) capacity of reinforced concrete bridge columns by using a cyclic dynamic Fiber Element computational model. The results were used with a smooth hysteretic rule to generate seismic energy demand. By comparing the ratio of energy demand to capacity, inferences of column damageability or fatigue resistance were made.

A complete analysis methodology for bridge columns was developed starting from the basic principles of nonlinear mechanics of materials. The hysteretic behavior of steel reinforcement was dealt with in detail: stability, degradation and consistency of cyclic behavior was explained. An energy based universally applicable low cycle fatigue model for steel was proposed. A hysteretic model for confined and unconfined concrete subjected to both tension or compression cyclic loading was advanced, which is also capable of simulating gradual crack closure. A Cyclic Inelastic Strut-Tie (CIST) model was developed, in which the comprehensive concrete model proved to be suitable. The CIST model was shown to be capable of assessing inelastic shear deformations with a high degree of accuracy, within the context of a Fiber Element (FE) program. A parabolic fiber element with parabolic stress function element for uniaxial flexure was developed, as well as a rectangular fiber element with a quadratic interpolation function suitable for biaxial flexure.

5.2 Specific Conclusions

1. Steel Stress-Strain Modeling

A universally applicable stress-strain model for mild and high strength reinforcing steels was developed. This model includes the effects of low cycle fatigue and is capable of accurately predicting bar fracture-- an important phenomenon in the seismic damage analysis of bridge columns. The prediction of bar fracture is achieved by tracking hysteretic energy absorption. This method gives superior results to the best alternative-- the rainflow counting method.

2. Concrete Stress-Strain Modeling

A universally applicable stress-strain model for concrete has also been advanced. This model is an enhanced version of that originally proposed by Mander et al. (1988a). Some of the new features include:

- (i) An improved monotonic stress-strain idealization using the equation of Tsai (1988), which can now cater to low to very high strength concrete.
- (ii) Enhanced cyclic loading stress-strain relations that couple tensile and compressive excursions and allows for gradual crack closure. This greatly improves the moment-curvature, force-displacement prediction of beams and columns with low levels of axial load.
- (iii) Cyclic stress-strain relations in tension. This enables the reliable prediction of cyclic inelastic shear displacements.

3. Fiber-Element Analysis

A computer program UB-COLA was developed that uses "Fiber-Element" for the prediction of both the non-linear moment-curvature, and force-displacement behavior of structural concrete beam-columns under dynamic cyclic lateral (shear) loading. The program is capable of predicting the modes of failure that generally lead to column collapse, namely:

- (i) Low cyclic fatigue of the longitudinal reinforcement-- common in beams and columns with low axial loads ($P_e < 0.15 f'_c A_g$)
- (ii) Fracture of transverse hoops-- common in confined columns with high axial load ($P_e > 0.2 f'_c A_g$)
- (iii) Buckling of the longitudinal compression reinforcement and subsequent crushing of the concrete-- common in columns where the transverse hoop spacing exceeds six longitudinal bar diameters.
- (iv) Shear failure, when the concrete struts crush.

The program has the unique feature of being able to reliably track inelastic shear displacements in lightly reinforced columns which have not been detailed in accordance with capacity design principles.

5.3 Recommendations for Future Research

(1) The nature of the cyclic behavior of concrete with incursions into tension and compression needs to be established. Very limited experimental information exists regarding the cyclic behavior of concrete.

(2) The fatigue model needs to be calibrated with additional experimental results to more reliably establish its parameters.

(3) Well-designed experiments to assess shear deformations and crack formation are needed, to validate or refine the proposed Cyclic Inelastic Strut-Tie model.

(4) The fiber element analysis in its present form is "curvature" controlled. That is, for a given curvature the moment, and hence shear, is assessed, then the inelastic shear strain is determined from a "force" (shear) controlled algorithm. This process works well except for columns failing prematurely in shear. It is therefore recommended that an inverse form of the solution be explored for such shear-critical elements, where the response is perhaps "shear-strain" controlled. In this approach shear force would be determined for a given level of share strain. From the requested moment the curvature would be assessed from a "force" controlled algorithm.

(5) Parametric studies to measure the influence of various proposed model parameters may clarify their range and validity.

(6) A study on the interaction between the orthogonal cracking and yielding on biaxial flexure is needed.

(7) A modified shear model for the assessment of shear deformation on biaxial shear needs to be developed.

Section 6

References

References - Section 1

- _____ ATC 6-2 (1983), *Seismic Retrofitting Guidelines for Highway Bridges*, Applied Technology Council, 220 pp.
- _____ ACI Committee 318, (1989), *Building Code Requirements for Reinforced Concrete (ACI 318-89) and Commentary ACI 318 R-89*, American Concrete Institute, Detroit, 353 pp.
- Allahabadi, R. and Powell, G.H., (1988), *DRAIN-2DX User's Guide*, Report No. UCB/EERC-88-06, University of California, Berkeley, 1988.
- Bouc, R., (1967), *Forced Vibrations of Mechanical Systems with Hysteresis*, Proceedings of 4th Conference on Nonlinear Oscillation, Prague, 1967.
- Collins, P.M. and Mitchell, D., (1991), *Prestressed Concrete Structures*, Prentice Hall, New Jersey, 1991.
- Hsu, T.T.C., (1993), *Unified Theory of Reinforced Concrete*, CRC Press, Boca Raton, 1993.
- Kanaan, A.E. and Powell, G.H., (1973), *DRAIN-2D A General Purpose Computer Program for Dynamic Analysis of Inelastic Plane Structures*, Report No. UCB/EERC/73/06 and 73/22, University of California, Berkeley, 1973.
- Kohnke, P.C., (1983), *ANSYS Engineering Analysis System - Theoretical Manual*, Swanson Analysis System, Houston, Pennsylvania, 1983.
- Mander, J.B., Priestley, M.J.N. and Park, R., (1984), *Seismic Design of Bridge Piers*, Department of Civil Engineering, University of Canterbury, Report 84-2, Feb-84, 483 pp.

- Mander, J.B., Priestley, M.J.N. and Park, R., (1988a), *Theoretical Stress-Strain Model for Confined Concrete*, Journal of Structural Engineering, Vol. 114, No. 8, Aug-88, pp. 1804-1826.
- Mander, J.B., Priestley, M.J.N. and Park, R., (1988b), *Observed Stress-Strain Behavior of Confined Concrete*, Journal of Structural Engineering, Vol. 114, No. 8, Aug-88, pp. 1827-1849.
- Park, Y.J., Reinhorn, A.M., and Kunnath, S.K., (1987), *IDARC: Inelastic Damage analysis of Reinforced Concrete Frame-Shear Wall Structures*, Technical Report NCEER-87-0008, SUNY/Buffalo, 1987.
- Wen, Y.K., (1975), *Approximate Method for Nonlinear Random Vibration*, Journal of Engineering Mechanics Division, ASCE, Vol. 101, EM4, 1975.
- Zahn, F.A., Park, R. and Priestley, M.J.N., (1990), *Flexural Strength and Ductility of Circular Hollow Reinforced Concrete Columns without Confinement on Inside Face*, ACI Structural Journal, Vol. 87, No. 2, Mar-Apr 90, pp.156-166.

References - Section 2

- Adriano, T. and Park, R., (1986), *Seismic Design Considerations of the Properties of New Zealand Manufactured Steel Reinforcing Bars*, Bulletin of the New Zealand National Society for Earthquake Engineering, Vol. 19, No. 3, Sep-86, pp. 213-246
- Coffin, L.F., Jr., (1954), *A Study of the Effects of Cyclic Thermal Stresses in a Ductile Metal*, ASME Transactions, Vol. 16, 1954, pp. 931-950.
- Coffin, L.F., Jr., (1955), *Design Aspects of High Temperature Fatigue with Particular Reference to Thermal Stresses*, ASME Transactions, Vol. 78, 1955, pp. 527-532.
- De Martino, A., Landolfo, R. and Mazzolani, F.M., (1990), *The Use of the Ramberg-Osgood Law for Materials of Round-House Type*, Journal of Materials and Structures, Vol. 23, 1990, pp. 59-67.

- Dowling, N.E., (1972), *Fatigue Failure Predictions for Complicated Stress-Strain Histories*, Journal of Materials, Vol.7, No. 1, Jan-72, pp. 71-87.
- El-Metwally, S.E. and Chen, W.F., (1987), *Moment-Rotation Modeling of Reinforced Concrete Beam-Column Connections*, ACI Structural Journal, Vol. 85, No. 4, Aug-87, pp. 384-394.
- Espion, B. and Halleux, P., (1988), *Moment Curvature Relationship of Reinforced Concrete Sections Under Combined Bending and Normal Force*, Materials and Structures / Matériaux et Constructions, Vol. 21, No. 125, Sep-88, pp. 341-351.
- Glinka, G. and Kam, J.C.P., (1987), *Rainflow Continuing Algorithm for Very Long Stress Histories*, International Journal of Fatigue, Oct-87, pp. 223-228.
- Kato, B., (1990), *Tension Testing of Metallic Structural Materials for Determining Stress-Strain Relations Under Monotonic and Uniaxial Tensile Loading*, Journal of Materials and Structures, Vol. 23, 1990, pp. 35-46.
- Kato, B., Aoki, H. and Yamanouchi, H., (1990), *Standardized Mathematical Expression for Stress-Strain Relations of Structural Steel for Monotonic and Uniaxial Tension Loading*, Journal of Materials and Structures, Vol. 23, 1990, pp. 47-58.
- Kent, D.C., and Park, R., (1973), *Cyclic Load Behavior of Reinforcing Steel*, Strain, Vol. 9, No. 3, July 1973, pp. 98-103.
- Koh, S.K. and Stephens, R.I., (1991), *Mean Stress Effects on Low Cycle Fatigue for a High Strength Steel*, Journal of Fatigue Fracture of Engineering Materials, Vol.14, No.4, 1991, pp. 413-428.
- Lindgren, G. and Rychlik, I., (1987), *Rain Flow Cycle Distributions for Fatigue Life Prediction Under Gaussian Load Processes*, Fatigue of Engineering Materials and Structures, Vol. 10, No. 3, Mar-87, pp. 251-260.
- Lorenzo, F. and Laird, C., (1984), *A New Approach to Predicting Fatigue Life Behavior under the Action of Mean Stresses*, Journal of Materials Science and Engineering, Vol. 62, 1984, pp. 205-210.

- Ma, S.M., Bertero, V.V. and Popov, (1976), E.P., *Experimental and Analytical Studies on the Hysteretic Behavior of Reinforced Concrete Rectangular and T-Beams*, EERC, Report No. 76/02, May 1976.
- Mander, J.B., Priestley, M.J.N. and Park, R., (1984), *Seismic Design of Bridge Piers*, Department of Civil Engineering, University of Canterbury, Report 84-2, Feb-84, 483 pp.
- Mander, J.B., Priestley, M.J.N. and Park, R., (1988a), *Theoretical Stress-Strain Model for Confined Concrete*, Journal of Structural Engineering, Vol. 114, No. 8, Aug-88, pp. 1804-1826.
- Mander, J.B., Priestley, M.J.N. and Park, R., (1988b), *Observed Stress-Strain Behavior of Confined Concrete*, Journal of Structural Engineering, Vol. 114, No. 8, Aug-88, pp. 1827-1849.
- Mander, J.B., Panthaki, F.D. and Chaudhary, M.T., (1992), *Evaluation of Seismic Vulnerability of Highway Bridges in the Eastern United States*, Lifeline Earthquake Engineering, 1992, pp. 72-86.
- Manson, S.S., (1954), *Behavior of Materials under Conditions of Thermal Stresses*, NACA TN-2933, National Advisory Committee for Aeronautics, Cleveland, 1954.
- McCabe, S.L. and Hall, W.J., (1989), *Assessment of Seismic Structural Damage*, Journal of Structural Engineering, Vol. 115, No. 9, Sep-89, pp. 2166-2183.
- Menegotto, M. and Pinto, (1973), P.E., *Method of Analysis for Cyclically Loaded Reinforced Concrete Plane Frames Including Changes in Geometry and Non-elastic Behavior of Elements Under Combined Normal Force and Bending*. IABSE Symposium on the Resistance and Ultimate Deformability of Structures Acted on by Well-Defined Repeated Loads, Lisbon 1973.
- Miner, M.A., (1945), *Cumulative Damage in Fatigue*, Trans. ASME, Journal of Applied Mechanics, Vol. 67, Sept. 1945, pp. A 159 - A 164.

- Palmgren, A., (1924), *Durability of Ball Bearings*, ZVDI, Vol. 68, No. 14, 1924, pp. 339-341 (in German).
- Panthaki, F.D., (1991), *Low Cycle Fatigue Behavior of High Strength and Ordinary Reinforcing Steels*, MS-Thesis, SUNY/Buffalo, 1991.
- Rychlik, I., (1993), *Note on Cyclic Counts in Irregular Loads*, *Fatigue Fracture Engineering Materials Structures*, Vol. 16, No. 4, 1993, pp. 377-390.
- Rychlik, I., (1993), *On the 'Narrow-Band' Approximation for Expected Fatigue Damage*, *Probabilistic Engineering Mechanics*, Vol. 8, pp. 1-4.
- Rychlik, I., (1987), *A New Definition of the Rain-Flow Cycle Counting Method*, *International Journal of Fatigue*, Vol. 9, 1987, pp. 119-121.
- Smith, K.N., Watson, P. and Topper, T.H., (1970), *A Stress-Strain Function for the Fatigue of Metals*, *Journal of Materials*, Vol. 5, No. 4, Dec-70, pp. 767-778.
- Sobczyk, K. and Spencer, B.F. Jr., (1992), *Random Fatigue: From Data to Theory*, Academic Press, Inc., San Diego, CA, 1992.
- Soroushian, P. and Choi, K.B., (1987), *Steel Mechanical Properties at Different Strain Rates*, *Journal of Structural Engineering*, Vol.113, No.4, Apr-87, pp. 663-672.
- Svensson, T. and Holmgren, M., (1992), *Numerical and Experimental Verification of a New Model for Fatigue Life*, *Fatigue & Fracture of Engineering Materials & Structures*, Dec-92, pp. 481-493.
- Xiao-yan, T., De-Jun, W. and Hao, X., (1989), *Investigation of Cyclic Hysteresis Energy in Fatigue Failure Process*, *International Journal of Fatigue*, Vol. 11, No. 5, Sept-1989, pp. 353-359.
- Xiulin, Z. and Baotong, L., (1987), *On a Fatigue Formula Under Stress Cycling*, *International Journal of Fatigue*, Vol. 9, No. 2, July 1987, pp. 169-174.

Zahn, F.A., Park, R. and Priestley, M.J.N., (1987), *The Use of Grade 380 Steel for Transverse Confining Reinforcement in Columns*, Bulletin of New Zealand National Society for Earthquake Engineering, Vol. 20, No. 2, Jun-87, pp. 99-115.

Zahn, F.A., Park, R. and Priestley, M.J.N., (1990), *Flexural Strength and Ductility of Circular Hollow Reinforced Concrete Columns without Confinement on Inside Face*, ACI Structural Journal, Vol. 87, No. 2, Mar-Apr 90, pp.156-166.

References - Section 3

_____ ACI Committee 439, (1969), *Effect of Steel Strength and of Reinforcement Ratio on the Mode of Failure and Strain Energy Capacity of Reinforced Concrete Beams*, Journal of the American Concrete Institute, Title No. 66-16, Mar-69, pp.165-173.

Abu-Lebdeh, T.M. and Voyiadjis, G.Z., (1993), *Plasticity-Damage Model for Concrete Under Cyclic Multiaxial Loading*, Journal of Engineering Mechanics, Vol. 119, No. 7, July-1993, pp.1465-1484.

Agrawal, G.L., Tulin, L.G. and Gerstle, K.H., (1965), *Response of Doubly Reinforced Concrete Beams to Cyclic Loading*, Journal of the American Concrete Institute, Vol. 62, No. 7, Jul-65, pp. 823-835.

Ahmad, S.H. and Shah, S.P., (1982), *Stress-Strain Curves of Concrete Confined by Spiral Reinforcement*, Journal of the American Concrete Institute, Vol. 79, No. 6, Dec-82, pp. 484-490.

Ahmad, S.H. and Shah, S.P., (1985), *Behavior of Hoop Confined Concrete Under High Strain Rates*, Journal of the American Concrete Institute, Vol. 82, No. 5, Oct-85, pp. 634-647.

Ahmad, S.H. and Shah, S.P., (1982), *Complete Triaxial Stress-Strain Curves for Concrete*, Journal of the Structural Division, ASCE, Vol. 108, No. ST4, Apr-82, pp. 728-742.

- Al-Noury, S.I. and Chen, W.F., (1989), *Behavior and Design of Reinforced and Composite Concrete Sections*, Journal of the Structural Division, ASCE, Vol. 108, No. ST6, Jun-82, pp. 1266-1284.
- Ang, B.G., Priestley, M.J.N. and Paulay, T., (1989), *Seismic Shear Strength of Circular Reinforced Concrete Columns*, ACI Structural Journal, Vol. 86, No.1, Jan-89, pp. 45-60.
- Balmer, G.G., (1949), *Shearing Strength of Concrete under High Triaxial Stress Computation of Mohrs Envelope as a Curve*, Denver, U.S. Department of the Interior (Research and Geology Division), Bureau of Reclamation, Structural Research Laboratory Report SP 23, Jan-49, pp. 13-26.
- Barnard, P.R., (1964), *Researches into the Complete Stress-Strain Curve for Concrete*, Magazine of Concrete Research, Vol. 16, No. 49, Dec-64, pp. 203-210.
- Bazant, Z.P and Tsubaki, T., (1980), *Total Strain Theory and Path-Dependence of Concrete*, Journal of the Engineering Mechanics Division, ASCE, Vol. 106, No. EM6, Dec-80, pp. 1151-1173.
- Bazant, Z.P. and Kim, S.S., (1979), *Plastic-Fracturing Theory for Concrete*, Journal of the Engineering Mechanics Division, ASCE, Vol. 105, No. EM3, Jun-79, pp. 407-428.
- Bazant, Z.P. and Oh, B.H., (1984), *Deformation of Progressively Cracking Reinforced Concrete*, Journal of the American Concrete Institute, Vol. 81, No. 3, Jun-84, pp. 268-278.
- Bertero, V.V., Popov, E.P. and Forzani, B., (1980), *Seismic Behavior of Lightweight Concrete Beam-Column Subassemblages*, Journal of the American Concrete Institute, Vol. 77, No. 1, Feb-80, pp. 44-52.
- Bing, L., Park, R. and Tanaka, H., (1991), *Effect of Confinement on the Behavior of High Strength Concrete Columns under Seismic Loading*, Pacific Conference on Earthquake Engineering, New Zealand, Nov-91, pp. 183-194.
- Bischoff, P.H. and Perry, S.H., (1991), *Compressive Behavior of Concrete at High Strain Rates*, Materials and Structures / Matériaux et Constructions, Vol. 24, Feb-91, pp. 425-452.

- Blume, J.A., Newmark, N.M. and Corning, L.H., (1961), *Design of Multi-Story Reinforced Concrete Buildings for Earthquake Motions*, Portland Cement Association, Chicago, Chapter 5, Jan-61.
- Bresler, B. and Gilbert, P.H., (1961), *Tie Requirements for Reinforced Concrete Columns*, Journal of the American Concrete Institute, Vol. 58, No. 5, Nov-61, pp. 555-569.
- Burdette, E.G. and Hilsdorf, H.K., (1971), *Behavior of Laterally Reinforced Concrete Columns*, Journal of the Structural Division, ASCE, Vol. 97, No. ST2, Feb-71, pp. 587-602.
- Burns, N.H. and Siess, C.P., (1966), *Plastic Hinging in Reinforced Concrete*, Journal of the Structural Division, ASCE, Vol. 92, No. ST5, Oct-66, pp. 45-64.
- Burns, N.H. and Siess, C.P., (1966), *Repeated and Reversed Loading in Reinforced Concrete*, Journal of the Structural Division, ASCE, Vol. 92, No. ST5, Oct-66, pp. 65-78.
- Carrasquillo, R.L., Nilson, A.H. and Slate, F.O., (1981), *Properties of High Strength Concrete Subjected to Short-Term Loads*, Journal of the American Concrete Institute, Vol. 78, No. 3, May-81, pp. 171-178.
- Carreira, D.J. and Chu, K.H., (1985), *Stress-Strain Relationship for Plain Concrete in Compression*, Journal of the American Concrete Institute, Vol. 82, No. 6, Dec-85, pp. 797-804.
- Carreira, D.J. and Chu, K.H., (1986), *Stress-Strain Relationship for Plain Concrete in Tension*, Journal of the American Concrete Institute, Vol. 83, No. 1, Feb-86, pp. 21-28.
- Carreira, D.J. and Chu, K.H., (1986), *The Moment-Curvature Relationship of Reinforced Concrete Member*, Journal of the American Concrete Institute, Vol. 83, No. 2, Apr-86, pp. 191-198.
- Cedolin, L., Crutzen, Y.R.J. and Poli, S.D., (1977), *Triaxial Stress-Strain Relationship for Concrete*, Journal of the Engineering Mechanics Division, ASCE, Vol. 103, No. EM3, Jun-77, pp. 423-439.

- Chan, W. W. L., (1955), *The Ultimate Strength and Deformation of Plastic Hinges in Reinforced Concrete Frameworks*, Magazine of Concrete Research, Vol. 7, No. 21, Nov-55, pp. 121-132.
- Chen, A.C.T. and Chen, W.F., (1975), *Constitutive Relations for Concrete*, Journal of the Engineering Mechanics Division, ASCE, Vol. 101, No. EM4, Aug-75, pp. 465-481.
- Chen, E.S. and Buyukozturk, O., (1985), *Constitutive Model for Concrete in Cyclic Compression*, Journal of Structural Engineering, Vol. 111, No. 6, Jun-85, pp. 797-814.
- Chen, W.F. and Ting, E.C., (1980), *Constitutive Models for Concrete Structures*, Journal of the Engineering Mechanics Division, ASCE, Vol. 106, No. EM1, Feb-80, pp. 1-19.
- Chuan-zhi, W., Zhen-hai, G. and Zhang, X., (1987), *Experimental Investigation of Biaxial and Triaxial Compressive Concrete Strength*, ACI Materials Journal, Vol. 84, No. 2, Apr-87, pp. 92-100.
- Collins, P.M. and Mitchell, D., (1991), *Prestressed Concrete Structures*, Prentice Hall, New Jersey, 1991.
- Cook, D.J. and Chindapasirt, P., (1980), *Influence of Loading History upon the Compressive Properties of Concrete*, Magazine of Concrete Research, Vol. 32, No. 111, Jun-80, pp.89-100.
- Corley, W.G., (1966), *Rotational Capacity of Reinforced Concrete Beams*, Journal of the Structural Division, ASCE, Vol. 92, No. ST5, Oct-66, pp. 121-146.
- Darwin, D. and Pecknold, D.A., (1977), *Nonlinear Biaxial Stress-Strain Law for Concrete*, Journal of the Engineering Mechanics Division, ASCE, Vol. 103, No. EM2, Apr-77, pp. 229-241.
- Desayi, P. and Krishnan, S., (1964), *Equation for the Stress-Strain Curve of Concrete*, Journal of the American Concrete Institute, Vol. 61, No. 3, Mar-64, pp. 345-350.

- Dilger, W.H., Koch, R. and Kowalczyk, R., (1984), *Ductility of Plain and Confined Concrete Under Different Strain Rates*, Journal of the American Concrete Institute, Vol. 81, No.1, Feb-84, pp. 73-81.
- El-Metwally, S.E. and Chen, W.F., (1987), *Moment-Rotation Modeling of Reinforced Concrete Beam-Column Connections*, ACI Structural Journal, Vol. 85, No. 4, Aug-87, pp. 384-394.
- Elwi, A.A. and Murray, D.W., (1979), *A 3-D Hypoelastic Concrete Constitutive Relationship*, ASCE, Vol. 105, EM4, Aug-79.
- Espion, B. and Halleux, P., (1988), *Moment Curvature Relationship of Reinforced Concrete Sections Under Combined Bending and Normal Force*, Materials and Structures / Matériaux et Constructions, Vol. 21, No. 125, Sep-88, pp. 341-351.
- Fafitis, A. and Shah, S.P., (1984), *Rheological Model for Cyclic Loading of Concrete*, Journal of Structural Engineering, Vol. 110, No. 9, Sep-84, pp.2085-2102.
- Fafitis, A. and Shah, S.P., (1985), *Predictions of Ultimate Behavior of Confined Columns Subjected to Large Deformations*, Journal of the American Concrete Institute, Vol. 82, No. 4, Aug-85, pp. 423-442.
- Ghosh, S.K., (1970), *Behavior of Concrete under Compressive Loadings* (Discussion), Journal of the Structural Division, ASCE, Vol. 96, No. ST6, Jun-70, pp. 1254-1256.
- Gopalaratnman, V.S. and Shah, S.P., (1985), *Softening Response of Plain Concrete in Direct Tension*, ACI Journal, Vol. 82, No. 3, May-June 1985, pp. 310-323.
- Hanson, N.W. and Connor, H.W., (1967), *Seismic Resistance of Reinforced Concrete Beam-Column Joints*, Journal of the Structural Division, ASCE, Vol. 93, No. ST5, Oct-67, pp. 533-560.
- Hays, C.O. Jr., (1981), *Inelastic Material Models in Earthquake Response*, Journal of the Structural Division, ASCE, Vol. 107, No. ST1, Jan-81, pp. 13-28.

- Hognestad, E., Hanson, N.W. and McHenry, D., (1955), *Concrete Stress Distribution in Ultimate Strength Design*, Journal of the American Concrete Institute, Vol. 27, No. 4, Dec-55, pp. 455-479.
- Hughes, B.P. and Gregory, R., (1972), *Concrete Subjected to High Rates of Loading in Compression*, Magazine of Concrete Research, Vol. 24, No. 78, Mar-72, pp. 25-36.
- Hussein, R., (1983), *Analytical Model for Concrete Confinement in Tied Columns* (Discussion), Journal of Structural Engineering, Vol. 109, No. 12, Dec-83, pp. 2951-2954.
- Iyengar, S.R., Desayi, P. and Reddy, K.N., (1970), *Stress-Strain Characteristics of Concrete Confined in Steel Binders*, Magazine of Concrete Research, Vol. 22, No. 72, Sep-70, pp. 173-184.
- Joen, P.H. and Park, R., (1990), *Simulated Seismic Load Tests on Prestressed Concrete Piles and Pile-Pile Cap Connections*, PCI Journal Vol. 35, No. 6, Nov-90, pp. 42-61.
- Kabaila, A., (1964), *Equation for the Stress-Strain Curve of Concrete* (Discussion), Journal of the American Concrete Institute, Vol. 61, No. 9, Sep-64, pp.1227-1229.
- Kani, G.N., (1969), *A Rational Theory for the Function of Web Reinforcement*, Journal of the American Concrete Institute, Title No. 66-18, Mar-69, pp. 185-197.
- Karsan, I.D. and Jirsa, J.O., (1969), *Behavior of Concrete under Compressive Loadings*, Journal of the Structural Division, ASCE, Vol. 95, No. ST12, Dec-69, pp. 2543-2563.
- Karsan, I.D. and Jirsa, J.O., (1970), *Behavior of Concrete under Varying Strain Gradients*, Journal of the Structural Division, ASCE, Vol. 96, No. ST8, Aug-70, pp. 1675-1697.
- Kent, D.C. and Park, R., (1971), *Flexural Members with Confined Concrete*, Journal of the Structural Division, ASCE, Vol. 97, No. ST7, Jul-71, pp. 1969-1990.
- Klink, S.A., (1969), *Actual Elastic Modulus of Concrete*, Journal of the American Concrete Institute, Vol. 82, No. 5, Oct-85, pp. 630-633.

- Komlos, K., (1969), *Factors Affecting the Stress-Strain Relation of Concrete in Uniaxial Tension*, Journal of the American Concrete Institute, Vol. 66, No. 2, Feb-69, pp. 111-114.
- Kotsovos, M.D. and Newman, J.B., (1979), *A Mathematical Description of the Deformational Behavior of Concrete Under Complex Loading*, Magazine of Concrete Research, Vol. 31, No. 107, Jun-79.
- Kotsovos, M.D., (1979), *A Mathematical Description of the Deformational Behavior of Concrete under Complex Loading*, Magazine of Concrete Research, Vol. 31, No. 107, Jun-79, pp. 77-90.
- Kotsovos, M.D., (1980), *Constitutive Model for Short-Time Loading of Concrete* (Discussion), Journal of the Engineering Mechanics Division, ASCE, Vol. 106, No. EM1, Feb-80, pp. 193-196.
- Krauthammer, T. and Hall, W.J., (1982), *Modified Analysis of Reinforced Concrete Beams*, Journal of the Structural Division, ASCE, Vol. 108, No. ST2, Feb-82, pp. 457-475.
- Kupfer, H.B. and Gerstle, K.H., (1973), *Behavior of Concrete under Biaxial Stresses*, Journal of the Engineering Mechanics Division, ASCE, Vol. 99, No. EM4, Aug-73, pp. 853-866.
- Leslie, P.D., (1974), *Ductility of Reinforced Concrete Bridge Piers*, M.E. Report, University of Canterbury, New Zealand, 1974.
- Li, X., Park, R. and Tanaka, H., (1991), *Effects of Variations in Axial Load Level on the Strength and Ductility of Reinforced Concrete Columns*, Pacific Conference on Earthquake Engineering, New Zealand, Nov-91, pp. 147-158.
- Liu, T.C.Y., Nilson, A.H. and Slate, F.O., (1972), *Biaxial Stress-Strain Relations for Concrete*, Journal of the Structural Division, ASCE, Vol. 98, No. ST5, May-72, pp. 1025-1034.
- Madas, P. and Elnashai, A.S., (1992), *A New Passive Confinement Model for the Analysis of Concrete Structures Subjected to Cyclic and Transient Dynamic Loading*, Earthquake Engineering and Structural Dynamics, Vol. 21, 1992, pp. 409-431.

- Mander, J.B., Priestley, M.J.N. and Park, R., (1984), *Seismic Design of Bridge Piers*, Department of Civil Engineering, University of Canterbury, Report 84-2, Feb-84, 483 pp.
- Mander, J.B., Priestley, M.J.N. and Park, R., (1983), *Behavior of Ductile Hollow Reinforced Concrete Columns*, Bulletin of the New Zealand National Society for Earthquake Engineering, Vol. 16, No. 4, Dec-83, pp. 273-290.
- Mander, J.B., Priestley, M.J.N. and Park, R., (1988a), *Theoretical Stress-Strain Model for Confined Concrete*, Journal of Structural Engineering, Vol. 114, No. 8, Aug-88, pp. 1804-1826.
- Mander, J.B., Priestley, M.J.N. and Park, R., (1988b), *Observed Stress-Strain Behavior of Confined Concrete*, Journal of Structural Engineering, Vol. 114, No. 8, Aug-88, pp. 1827-1849.
- Medland, I.C. and Taylor, D.A., (1971), *Flexural Rigidity of Concrete Column Sections*, Journal of the Structural Division, ASCE, Vol. 97, No. ST2, Feb-71, pp. 573-586.
- Mills, L.L. and Zimmerman, R.M., (1970), *Compressive Strength of Plain Concrete under Multiaxial Loading Conditions*, Journal of the American Concrete Institute, Vol. 67, No. 10, Oct-70, pp. 802-807.
- Mirza, M.S. and Hsu, C.T., (1969), *Progress Report on Code Clauses for Limit Design (Discussion)*, Journal of the American Concrete Institute, Vol. 66, No. 3, Mar-69, pp. 221-223.
- Muguruma, H., Nishiyama, M. and Watanabe, F., (1991), *Ductility Evaluation of Reinforced Concrete Columns with Normal and High Strength Concrete*, Pacific Conference on Earthquake Engineering, New Zealand, Nov-91, pp. 159-170.
- Nawy, E.G., Danesi, R.F. and Grosko, J.J., (1968), *Rectangular Spiral Binders Effect on Plastic Hinge Rotation Capacity in Reinforced Concrete Beams*, Journal of the American Concrete Institute, Vol. 65, No. 12, Dec-68, pp. 1001-1010.

- Okamoto, S., Shiomi, S. and Yamabe, K., (1976), *Earthquake Resistance of Prestressed Concrete Structures*, Proceeding, Annual Convention, AIJ, Jan-76, pp. 1251-1252.
- Ottosen, N.S., (1979), *Constitutive Model for Short-Time Loading of Concrete*, Journal of the Engineering Mechanics Division, ASCE, Vol. 105, No. EM1, Feb-79, pp. 127-141.
- Park, R., Kent, D.C. and Sampson, R.A., (1972), *Reinforced Concrete Members with Cyclic Loading*, Journal of the Structural Division, ASCE, Vol. 98, No. ST7, Jul-72, pp. 1341-1358.
- Park, R. and Sampson, R.A., (1972), *Ductility of Reinforced Concrete Column Sections in Seismic Design*, Journal of the American Concrete Institute, Vol. 69, No. 9, Sep-72, pp. 543-551.
- Park, R. and Priestley, M.J.N., (1982), *Ductility of Square-Confined Concrete Columns*, Journal of the Structural Division, ASCE, Vol. 108, No. ST4, Apr-82, pp. 929-950.
- Park, R. and Paulay, T., (1975), *Reinforced Concrete Structures*, John Wiley, New York, 1975.
- Pauw, A., (1960), *Static Modulus of Elasticity of Concrete as Affected by Density*, Journal of the American Concrete Institute, Vol. 32, No. 6, Dec-60, pp. 679-687.
- Popov, E.P., (1980), *Seismic Behavior of Structural Subassemblages*, Journal of the Structural Division, ASCE, Vol. 106, No. ST7, Jul-80 pp. 1451, 1474.
- Popovics, S., (1970), *A Review of Stress-Strain Relationships for Concrete*, Journal of the American Concrete Institute, Vol. 67, No. 3, Mar-70, pp. 243-248.
- Popovics, S., (1973), *A Numerical Approach to the Complete Stress-Strain Curve of Concrete*, Cement and Concrete Research, Vol. 3, No. 4, Sep-73, pp. 583-599.
- Pozzo, E., (1987), *The Influence of Axial Load and Rate of Loading on Experimental Post-Elastic Behavior and Ductility of Reinforced Concrete Members*, Materials and Structures / Matériaux et Constructions, Vol. 20, No. 118, Jul-87, pp. 303-314.
- Priestley, M.J.N., Park, R. and Potangaroa, R.T., (1981), *Ductility of Spirally-Confined Concrete Columns*, Journal of the Structural Division, ASCE, Vol. 107, No. ST1, Jan-81, pp. 181-202.

- Priestley, M.J.N., (1986), *Seismic Design of Concrete Masonry Shearwalls*, Journal of the American Concrete Institute, Vol. 83, No. 1, Feb-86, pp. 58-68.
- Priestley, M.J.N. and Park, R., (1987), *Strength and Ductility of Concrete Bridge Columns Under Seismic Loading*, ACI Structural Journal, Vol. 84, No. 1, Feb-87, pp. 61-76.
- Priestley, M.J.N. and Park, R., (1984), *Strength and Ductility of Bridge Substructures*, Road Research Unit, National Roads Board, Bulletin 71, Jan-84, 120 pp.
- Rabbat, B.G., Daniel, J.I., Weinmann, T.L. and Hanson, N.W., (1986), *Seismic Behavior of Lightweight and Normal Weight Concrete Columns*, Journal of the American Concrete Institute, Vol. 83, No. 1, Feb-86, pp. 69-79.
- Richardt, F.E., Brandtzaeg, A. and Brown, R.L., (1928), *A Study of the Failure of Concrete Under Combined Compressive Stresses*, University of Illinois Engineering Experimental Station, Bulletin No. 185, Jan-28, p. 104.
- Richardt, F.E., Brandtzaeg, A. and Brown, R.L., (1929), *The Failure of Plain and Spirally Reinforced Columns in Compression*, University of Illinois Engineering Experimental Station, Bulletin No. 190, Jan-29, p. 74.
- Roufaiel, M.S.L. and Meyer, C., (1987), *Analytical Modeling of Hysteretic Behavior of R/C Frames*, Journal of Structural Engineering, Vol. 113, No. 3, Mar-87, pp. 429-444.
- Roy, H.E.H. and Sozen, M.A., (1964), *Ductility of Concrete*, Proceedings of the International Symposium on the Flexural Mechanics of Reinforced Concrete, ASCE-ACI, Miami, Nov-64, pp. 213-224.
- Saatcioglu, M. and Razvi, S.R., (1992), *Strength and Ductility of Confined Concrete*, Journal of Structural Engineering, Vol.118, No. 6, Jun-92, pp. 1590-1607.
- Saenz, L.P., (1964), *Equation for the Stress-Strain Curve of Concrete* (Discussion), Journal of the American Concrete Institute, Vol. 61, No. 9, Sep-64, pp.1229-1235.

- Sakai, Y., Otani, S. and Aoyama, H., (1991), *Ductility of Reinforced Concrete Columns Using High-Strength Concrete Under Flexural Compression*, Pacific Conference on Earthquake Engineering, New Zealand, Nov-91, pp. 171-182.
- Sangha, C.M. and Dhir, R.K., (1972), *Strength and Complete Stress-Strain Relationships for Concrete Tested in Uniaxial Compression Under Different Test Conditions*, Materials and Structures, Research and Testing (RILEM Paris), Vol. 5, No. 30, Nov-72, pp. 361-370.
- Scott, B.D., Park, R. and Priestley, M.J.N., (1982), *Stress-Strain Behavior of Concrete Confined by Overlapping Hoops at Low and High Strain Rates*, Journal of the American Concrete Institute, Vol. 79, No.1, Feb-82, pp. 13-27.
- Shah, S.P., Wang, M.L. and Chung, L., (1987), *Model Concrete Beam-Column Joints Subjected to Cyclic Loading at Two Rates*, Materials and Structures / Matériaux et Constructions, Vol. 20, No. 116, Mar-87, pp. 85-95.
- Shah, S.P., Fafitis, A. and Arnold, R., (1983), *Cyclic Loading of Spirally Reinforced Concrete*, Journal of Structural Engineering, Vol. 109, No. 7, Jul-83, pp. 1695-1710.
- Shah, S.P. and Rangan, B.V., (1970), *Effects of Reinforcements on Ductility of Concrete*, Journal of the Structural Division, ASCE, Vol. 96, No. ST6, Jun-70, pp. 1167-1184.
- Shah, S.P. and Chandra, S., (1970), *Fracture of Concrete Subjected to Cyclic and Sustained Loading*, Journal of the American Concrete Institute, Vol. 67, No. 10, Oct-70, pp. 816-825.
- Sheikh, S.A. and Uzumeri, S.M., (1980), *Strength and Ductility of Tied Concrete Columns*, Journal of the Structural Division, ASCE, Vol. 106, No. ST5, May-80, pp. 1079-1102.
- Sheikh, S.A. and Uzumeri, S.M., (1982), *Analytical Model for Concrete Confinement in Tied Columns*, Journal of the Structural Division, ASCE, Vol. 108, No. ST12, Dec-82, pp. 2703-2722.
- Sheikh, S.A., (1982), *A Comparative Study of Confinement Models*, Journal of the American Concrete Institute, Vol. 79, No. 4, Aug-82, pp. 296-306.

- Sheikh, S.A. and Yeh, C.C., (1986), *Flexural Behavior of Confined Concrete Columns*, Journal of the American Concrete Institute, Vol. 83, No. 3, Jun-86, pp. 389-404.
- Sinha, B.P., Gerstle, K.H. and Tulin, L.G., (1964), *Stress-Strain Relations for Concrete under Cyclic Loading*, Journal of the American Concrete Institute, Vol. 61, No. 2, Feb-64, pp. 195-211.
- Smith, R.G. and Orangun, C.O., (1969), *Evaluation of the Stress-Strain Curve of Concrete in Flexure using Method of Least Squares*, Journal of the American Concrete Institute, Vol. 66, No. 7, Jul-69, pp. 553-559.
- Smith, G.M. and Young, L.E., (1955), *Ultimate Theory in Flexure by Exponential Function*, Journal of the American Concrete Institute, Vol. 27, No. 3, Nov-55, pp. 349-359.
- Soliman, M.T.M. and Yu, C.W., (1967), *The Flexural Stress-Strain Relationship of Concrete Confined by Rectangular Transverse Reinforcement*, Magazine of Concrete Research, Vol. 19, No. 61, Dec-67, pp. 223-238.
- Somes, N.F., (1970), *Compression Tests on Hoop-Reinforced Concrete*, Journal of the Structural Division, ASCE, Vol. 96, No. ST7, Jul-70, pp. 1495-1509.
- Soroushian, P. and Obaseki, K., (1986), *Strain Rate-Dependent Interaction Diagrams for Reinforced Concrete Sections*, Journal of the American Concrete Institute, Vol. 83, No. 1, Feb-86, pp. 108-116.
- Soroushian, P., Choi, K.B. and Alhamad, A., (1986), *Dynamic Constitutive Behavior of Concrete*, Journal of the American Concrete Institute, Vol. 83, No. 2, Apr-86, pp. 251-259.
- Spooner, D.C. and Dougill, J.W., (1975), *A Quantitative Assessment of Damage Sustained in Concrete During Compression Loading*. Magazine of Concrete Research, Vol. 27, No. 92, Sep-75, pp. 151-160.
- Sturman, G.M., Shah, S.P. and Winter, G., (1965), *Effects of Flexural Strain Gradients on Microcracking and Stress-Strain Behavior of Concrete*, Journal of the American Concrete Institute, Vol. 62, No. 7, Jul-65, pp. 805-822.

- Sulayfani, A. and Lamirault, J., (1987), *Contribution à l'analyse expérimentale du comportement mécanique cyclique du béton* (in French). Materials and Structures / Matériaux et Constructions, Vol. 20, No. 118, Jul-87, pp. 283-292.
- Tanigawa, Y. and Uchida, Y., (1979), *Hysteretic Characteristics of Concrete in the Domain of High Compressive Strain*, Proceeding, Annual Convention, AIJ, Jan-79, pp. 449-450.
- Thompson, K.J. and Park, R., (1980), *Seismic Response of Partially Prestressed Concrete*, Journal of the Structural Division, ASCE, Vol. 106, No. ST8, Aug-80, pp. 1755-1775.
- Tsai, W.T., (1988), *Uniaxial Compressional Stress-Strain Relation of Concrete*, Journal of Structural Engineering, Vol. 114, No. 9, Sep-88, pp. 2133-2136.
- Tulin, L.G. and Gerstle, K.H., (1964), *Equation for the Stress-Strain Curve of Concrete* (Discussion), Journal of the American Concrete Institute, Vol. 61, No. 9, Sep-64, pp.1236-1238.
- Vallenas, J., Bertero, V.V. and Popov, E.P., (1977), *Concrete Confined by Rectangular Hoops Subjected to Axial Loads*, University of California, Berkeley, Report No. UBC/EERC-77/13, Aug-77.
- Vecchio, F.J. and Collins, M.P., (1986), *The Modified Compression-Field Theory for Reinforced Concrete Elements Subjected to Shear*, Journal of the American Concrete Institute, Vol. 83, No. 2, Apr-86, pp. 219-231.
- Vecchio, F.J., (1989), *Nonlinear Finite Element Analysis of Reinforced Concrete Membranes*, ACI Structural Journal, Vol. 6, No.1, Jan.-Feb 1989, pp. 26-35.
- Vecchio, F.J. and Collins, M.P., (1993), *Compression Response of Cracked Reinforced Concrete*. Journal of Structural Engineering, Vol. 119, No. 12, Dec-93, pp. 3590-3610.
- Wang, P.T., Shah, S.P. and Naaman, A.E., (1978), *High-Strength Concrete in Ultimate Strength Design*, Journal of the Structural Division, ASCE, Vol. 104, No. ST11, Nov-78, pp. 1761-1773.

- Warner, R.F., (1969), *Biaxial Moment Thrust Curvature Relations*. Journal of the Structural Division, ASCE, Vol. 95, No. ST5, May-69, pp. 923-940.
- Wastiels, J., (1980), *Constitutive Model for Short-Time Loading of Concrete* (Discussion), Journal of the Engineering Mechanics Division, ASCE, Vol. 106, No. EM1, Feb-80, pp. 192-193.
- Watstein, D., (1953), *Effect of Straining Rate on the Compressive Strength and Elastic Properties of Concrete*, Journal of the American Concrete Institute, Vol. 27, No. 6, Jun-53, pp. 729-744.
- William, K.J. and Warnke, E.P., (1975), *Constitutive Model for the Triaxial Behavior of Concrete*, International Association for Bridge and Structural Engineering, Proceedings, Vol. 19, Jan-75.
- Yankelevsky, D.Z. and Reinhardt, H.W., (1987a), *Model for Cyclic Compressive Behavior of Concrete*, Journal of Structural Engineering, Vol. 113, No. 2, Feb-87, pp. 228-240.
- Yankelevsky, D.Z. and Reinhardt, H.W., (1987b), *Response of Plain Concrete to Cyclic Tension*, ACI Materials Journal, Vol. 84, No. 5, Oct-87, pp. 365-373.
- Young, L.E., (1960), *Simplifying Ultimate Flexural Theory by Maximizing the Moment of the Stress Block*, Journal of the American Concrete Institute, Vol. 32, No. 5, Nov-60, pp. 549-556.
- Zahn, F.A., Park, R. and Priestley, M.J.N., (1990), *Flexural Strength and Ductility of Circular Hollow Reinforced Concrete Columns without Confinement on Inside Face*, ACI Structural Journal, Vol. 87, No.2, Apr-90, pp. 156-166.

References - Section 4

- Ang, B.G., Priestley, M.J.N. and Paulay, T., (1989), *Seismic Shear Strength of Circular Reinforced Concrete Columns*, ACI Structural Journal, Jan-Feb 1989, pp. 45-59.

- Aycardi, L.E., Mander, J.B. and Reinhorn, A.M., (1992), *Seismic Resistance of Reinforced Concrete Frame Structures Designed Only for Gravity Loads: Part II - Experimental Performance of Subassemblages*, National Center for Earthquake Engineering Research, State University of New York at Buffalo, Dec-1992.
- Belabri, A. and Hsu, T.T.C., (1990), *Stirrup Stresses in Reinforced Concrete Beams*, ACI Structural Journal, Vol. 87, No. 5, Sept-Oct 1990, pp. 530-538.
- Bhide, S.B. and Collins, M.P., (1989), *Influence of Axial Tension on the Shear Capacity of Reinforced Concrete Members*, ACI Journal, Vol. 86, No. 5, Sept-Oct 1989, pp. 570-580.
- Collins, M.P. and Mitchell, D., (1991), *Prestressed Concrete Structures*, Prentice-Hall, New Jersey, 1991.
- Collins, M.P., (1992), *The Response of Reinforced Concrete Elements Subjected to Shear*, Concrete Shear in Earthquake, Edited by T.C.C. Hsu and S.T. Mau, Elsevier Science Publishers Ltd., 1992, pp. 13-23.
- Fafitis, A. and Shah, S.P., (1985), *Predictions of Ultimate Behavior of Confined Columns Subjected to Large Deformations*, ACI Journal, July-August 1985, pp. 423-433.
- Hsu, T.T.C., (1991), *Nonlinear Analysis of Concrete Membrane Elements*, ACI Structural Journal, July-August 1991, pp. 552-561.
- Hsu, T.T.C., (1988), *Softened Truss Model Theory for Shear and Torsion*, ACI Structural Journal, Vol. 85, No. 6, Nov-Dec 1988, pp. 624-635.
- Hsu, T.T.C., Belarbi, A. and Pang, X.B., (1992), *Stress-Strain Relationships for Reinforced Concrete Membrane Elements*, Concrete Shear in Earthquake, Edited by T.C.C. Hsu and S.T. Mau, Elsevier Science Publishers Ltd., 1992, pp. 43-54.
- Hsu, T.T.C., (1993), *Unified Theory of Reinforced Concrete*, CRC Press, Boca Raton, 1993.
- Ichinose, T., (1992), *A Shear Design Equation for Ductile R/C Members*, Earthquake Engineering and Structural Dynamics, Vol. 21, 1992, pp. 197-214.

- Kani, G.H.J., (1969), *A Rational Theory for the Function of Web Reinforcement*, ACI Journal, March-1969, pp. 185-197.
- Mander, J.B., Priestley, M.J.N. and Park, R., (1984), *Seismic Design of Bridge Piers*, Department of Civil Engineering, University of Canterbury, Report 84-2, Feb-84, 483 pp.
- Mander, J.B., Waheed, S.M., Chaudary, M.T.A. and Chen, S.S., (1993), *Seismic Performance of Shear-Critical Reinforced Concrete Bridge Piers*, April 1993, Technical Report NCEER-93-0010.
- Marti, P. and Meyboom, J., (1992), *Response of Prestressed Concrete Elements to In-Plane Shear Forces*, ACI Structural Journal, Sept-Oct 1992, pp. 503-514.
- Ozcebe, G. and Saatcioglu, M., (1989), *Hysteretic Shear Model for Reinforced Concrete Members*, Journal of Structural Engineering, Vol. 115, No. 1, Jan 1989, pp. 132-149.
- Park, R. and Paulay, T., (1975), *Reinforced Concrete Structures*, John Wiley, New York, 1975.
- Press, W.H., Flannery, B.P., Teukolsky, S.A. and Vetterling, W.T., (1989), *Numerical Recipes: The Art of Scientific Computing (FORTRAN Version)*, Cambridge University Press, Cambridge, 1989, 702 pp.
- Roufaiel, M.S.L. and Meyer, C., (1987), *Analytical Modeling of Hysteretic Behavior of R/C Frames*, Journal of Structural Engineering, Vol. 113, No. 3, ASCE, March-1987, pp.429-444.
- Vecchio, F.J. and Collins, M.P., (1986), *The Modified Compression-Field Theory of Reinforced Concrete Elements Subjected to Shear*, ACI Structural Journal, March-April 1986, pp. 219-231.
- Vecchio, F.J., (1989), *Nonlinear Finite Element Analysis of Reinforced Concrete Membranes*, ACI Structural Journal, January-February 1989, pp. 26-35.
- Vecchio, F.J. and Emara, M.B., (1992), *Shear Deformations in Reinforced Concrete Frames*, ACI Structural Journal, Vol. 89, No. 1, Jan-Feb 1992, pp. 45-56.

Zahn, F.A. Park, R. and Priestley, M.J.N., (1990), *Flexural Strength and Ductility of Circular Hollow Reinforced Concrete Columns without Confinement on Inside Face*, ACI Structural Journal, Vol. 87, No.2 March-April 1990, pp.156-166.

**NATIONAL CENTER FOR EARTHQUAKE ENGINEERING RESEARCH
LIST OF TECHNICAL REPORTS**

The National Center for Earthquake Engineering Research (NCEER) publishes technical reports on a variety of subjects related to earthquake engineering written by authors funded through NCEER. These reports are available from both NCEER's Publications Department and the National Technical Information Service (NTIS). Requests for reports should be directed to the Publications Department, National Center for Earthquake Engineering Research, State University of New York at Buffalo, Red Jacket Quadrangle, Buffalo, New York 14261. Reports can also be requested through NTIS, 5285 Port Royal Road, Springfield, Virginia 22161. NTIS accession numbers are shown in parenthesis, if available.

- NCEER-87-0001 "First-Year Program in Research, Education and Technology Transfer," 3/5/87, (PB88-134275).
- NCEER-87-0002 "Experimental Evaluation of Instantaneous Optimal Algorithms for Structural Control," by R.C. Lin, T.T. Soong and A.M. Reinhorn, 4/20/87, (PB88-134341).
- NCEER-87-0003 "Experimentation Using the Earthquake Simulation Facilities at University at Buffalo," by A.M. Reinhorn and R.L. Ketter, to be published.
- NCEER-87-0004 "The System Characteristics and Performance of a Shaking Table," by J.S. Hwang, K.C. Chang and G.C. Lee, 6/1/87, (PB88-134259). This report is available only through NTIS (see address given above).
- NCEER-87-0005 "A Finite Element Formulation for Nonlinear Viscoplastic Material Using a Q Model," by O. Gyebi and G. Dasgupta, 11/2/87, (PB88-213764).
- NCEER-87-0006 "Symbolic Manipulation Program (SMP) - Algebraic Codes for Two and Three Dimensional Finite Element Formulations," by X. Lee and G. Dasgupta, 11/9/87, (PB88-218522).
- NCEER-87-0007 "Instantaneous Optimal Control Laws for Tall Buildings Under Seismic Excitations," by J.N. Yang, A. Akbarpour and P. Ghaemmaghami, 6/10/87, (PB88-134333). This report is only available through NTIS (see address given above).
- NCEER-87-0008 "IDARC: Inelastic Damage Analysis of Reinforced Concrete Frame - Shear-Wall Structures," by Y.J. Park, A.M. Reinhorn and S.K. Kunnath, 7/20/87, (PB88-134325).
- NCEER-87-0009 "Liquefaction Potential for New York State: A Preliminary Report on Sites in Manhattan and Buffalo," by M. Budhu, V. Vijayakumar, R.F. Giese and L. Baumgras, 8/31/87, (PB88-163704). This report is available only through NTIS (see address given above).
- NCEER-87-0010 "Vertical and Torsional Vibration of Foundations in Inhomogeneous Media," by A.S. Veletsos and K.W. Dotson, 6/1/87, (PB88-134291).
- NCEER-87-0011 "Seismic Probabilistic Risk Assessment and Seismic Margins Studies for Nuclear Power Plants," by Howard H.M. Hwang, 6/15/87, (PB88-134267).
- NCEER-87-0012 "Parametric Studies of Frequency Response of Secondary Systems Under Ground-Acceleration Excitations," by Y. Yong and Y.K. Lin, 6/10/87, (PB88-134309).
- NCEER-87-0013 "Frequency Response of Secondary Systems Under Seismic Excitation," by J.A. HoLung, J. Cai and Y.K. Lin, 7/31/87, (PB88-134317).
- NCEER-87-0014 "Modelling Earthquake Ground Motions in Seismically Active Regions Using Parametric Time Series Methods," by G.W. Ellis and A.S. Cakmak, 8/25/87, (PB88-134283).
- NCEER-87-0015 "Detection and Assessment of Seismic Structural Damage," by E. DiPasquale and A.S. Cakmak, 8/25/87, (PB88-163712).

- NCEER-87-0016 "Pipeline Experiment at Parkfield, California," by J. Isenberg and E. Richardson, 9/15/87, (PB88-163720). This report is available only through NTIS (see address given above).
- NCEER-87-0017 "Digital Simulation of Seismic Ground Motion," by M. Shinozuka, G. Deodatis and T. Harada, 8/31/87, (PB88-155197). This report is available only through NTIS (see address given above).
- NCEER-87-0018 "Practical Considerations for Structural Control: System Uncertainty, System Time Delay and Truncation of Small Control Forces," J.N. Yang and A. Akbarpour, 8/10/87, (PB88-163738).
- NCEER-87-0019 "Modal Analysis of Nonclassically Damped Structural Systems Using Canonical Transformation," by J.N. Yang, S. Sarkani and F.X. Long, 9/27/87, (PB88-187851).
- NCEER-87-0020 "A Nonstationary Solution in Random Vibration Theory," by J.R. Red-Horse and P.D. Spanos, 11/3/87, (PB88-163746).
- NCEER-87-0021 "Horizontal Impedances for Radially Inhomogeneous Viscoelastic Soil Layers," by A.S. Veletsos and K.W. Dotson, 10/15/87, (PB88-150859).
- NCEER-87-0022 "Seismic Damage Assessment of Reinforced Concrete Members," by Y.S. Chung, C. Meyer and M. Shinozuka, 10/9/87, (PB88-150867). This report is available only through NTIS (see address given above).
- NCEER-87-0023 "Active Structural Control in Civil Engineering," by T.T. Soong, 11/11/87, (PB88-187778).
- NCEER-87-0024 "Vertical and Torsional Impedances for Radially Inhomogeneous Viscoelastic Soil Layers," by K.W. Dotson and A.S. Veletsos, 12/87, (PB88-187786).
- NCEER-87-0025 "Proceedings from the Symposium on Seismic Hazards, Ground Motions, Soil-Liquefaction and Engineering Practice in Eastern North America," October 20-22, 1987, edited by K.H. Jacob, 12/87, (PB88-188115).
- NCEER-87-0026 "Report on the Whittier-Narrows, California, Earthquake of October 1, 1987," by J. Pantelic and A. Reinhorn, 11/87, (PB88-187752). This report is available only through NTIS (see address given above).
- NCEER-87-0027 "Design of a Modular Program for Transient Nonlinear Analysis of Large 3-D Building Structures," by S. Srivastav and J.F. Abel, 12/30/87, (PB88-187950).
- NCEER-87-0028 "Second-Year Program in Research, Education and Technology Transfer," 3/8/88, (PB88-219480).
- NCEER-88-0001 "Workshop on Seismic Computer Analysis and Design of Buildings With Interactive Graphics," by W. McGuire, J.F. Abel and C.H. Conley, 1/18/88, (PB88-187760).
- NCEER-88-0002 "Optimal Control of Nonlinear Flexible Structures," by J.N. Yang, F.X. Long and D. Wong, 1/22/88, (PB88-213772).
- NCEER-88-0003 "Substructuring Techniques in the Time Domain for Primary-Secondary Structural Systems," by G.D. Manolis and G. Juhn, 2/10/88, (PB88-213780).
- NCEER-88-0004 "Iterative Seismic Analysis of Primary-Secondary Systems," by A. Singhal, L.D. Lutes and P.D. Spanos, 2/23/88, (PB88-213798).
- NCEER-88-0005 "Stochastic Finite Element Expansion for Random Media," by P.D. Spanos and R. Ghanem, 3/14/88, (PB88-213806).

- NCEER-88-0006 "Combining Structural Optimization and Structural Control," by F.Y. Cheng and C.P. Pantelides, 1/10/88, (PB88-213814).
- NCEER-88-0007 "Seismic Performance Assessment of Code-Designed Structures," by H.H-M. Hwang, J-W. Jaw and H-J. Shau, 3/20/88, (PB88-219423).
- NCEER-88-0008 "Reliability Analysis of Code-Designed Structures Under Natural Hazards," by H.H-M. Hwang, H. Ushiba and M. Shinozuka, 2/29/88, (PB88-229471).
- NCEER-88-0009 "Seismic Fragility Analysis of Shear Wall Structures," by J-W Jaw and H.H-M. Hwang, 4/30/88, (PB89-102867).
- NCEER-88-0010 "Base Isolation of a Multi-Story Building Under a Harmonic Ground Motion - A Comparison of Performances of Various Systems," by F-G Fan, G. Ahmadi and I.G. Tadjbakhsh, 5/18/88, (PB89-122238).
- NCEER-88-0011 "Seismic Floor Response Spectra for a Combined System by Green's Functions," by F.M. Lavelle, L.A. Bergman and P.D. Spanos, 5/1/88, (PB89-102875).
- NCEER-88-0012 "A New Solution Technique for Randomly Excited Hysteretic Structures," by G.Q. Cai and Y.K. Lin, 5/16/88, (PB89-102883).
- NCEER-88-0013 "A Study of Radiation Damping and Soil-Structure Interaction Effects in the Centrifuge," by K. Weissman, supervised by J.H. Prevost, 5/24/88, (PB89-144703).
- NCEER-88-0014 "Parameter Identification and Implementation of a Kinematic Plasticity Model for Frictional Soils," by J.H. Prevost and D.V. Griffiths, to be published.
- NCEER-88-0015 "Two- and Three- Dimensional Dynamic Finite Element Analyses of the Long Valley Dam," by D.V. Griffiths and J.H. Prevost, 6/17/88, (PB89-144711).
- NCEER-88-0016 "Damage Assessment of Reinforced Concrete Structures in Eastern United States," by A.M. Reinhorn, M.J. Seidel, S.K. Kunnath and Y.J. Park, 6/15/88, (PB89-122220).
- NCEER-88-0017 "Dynamic Compliance of Vertically Loaded Strip Foundations in Multilayered Viscoelastic Soils," by S. Ahmad and A.S.M. Israil, 6/17/88, (PB89-102891).
- NCEER-88-0018 "An Experimental Study of Seismic Structural Response With Added Viscoelastic Dampers," by R.C. Lin, Z. Liang, T.T. Soong and R.H. Zhang, 6/30/88, (PB89-122212). This report is available only through NTIS (see address given above).
- NCEER-88-0019 "Experimental Investigation of Primary - Secondary System Interaction," by G.D. Manolis, G. Juhn and A.M. Reinhorn, 5/27/88, (PB89-122204).
- NCEER-88-0020 "A Response Spectrum Approach For Analysis of Nonclassically Damped Structures," by J.N. Yang, S. Sarkani and F.X. Long, 4/22/88, (PB89-102909).
- NCEER-88-0021 "Seismic Interaction of Structures and Soils: Stochastic Approach," by A.S. Veletsos and A.M. Prasad, 7/21/88, (PB89-122196).
- NCEER-88-0022 "Identification of the Serviceability Limit State and Detection of Seismic Structural Damage," by E. DiPasquale and A.S. Cakmak, 6/15/88, (PB89-122188). This report is available only through NTIS (see address given above).
- NCEER-88-0023 "Multi-Hazard Risk Analysis: Case of a Simple Offshore Structure," by B.K. Bhartia and E.H. Vanmarcke, 7/21/88, (PB89-145213).

- NCEER-88-0024 "Automated Seismic Design of Reinforced Concrete Buildings," by Y.S. Chung, C. Meyer and M. Shinozuka, 7/5/88, (PB89-122170). This report is available only through NTIS (see address given above).
- NCEER-88-0025 "Experimental Study of Active Control of MDOF Structures Under Seismic Excitations," by L.L. Chung, R.C. Lin, T.T. Soong and A.M. Reinhorn, 7/10/88, (PB89-122600).
- NCEER-88-0026 "Earthquake Simulation Tests of a Low-Rise Metal Structure," by J.S. Hwang, K.C. Chang, G.C. Lee and R.L. Ketter, 8/1/88, (PB89-102917).
- NCEER-88-0027 "Systems Study of Urban Response and Reconstruction Due to Catastrophic Earthquakes," by F. Kozin and H.K. Zhou, 9/22/88, (PB90-162348).
- NCEER-88-0028 "Seismic Fragility Analysis of Plane Frame Structures," by H.H.-M. Hwang and Y.K. Low, 7/31/88, (PB89-131445).
- NCEER-88-0029 "Response Analysis of Stochastic Structures," by A. Karama, C. Bucher and M. Shinozuka, 9/22/88, (PB89-174429).
- NCEER-88-0030 "Nonnormal Accelerations Due to Yielding in a Primary Structure," by D.C.K. Chen and L.D. Lutes, 9/19/88, (PB89-131437).
- NCEER-88-0031 "Design Approaches for Soil-Structure Interaction," by A.S. Veletsos, A.M. Prasad and Y. Tang, 12/30/88, (PB89-174437). This report is available only through NTIS (see address given above).
- NCEER-88-0032 "A Re-evaluation of Design Spectra for Seismic Damage Control," by C.J. Turkstra and A.G. Tallin, 11/7/88, (PB89-145221).
- NCEER-88-0033 "The Behavior and Design of Noncontact Lap Splices Subjected to Repeated Inelastic Tensile Loading," by V.E. Sagan, P. Gergely and R.N. White, 12/8/88, (PB89-163737).
- NCEER-88-0034 "Seismic Response of Pile Foundations," by S.M. Mamoon, P.K. Banerjee and S. Ahmad, 11/1/88, (PB89-145239).
- NCEER-88-0035 "Modeling of R/C Building Structures With Flexible Floor Diaphragms (IDARC2)," by A.M. Reinhorn, S.K. Kunnath and N. Panahshahi, 9/7/88, (PB89-207153).
- NCEER-88-0036 "Solution of the Dam-Reservoir Interaction Problem Using a Combination of FEM, BEM with Particular Integrals, Modal Analysis, and Substructuring," by C-S. Tsai, G.C. Lee and R.L. Ketter, 12/31/88, (PB89-207146).
- NCEER-88-0037 "Optimal Placement of Actuators for Structural Control," by F.Y. Cheng and C.P. Pantelides, 8/15/88, (PB89-162846).
- NCEER-88-0038 "Teflon Bearings in Aseismic Base Isolation: Experimental Studies and Mathematical Modeling," by A. Mokha, M.C. Constantinou and A.M. Reinhorn, 12/5/88, (PB89-218457). This report is available only through NTIS (see address given above).
- NCEER-88-0039 "Seismic Behavior of Flat Slab High-Rise Buildings in the New York City Area," by P. Weidlinger and M. Ettouney, 10/15/88, (PB90-145681).
- NCEER-88-0040 "Evaluation of the Earthquake Resistance of Existing Buildings in New York City," by P. Weidlinger and M. Ettouney, 10/15/88, to be published.
- NCEER-88-0041 "Small-Scale Modeling Techniques for Reinforced Concrete Structures Subjected to Seismic Loads," by W. Kim, A. El-Attar and R.N. White, 11/22/88, (PB89-189625).

- NCEER-88-0042 "Modeling Strong Ground Motion from Multiple Event Earthquakes," by G.W. Ellis and A.S. Cakmak, 10/15/88, (PB89-174445).
- NCEER-88-0043 "Nonstationary Models of Seismic Ground Acceleration," by M. Grigoriu, S.E. Ruiz and E. Rosenblueth, 7/15/88, (PB89-189617).
- NCEER-88-0044 "SARCF User's Guide: Seismic Analysis of Reinforced Concrete Frames," by Y.S. Chung, C. Meyer and M. Shinozuka, 11/9/88, (PB89-174452).
- NCEER-88-0045 "First Expert Panel Meeting on Disaster Research and Planning," edited by J. Pantelic and J. Stoye, 9/15/88, (PB89-174460).
- NCEER-88-0046 "Preliminary Studies of the Effect of Degrading Infill Walls on the Nonlinear Seismic Response of Steel Frames," by C.Z. Chrysostomou, P. Gergely and J.F. Abel, 12/19/88, (PB89-208383).
- NCEER-88-0047 "Reinforced Concrete Frame Component Testing Facility - Design, Construction, Instrumentation and Operation," by S.P. Pessiki, C. Conley, T. Bond, P. Gergely and R.N. White, 12/16/88, (PB89-174478).
- NCEER-89-0001 "Effects of Protective Cushion and Soil Compliancy on the Response of Equipment Within a Seismically Excited Building," by J.A. HoLung, 2/16/89, (PB89-207179).
- NCEER-89-0002 "Statistical Evaluation of Response Modification Factors for Reinforced Concrete Structures," by H.H-M. Hwang and J-W. Jaw, 2/17/89, (PB89-207187).
- NCEER-89-0003 "Hysteretic Columns Under Random Excitation," by G-Q. Cai and Y.K. Lin, 1/9/89, (PB89-196513).
- NCEER-89-0004 "Experimental Study of 'Elephant Foot Bulge' Instability of Thin-Walled Metal Tanks," by Z-H. Jia and R.L. Ketter, 2/22/89, (PB89-207195).
- NCEER-89-0005 "Experiment on Performance of Buried Pipelines Across San Andreas Fault," by J. Isenberg, E. Richardson and T.D. O'Rourke, 3/10/89, (PB89-218440). This report is available only through NTIS (see address given above).
- NCEER-89-0006 "A Knowledge-Based Approach to Structural Design of Earthquake-Resistant Buildings," by M. Subramani, P. Gergely, C.H. Conley, J.F. Abel and A.H. Zaghaw, 1/15/89, (PB89-218465).
- NCEER-89-0007 "Liquefaction Hazards and Their Effects on Buried Pipelines," by T.D. O'Rourke and P.A. Lane, 2/1/89, (PB89-218481).
- NCEER-89-0008 "Fundamentals of System Identification in Structural Dynamics," by H. Imai, C-B. Yun, O. Maruyama and M. Shinozuka, 1/26/89, (PB89-207211).
- NCEER-89-0009 "Effects of the 1985 Michoacan Earthquake on Water Systems and Other Buried Lifelines in Mexico," by A.G. Ayala and M.J. O'Rourke, 3/8/89, (PB89-207229).
- NCEER-89-R010 "NCEER Bibliography of Earthquake Education Materials," by K.E.K. Ross, Second Revision, 9/1/89, (PB90-125352).
- NCEER-89-0011 "Inelastic Three-Dimensional Response Analysis of Reinforced Concrete Building Structures (IDARC-3D), Part I - Modeling," by S.K. Kunnath and A.M. Reinhorn, 4/17/89, (PB90-114612).
- NCEER-89-0012 "Recommended Modifications to ATC-14," by C.D. Poland and J.O. Malley, 4/12/89, (PB90-108648).

- NCEER-89-0013 "Repair and Strengthening of Beam-to-Column Connections Subjected to Earthquake Loading," by M. Corazao and A.J. Durrani, 2/28/89, (PB90-109885).
- NCEER-89-0014 "Program EXKAL2 for Identification of Structural Dynamic Systems," by O. Maruyama, C-B. Yun, M. Hoshiya and M. Shinozuka, 5/19/89, (PB90-109877).
- NCEER-89-0015 "Response of Frames With Bolted Semi-Rigid Connections, Part I - Experimental Study and Analytical Predictions," by P.J. DiCorso, A.M. Reinhorn, J.R. Dickerson, J.B. Radzinski and W.L. Harper, 6/1/89, to be published.
- NCEER-89-0016 "ARMA Monte Carlo Simulation in Probabilistic Structural Analysis," by P.D. Spanos and M.P. Mignolet, 7/10/89, (PB90-109893).
- NCEER-89-P017 "Preliminary Proceedings from the Conference on Disaster Preparedness - The Place of Earthquake Education in Our Schools," Edited by K.E.K. Ross, 6/23/89, (PB90-108606).
- NCEER-89-0017 "Proceedings from the Conference on Disaster Preparedness - The Place of Earthquake Education in Our Schools," Edited by K.E.K. Ross, 12/31/89, (PB90-207895). This report is available only through NTIS (see address given above).
- NCEER-89-0018 "Multidimensional Models of Hysteretic Material Behavior for Vibration Analysis of Shape Memory Energy Absorbing Devices, by E.J. Graesser and F.A. Cozzarelli, 6/7/89, (PB90-164146).
- NCEER-89-0019 "Nonlinear Dynamic Analysis of Three-Dimensional Base Isolated Structures (3D-BASIS)," by S. Nagarajaiah, A.M. Reinhorn and M.C. Constantinou, 8/3/89, (PB90-161936). This report is available only through NTIS (see address given above).
- NCEER-89-0020 "Structural Control Considering Time-Rate of Control Forces and Control Rate Constraints," by F.Y. Cheng and C.P. Pantelides, 8/3/89, (PB90-120445).
- NCEER-89-0021 "Subsurface Conditions of Memphis and Shelby County," by K.W. Ng, T-S. Chang and H-H.M. Hwang, 7/26/89, (PB90-120437).
- NCEER-89-0022 "Seismic Wave Propagation Effects on Straight Jointed Buried Pipelines," by K. Elhadi and M.J. O'Rourke, 8/24/89, (PB90-162322).
- NCEER-89-0023 "Workshop on Serviceability Analysis of Water Delivery Systems," edited by M. Grigoriu, 3/6/89, (PB90-127424).
- NCEER-89-0024 "Shaking Table Study of a 1/5 Scale Steel Frame Composed of Tapered Members," by K.C. Chang, J.S. Hwang and G.C. Lee, 9/18/89, (PB90-160169).
- NCEER-89-0025 "DYNA1D: A Computer Program for Nonlinear Seismic Site Response Analysis - Technical Documentation," by Jean H. Prevost, 9/14/89, (PB90-161944). This report is available only through NTIS (see address given above).
- NCEER-89-0026 "1:4 Scale Model Studies of Active Tendon Systems and Active Mass Dampers for Aseismic Protection," by A.M. Reinhorn, T.T. Soong, R.C. Lin, Y.P. Yang, Y. Fukao, H. Abe and M. Nakai, 9/15/89, (PB90-173246).
- NCEER-89-0027 "Scattering of Waves by Inclusions in a Nonhomogeneous Elastic Half Space Solved by Boundary Element Methods," by P.K. Hadley, A. Askar and A.S. Cakmak, 6/15/89, (PB90-145699).
- NCEER-89-0028 "Statistical Evaluation of Deflection Amplification Factors for Reinforced Concrete Structures," by H.H.M. Hwang, J-W. Jaw and A.L. Ch'ng, 8/31/89, (PB90-164633).

- NCEER-89-0029 "Bedrock Accelerations in Memphis Area Due to Large New Madrid Earthquakes," by H.H.M. Hwang, C.H.S. Chen and G. Yu, 11/7/89, (PB90-162330).
- NCEER-89-0030 "Seismic Behavior and Response Sensitivity of Secondary Structural Systems," by Y.Q. Chen and T.T. Soong, 10/23/89, (PB90-164658).
- NCEER-89-0031 "Random Vibration and Reliability Analysis of Primary-Secondary Structural Systems," by Y. Ibrahim, M. Grigoriu and T.T. Soong, 11/10/89, (PB90-161951).
- NCEER-89-0032 "Proceedings from the Second U.S. - Japan Workshop on Liquefaction, Large Ground Deformation and Their Effects on Lifelines, September 26-29, 1989," Edited by T.D. O'Rourke and M. Hamada, 12/1/89, (PB90-209388).
- NCEER-89-0033 "Deterministic Model for Seismic Damage Evaluation of Reinforced Concrete Structures," by J.M. Bracci, A.M. Reinhorn, J.B. Mander and S.K. Kunnath, 9/27/89.
- NCEER-89-0034 "On the Relation Between Local and Global Damage Indices," by E. DiPasquale and A.S. Cakmak, 8/15/89, (PB90-173865).
- NCEER-89-0035 "Cyclic Undrained Behavior of Nonplastic and Low Plasticity Silts," by A.J. Walker and H.E. Stewart, 7/26/89, (PB90-183518).
- NCEER-89-0036 "Liquefaction Potential of Surficial Deposits in the City of Buffalo, New York," by M. Budhu, R. Giese and L. Baumgrass, 1/17/89, (PB90-208455).
- NCEER-89-0037 "A Deterministic Assessment of Effects of Ground Motion Incoherence," by A.S. Veletsos and Y. Tang, 7/15/89, (PB90-164294).
- NCEER-89-0038 "Workshop on Ground Motion Parameters for Seismic Hazard Mapping," July 17-18, 1989, edited by R.V. Whitman, 12/1/89, (PB90-173923).
- NCEER-89-0039 "Seismic Effects on Elevated Transit Lines of the New York City Transit Authority," by C.J. Costantino, C.A. Miller and E. Heymsfield, 12/26/89, (PB90-207887).
- NCEER-89-0040 "Centrifugal Modeling of Dynamic Soil-Structure Interaction," by K. Weissman, Supervised by J.H. Prevost, 5/10/89, (PB90-207879).
- NCEER-89-0041 "Linearized Identification of Buildings With Cores for Seismic Vulnerability Assessment," by I-K. Ho and A.E. Aktan, 11/1/89, (PB90-251943).
- NCEER-90-0001 "Geotechnical and Lifeline Aspects of the October 17, 1989 Loma Prieta Earthquake in San Francisco," by T.D. O'Rourke, H.E. Stewart, F.T. Blackburn and T.S. Dickerman, 1/90, (PB90-208596).
- NCEER-90-0002 "Nonnormal Secondary Response Due to Yielding in a Primary Structure," by D.C.K. Chen and L.D. Lutes, 2/28/90, (PB90-251976).
- NCEER-90-0003 "Earthquake Education Materials for Grades K-12," by K.E.K. Ross, 4/16/90, (PB91-251984).
- NCEER-90-0004 "Catalog of Strong Motion Stations in Eastern North America," by R.W. Busby, 4/3/90, (PB90-251984).
- NCEER-90-0005 "NCEER Strong-Motion Data Base: A User Manual for the GeoBase Release (Version 1.0 for the Sun3)," by P. Friberg and K. Jacob, 3/31/90 (PB90-258062).
- NCEER-90-0006 "Seismic Hazard Along a Crude Oil Pipeline in the Event of an 1811-1812 Type New Madrid Earthquake," by H.H.M. Hwang and C-H.S. Chen, 4/16/90(PB90-258054).

- NCEER-90-0007 "Site-Specific Response Spectra for Memphis Sheahan Pumping Station," by H.H.M. Hwang and C.S. Lee, 5/15/90, (PB91-108811).
- NCEER-90-0008 "Pilot Study on Seismic Vulnerability of Crude Oil Transmission Systems," by T. Ariman, R. Dobry, M. Grigoriu, F. Kozin, M. O'Rourke, T. O'Rourke and M. Shinozuka, 5/25/90, (PB91-108837).
- NCEER-90-0009 "A Program to Generate Site Dependent Time Histories: EQGEN," by G.W. Ellis, M. Srinivasan and A.S. Cakmak, 1/30/90, (PB91-108829).
- NCEER-90-0010 "Active Isolation for Seismic Protection of Operating Rooms," by M.E. Talbott, Supervised by M. Shinozuka, 6/8/9, (PB91-110205).
- NCEER-90-0011 "Program LINEARID for Identification of Linear Structural Dynamic Systems," by C-B. Yun and M. Shinozuka, 6/25/90, (PB91-110312).
- NCEER-90-0012 "Two-Dimensional Two-Phase Elasto-Plastic Seismic Response of Earth Dams," by A.N. Yiagos, Supervised by J.H. Prevost, 6/20/90, (PB91-110197).
- NCEER-90-0013 "Secondary Systems in Base-Isolated Structures: Experimental Investigation, Stochastic Response and Stochastic Sensitivity," by G.D. Manolis, G. Juhn, M.C. Constantinou and A.M. Reinhorn, 7/1/90, (PB91-110320).
- NCEER-90-0014 "Seismic Behavior of Lightly-Reinforced Concrete Column and Beam-Column Joint Details," by S.P. Pessiki, C.H. Conley, P. Gergely and R.N. White, 8/22/90, (PB91-108795).
- NCEER-90-0015 "Two Hybrid Control Systems for Building Structures Under Strong Earthquakes," by J.N. Yang and A. Danielians, 6/29/90, (PB91-125393).
- NCEER-90-0016 "Instantaneous Optimal Control with Acceleration and Velocity Feedback," by J.N. Yang and Z. Li, 6/29/90, (PB91-125401).
- NCEER-90-0017 "Reconnaissance Report on the Northern Iran Earthquake of June 21, 1990," by M. Mehraein, 10/4/90, (PB91-125377).
- NCEER-90-0018 "Evaluation of Liquefaction Potential in Memphis and Shelby County," by T.S. Chang, P.S. Tang, C.S. Lee and H. Hwang, 8/10/90, (PB91-125427).
- NCEER-90-0019 "Experimental and Analytical Study of a Combined Sliding Disc Bearing and Helical Steel Spring Isolation System," by M.C. Constantinou, A.S. Mokha and A.M. Reinhorn, 10/4/90, (PB91-125385).
- NCEER-90-0020 "Experimental Study and Analytical Prediction of Earthquake Response of a Sliding Isolation System with a Spherical Surface," by A.S. Mokha, M.C. Constantinou and A.M. Reinhorn, 10/11/90, (PB91-125419).
- NCEER-90-0021 "Dynamic Interaction Factors for Floating Pile Groups," by G. Gazetas, K. Fan, A. Kaynia and E. Kausel, 9/10/90, (PB91-170381).
- NCEER-90-0022 "Evaluation of Seismic Damage Indices for Reinforced Concrete Structures," by S. Rodriguez-Gomez and A.S. Cakmak, 9/30/90, PB91-171322).
- NCEER-90-0023 "Study of Site Response at a Selected Memphis Site," by H. Desai, S. Ahmad, E.S. Gazetas and M.R. Oh, 10/11/90, (PB91-196857).
- NCEER-90-0024 "A User's Guide to Strongmo: Version 1.0 of NCEER's Strong-Motion Data Access Tool for PCs and Terminals," by P.A. Friberg and C.A.T. Susch, 11/15/90, (PB91-171272).

- NCEER-90-0025 "A Three-Dimensional Analytical Study of Spatial Variability of Seismic Ground Motions," by L-L. Hong and A.H.-S. Ang, 10/30/90, (PB91-170399).
- NCEER-90-0026 "MUMOID User's Guide - A Program for the Identification of Modal Parameters," by S. Rodriguez-Gomez and E. DiPasquale, 9/30/90, (PB91-171298).
- NCEER-90-0027 "SARCF-II User's Guide - Seismic Analysis of Reinforced Concrete Frames," by S. Rodriguez-Gomez, Y.S. Chung and C. Meyer, 9/30/90, (PB91-171280).
- NCEER-90-0028 "Viscous Dampers: Testing, Modeling and Application in Vibration and Seismic Isolation," by N. Makris and M.C. Constantinou, 12/20/90 (PB91-190561).
- NCEER-90-0029 "Soil Effects on Earthquake Ground Motions in the Memphis Area," by H. Hwang, C.S. Lee, K.W. Ng and T.S. Chang, 8/2/90, (PB91-190751).
- NCEER-91-0001 "Proceedings from the Third Japan-U.S. Workshop on Earthquake Resistant Design of Lifeline Facilities and Countermeasures for Soil Liquefaction, December 17-19, 1990," edited by T.D. O'Rourke and M. Hamada, 2/1/91, (PB91-179259).
- NCEER-91-0002 "Physical Space Solutions of Non-Proportionally Damped Systems," by M. Tong, Z. Liang and G.C. Lee, 1/15/91, (PB91-179242).
- NCEER-91-0003 "Seismic Response of Single Piles and Pile Groups," by K. Fan and G. Gazetas, 1/10/91, (PB92-174994).
- NCEER-91-0004 "Damping of Structures: Part 1 - Theory of Complex Damping," by Z. Liang and G. Lee, 10/10/91, (PB92-197235).
- NCEER-91-0005 "3D-BASIS - Nonlinear Dynamic Analysis of Three Dimensional Base Isolated Structures: Part II," by S. Nagarajaiah, A.M. Reinhorn and M.C. Constantinou, 2/28/91, (PB91-190553).
- NCEER-91-0006 "A Multidimensional Hysteretic Model for Plasticity Deforming Metals in Energy Absorbing Devices," by E.J. Graesser and F.A. Cozzarelli, 4/9/91, (PB92-108364).
- NCEER-91-0007 "A Framework for Customizable Knowledge-Based Expert Systems with an Application to a KBES for Evaluating the Seismic Resistance of Existing Buildings," by E.G. Ibarra-Anaya and S.J. Fenves, 4/9/91, (PB91-210930).
- NCEER-91-0008 "Nonlinear Analysis of Steel Frames with Semi-Rigid Connections Using the Capacity Spectrum Method," by G.G. Deierlein, S-H. Hsieh, Y-J. Shen and J.F. Abel, 7/2/91, (PB92-113828).
- NCEER-91-0009 "Earthquake Education Materials for Grades K-12," by K.E.K. Ross, 4/30/91, (PB91-212142).
- NCEER-91-0010 "Phase Wave Velocities and Displacement Phase Differences in a Harmonically Oscillating Pile," by N. Makris and G. Gazetas, 7/8/91, (PB92-108356).
- NCEER-91-0011 "Dynamic Characteristics of a Full-Size Five-Story Steel Structure and a 2/5 Scale Model," by K.C. Chang, G.C. Yao, G.C. Lee, D.S. Hao and Y.C. Yeh, 7/2/91, (PB93-116648).
- NCEER-91-0012 "Seismic Response of a 2/5 Scale Steel Structure with Added Viscoelastic Dampers," by K.C. Chang, T.T. Soong, S-T. Oh and M.L. Lai, 5/17/91, (PB92-110816).
- NCEER-91-0013 "Earthquake Response of Retaining Walls; Full-Scale Testing and Computational Modeling," by S. Alampalli and A-W.M. Elgarnal, 6/20/91, to be published.

- NCEER-91-0014 "3D-BASIS-M: Nonlinear Dynamic Analysis of Multiple Building Base Isolated Structures," by P.C. Tsopelas, S. Nagarajaiah, M.C. Constantinou and A.M. Reinhorn, 5/28/91, (PB92-113885).
- NCEER-91-0015 "Evaluation of SEAOC Design Requirements for Sliding Isolated Structures," by D. Theodossiou and M.C. Constantinou, 6/10/91, (PB92-114602).
- NCEER-91-0016 "Closed-Loop Modal Testing of a 27-Story Reinforced Concrete Flat Plate-Core Building," by H.R. Somprasad, T. Toksoy, H. Yoshiyuki and A.E. Aktan, 7/15/91, (PB92-129980).
- NCEER-91-0017 "Shake Table Test of a 1/6 Scale Two-Story Lightly Reinforced Concrete Building," by A.G. El-Attar, R.N. White and P. Gergely, 2/28/91, (PB92-222447).
- NCEER-91-0018 "Shake Table Test of a 1/8 Scale Three-Story Lightly Reinforced Concrete Building," by A.G. El-Attar, R.N. White and P. Gergely, 2/28/91, (PB93-116630).
- NCEER-91-0019 "Transfer Functions for Rigid Rectangular Foundations," by A.S. Veletsos, A.M. Prasad and W.H. Wu, 7/31/91.
- NCEER-91-0020 "Hybrid Control of Seismic-Excited Nonlinear and Inelastic Structural Systems," by J.N. Yang, Z. Li and A. Danielians, 8/1/91, (PB92-143171).
- NCEER-91-0021 "The NCEER-91 Earthquake Catalog: Improved Intensity-Based Magnitudes and Recurrence Relations for U.S. Earthquakes East of New Madrid," by L. Seeber and J.G. Armbruster, 8/28/91, (PB92-176742).
- NCEER-91-0022 "Proceedings from the Implementation of Earthquake Planning and Education in Schools: The Need for Change - The Roles of the Changemakers," by K.E.K. Ross and F. Winslow, 7/23/91, (PB92-129998).
- NCEER-91-0023 "A Study of Reliability-Based Criteria for Seismic Design of Reinforced Concrete Frame Buildings," by H.H.M. Hwang and H-M. Hsu, 8/10/91, (PB92-140235).
- NCEER-91-0024 "Experimental Verification of a Number of Structural System Identification Algorithms," by R.G. Ghanem, H. Gavin and M. Shinozuka, 9/18/91, (PB92-176577).
- NCEER-91-0025 "Probabilistic Evaluation of Liquefaction Potential," by H.H.M. Hwang and C.S. Lee, 11/25/91, (PB92-143429).
- NCEER-91-0026 "Instantaneous Optimal Control for Linear, Nonlinear and Hysteretic Structures - Stable Controllers," by J.N. Yang and Z. Li, 11/15/91, (PB92-163807).
- NCEER-91-0027 "Experimental and Theoretical Study of a Sliding Isolation System for Bridges," by M.C. Constantinou, A. Kartoum, A.M. Reinhorn and P. Bradford, 11/15/91, (PB92-176973).
- NCEER-92-0001 "Case Studies of Liquefaction and Lifeline Performance During Past Earthquakes, Volume 1: Japanese Case Studies," Edited by M. Hamada and T. O'Rourke, 2/17/92, (PB92-197243).
- NCEER-92-0002 "Case Studies of Liquefaction and Lifeline Performance During Past Earthquakes, Volume 2: United States Case Studies," Edited by T. O'Rourke and M. Hamada, 2/17/92, (PB92-197250).
- NCEER-92-0003 "Issues in Earthquake Education," Edited by K. Ross, 2/3/92, (PB92-222389).
- NCEER-92-0004 "Proceedings from the First U.S. - Japan Workshop on Earthquake Protective Systems for Bridges," Edited by I.G. Buckle, 2/4/92, (PB94-142239, A99, MF-A06).
- NCEER-92-0005 "Seismic Ground Motion from a Haskell-Type Source in a Multiple-Layered Half-Space," A.P. Theoharis, G. Deodatis and M. Shinozuka, 1/2/92, to be published.

- NCEER-92-0006 "Proceedings from the Site Effects Workshop," Edited by R. Whitman, 2/29/92, (PB92-197201).
- NCEER-92-0007 "Engineering Evaluation of Permanent Ground Deformations Due to Seismically-Induced Liquefaction," by M.H. Baziar, R. Dobry and A.W.M. Elgamal, 3/24/92, (PB92-222421).
- NCEER-92-0008 "A Procedure for the Seismic Evaluation of Buildings in the Central and Eastern United States," by C.D. Poland and J.O. Malley, 4/2/92, (PB92-222439).
- NCEER-92-0009 "Experimental and Analytical Study of a Hybrid Isolation System Using Friction Controllable Sliding Bearings," by M.Q. Feng, S. Fujii and M. Shinozuka, 5/15/92, (PB93-150282).
- NCEER-92-0010 "Seismic Resistance of Slab-Column Connections in Existing Non-Ductile Flat-Plate Buildings," by A.I. Durrani and Y. Du, 5/18/92.
- NCEER-92-0011 "The Hysteretic and Dynamic Behavior of Brick Masonry Walls Upgraded by Ferrocement Coatings Under Cyclic Loading and Strong Simulated Ground Motion," by H. Lee and S.P. Prawel, 5/11/92, to be published.
- NCEER-92-0012 "Study of Wire Rope Systems for Seismic Protection of Equipment in Buildings," by G.F. Demetriades, M.C. Constantinou and A.M. Reinhorn, 5/20/92.
- NCEER-92-0013 "Shape Memory Structural Dampers: Material Properties, Design and Seismic Testing," by P.R. Witting and F.A. Cozzarelli, 5/26/92.
- NCEER-92-0014 "Longitudinal Permanent Ground Deformation Effects on Buried Continuous Pipelines," by M.J. O'Rourke, and C. Nordberg, 6/15/92.
- NCEER-92-0015 "A Simulation Method for Stationary Gaussian Random Functions Based on the Sampling Theorem," by M. Grigoriu and S. Balopoulou, 6/11/92, (PB93-127496).
- NCEER-92-0016 "Gravity-Load-Designed Reinforced Concrete Buildings: Seismic Evaluation of Existing Construction and Detailing Strategies for Improved Seismic Resistance," by G.W. Hoffmann, S.K. Kunnath, A.M. Reinhorn and J.B. Mander, 7/15/92, (PB94-142007, A08, MF-A02).
- NCEER-92-0017 "Observations on Water System and Pipeline Performance in the Limón Area of Costa Rica Due to the April 22, 1991 Earthquake," by M. O'Rourke and D. Ballantyne, 6/30/92, (PB93-126811).
- NCEER-92-0018 "Fourth Edition of Earthquake Education Materials for Grades K-12," Edited by K.E.K. Ross, 8/10/92.
- NCEER-92-0019 "Proceedings from the Fourth Japan-U.S. Workshop on Earthquake Resistant Design of Lifeline Facilities and Countermeasures for Soil Liquefaction," Edited by M. Hamada and T.D. O'Rourke, 8/12/92, (PB93-163939).
- NCEER-92-0020 "Active Bracing System: A Full Scale Implementation of Active Control," by A.M. Reinhorn, T.T. Soong, R.C. Lin, M.A. Riley, Y.P. Wang, S. Aizawa and M. Higashino, 8/14/92, (PB93-127512).
- NCEER-92-0021 "Empirical Analysis of Horizontal Ground Displacement Generated by Liquefaction-Induced Lateral Spreads," by S.F. Bartlett and T.L. Youd, 8/17/92, (PB93-188241).
- NCEER-92-0022 "IDARC Version 3.0: Inelastic Damage Analysis of Reinforced Concrete Structures," by S.K. Kunnath, A.M. Reinhorn and R.F. Lobo, 8/31/92, (PB93-227502, A07, MF-A02).
- NCEER-92-0023 "A Semi-Empirical Analysis of Strong-Motion Peaks in Terms of Seismic Source, Propagation Path and Local Site Conditions," by M. Kamiyama, M.J. O'Rourke and R. Flores-Berrones, 9/9/92, (PB93-150266).
- NCEER-92-0024 "Seismic Behavior of Reinforced Concrete Frame Structures with Nonductile Details, Part I: Summary of Experimental Findings of Full Scale Beam-Column Joint Tests," by A. Beres, R.N. White and P. Gergely, 9/30/92, (PB93-227783, A05, MF-A01).

- NCEER-92-0025 "Experimental Results of Repaired and Retrofitted Beam-Column Joint Tests in Lightly Reinforced Concrete Frame Buildings," by A. Beres, S. El-Borgi, R.N. White and P. Gergely, 10/29/92, (PB93-227791, A05, MF-A01).
- NCEER-92-0026 "A Generalization of Optimal Control Theory: Linear and Nonlinear Structures," by J.N. Yang, Z. Li and S. Vongchavalitkul, 11/2/92, (PB93-188621).
- NCEER-92-0027 "Seismic Resistance of Reinforced Concrete Frame Structures Designed Only for Gravity Loads: Part I - Design and Properties of a One-Third Scale Model Structure," by J.M. Bracci, A.M. Reinhorn and J.B. Mander, 12/1/92, (PB94-104502, A08, MF-A02).
- NCEER-92-0028 "Seismic Resistance of Reinforced Concrete Frame Structures Designed Only for Gravity Loads: Part II - Experimental Performance of Subassemblages," by L.E. Aycardi, J.B. Mander and A.M. Reinhorn, 12/1/92, (PB94-104510, A08, MF-A02).
- NCEER-92-0029 "Seismic Resistance of Reinforced Concrete Frame Structures Designed Only for Gravity Loads: Part III - Experimental Performance and Analytical Study of a Structural Model," by J.M. Bracci, A.M. Reinhorn and J.B. Mander, 12/1/92, (PB93-227528, A09, MF-A01).
- NCEER-92-0030 "Evaluation of Seismic Retrofit of Reinforced Concrete Frame Structures: Part I - Experimental Performance of Retrofitted Subassemblages," by D. Choudhuri, J.B. Mander and A.M. Reinhorn, 12/8/92, (PB93-198307, A07, MF-A02).
- NCEER-92-0031 "Evaluation of Seismic Retrofit of Reinforced Concrete Frame Structures: Part II - Experimental Performance and Analytical Study of a Retrofitted Structural Model," by J.M. Bracci, A.M. Reinhorn and J.B. Mander, 12/8/92, (PB93-198315, A09, MF-A03).
- NCEER-92-0032 "Experimental and Analytical Investigation of Seismic Response of Structures with Supplemental Fluid Viscous Dampers," by M.C. Constantinou and M.D. Symans, 12/21/92, (PB93-191435).
- NCEER-92-0033 "Reconnaissance Report on the Cairo, Egypt Earthquake of October 12, 1992," by M. Khater, 12/23/92, (PB93-188621).
- NCEER-92-0034 "Low-Level Dynamic Characteristics of Four Tall Flat-Plate Buildings in New York City," by H. Gavin, S. Yuan, J. Grossman, E. Pekelis and K. Jacob, 12/28/92, (PB93-188217).
- NCEER-93-0001 "An Experimental Study on the Seismic Performance of Brick-Infilled Steel Frames With and Without Retrofit," by J.B. Mander, B. Nair, K. Wojtkowski and J. Ma, 1/29/93, (PB93-227510, A07, MF-A02).
- NCEER-93-0002 "Social Accounting for Disaster Preparedness and Recovery Planning," by S. Cole, E. Pantoja and V. Razak, 2/22/93, (PB94-142114, A12, MF-A03).
- NCEER-93-0003 "Assessment of 1991 NEHRP Provisions for Nonstructural Components and Recommended Revisions," by T.T. Soong, G. Chen, Z. Wu, R-H. Zhang and M. Grigoriu, 3/1/93, (PB93-188639).
- NCEER-93-0004 "Evaluation of Static and Response Spectrum Analysis Procedures of SEAOC/UBC for Seismic Isolated Structures," by C.W. Winters and M.C. Constantinou, 3/23/93, (PB93-198299).
- NCEER-93-0005 "Earthquakes in the Northeast - Are We Ignoring the Hazard? A Workshop on Earthquake Science and Safety for Educators," edited by K.E.K. Ross, 4/2/93, (PB94-103066, A09, MF-A02).
- NCEER-93-0006 "Inelastic Response of Reinforced Concrete Structures with Viscoelastic Braces," by R.F. Lobo, J.M. Bracci, K.L. Shen, A.M. Reinhorn and T.T. Soong, 4/5/93, (PB93-227486, A05, MF-A02).

- NCEER-93-0007 "Seismic Testing of Installation Methods for Computers and Data Processing Equipment," by K. Kosar, T.T. Soong, K.L. Shen, J.A. HoLung and Y.K. Lin, 4/12/93, (PB93-198299).
- NCEER-93-0008 "Retrofit of Reinforced Concrete Frames Using Added Dampers," by A. Reinhorn, M. Constantinou and C. Li, to be published.
- NCEER-93-0009 "Seismic Behavior and Design Guidelines for Steel Frame Structures with Added Viscoelastic Dampers," by K.C. Chang, M.L. Lai, T.T. Soong, D.S. Hao and Y.C. Yeh, 5/1/93, (PB94-141959, A07, MF-A02).
- NCEER-93-0010 "Seismic Performance of Shear-Critical Reinforced Concrete Bridge Piers," by J.B. Mander, S.M. Waheed, M.T.A. Chaudhary and S.S. Chen, 5/12/93, (PB93-227494, A08, MF-A02).
- NCEER-93-0011 "3D-BASIS-TABS: Computer Program for Nonlinear Dynamic Analysis of Three Dimensional Base Isolated Structures," by S. Nagarajaiah, C. Li, A.M. Reinhorn and M.C. Constantinou, 8/2/93, (PB94-141819, A09, MF-A02).
- NCEER-93-0012 "Effects of Hydrocarbon Spills from an Oil Pipeline Break on Ground Water," by O.J. Helweg and H.H.M. Hwang, 8/3/93, (PB94-141942, A06, MF-A02).
- NCEER-93-0013 "Simplified Procedures for Seismic Design of Nonstructural Components and Assessment of Current Code Provisions," by M.P. Singh, L.E. Suarez, E.E. Matheu and G.O. Maldonado, 8/4/93, (PB94-141827, A09, MF-A02).
- NCEER-93-0014 "An Energy Approach to Seismic Analysis and Design of Secondary Systems," by G. Chen and T.T. Soong, 8/6/93, (PB94-142767, A11, MF-A03).
- NCEER-93-0015 "Proceedings from School Sites: Becoming Prepared for Earthquakes - Commemorating the Third Anniversary of the Loma Prieta Earthquake," Edited by F.E. Winslow and K.E.K. Ross, 8/16/93.
- NCEER-93-0016 "Reconnaissance Report of Damage to Historic Monuments in Cairo, Egypt Following the October 12, 1992 Dahshur Earthquake," by D. Sykora, D. Look, G. Croci, E. Karaesmen and E. Karaesmen, 8/19/93, (PB94-142221, A08, MF-A02).
- NCEER-93-0017 "The Island of Guam Earthquake of August 8, 1993," by S.W. Swan and S.K. Harris, 9/30/93, (PB94-141843, A04, MF-A01).
- NCEER-93-0018 "Engineering Aspects of the October 12, 1992 Egyptian Earthquake," by A.W. Elgamal, M. Amer, K. Adalier and A. Abul-Fadl, 10/7/93, (PB94-141983, A05, MF-A01).
- NCEER-93-0019 "Development of an Earthquake Motion Simulator and its Application in Dynamic Centrifuge Testing," by I. Krstelj, Supervised by J.H. Prevost, 10/23/93.
- NCEER-93-0020 "NCEER-Taisei Corporation Research Program on Sliding Seismic Isolation Systems for Bridges: Experimental and Analytical Study of a Friction Pendulum System (FPS)," by M.C. Constantinou, P. Tsopelas, Y-S. Kim and S. Okamoto, 11/1/93, (PB94-142773, A08, MF-A02).
- NCEER-93-0021 "Finite Element Modeling of Elastomeric Seismic Isolation Bearings," by L.J. Billings, Supervised by R. Shepherd, 11/8/93, to be published.
- NCEER-93-0022 "Seismic Vulnerability of Equipment in Critical Facilities: Life-Safety and Operational Consequences," by K. Porter, G.S. Johnson, M.M. Zadeh, C. Scawthorn and S. Eder, 11/24/93.
- NCEER-93-0023 "Hokkaido Nansei-oki, Japan Earthquake of July 12, 1993, by P.I. Yanev and C.R. Scawthorn, 12/23/93.
- NCEER-94-0001 "An Evaluation of Seismic Serviceability of Water Supply Networks with Application to San Francisco Auxiliary Water Supply System," by I. Markov, Supervised by M. Grigoriu and T. O'Rourke, 1/21/94.

- NCEER-94-0002 "NCEER-Taisei Corporation Research Program on Sliding Seismic Isolation Systems for Bridges: Experimental and Analytical Study of Systems Consisting of Sliding Bearings, Rubber Restoring Force Devices and Fluid Dampers," Volumes I and II, by P. Tsopelas, S. Okamoto, M.C. Constantinou, D. Ozaki and S. Fujii, 2/4/94.
- NCEER-94-0003 "A Markov Model for Local and Global Damage Indices in Seismic Analysis," by S. Rahman and M. Grigoriu, 2/18/94, to be published.
- NCEER-94-0004 "Proceedings from the NCEER Workshop on Seismic Response of Masonry Infills," edited by D.P. Abrams, 3/1/94.
- NCEER-94-0005 "The Northridge, California Earthquake of January 17, 1994: General Reconnaissance Report," edited by J.D. Goltz, 3/11/94.
- NCEER-94-0006 "Seismic Energy Based Fatigue Damage Analysis of Bridge Columns: Part I - Evaluation of Seismic Capacity," by G.A. Chang and J.B. Mander, 3/14/94.